



UNIWERSYTET ŚLĄSKI  
INSTYTUT FIZYKI  
IM. AUGUSTA CHEŁKOWSKIEGO

**Uniwersytet Śląski w Katowicach**  
**INSTYTUT FIZYKI**  
**Wydział Nauk Ścisłych i Technicznych**

PRACA DOKTORSKA

Badania dynamiki molekularnej układów nisko- i wysokocząsteczkowych w układach  
porowatych

mgr Agnieszka Talik

PROMOTOR PRACY:

Prof. dr hab. Kamil Kamiński

PROMOTOR POMOCNICZY PRACY:

dr hab. Magdalena Tarnacka, prof. UŚ

CHORZÓW 2021

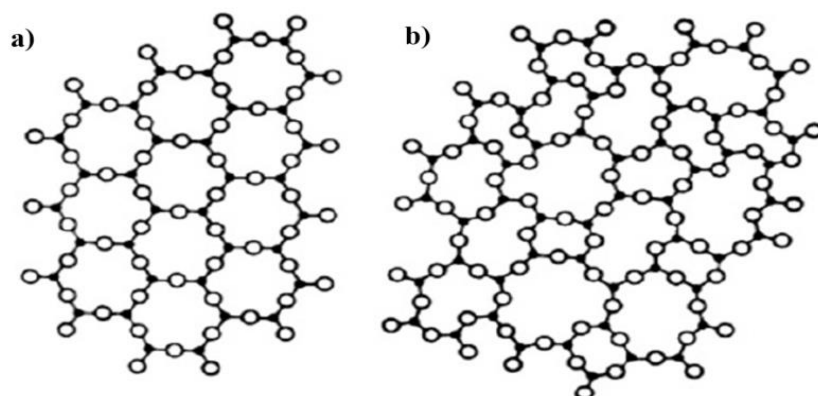
## SPIS TREŚCI

I. WSTĘP .....	3
II. OMÓWIENIE OTRZYMANYCH WYNIKÓW .....	15
A. Określenie roli energii międzyfazowej i specyficznych interakcji na zachowanie poli(glikolu propylenowego) i jego pochodnych w dwuwymiarowym ograniczeniu przestrzennym oraz wpływu ograniczenia przestrzennego na dynamikę oraz zachowanie wiązań wodorowych w poli(glikolach propylenowych) o niskiej masie cząsteczkowej .....	15
B. Określenie wpływu krzywizny powierzchni na właściwości układów w dwuwymiarowym ograniczeniu przestrzennym na przykładzie glicerolu .....	27
C. Prześledzenie wpływu dwu-wymiarowego ograniczenia przestrzennego na specyficzne oddziaływania wodorowe a także na supramolekularne struktury o różnej architekturze na przykładzie wybranych monohydroksy alkoholi.....	30
III. TREŚCI ARTYKUŁÓW STANOWIĄCYCH PODSTAWĘ ROZPRAWY DOKTORSKIEJ WRAZ Z OŚWIADCZENIAMI WSPÓŁAUTORÓW .....	34
A1. The Role of Interfacial Energy and Specific Interactions on the Behavior of Poly(propylene glycol) Derivatives under 2D Confinement. ....	34
A2. Impact of the Interfacial Energy and Density Fluctuation on the Shift of the Glass-Transition Temperature of Liquids Confined in Pores. ....	48
A3. The influence of the nanocurvature on the surface interactions and molecular dynamics of model liquid confined in cylindrical pores .....	57
A4. Are hydrogen supramolecular structures being suppressed upon nanoscale confinement? The case of monohydroxy alcohols .....	65
A5. Impact of Confinement on the Dynamics and H-Bonding Pattern in Low-Molecular Weight Poly(propylene glycols) .....	79
IV. PODSUMOWANIE .....	108
V. Bibliografia .....	111

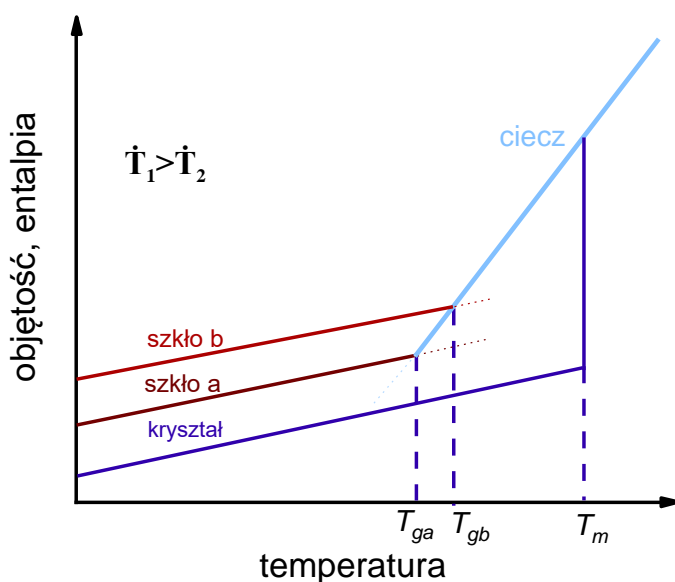
## I. WSTĘP

Według amerykańskiej Agencji Ochrony Środowiska (EPA) nanotechnologia definiowana jest jako "tworzenie i wykorzystywanie struktur, urządzeń i systemów o nowych właściwościach i funkcjach z powodu ich niewielkich rozmiarów" w kontekście zrozumienia i kontroli materii o wymiarach od około 1 do 100 nm<sup>1,2</sup>. Za historyczny początek nanotechnologii uważa się wygłoszenie w latach 50. XX w. przez naukowca i noblistę w dziedzinie fizyki Richarda Feynmana wykładu pt. „*There is plenty of room at the bottom*” odnoszącego się do możliwości poznawczych w świecie mikroskopowym, możliwości manipulacji i kontroli poszczególnych atomów i molekuł w skali nanometrycznej<sup>3,4</sup>. Ten słynny wykład zainicjował trend miniaturyzacji trwający do dnia dzisiejszego.

Dynamiczny rozwój przemysłu w ostatnich dekadach spowodował, że nanomateriały wzbudziły duże zainteresowanie ze względu na wyjątkowe właściwości fizyko-chemiczne oraz możliwość uzyskania unikalnych morfologii różniących się od tych otrzymywanych w skali makroskopowej. Znalazły one szerokie zastosowanie w przemyśle m.in. jako nośniki leków, nanodrut, implanty, a także w układach elektronicznych, elektrooptycznych czy w ogniwach fotowoltaicznych<sup>5,6,7,8,9,10</sup>. To szerokie spektrum zastosowań nanomateriałów powoduje, że w ostatnich latach coraz większego znaczenia nabiera poszukiwanie odpowiedzi na pytanie jak zmieniają się dynamiczne właściwości materiałów w nanoskali, takie jak dyfuzja, czasy relaksacji, temperatury przejść fazowych, temperatura przejścia szklistego ( $T_g$ ) substancji formujących szkło.



**Rys.1** Schematyczne przedstawienie struktur a) krystalicznej i b) amorficznej [11].



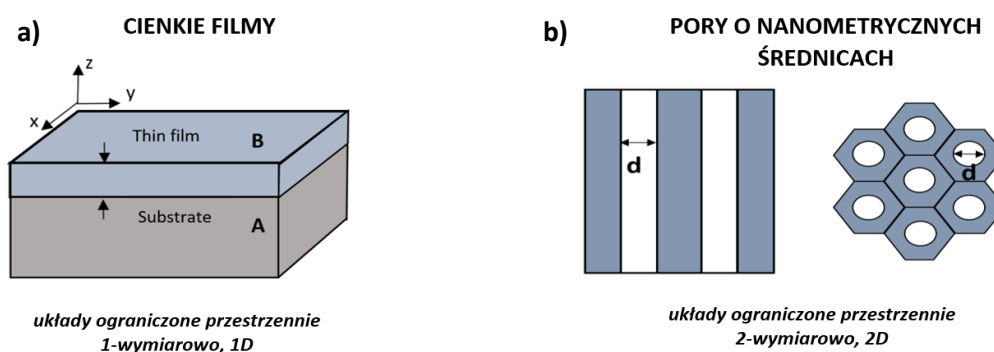
**Rys. 2** Wykres zależności objętości układu oraz jego entalpii od temperatury [12].

Temperatura przejścia szklistego ( $T_g$ ) jest centralnym zagadnieniem w większości badań substancji formujących fazę szklistą w ograniczeniu przestrzennym oraz dla materiałów litych (*ang. bulk*). Pomimo dziesięcioleci badań zarówno teoretyków jak i eksperymentatorów, zmierzających do odkrycia mechanizmu prowadzącego do powstawania szkła, zjawisko to jest nadal nierozwiązanym problemem fizyki materii skondensowanej<sup>13,14,15,16</sup>. Szkło wykazuje makroskopijne właściwości ciała stałego ale mikroskopijnie zachowuje nieuporządkowany charakter cieczy nie wykazując dalekozasięgowego uporządkowania charakterystycznego dla

struktur krystalicznych (**Rys. 1**)<sup>17</sup>. Podczas wolnego ochładzania poniżej temperatury topnienia ( $T_m$ ) ciecz może skryształizować bądź jeżeli tempo schładzania jest dostatecznie szybkie ( $\dot{T} = dT/dt$ ), może ulec przechłodzeniu i w konsekwencji przejść do stanu szklanego (**Rys. 1**)<sup>18</sup>. Ponadto, po ochłodzeniu wielkości takie jak lepkość, współczynnik dyfuzji czy czas relaksacji strukturalnej zmieniają się (pomiędzy  $T_m$  i  $T_g$ ) o kilkanaście rzędów wielkości, czego skutkiem jest spowolnienie ruchliwości (dynamiki) molekularnej (**Rys. 2**). W obrębie  $T_g$  lepkość i czasy relaksacji osiągają odpowiednio wartości  $\eta = 10^{13}$  P i  $\tau_\alpha = 100$  s<sup>12,19</sup>. Jednak fizyczna natura tego zjawiska, pomimo wielu doniesień literaturowych, jest nadal nieznana. Dlatego zbadanie i pełne zrozumienie tego procesu ma istotne znaczenie przyczyniające się do sformułowania ogólnej, molekularnej teorii przejścia szklanego, która w następstwie posłuży do lepszego wykorzystania materiałów amorficznych w szeroko rozumianym przemyśle.

Jedną z podstawowych koncepcji opisujących zmiany we właściwościach materiałów w pobliżu  $T_g$  jest teoria dynamicznych heterogeniczności, zgodnie z którą dla cieczy przechłodzonej tworzą się regiony, w których przegrupowania molekuł odbywają się w sposób kooperatywny, składające się z wysoce mobilnych i słabo ruchliwych cząsteczek. Koncepcję tą wprowadził G. Adam i J.H. Gibbs w latach 60-tych ubiegłego wieku<sup>20</sup>, w której postulowano, iż wraz z ochładzaniem cieczy rośnie czas relaksacji układu ze względu na zwiększenie rozmiaru tzw. kooperatywnie reorientujących domen (z ang. *Cooperatively rearranging regions*) CRR. W swoim modelu powiązali oni czas relaksacji, który definiuje dynamikę układu z entropią konfiguracyjną, która jest wielkością termodynamiczną ( $\tau = \tau_0 \exp[C/(TS_c)]$ )<sup>21</sup>. Opis zaproponowany przez Adama i Gibbsa zainspirował wielu naukowców do ukierunkowania swoich badań i powiązania przejścia szklanego z efektami entropowymi. Podejście to jest w pełni uzasadnione biorąc pod uwagę termodynamiczny opis przejść fazowych. Chociaż jest wiele przesłanek eksperymentalnych wskazujących, iż proces witrifikacji z powodu zmiany stanu układu z metastabilnego równowagowego na metastabilny

nierównowagowy nie może być klasyfikowany jako typowe przejście fazowe w klasycznym ujęciu Ehrenfesta<sup>22</sup>. Niemniej jednak koncepcja obszarów dynamicznie skorelowanych jest wciąż rozwijana, w tym kontekście można przywołać prace opublikowane w prestiżowych czasopismach m.in w Science<sup>23,24</sup>. Niezwykle ciekawym podejściem do weryfikacji modeli zakładających istnienie dynamicznych heterogeniczności, których rozmiar ma wpływ na czas relaksacji strukturalnej czy też segmentalnej są eksperymenty prowadzone dla układów ograniczonych przestrzennie w nanoskali. Dotychczas prowadzone badania pokazały, że rozmiar dynamicznych heterogeniczności jest rzędu kilku nanometrów<sup>25,26,27</sup>. Jest to skala ograniczenia przestrzennego jakie możemy wytworzyć eksperymentalnie w laboratorium dla układów miękkiej materii. Niestety badania nad układami ograniczonymi przestrzennie jasno pokazały, że weryfikacja modeli bazujących na koncepcji dynamicznych heterogeniczności jest niebywale trudna ze względu na duży wpływ substratu, który bardzo często mocno oddziałuje z badaną próbką i wprowadza gradient gęstości, mobilności, zmieniający się w sposób trudny do przewidzenia wraz z odległością.



**Rys. 3** Układy ograniczone przestrzennie.

Należy nadmienić, iż układy w geometrycznym ograniczeniu można przede wszystkim otrzymać w postaci nanocząstek, warstw o nanometrycznych grubościach osadzanych na twardym podłożu gdzie badana substancja jest ograniczana wzdłuż kierunku  $z$  (układy ograniczone przestrzennie jednowymiarowo, 1D, **Rys. 3a**), bądź też poprzez ich infiltrowanie

do porowatych membran o nanometrycznych średnicach porów, gdzie badany materiał jest ograniczony w dwóch wymiarach  $x$  i  $y$  (układy ograniczone przestrzennie dwuwymiarowo, 2D, **Rys. 3b**)<sup>28,29,30,31</sup>. Zmiany w dynamice molekularnej i we właściwościach materiału zachodzące w ograniczeniu przestrzennym, gdzie wymiary są zredukowane do skali nanometrycznej, są intensywnie badane przez naukowców<sup>14</sup>, zarówno teoretyków (symulacje)<sup>32,33,34,35</sup>, jak i eksperymentatorów<sup>31,36,37,38</sup>. Szczególnie ważną kwestią stało się wykrywanie i monitorowanie wielkości zmian/odchyień w zachowaniu materiału w ograniczeniu przestrzennym w stosunku do materiału litego<sup>39,40,41</sup>.

W ciągu ostatnich dziesięcioleci, ze względu na duże znaczenie poznawcze i ogromny potencjał użytkowy, podjęto duże wysiłki w celu zbadania wpływu nisko- i wysokocząsteczkowych substancji m.in polimerów, w warunkach nano-wymiarowego ograniczenia przestrzennego na przebieg procesu zeszklenia<sup>42,43</sup>. Badania te mają na celu zarówno osiągnięcie głębszego zrozumienia efektu i wpływu rozmiarowości oraz zbadanie jak substrat, zakrzywienie ścianek w układach porowatych wpływa na dynamikę polimeru w ograniczeniu przestrzennym<sup>13</sup>.

Pionierskie prace nad polimerami w warunkach ograniczenia przestrzennego koncentrowały się początkowo głównie na cienkich warstwach<sup>31,41,44,45,46,47,48,49</sup>. Wynikało to w szczególności z odmiennych i nieco kontrowersyjnych wyników opublikowanych przez różne grupy badawcze, wykazujące duży rozrzut w wartości  $T_g$  dla takich materiałów w odniesieniu do wartości otrzymywanej dla substancji litej<sup>31,36,50,51,52,53</sup>. Pierwsze doniesienia literaturowe wykazały silną redukcję  $T_g$  w porównaniu do próbki litej. Jednakże dalsze eksperymenty dla polistyrenu (PS) ujawniły że  $T_g$  substancji w jednowymiarowym ograniczeniu przestrzennym wzrasta, maleje, bądź pozostaje stałe<sup>54,55,56,57</sup>. Osiągnięcie spójnej teorii dla tak zróżnicowanych wyników, zwłaszcza gdy raportowane  $T_g$  zmienia się o ponad 70 K w porównaniu z materiałem litym, okazało się dużym wyzwaniem<sup>58</sup>. Kolejne badania

substancji osadzanych w postaci cienkich warstw pokazały, że zmiany w temperaturze zeszklenia w porównaniu do  $T_g$  polimerów w stanie litym zależą od zastosowanego substratu<sup>59</sup>. Dla poli(metakrylanu metylu) (PMMA) osadzanego na niepolarnych podłożach zaobserwowano, że interakcje polimeru z powierzchnią substratu są słabsze prowadząc do obniżenia wartości  $T_g$ , podczas gdy dla polarnych podłoży odnotowano wzrost  $T_g$ <sup>36,43</sup>, wnioskując tym samym, że temperatura zeszklenia dla ultracienkich warstw wzrasta jeśli pomiędzy łańcuchami a podłożem (substratem) istnieją silne oddziaływania np. wodorowe<sup>43,60</sup>. Wyniki te pokazują, że zarówno efekty powierzchniowe jak i międzyfazowe wydają się być kluczowymi czynnikami wpływającymi na właściwości ultracienkich warstw polimerowych<sup>60</sup>. Dalsze systematyczne badania wykazały, że zmiany w dynamice molekularnej mogą być związane z mobilnością warstwy zewnętrznej będącej w kontakcie z powietrzem, adsorpcją łańcuchów polimerowych na powierzchni substrat-substancja a także z zastosowaną techniką eksperymentalną<sup>61,46,62,52,63,64</sup>. Wykazano również, że kierunek i wielkość przesunięcia  $T_g$ , zależy w dużym stopniu od energii międzyfazowej ( $\gamma_{SL}$ , substancja badana - matryca), gdzie wzrost  $\gamma_{SL}$  prowadzi do zmniejszenia mobilności warstwy międzyfazowej, a tym samym do wzrostu  $T_g$ <sup>36,65</sup>. Ostatnie badania dowodzą, że zmiany w zachowaniu (m.in. odchylenia od temperatury zeszklenia pomiędzy materiałem litym a ograniczonym przestrzennie ( $\Delta T_g$ )) mogą też mocno zależeć od historii termicznej próbki. Oznacza to, że wartość zmian w  $T_g$  jest ściśle związana ze skalą czasową eksperymentu<sup>66</sup>, gdzie wygrzewanie układu powyżej  $T_g$  w funkcji czasu, może prowadzić do odzyskania właściwości podobnych do materiału litego niezależnie od grubości warstwy<sup>67</sup>. Wyniki te zostały omówione w kategoriach zmian gęstości na styku substrat-substancja oraz wzrostu liczby nieodwracalnie zaadsorbowanych łańcuchów na granicy faz podczas osiągnięcia stanu równowagi w skali czasowej znacznie dłuższej niż czas reptacji, bardzo często utożsamiany jako czas relaksacji segmentalnej<sup>41,68</sup>.



Odmienny wzorzec zachowań został odnotowany w literaturze dla substancji infiltrowanych do porowatych matryc o nanometrycznych średnicach, gdzie zaobserwowano obniżenie  $T_g$  w porównaniu do materiału litego wraz ze zmniejszaniem rozmiarów porów<sup>39,69,70,71,72</sup>. Dla tych systemów w pobliżu  $T_g$  skala czasowa ruchliwości molekularnej w danej temperaturze skraca się wraz ze zwiększeniem krzywizny ścianki<sup>65</sup>. W tego typu układach, molekuly są ograniczone w dwóch wymiarach (**Rys. 3**), gdzie fluktuacje gęstości materiału spowodowane zmianami energii międzyfazowej są silniejsze w porównaniu do materiałów 1D. Porównanie dynamiki molekularnej na przykładzie polimeru poli(metylofenylo-siloksanu) (PMPS) w ograniczeniu przestrzennym jedno- i dwu-wymiarowym wykazało, że dynamika segmentalna dla cienkich warstw pozostała taka sama jak dla materiału litego, podczas gdy wartość  $T_g$  polimerów infiltrowanych do porowatych matryc zmalała<sup>73</sup>. Ponadto badania polistyrenu (PS) infiltrowanego do porowatych matryc pokazały, że  $T_g$  jest niezmiennie w porównaniu do materiału litego, jeżeli rozmiar porów jest mniejszy niż wymiary łańcucha ( $2R_g$ )<sup>48,74</sup>. Oznacza to, że dynamika molekularna w dwuwymiarowym ograniczeniu przestrzennym jest regulowana poprzez interakcję pomiędzy efektami powierzchniowymi a ograniczeniem rozmiarowości<sup>75</sup>. W związku z powyższym stosunkiem powierzchni do objętości dla układów dwuwymiarowych (2D) - efekt powierzchniowy staje się znacznie większy niż dla układów 1D. Ograniczone przestrzenie molekuly w środku porowatych matryc często wykazują zwiększoną mobilność w porównaniu do materiału w stanie litym. Wpływ ograniczenia przestrzennego na  $T_g$  został dość szeroko omówiony w literaturze między innymi w kontekście (i) wolnej objętości (ang. *free volume*)<sup>76,77</sup>, (ii) entropii konfiguracyjnej (liczby różnych sposobów ułożenia atomów w węzłach sieci) zaproponowanej przez Gibbsa i DiMarzio<sup>78,79</sup> (iii) efektów gęstości<sup>80,67</sup> czy (vi) teorii kooperatywnie reorientujących domen CRR (ang. *Cooperative Rearrangement Regions*), zgodnie z którą, wraz z obniżaniem temperatury liczba cząsteczek lub segmentów polimerowych w obrębie CRR wzrasta,

powodując gwałtowny wzrost lepkości, spowalniając tym samym czas relaksacji w pobliżu  $T_g$ <sup>81,82</sup>. Zaproponowano również, że spadek  $T_g$  dla niskocząsteczkowych molekuł w mezoporach może być połączony ze zjawiskiem ujemnego ciśnienia<sup>39,83,84</sup>.

Najnowsze badania pokazały, że obniżenie  $T_g$  jest w dużej mierze spowodowane wzrostem energii międzyfazowej ( $\gamma_{SL}$ )<sup>65</sup>. Jednakże przedstawiona korelacja jest sprzeczna z dotychczas obserwowanym zachowaniem materiałów ograniczonych przestrzennie jednowymiarowo, gdzie zgodnie z literaturą, wzrost energii międzyfazowej powoduje wzrost  $T_g$  w wyniku zmniejszonej mobilności molekuł<sup>65</sup>. W tym kontekście wydaje się zaskakujące, że zmiana geometrii ograniczenia przestrzennego może spowodować aż tak dramatyczną zmianę obserwowanego trendu zachowań. Choć większość prac dowiodła istnienie silnego efektu ograniczenia przestrzennego i wpływu na zmiany w  $T_g$ , jednak raportowane sprzeczne obserwacje utrudniły opracowanie spójnego obrazu dotychczasowych efektów obserwowanych w nanoskali.

W niniejszej rozprawie przeprowadzono badania dynamiki molekularnej substancji nisko- i wysokocząsteczkowych formujących fazę szklistą w stanie litym oraz w dwuwymiarowym ograniczeniu przestrzennym, za pomocą szerokopasmowej spektroskopii dielektrycznej (BDS). Użycie tej techniki pozwala na monitorowanie dynamiki molekularnej, charakterystycznych czasów relaksacji w szerokim zakresie częstotliwości  $10^{-2}$  -  $10^6$  Hz oraz temperatur (-140 - 400°C). Metoda ta umożliwia śledzenie odpowiedzi badanej substancji na przyłożone zewnętrznie zmienne pole elektryczne mierząc zmiany wypadkowego wektora polaryzacji, składającego się z wkładu polaryzacji indukowanej (polaryzacji elektronowej i atomowej) oraz orientacyjnej. Relacja pomiędzy zewnętrznym polem elektrycznym  $E$  a wektorem polaryzacji  $P$  w funkcji częstotliwości przedstawiona jest jako:

$$P^*(\omega) = \varepsilon^*(\omega) E(\omega) \quad (1)$$

gdzie  $\varepsilon^*(\omega)$  oznacza zespoloną przenikalność dielektryczną wyrażoną jako:

$$\varepsilon^*(\omega) = \varepsilon'(\omega) - i \varepsilon''(\omega) \quad (2)$$

W powyższym wzorze  $\varepsilon' = C/C_0$  ( $C$ - pojemność kondensatora z dielektrykiem;  $C_0$ - pojemność pustego kondensatora) to część rzeczywista, natomiast  $\varepsilon'' = 1/\omega RC_0$  reprezentuje część urojoną (straty dielektryczne). W eksperymencie prowadzonym z użyciem spektroskopii dielektrycznej wykorzystywane jest sinusoidalne zmienne pole elektryczne. Badany materiał umieszcza się pomiędzy dwoma okładkami kondensatora (stałą odległość między okładkami zapewnia teflonowa wkładka) i instaluje się w głowicy pomiarowej połączonej z analizatorem impedancji. Kondensator wypełniony dielektrykiem można schematycznie zobrazować jako połączony szeregowo kondensator o pojemności  $C$  oraz opornik o oporze  $R$ . Stosunek napięcia przyłożonego do kondensatora oraz natężenia prądu przepływającego przez materiał nosi nazwę zespolonej impedancji ( $Z^*(\omega) = U^*/I^*$ ). W konsekwencji z otrzymanej relacji zespolona przenikalność dielektryczna przyjmuje postać:

$$\varepsilon^*(\omega) = -\frac{i}{\omega Z_s^*(\omega) C_0} \quad (3)$$

Pojemność pustego kondensatora  $C_0 = \varepsilon_0 S/d$ , zależy od geometrii, gdzie  $S$  to pole powierzchni okładki,  $d$  – odległość między okładkami, natomiast  $\varepsilon_0$  - przenikalność dielektryczna próżni.

Ponadto dla substancji infiltrowanych do porowatych matryc należy uwzględnić dwie składowe równoległych kondensatorów:  $\varepsilon^*_{substancja}$  i  $\varepsilon^*_{matryca}$ . Zatem całkowita impedancja jest związana z poszczególnymi wartościami poprzez  $1/Z^* = 1/Z^*_{substancja} + 1/Z^*_{matryca}$ .

Charakterystyka własności fizyko-chemicznych badanych układów przedstawiona w niniejszej rozprawie została rozszerzona o pomiary przy wykorzystaniu komplementarnych technik eksperymentalnych, tj. różnicowej kalorymetrii skaningowej (DSC), spektroskopii w podczerwieni (FT-IR), kątów zwilżania, a także pionierskich badań za pomocą mikroskopii sił atomowych (AFM).

Celem niniejszej pracy doktorskiej pt. „*Badania dynamiki molekularnej układów nisko- i wysokocząsteczkowych w układach porowatych*” było znalezienie odpowiedzi na fundamentalne pytanie, jaki czynnik determinuje zachowanie miękkiej materii w ograniczeniu przestrzennym dwu-wymiarowym, w szczególności:

- A. Określenie roli energii międzyfazowej i specyficznych interakcji na zachowanie poli(glikolu propylenowego) i jego pochodnych w dwuwymiarowym ograniczeniu przestrzennym oraz wpływu ograniczenia przestrzennego na dynamikę oraz zachowanie wiązań wodorowych w poli(glikolach propylenowych) o niskiej masie cząsteczkowej.
- B. Określenie wpływu krzywizny powierzchni na właściwości układów w dwuwymiarowym ograniczeniu przestrzennym na przykładzie glicerolu.
- C. Prześledzenie wpływu dwu-wymiarowego ograniczenia przestrzennego na specyficzne oddziaływania wodorowe, a także na supramolekularne struktury o różnej architekturze na przykładzie wybranych monohydroksy alkoholi.

Rezultaty prowadzonych badań zostały opublikowane w prestiżowych czasopismach naukowych:

- A1. A. Talik, M. Tarnacka, I. Grudzka-Flak, P. Maksym, M. Geppert-Rybczynska, K. Wolnica, E. Kaminska, K. Kaminski, M. Paluch. **The Role of Interfacial Energy and Specific Interactions on the Behavior of Poly(propylene glycol) Derivatives under 2D Confinement.** *Macromolecules*, 2018, 51(13), 4840-4852.
- A2. A. Talik, M. Tarnacka, M. Geppert-Rybczynska, A. Minecka, E. Kaminska, K. Kaminski, M. Paluch. **Impact of the Interfacial Energy and Density Fluctuations on the Shift of the Glass-Transition Temperature of Liquids Confined in Pores.** *Journal of Physical Chemistry C*, 2019, 123(9), 5549-5556.

- A3. A. Talik, M. Tarnacka, M. Wojtyniak, E. Kaminska, K. Kaminski, M. Paluch. **The influence of the nanocurvature on the surface interactions and molecular dynamics of model liquid confined in cylindrical pores.** *Journal of Molecular Liquids*, 2019, 111973.
- A4. A. Talik, M. Tarnacka, M. Geppert-Rybczynska, B. Hachuła, R. Bernat, A. Chrzanowska, K. Kaminski, M. Paluch. **Are hydrogen supramolecular structures being suppressed upon nanoscale confinement? The case of monohydroxy alcohols.** *Journal of Colloid and Interface Science*, 2020, 576, 217-229.
- A5. A. Talik, M. Tarnacka, M. Geppert-Rybczynska, B. Hachuła, K. Kaminski, M. Paluch. **Impact of Confinement on the Dynamics and H-Bonding Pattern in Low-Molecular Weight Poly(propylene glycols).** *Journal of Physical Chemistry C* 2020, 124, 17607-17621.

Treść powyższych publikacji stanowiących podstawę niniejszej pracy doktorskiej można znaleźć w **Rozdziale 2**. Wyniki uzyskane w trakcie mojego doktoratu zostały zaprezentowane na konferencjach naukowych:

1. „XII Copernican International Young Scientists Conference” (2018) Toruń, Polska.
2. „10th Conference on Broadband Dielectric Spectroscopy and its Applications” (2018) Bruksela, Belgia.
3. „XIII Kopernikańskie Seminarium Doktoranckie” (2019) Toruń, Polska.
4. „InterNanoPoland” (2019) Katowice, Polska.

Ponadto jestem współautorem 14 artykułów naukowych, które nie zostały włączone do rozprawy:

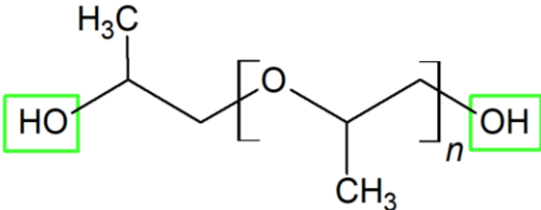
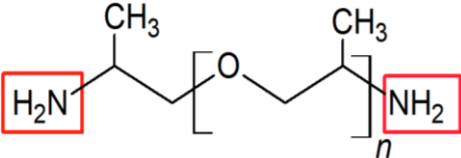
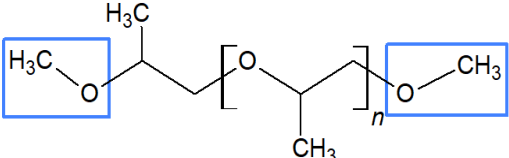
1. A. Minecka, E. Kamińska, M. Tarnacka, A. Talik, I. Grudzka-Flak, K. Wolnica, M. Dulski, K. Kamiński, M. Paluch. **Conformational changes underlying variation in the structural dynamics of materials confined at the nanometric scale.** *Physical Chemistry Chemical Physics*, 2018, 20(48), 30200-30208.
2. D. Heczko, E. Kamińska, A. Minecka, A. Dzień, K. Jurkiewicz, M. Tarnacka, A. Talik, K. Kamiński, M. Paluch. **High-pressure dielectric studies on 1,6-anhydro-  $\beta$ -D-mannopyranose (plastic crystal) and 2,3,4-tri-O-acetyl-1,6-anhydro-  $\beta$ -D-glucopyranose (canonical glass).** *Journal of Chemical Physics*, 2018, 148(20), 204510.
3. M. Tarnacka, A. Dzień, P. Maksym, A. Talik, A. Zięba, R. Bielas, K. Kamiński, M. Paluch. **Highly Efficient ROP Polymerization of  $\epsilon$ -Caprolactone Catalyzed by Nanoporous Alumina Membranes. How the Confinement Affects the Progress and Product of ROP Reaction.** *Macromolecules*, 2018, 51(12), 4588-4597.

4. M. Tarnacka, M. Dulski, M. Geppert-Rybczyńska, A. Talik, E. Kamińska, K. Kamiński, M. Paluch. **Variation in the Molecular Dynamics of DGEBA Confined within AAO Templates above and below the Glass-Transition Temperature.** *Journal of Physical Chemistry C*, 2018, 122(49), 28033-28044.
5. M. Tarnacka, A. Talik, E. Kaminska, M. Geppert-Rybczynska, K. Kaminski and M. Paluch. **The Impact of Molecular Weight on the Behavior of Poly(propylene glycol) Derivatives Confined within Alumina Templates.** *Macromolecules*, 2019, 52(9), 3516-3529.
6. A. Minecka, E. Kaminska, D. Heczko, K. Jurkiewicz, K. Wolnica, M. Dulski, B. Hachuła, W. Pisarski, M. Tarnacka, A. Talik, K. Kamiński and M. Paluch. **Studying structural and local dynamics in model H-bonded active ingredient — Curcumin in the supercooled and glassy states at various thermodynamic conditions.** *European Journal of Pharmaceutical Sciences*, 2019, 135, 38-50.
7. A. Minecka, K. Kamińska, M. Tarnacka, K. Jurkiewicz, A. Talik, K. Wolnica, M. Dulski, A. Kasprzycka, P. Spsychalska, G. Garbacz, K. Kamiński, M. Paluch. **Does the molecular mobility and flexibility of the saccharide ring affect the glass-forming ability of naproxen in binary mixtures?** *European Journal of Pharmaceutical Sciences*, 2020, 141, 105091.
8. A. Talik, M. Tarnacka, A. Dzienia, E. Kaminska, K. Kaminski and M. Paluch. **High-Pressure Studies on the Chain and Segmental Dynamics of a Series of Poly(propylene glycol) Derivatives.** *Macromolecules*, 2019, 52(15), 5658-5669.
9. M. Tarnacka, M. Wojtyniak, A. Brzózka, A. Talik, B. Hachuła, E. Kamińska, G.D.Sulka, K.Kamiński, M.Paluch. **Unique Behavior of Poly(propylene glycols) Confined within Alumina Templates Having a Nanostructured Interface.** *Nano letters*, 20(8), 2020, 5714-5719.
10. K. Jurkiewicz, S. Kołodziej, B. Hachuła, K. Grzybowska, M. Musiał, J. Grelska, R. Bielas, A. Talik, S. Pawlus, K. Kamiński, M. Paluch. **Interplay between structural static and dynamical parameters as a key factor to understand peculiar behaviour of associated liquids.** *Journal of Molecular Liquids*, 2020, 319, 114084.
11. D. Tarnawska, K. Balin, M. Jastrzębska, A. Talik, R. Wrzalik. **Physicochemical Analysis of Sediments Formed on the Surface of Hydrophilic Intraocular Lens after Descemet's Stripping Endothelial Keratoplasty.** *Materials*, 2020, 13(18), 4145.
12. M. Tarnacka, K. Jurkiewicz, B. Hachuła, Z. Wojnarowska, R. Wrzalik, R. Bielas, A. Talik, P. Maksym, K. Kaminski, M. Paluch. **Correlation between locally ordered (hydrogen-bonded) nanodomains and puzzling dynamics of polymethylsiloxane derivative.** *Macromolecules*, 2020, 53(22), 10225–10233.
13. A. Talik, M. Tarnacka, A. Minecka, B. Hachuła, J. Grelska, K. Jurkiewicz, K. Kamiński, M. Paluch, E. Kaminska. **Anormal thermal history effect on the structural dynamics of probucol infiltrated into porous alumina.** *Journal of Physical Chemistry C*, 2021, 125(7) 3901-3912.
14. R. Bielas, P. Maksym, M. Tarnacka, A. Minecka, K. Jurkiewicz, A. Talik, M. Geppert-Rybczyńska, Ł. Mielańczyk, R. Bernat, K. Kamiński, M. Paluch, E. Kamińska. **Synthetic strategy matters: The study of a different kind of PVP as micellar vehicles of metronidazole.** *Journal of Molecular Liquids*, 2021, 332, 115789.

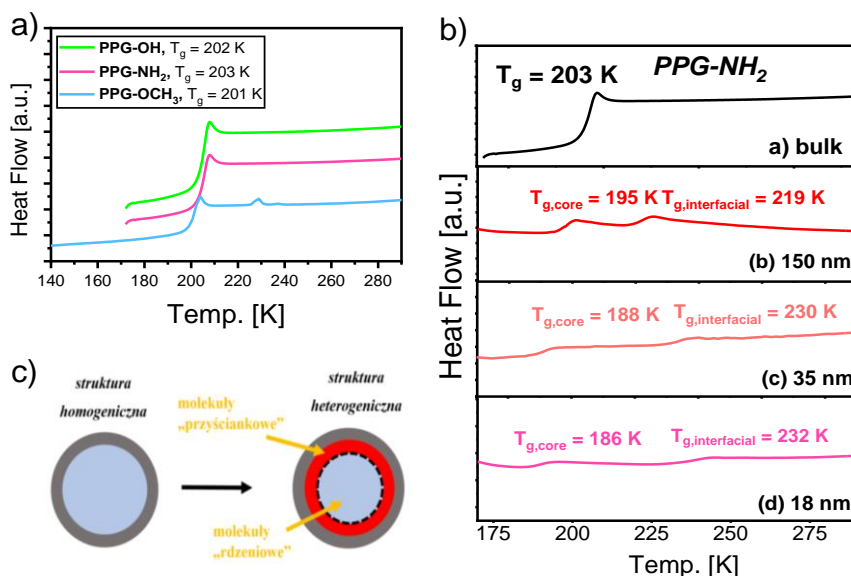
## II. OMÓWIENIE OTRZYMANYCH WYNIKÓW

### A. Określenie roli energii międzyfazowej i specyficznych interakcji na zachowanie poli(glikolu propylenowego) i jego pochodnych w dwuwymiarowym ograniczeniu przestrzennym oraz wpływu ograniczenia przestrzennego na dynamikę oraz zachowanie wiązań wodorowych w poli(glikolach propylenowych) o niskiej masie cząsteczkowej

W celu zbadania wpływu ograniczonej geometrii, specyficznych oddziaływań oraz energii międzyfazowej (ciało stałe-ciecz) na dynamikę molekularną a także temperaturę przejścia szklistego w **artykule A1** wybrano modelową substancję glikol polipropylenowy, PPG-OH, i jego dwie pochodne PPG-NH<sub>2</sub> oraz PPG-OCH<sub>3</sub>. Należy podkreślić że badane polimery charakteryzują się stałą dyspersyjnością i ciężarem cząsteczkowym  $M_n = 4\ 000$  g/mol oraz różnymi oddziaływaniami międzycząsteczkowymi uzyskanymi dzięki modyfikacji terminalnej grupy funkcyjnej. Badane substancje zostały infiltrowane do porów wykonanych z tlenku glinu (ang. *anodic aluminium oxide*, AAO) o stałej średnicy porów,  $d = 18-150$  nm. Podstawowe informacje dotyczące struktury i nazewnictwa zebrano w **Tabeli 1**.

<b>Glikol polipropylenowy (PPG-OH)</b>	
	
<b>Eter bis (2-aminopropyłowy) poli (glikolu propylenowego) (PPG-NH<sub>2</sub>)</b>	<b>Eter dimetyłowy poli (glikolu propylenowego) (PPG-OCH<sub>3</sub>)</b>
	

**Tabela 1.** Struktura i nazewnictwo badanych substancji.

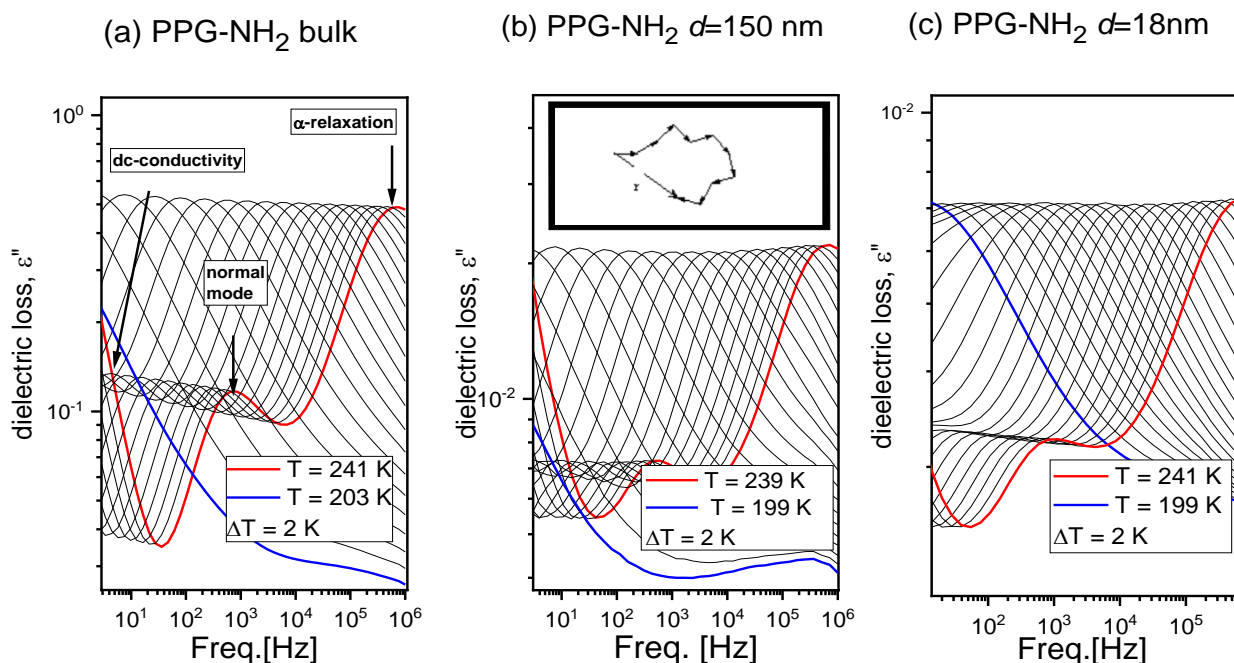


**Rys. 4.** (a) Termogramy DSC uzyskane dla substancji litych PPG-OH, PPG-NH<sub>2</sub>, PPG-OCH<sub>3</sub> ( $M_n = 4000$  g/mol); (b) termogramy PPG-NH<sub>2</sub> infiltrowanego do porów wykonanych z tlenku glinu o średnicach  $d = 150$ - $18$  nm; (c) schemat dwuwarstwowego modelu dla substancji w dwuwymiarowym ograniczeniu przestrzennym.

Uzyskane termogramy DSC dla polimerów o masie  $M_n = 4000$  g/mol w stanie litym przedstawione na **Rys. 4a** wykazały jeden proces endotermiczny zlokalizowany około temperatury  $T_g \sim 202$  K niezależnie od grupy końcowej badanego PPG. Podczas gdy krzywe kalorymetryczne uzyskane dla PPGs ograniczonych przestrzennie wykazały istnienie dwóch procesów endotermicznych znajdujących się odpowiednio poniżej i powyżej  $T_g$  materiałów litych, niezależnie od średnicy użytych porów. Zjawisko to potwierdziło istnienie podwójnego przejścia szklistego dla tych systemów. Zgodnie z modelem dwuwarstwowym zaproponowanym przez McKenne<sup>85</sup> i współpracowników jest ono związane z dwoma frakcjami molekuł o różnej mobilności (**Rys. 4c**). Pierwsza z nich odnosi się do molekuł „przysciankowych” ( $T_{g,interfacial}$ ) oddziałujących ze ścianami matrycy, o zmniejszonej mobilności ze względu na występujące oddziaływania między substancją a powierzchnią porów, charakteryzujące się  $T_g$  wyższym od materiału litego. Druga frakcja to molekuły znajdujące się w centrum/rdzeniu porów ( $T_{g,core}$ ) charakteryzujące się niższą gęstością upakowania, a tym samym większą objętością swobodną, gdzie wartość  $T_g$  jest niższa niż dla



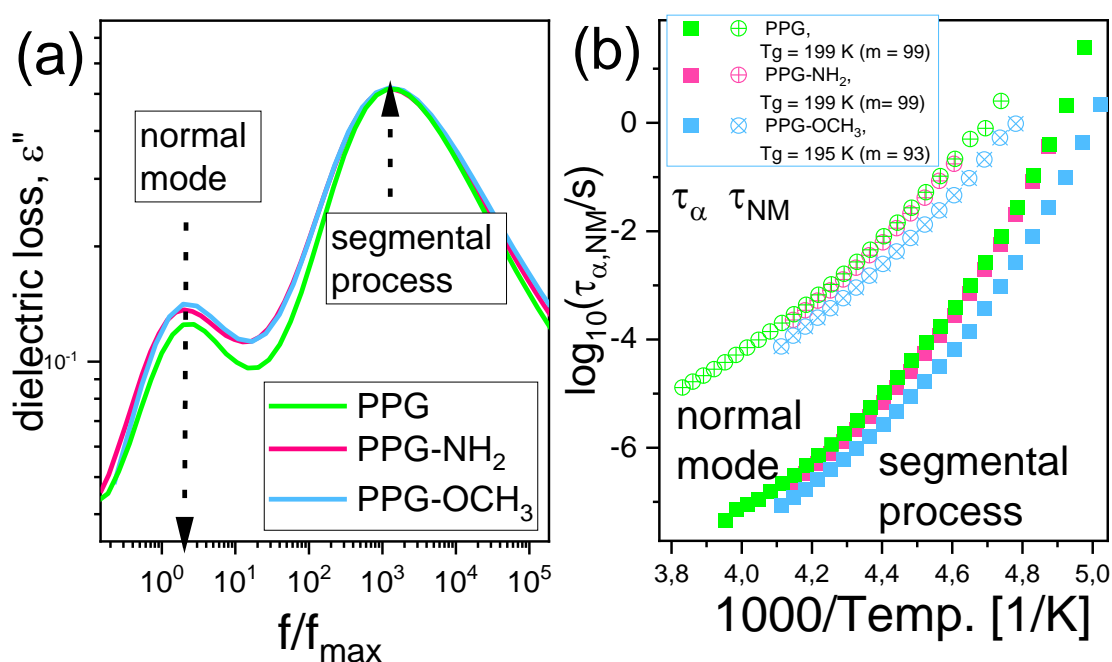
materiału litego. Obie wartości zmieniają się wraz ze zmniejszaniem średnicy mezooporów, gdzie  $T_{g,core}$  maleje, podczas gdy  $T_{g,interfacial}$  wzrasta wraz z rosnącym ograniczeniem przestrzennym (**Rys. 4b**).



**Rys. 5** Widma dielektryczne dla (a) PPH-NH<sub>2</sub> w stanie litym oraz infiltrowane do matrycy o średnicach (b)  $d = 150$  nm oraz (c)  $d = 18$  nm.

Dalsze badania dynamiki molekularnej poli(glikoli propylenowych) za pomocą szerokopasmowej spektroskopii dielektrycznej potwierdziły istnienie zjawiska podwójnego przejścia szklistego. Glikol polipropylenowy (PPG) należy do polimerów *typu A*, dla których moment dipolowy całego łańcucha jest dany przez sumowanie indywidualnych momentów dipolowych równoległych do szkieletu łańcucha (**Rys. 5b**), umożliwiając tym samym obserwację dodatkowego procesu relaksacji wektora łączącego końce łańcucha zwanego w literaturze „normal mode” ( $\alpha_{NM}$ ), **Rys. 5a**. Dzięki czemu informacje o lokalnej (segmentowej) i globalnej (łańcuchowej) dynamice można uzyskać bezpośrednio z pomiarów dielektrycznych. Jednakże dla glikoli o masie cząsteczkowej  $M_n > 1000$  g/mol relaksacja typu normal mode nie jest obserwowana, tak jak w przypadku badanych glikoli o  $M_n = 400$  g/mol w artykule **A5**.

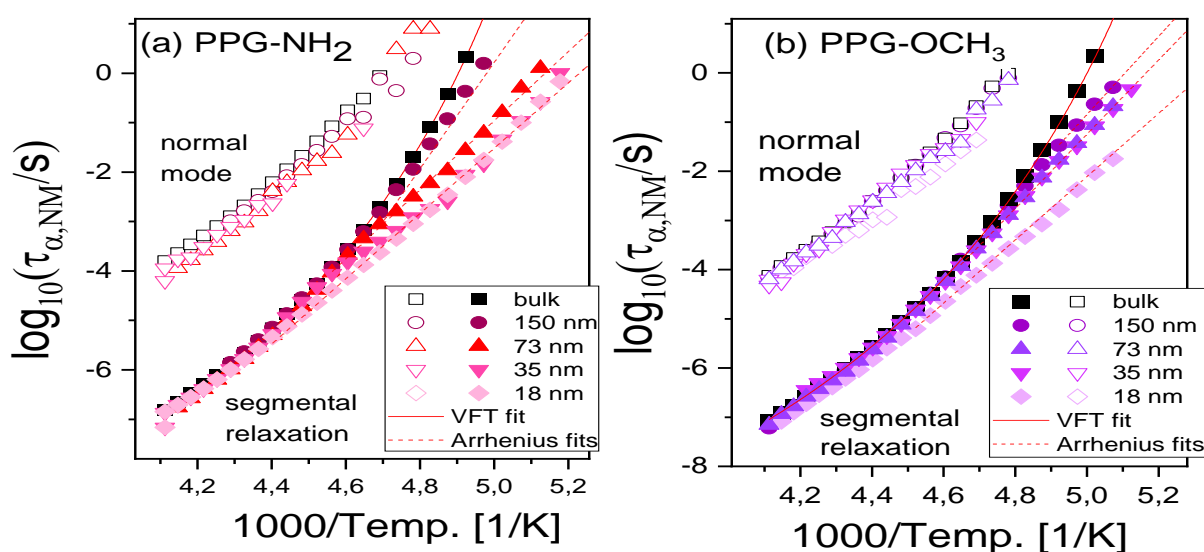
Badane substancje wykazały obecność trzech procesów relaksacyjnych: (i) przewodnictwo stałoprądowe (dc-conductivity) związane z transportem ładunków, zlokalizowane przy najniższych częstotliwościach, (ii) relaksację „normal mode” odzwierciedlającą procesy związane z globalną dynamiką/dyfuzją łańcucha i fluktuacjami wektora łączącego końce łańcucha, oraz (iii) relaksację segmentalną ( $\alpha$ ) przy najwyższych częstotliwościach, przypisaną do kooperatywnych ruchów segmentów, odpowiedzialną za przejście z fazy ciekłej w szklistą (**Rys. 5**).



**Rys. 6.** (a) Porównanie kształtu relaksacji segmentalnej dla materiałów litych (b) czasy relaksacji wykreślone w funkcji temperatury dla PPG-OH, PPG-NH<sub>2</sub> i PPG-OCH<sub>3</sub>.

Analiza widm dielektrycznych za pomocą modelu Havriliaka-Negami (HN) pozwoliła wyznaczyć czasy relaksacji  $\tau_{\alpha}$  i  $\tau_{NM}$  w funkcji temperatury (**Rys. 6**). Dla materiałów litych zauważono, że modyfikacja końców PPG nie wpływa na rozkład czasów relaksacji segmentalnej, a kształt procesu  $\alpha$  jest identyczny dla wszystkich badanych polimerów (**Rys. 6a**). Ten sam scenariusz jest również obserwowany w przypadku relaksacji  $\tau_{NM}$ . Użycie funkcji Vogela-Fulchera-Tammanna (VFT) umożliwiło wyznaczenie temperatur przejścia szklistego dla

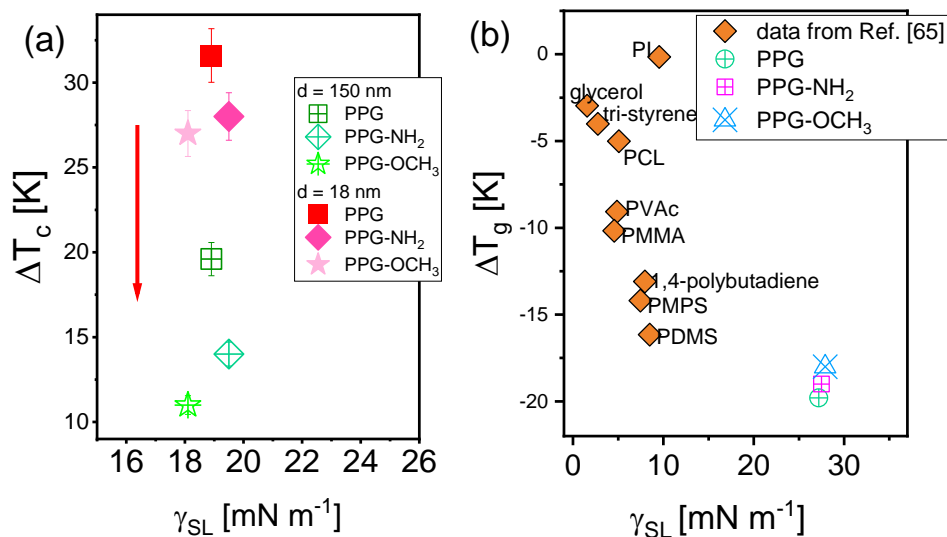
$\tau_\alpha = 100$  s. Dla tych substancji odnotowano jedno przejście szkliste zgodne z wartościami uzyskanymi z różnicowej kalorymetrii skaningowej, gdzie dla PPG-OCH<sub>3</sub> wartość  $T_g$  nieznacznie spadła w porównaniu do PPG-OH i PPG-NH<sub>2</sub> (**Rys. 6b**). Można zatem wnioskować, że niewielka modyfikacja chemiczna (zamiana grupy końcowej) ma zauważalny wpływ na dynamikę molekularną.



**Rys. 7.** Temperaturowa zależność czasów relaksacji segmentalnej dla (a) PPG-NH<sub>2</sub> oraz (b) PPG-OCH<sub>3</sub> w stanie litym oraz infiltrowanych do porów o średnicach  $d = 150$ - $18$  nm.

Zupełnie odmienne zachowanie odnotowano dla substancji infiltrowanych do porowatych matryc. Wyznaczone czasy relaksacji ujawniły temperaturową zmianę zależności od zachowania eksponencjalnego (opisywanego równaniem VFT) do bardziej liniowego (charakterystycznego dla modelu Arrhenius'a) (**Rys. 7**). Temperatura przejścia szklistego jak i czasy relaksacji dla PPG infiltrowanego do porów o różnych średnicach wykazują zachowanie przypominające materiał lity (brak efektu ograniczenia przestrzennego) w wysokich temperaturach, podczas gdy w pewnej określonej temperaturze (oznaczanej jako  $T_c$ ) obserwuje się zmianę w temperaturowej zależności  $\tau_\alpha$  w porównaniu do materiału litego niezależnie od badanej substancji (**Rys. 7a i 7b**). Okazuje się, że  $T_c$  silnie zależy od średnicy porów

zastosowanych membran, gdzie im mniejsze  $d$ , tym wyższa temperatura w której czasy relaksacji zaczynają odbiegać od wyznaczonych dla materiału litego. Porównując uzyskane wartości z obu technik eksperymentalnych można stwierdzić dobrą zgodność pomiędzy  $T_c$  (oszacowaną z BDS) i  $T_{g,interfacial}$  (wyznaczoną z DSC). Dlatego też odchylenie w  $\tau_\alpha(T)$  dla PPG infiltrowanego do porowatych matryc, obserwowane w temperaturze  $T_c$  jest dobrze skorelowane z zeszkleniem polimerów zaadsorbowanych na ścianach porów (warstwa „przyściankowa”). Jak zaobserwowano, temperatura przejścia szklistego tych molekuł zależy od badanej substancji i maleje wraz z malejącą zdolnością do tworzenia wiązań wodorowych w następującej kolejności: PPG-OH  $\rightarrow$  PPG-NH<sub>2</sub>  $\rightarrow$  PPG-OCH<sub>3</sub>. Można więc przyjąć, że odchylenia w zależnościach  $\tau_\alpha(T)$  i  $T_c$  mogą być związane ze zmianą oddziaływań z powierzchnią (w tym wiązań wodorowych) w wyniku modyfikacji grupy końcowej PPG, oczekując tym samym, że im silniejsze oddziaływanie między materiałem a matrycą, tym wyższa temperatura przejścia szklistego warstwy polimeru oddziałującej ze ścianami porów.



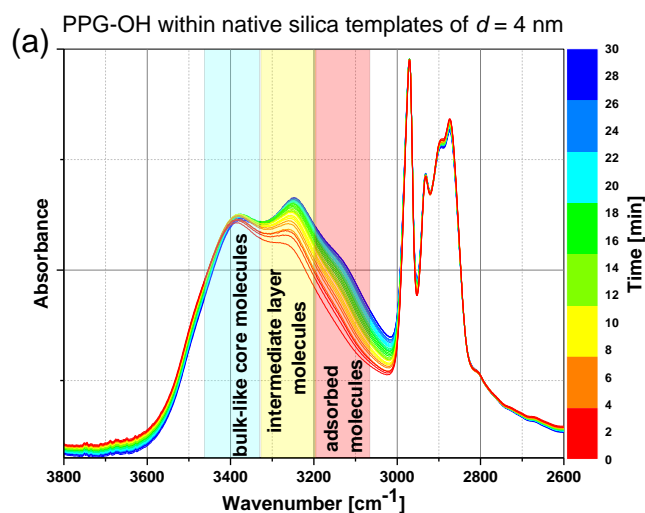
**Rys. 8.** (a) Różnice pomiędzy temperaturą przejścia szklistego molekuł przyściankowych i materiału litego, oznaczaną jako  $\Delta T_c$  (gdzie  $\Delta T_c = T_c - T_{g,bulk}$ ), (b) zależność  $\Delta T_g$  dla PPG-OH i jego pochodnych infiltrowanych do porów o średnicy  $d = 18$  nm w funkcji  $\gamma_{SL}$  ( $T = 298$  K). Dodatkowe dane uzyskane dla polimerów zamkniętych w porach o różnej średnicy (gdzie  $25$  nm  $< d < 65$  nm) zostały zaczerpnięte z Ref. [65].

Aby zbadać rolę oddziaływań powierzchniowych wpływających na zachowanie poli(glikoli propylenowych) ograniczonych dwu-wymiarowo zostały przeprowadzone dodatkowe pomiary kąta zwilżalności ( $\theta$ ) oraz napięcia powierzchniowego ( $\gamma_L$ ), umożliwiające obliczenie energii międzyfazowej (ciało stałe-ciecz,  $\gamma_{SL}$ ). Najmniejszą i największą wartość kąta zwilżalności zaobserwowano dla PPG-OH ( $\theta = 8.35^\circ$ ) i PPG-OCH<sub>3</sub> ( $\theta = 14^\circ$ ). W tym kontekście można założyć obecność silnych oddziaływań ciało stałe-ciecz, które zmniejszają się w następującej kolejności: PPG-OH  $\rightarrow$  PPG-NH<sub>2</sub>  $\rightarrow$  PPG-OCH<sub>3</sub>. Wykazano również korelację pomiędzy energią fazową,  $\gamma_{SL}$ , a obniżeniem temperatury zeszklenia w układach porowatych w stosunku do materiału litego, gdzie im wyższa  $\gamma_{SL}$ , tym niższe  $T_g$  molekuł rdzeniowych.

W pracy **A1** zbadano, jak zmienia się temperatura zeszklenia molekuł oddziałujących na ścianach porów, bezpośrednio związaną z oddziaływaniami międzyfazowymi, **Rys. 8a**. Zgodnie z wykreśloną zależnością,  $T_c$  zmienia się w zależności od zdolności do tworzenia wiązań wodorowych w następującej kolejności: PPG-OH  $\rightarrow$  PPG-NH<sub>2</sub>  $\rightarrow$  PPG-OCH<sub>3</sub> dla stałego  $\gamma_{SL}$ . Korelacja ta wyraźnie wskazuje, że poza energią międzyfazową również specyficzne oddziaływania, takie jak wiązania wodorowe muszą być brane pod uwagę, aby przewidzieć zmiany temperatury zeszklenia nie tylko frakcji znajdującej się w centrum mezoporów, ale także molekuł zaadsorbowanych na ich ścianach. Zgodnie z **Rys. 8b**, otrzymane wyniki dla PPG-OH i jego pochodnych wykreślono wraz z danymi literaturowymi różnych substancji infiltrowanych do porów o średnicach  $25 \text{ nm} < d < 65 \text{ nm}$ <sup>65</sup>. Zauważono dobrą zgodność z ogólnym trendem raportowanym wcześniej w literaturze, gdzie im większa energia międzyfazowa, tym niższe  $T_g$ . Jednakże wiele teoretycznych i doświadczalnych badań substancji m.in. polimerów w zamknięciu 1D wykazało odwrotne efekty. Zgodnie z tymi pracami sugeruje się, że silne oddziaływania powierzchniowe, w tym specyficzne

oddziaływania m.in. wodorowe, zmniejszają mobilność warstwy międzyfazowej, co prowadzi do zwiększenia  $T_g$ .

Analiza wpływu specyficznych oddziaływań oraz efektów powierzchniowych została kontynuowana i rozszerzona dla poli(glikoli propylenowych) o masie cząsteczkowej  $M_n = 400$  g/mol, mających różne powinowactwo do tworzenia wiązań wodorowych [A5] w zależności od materiału z którego wykonana jest matryca. PPG-OH i pochodne zostały infiltrowane do dwóch typów membran: (i) wykonanych z tlenku krzemu ( $d = 4$  nm) i (ii) tlenku glinu ( $d = 18$  nm). W badaniach potwierdzono, że napięcie międzyfazowe nie jest wystarczającym parametrem do opisu zmian dynamiki i temperatury zeszklenia układów w geometrycznym ograniczeniu przestrzennym. Dla tych systemów również odnotowano istnienie podwójnego przejścia szklistego. Wykazano, że dynamika segmentalna oligomerów PPG odbiega od dynamiki materiału litego przy tym samym czasie relaksacji, niezależnie od zastosowanego typu matrycy, rozmiaru porów i funkcjonalizacji. Ta obserwacja wskazuje na słaby wpływ charakteru powierzchni (hydrofobowość, hydrofilowość) na dynamikę warstwy międzyfazowej. Poprzez pomiary z użyciem spektroskopii w podczerwieni (IR) po raz pierwszy wykazano, że siła oddziaływań wiązań wodorowych między materiałem a matrycą różni się w zależności od zastosowanych membran, wskazując znaczne wzmocnienie wiązań wodorowych substancji infiltrowanych do porów krzemionkowych [A5].

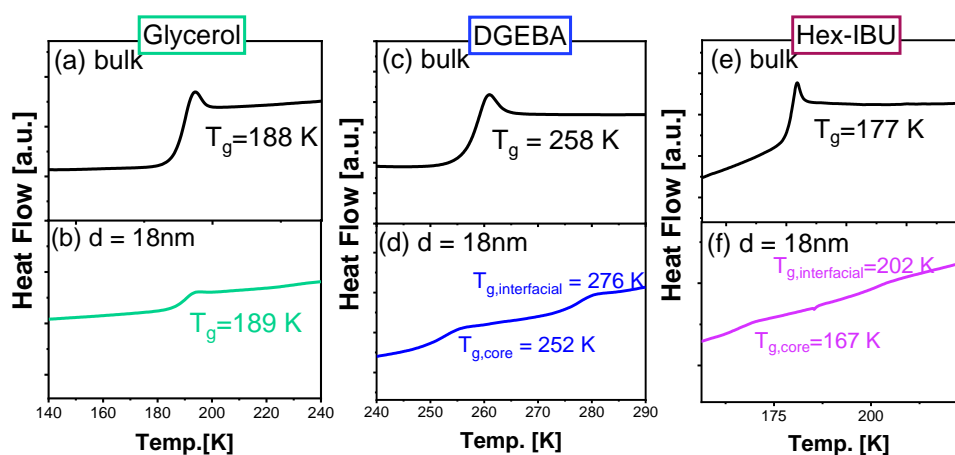


**Rys. 9.** Widma FTIR dla PPG-OH zamkniętego w natywnych porach krzemionkowych, w regionach O-H i C-H zarejestrowane w temperaturze  $T = 183\text{ K}$  w ciągu 30 min.

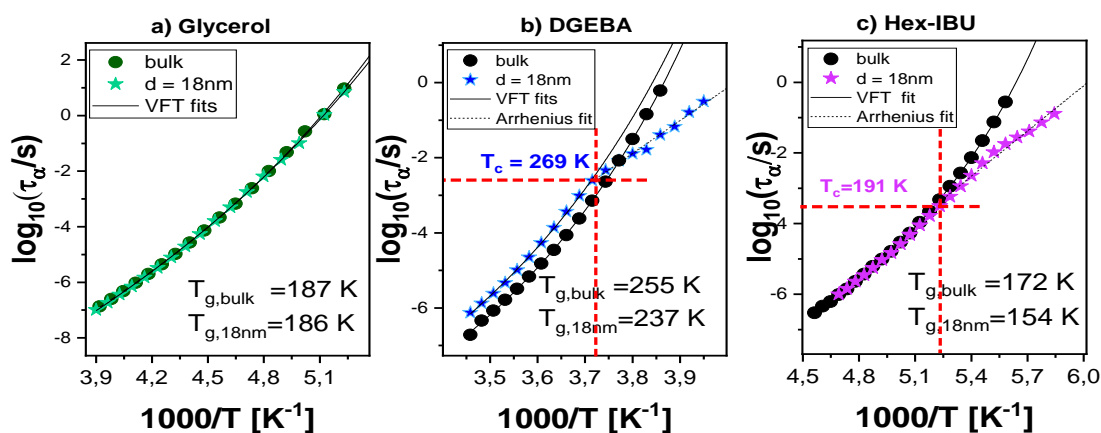
Ponadto przeprowadzono eksperymenty wygrzewania z wykorzystaniem spektroskopii FTIR, gdzie monitorowano zmiany w częstościach związanych z drganiami rozciągającymi grupy hydroksylowej które są odpowiedzialne za wiązania wodorowe. Badania te ujawniły reorganizację molekuł blisko powierzchni porów (ścian) i utworzenie trzech odrębnych frakcji molekuł: przyściankowej (międzyfazowej), pośredniej i rdzeniowej dla PPG infiltrowanego do porów krzemionkowych (**Rys. 9**). Tworzenie się trzeciej pośredniej warstwy zostało wcześniej opisane m.in. dla PMMA<sup>36</sup> i skorelowane ze słabnącymi oddziaływaniami polimer-matryca wraz ze wzrostem średnicy porów.

W związku z obserwowanym różnym wzorcem zachowań, tj. zmiany w  $T_g$  w zależności od energii międzyfazowej pomiędzy układami 1D i 2D, znalezienie rozwiązania a tym samym odpowiedzi na pytanie, co jest przyczyną obserwowanych różnic, ma ogromne znaczenie dla znalezienia jednolitego opisu wpływu ograniczenia jedno i dwu-wymiarowego na dynamikę przestrzennie ograniczonych materiałów. W związku z powyższym w artykule **A2** skupiłam się na próbie opisu i znalezienia spójnych zależności opisujących oba układy. W tym celu zbadano dwanaście różnych, nisko- i wysokocząsteczkowych substancji tworzących fazę szklaną. W

pracy wybrano trzy reprezentatywne układy: glicerol, heksylo-2-[4-(2-metylopropylo) fenylo]propanian (Hex-IBU) i eter diglicydylowy bisfenolu A (DGEBA) infiltrowane do matryc wykonanych z tlenku glinu o średnicach porów  $d = 18$  nm.



**Rys. 10.** Uzyskane termogramy dla trzech reprezentatywnych substancji w stanie litym oraz w ograniczeniu przestrzennym o średnicy porów  $d = 18$  nm.



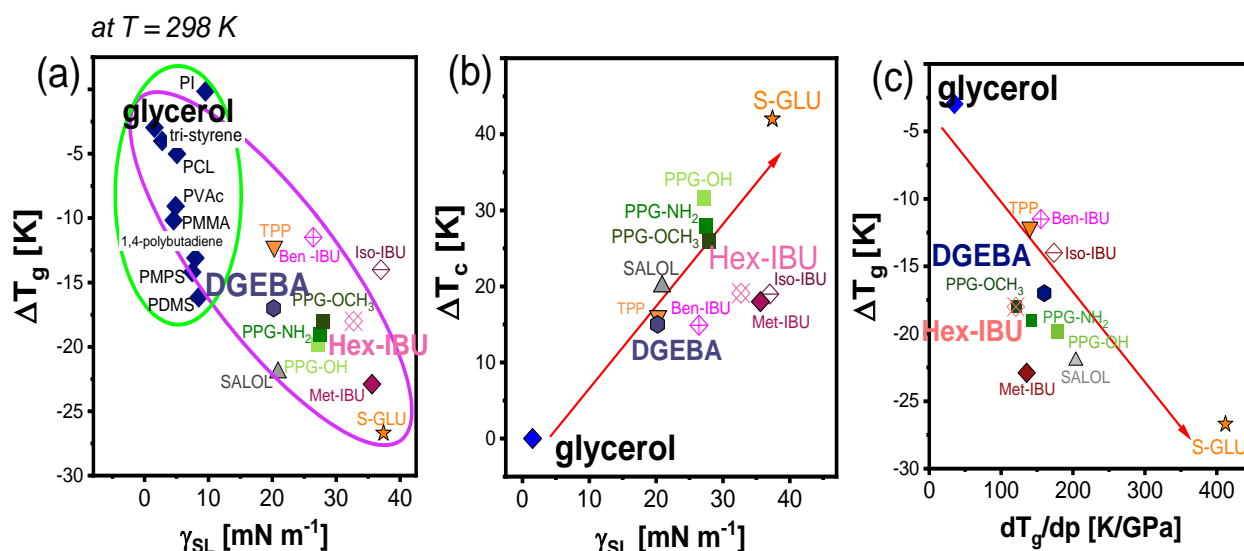
**Rys. 11.** Temperaturowa zależność czasów relaksacji strukturalnej dla (a) glicerolu (b) DGEBA oraz (c) Hex-IBU w stanie litym oraz infiltrowanych do porów o średnicach  $d = 18$  nm.

Termogramy DSC dla dwóch badanych substancji (DGEBA oraz Hex-IBU) infiltrowanych do porów o średnicach  $d = 18$  nm ujawniły istnienie dwóch procesów endotermicznych poniżej i powyżej  $T_g$  materiału litego, co jest potwierdzeniem istnienia podwójnego przejścia szklistego dla tych substancji (**Rys. 10**). Odmienne zjawisko



zobserwowano dla glicerolu infiltrowanego do mezoporów. Dla tej substancji zauważono tylko jeden proces odzwierciedlający nagły skok (zmianę) w pojemności cieplnej, odpowiadający jednemu przejściu szklistemu. To samo zjawisko zostało odnotowane na mapach relaksacyjnych (**Rys. 11**), gdzie dla glicerolu infiltrowanego do porowatych matryc czasy relaksacji pozostają takie same jak dla materiału litego w całym zakresie temperatur (**Rys. 11a**). Podczas gdy dla dwóch kolejnych badanych substancji zaobserwowano wyraźną zmianę dynamiki strukturalnej w pewnej określonej temperaturze,  $T_c$  (opisywane również jako  $T_{g,interfacial}$ ) (**Rys. 11b i 11c**). Brak wyższej temperatury zeszklenia dla glicerolu infiltrowanego do porów nie oznacza, że warstwa międzyfazowa nie może powstawać - w tym przypadku można przypuszczać, że obie frakcje molekuł (rdzeniowa i międzyfazowa) mają podobną dynamikę i temperatury zeszklenia. W celu głębszego zbadania co jest przyczyną obserwowanych różnic przeprowadzono pomiary napięcia powierzchniowego, kątów zwilżalności i energii międzyfazowej. Wykazano, że glicerol charakteryzuje się niezwykle niską energią międzyfazową  $\gamma_{SL} = 1.5 \text{ mN}\cdot\text{m}^{-1}$ , podczas gdy  $\gamma_{SL}$  pozostałych związków wynosi odpowiednio  $20 \text{ mN}\cdot\text{m}^{-1}$  i  $33 \text{ mN}\cdot\text{m}^{-1}$  dla DGEBY i Hex-IBU. Ponadto dla glicerolu odnotowano dużą wartość kąta zwilżalności,  $\theta = 63^\circ$  i napięcia powierzchniowego,  $\gamma_L = 60 \text{ mN}\cdot\text{m}^{-1}$ . W przypadku pozostałych materiałów wartości tych parametrów maleją odpowiednio dla DGEBY ( $\theta = 35^\circ$  i  $\gamma_L = 47,41 \text{ mN}\cdot\text{m}^{-1}$ ) oraz Hex-IBU ( $\theta = 7^\circ$  i  $\gamma_L = 26,5 \text{ mN}\cdot\text{m}^{-1}$ ), co pozwala stwierdzić, że w porównaniu do innych badanych substancji glicerol słabo zwilża i oddziałuje ze ścianami matrycy (ciało stałe- ciecz). Wydaje się więc, że te pomiary były kluczowe do wyjaśnienia braku podwójnego przejścia szklistego w tym materiale. Dla substancji charakteryzujących się wyższym  $\gamma_{SL}$  (w tym przypadku materiały o małej masie cząsteczkowej), czasy relaksacji strukturalnej wyznaczone dla próbek infiltrowanych do porów zaczynają odbiegać od tych otrzymanych dla materiałów litych, ze względu na zeszklenie cząsteczek międzyfazowych w temperaturze  $T_c$  (opisywane również jako  $T_{g,interfacial}$ ). Im

silniejsze są oddziaływania z matrycą, tym wartość  $T_c$  przesuwana się w kierunku wyższych temperatur. Zgadza się to z danymi przedstawionymi na **Rys. 11**, gdzie odchylenie zależności  $\tau_\alpha(T)$  od zachowania w stanie litym również zmienia się w ten sam sposób dla DGEBY i Hex-IBU infiltrowanych do matrycy o średnicach  $d = 18$  nm.



**Rys. 12.** Różnice pomiędzy temperaturą przejścia szklistego (a) molekuł rdzeniowych  $\Delta T_g$  (gdzie  $\Delta T_g = T_g - T_{g,bulk}$ ), oraz (b) molekuł przyściankowych i materiału litego, oznaczana jako  $\Delta T_c$  (gdzie  $\Delta T_c = T_c - T_{g,bulk}$ ) w zależności od  $\gamma_{SL}$ ; (c) zależność  $\Delta T_g$  od współczynnika ciśnieniowego  $dT_g/dp$ .

W konsekwencji,  $T_g$  materiałów w dwu-wymiarowym ograniczeniu przestrzennym maleje wraz ze wzrostem  $\gamma_{SL}$  (**Rys. 12a**). Efekt ten jest podobny do opisywanego wcześniej w literaturze<sup>65</sup>, gdzie wykazano, że czasy relaksacji w pobliżu temperatury przejścia szklistego są znacznie krótsze w porównaniu do materiału litego. Jednakże ta reguła nie zawsze jest spełniona, ponieważ łatwo można znaleźć układy charakteryzujące się tą samą energią międzyfazową i różną zmianą w temperaturach zeszklenia w warunkach ograniczenia przestrzennego.

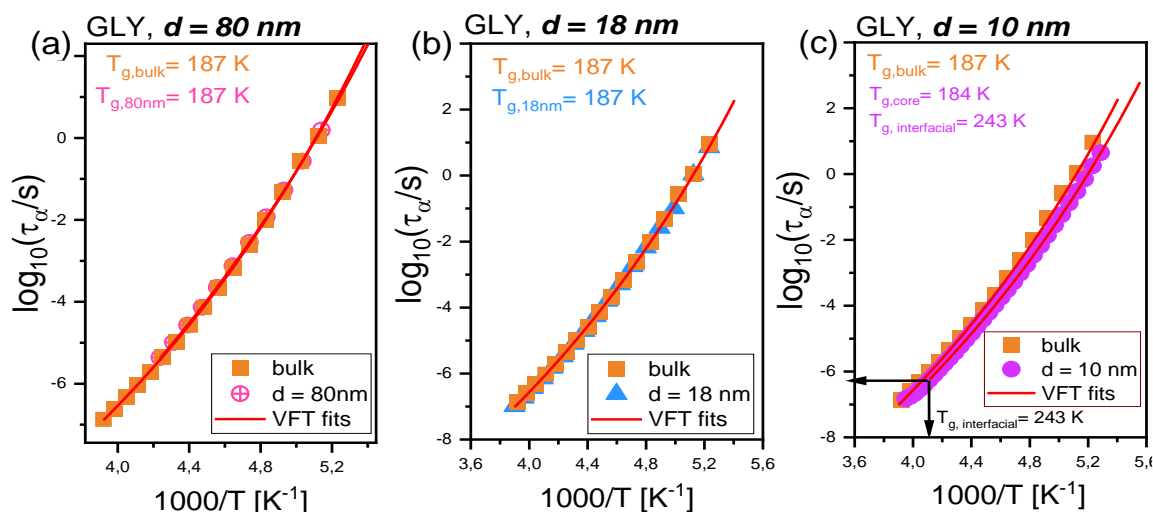
Aby wyjaśnić to odkrycie eksperymentalne w pracy **A2** oprócz trzech reprezentatywnych substancji, zbadano również dziewięć innych związków tworzących fazę szklistą. Wszystkie

substancje zostały infiltrowane do mezoporów o najmniejszych średnicach  $d = 18$  nm. W czasie pomiarów wszystkie próbki charakteryzowały się tą samą historią termiczną. Z **Rys. 12a** na pierwszy rzut oka można zauważyć dwie zależności: pierwsza dla makrocząsteczek i druga dla niskocząsteczkowych substancji formujących fazę szklistą (oznaczone odpowiednio na zielono i fioletowo) w zależności od energii międzyfazowej. W artykule **A2** postanowiłam również rozważyć wrażliwość relaksacji strukturalnej na fluktuacje gęstości, które mogą być określane ilościowo przez współczynnik ciśnieniowy temperatury zeszklenia,  $dT_g/dp$ . Na **Rys. 12c** pokazano, że spadek  $T_g$  frakcji rdzeniowej, dla substancji w ograniczeniu przestrzennym dobrze koreluje się ze wzrostem tego współczynnika. Dzięki tej korelacji można łatwo wytłumaczyć obniżenie  $T_g$  dla materiałów charakteryzujących się podobną energią międzyfazową. To daje stosunkowo łatwą i wiarygodną możliwość oszacowania kierunku i wielkości zmian temperatury zeszklenia cieczy infiltrowanych do porowatych matryc. Wyniki uzyskane w pracy **A2** sugerują jednoznacznie, że opisywany w literaturze spadek temperatury przejścia szklistego molekuł rdzenia dla substancji o silnych oddziaływaniach jest wynikiem wzrostu  $T_g$  cząsteczek zaadsorbowanych na ścianach zastosowanych porów. Ponadto po raz pierwszy opisano zależności pomiędzy energią międzyfazową a  $T_g$  molekuł przyściankowych (**Rys. 12b**). Kluczowym jest, że poprzez wykreślenie zmian  $T_g$  w funkcji  $\gamma_{SL}$ , dla różnych substancji wykazano, że badana relacja ma charakter uniwersalny i jest zgodna z danymi literaturowymi opublikowanymi dla układów 1D.

### **B. Określenie wpływu krzywizny powierzchni na właściwości układów w dwuwymiarowym ograniczeniu przestrzennym na przykładzie glicerolu**

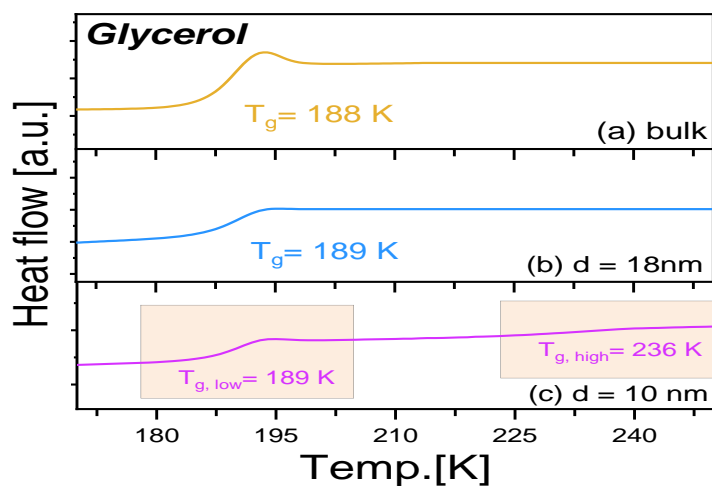
Wyniki uzyskane w pracy **A2** dla substancji które charakteryzują się niską wartością  $\gamma_{SL}$ , m.in. dla glicerolu o energii międzyfazowej  $\sim 1.5$  mNm<sup>-1</sup>, gdzie efekty ograniczenia przestrzennego (dla średnicy  $d = 18$  nm), mogą być niezauważalne skłoniły mnie do dalszych badań tej substancji. W artykule **A3** przeprowadzono analizę glicerolu infiltrowanego do membran o

mniejszej średnicy tj.  $d = 10$  nm, gdzie wykazano znaczną zmianę w temperaturowej zależności czasów relaksacji w porównaniu do materiału litego oraz infiltrowanego do membran o większych średnicach porów ( $d \geq 18$  nm).



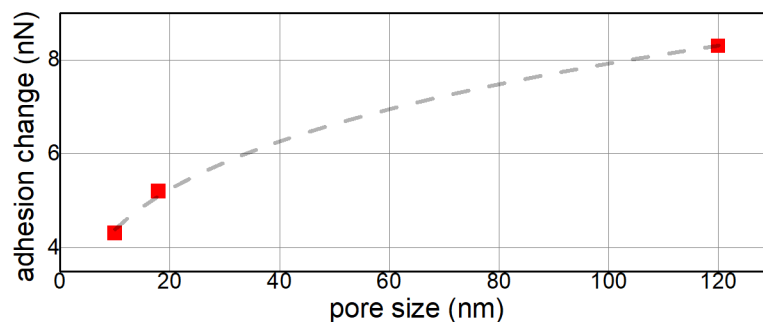
**Rys. 13.** Temperaturowa zależność czasów relaksacji strukturalnej dla glicerolu infiltrowanego do matryc o średnicy (a)  $d = 80$  nm (b)  $18$  nm oraz (c)  $10$  nm.

Na **Rys. 13c** zaobserwowano zmianę w temperaturowych zależnościach czasów relaksacji dla glicerolu infiltrowanego do matryc AAO o średnicach porów  $d = 10$  nm w porównaniu do litego materiału. Te dane mogły wskazywać na istnienie podwójnego przejścia szklistego w przypadku glicerolu infiltrowanego do porów o małej średnicy  $d = 10$  nm podczas gdy dla większego rozmiaru mezoporów efekt ten nie jest obserwowany a czasy relaksacji,  $\tau_{\alpha}$ , pozostają takie same jak dla materiału w stanie litym (**Rys. 13a i 13b**).



**Rys. 14.** Termogramy dla glicerolu w stanie litym oraz infiltrowanego do porów wykonanych z tlenku glinu o średnicach  $d = 18$  i  $10$  nm.

Obserwacje te potwierdziły badania za pomocą różnicowej kalorymetrii skaningowej, gdzie zjawisko podwójnego przejścia szklistego, a więc istnienie dwóch procesów endotermicznych w danym zakresie temperatur, zostało zaobserwowane dla najmniejszego zastosowanego ograniczenia przestrzennego,  $d = 10$  nm (**Rys. 14**). Należy nadmienić, że obserwowane zachowanie jest pierwszym doniesieniem literaturowym pokazującym istnienie dwóch przejść szklistych dla tego układu. W istocie powyższe dane wskazują, że efekt krzywizny powierzchni może być kluczowym parametrem mającym duży wpływ na przewidywanie zachowania nanomateriałów. Aby dokładniej sprawdzić to zjawisko, zdecydowałam się na wykonanie pionierskich pomiarów sił adhezji za pomocą mikroskopii sił atomowych (AFM), które wykazały, że wraz ze wzrostem geometrycznego ograniczenia przestrzennego siła adhezji igły do materiału maleje, co prowadzi do wniosku, że dany materiał lepiej zwilża powierzchnię. Pomiary zostały przeprowadzone wzdłuż przekroju poprzecznego zarówno pustej membrany, jak i wypełnionej glicerolem.



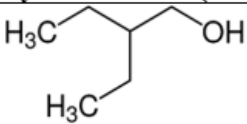
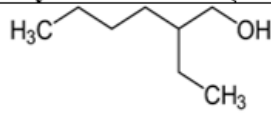
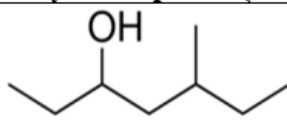
**Rys. 15.** Różnica pomiędzy siłą adhezji pomiędzy igłą a glicerolem w porach w stosunku do wartości wyznaczonych dla pustych membran (AAO) wykreślona w zależności od użytych średnic porów.

Uzupełniające badania AFM wskazały, że zmiana w zachowaniu substancji jest związana ze znacznym obniżeniem napięcia międzyfazowego substancji w geometrycznym ograniczeniu. W konsekwencji, w najmniejszych porach ( $d = 10$  nm) spodziewana jest lepsza zwilżalność i wzmocnienie oddziaływań międzyfazowych pomiędzy matrycą a substancją. Uzyskane wyniki zostały skorelowane z modelem Tolmana przewidującym, że obniżenie napięcia powierzchniowego jest ściśle związane ze wzrostem krzywizny powierzchni, stąd można wnioskować, że w przewidywaniu zachowania substancji należy również uwzględnić stopień zakrzywienia powierzchni (**Rys. 15**). Warto podkreślić, że są to pierwsze dane doświadczalne udowadniające istnienie korelacji między oddziaływaniami na powierzchni a jej krzywizną. Wyniki przedstawione w pracy **A3** pozwalają na głębsze zrozumienie zmienności dynamiki substancji w geometrycznym ograniczeniu przestrzennym i niewątpliwie pokazują, że bardzo trudno jest oddzielić wpływ efektów skończonego rozmiaru od efektów powierzchniowych, ponieważ oba wydają się być ze sobą ściśle związane.

### **C. Prześledzenie wpływu dwu-wymiarowego ograniczenia przestrzennego na specyficzne oddziaływania wodorowe a także na supramolekularne struktury o różnej architekturze na przykładzie wybranych monohydroksy alkoholi**

W dalszej części pracy badawczej postanowiłam sprawdzić, czy na przewidywanie kierunku i zmian w  $T_g$  oraz w dynamice molekularnej oprócz krzywizny powierzchni, a także rozmiarowości, może mieć wpływ typ zastosowanej matrycy oraz specyficzne oddziaływania,

w szczególności zdolność do tworzenia supramolekularnych struktur przy podłożu (ścianach porów). Wykorzystując komplementarne techniki eksperymentalne tj. BDS i FTIR w pracy **A4** zbadalam zachowanie monohydroksy alkoholi o różnej lokalizacji grup hydroksylowych (-OH) tj. 2-etylo-1-heksanol (2E1H), 2-etylo-1-butanol (2E1B) i 5-metylo-3-heptanol (5M3H) infiltrowanych do porów wykonanych z tlenku glinu ( $\text{Al}_2\text{O}_3$ ) oraz tlenku krzemu ( $\text{SiO}_2$ ): natywnych (hydrofilowych) oraz silanizowanych (hydrofobowych) o średnicach porów  $d = 4$  nm i  $d = 10$  nm. Struktury badanych substancji zostały zaprezentowane w **Tabeli 2**.

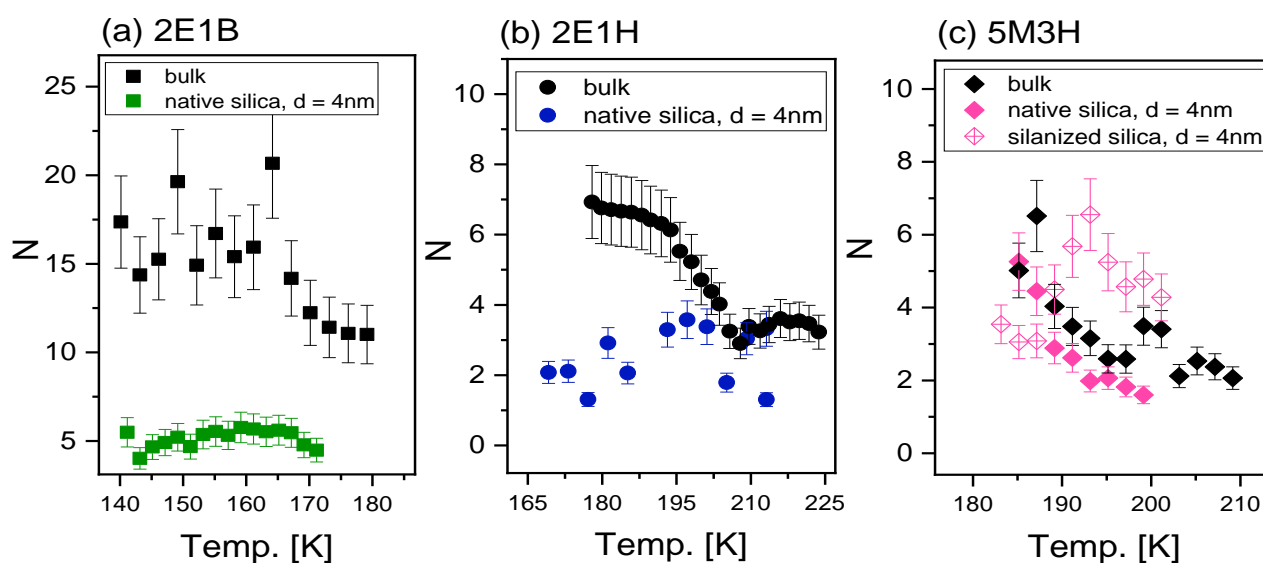
2-etylo-1-butanol (2E1B)	2-etylo-1-heksanol (2E1H)	5-metylo-3-heptanol (5M3H)
		

**Tabela 2.** Struktura badanych monohydroksy alkoholi.

Alkohole monohydroksylowe stanowią unikalną klasę cieczy posiadających jedną grupę hydroksylową, zdolnych do tworzenia struktur supramolekularnych o różnej architekturze (łańcuchowych, rozgałęzionych, pierścieniowych). Najbardziej interesującą cechą tych związków jest występowanie dodatkowego procesu Debye'a ( $D$ ) w widmach strat dielektrycznych ściśle związanego z tworzeniem wiązań wodorowych, opisujący relaksację dielektryczną molekuł polarnych charakteryzującą się jednym czasem relaksacji  $\tau_D$ . Monitorując właściwości dynamiczne tego procesu, w tym jego amplitudę i czasy relaksacji ( $\tau_D$ ), można uzyskać pośredni wgląd w zachowanie wiązań wodorowych oraz morfologię utworzonych asocjatów w różnych warunkach termodynamicznych i ograniczenia przestrzennego.

Analiza czasów relaksacji i siły dielektrycznej procesu międzyfazowego oraz relaksacji Debye'a molekuł „rdzeniowych” pozwoliła stwierdzić, że alkohole pierwszorzędowe o strukturze łańcuchowej tj. 2E1H i 2E1B, zachowują się inaczej w porównaniu do

drugorzędowego, 5M3H o budowie pierścieniowej, zbliżonej do miceli. Pomimo zmiany kątów zwilżania i energii międzyfazowych stwierdzono, że zmiana ewolucji temperaturowej czasów relaksacji Debye'a dla alkoholi infiltrowanych do hydrofilowych i hydrofobowych porów wykonanych z tlenku krzemu oraz tlenku glinu zachodzi przy podobnym  $\tau_D$  w porównaniu do próbek litych [A5]. Zjawisko to może być związane z podobnymi wartościami we współczynniku  $dT_g/dp$  dla wszystkich mierzonych monohydroksy alkoholi. Jednakże dynamika molekularna substancji infiltrowanych, pomimo zbliżonej wartości  $dT_g/dp$ , który jest istotnym czynnikiem wpływającym na zachowanie substancji w nanoskali, zmienia się, wskazując tym samym duży wpływ specyficznych oddziaływań wodorowych na obserwowane zachowanie. Ponadto hipotezę tą potwierdziły badania prowadzone za pomocą spektroskopii w podczerwieni [A5]. Dodatkowo z zależności zaproponowanej w Ref. 86 obliczono liczbę cząsteczek biorących udział w tworzeniu supramolekularnych struktur,  $N$ .



**Rys. 16.** Liczba cząstek  $N$  biorących udział w tworzeniu supramolekularnych struktur dla materiałów litych oraz alkoholi infiltrowanych do porów natywnych i silanizowanych.

Jak pokazano na **Rys. 16a i 16b** w przypadku 2E1B i 2E1H,  $N$  osiąga wartości  $N \sim 10-13$  i  $N \sim 7-8$  dla substancji w stanie litym. Jednakże, co ciekawe, liczba cząsteczek z wiązaniami wodorowymi zmniejsza się znacząco w geometrycznym ograniczeniu przestrzennym, co



wskazuje na redukcję długości łańcucha supramolekularnych asocjatów w tych układach. Wykonane eksperymenty sugerują również, że uporządkowana struktura może być zakłócana przez ograniczenie przestrzenne (oddziaływanie ze ścianami porów), zmieniające architekturę cząsteczek prowadząc do rozpadu form kulistych/miceli dla alkoholu drugorzędowego, zmieniając w pewnym stopniu strukturę na liniową. Utworzone asocjaty łańcuchowe w alkoholach pierwszorzędowych ulegają częściowemu zniszczeniu (liczba cząsteczek zaangażowanych w struktury łańcuchowe jest silnie zredukowana), podczas gdy drugorzędowe, tworzące micelle pozostają tylko w niewielkim stopniu naruszone przez ograniczenie przestrzenne ulegając w pewnym stopniu otwarciu i przekształceniu w liniowe asocjaty (**Rys. 16c**). Ponadto, obserwowana nie-Debye'owska funkcja odpowiedzi procesu międzyfazowego dla 5M3H może być związana z tym, że substancje te adsorbują się do porów krzemionki i wolą tworzyć wiązania wodorowe pomiędzy sobą aniżeli z powierzchnią. Dlatego, w przeciwieństwie do alkoholi pierwszorzędowych, występują tu bardzo słabe wiązania wodorowe o sile porównywalnej do oddziaływań dyspersyjnych pomiędzy strukturami supramolekularnymi a ścianami porów. Można więc stwierdzić, że ograniczenie przestrzenne ma większy wpływ na wiązania wodorowe w przypadku alkoholi pierwszorzędowych, podczas gdy w przypadku alkoholi drugorzędowych efekt ten nie jest tak istotny.

Wykonane eksperymenty sugerują jednoznacznie, że uporządkowana struktura może być zakłócana przez ograniczenie przestrzenne (oddziaływanie ze ścianami porów), zmieniające architekturę cząsteczek. Ponadto wykazano, że wiązania wodorowe stają się słabsze pod wpływem ograniczenia przestrzennego. Dodatkowo warto zaznaczyć, iż wpływ ograniczenia przestrzennego jest silniejszy dla alkoholi pierwszorzędowych sugerując tym samym istotną rolę struktury badanych związków.

### **III. TREŚCI ARTYKUŁÓW STANOWIĄCYCH PODSTAWĘ ROZPRAWY DOKTORSKIEJ WRAZ Z OŚWIADCZENIAMI WSPÓLAUTORÓW**

#### **A1. The Role of Interfacial Energy and Specific Interactions on the Behavior of Poly(propylene glycol) Derivatives under 2D Confinement.**

Autorzy: A. Talik, M. Tarnacka, I. Grudzka-Flak, P. Maksym, M. Geppert-Rybczynska, K.

Wolnica, E. Kaminska, K. Kaminski, M. Paluch.

Referencja: *Macromolecules*, 2018, 51, 4840-4852.

DOI: 10.1021/acs.macromol.8b00658

Impact Factor czasopisma z roku opublikowania pracy: 5.997

Liczba punktów ministerialnych MNiSW czasopisma (2018): 45

Mój udział w pracy polegał na: zebraniu danych literaturowych, współtworzeniu tezy badawczej, przygotowaniu próbek, wykonaniu pomiarów dielektrycznych a następnie analizie otrzymanych danych udziale w dyskusji wyników oraz współtworzeniu manuskryptu w tym przygotowaniu rysunków, opisie wyników i redagowaniu manuskryptu.

## The Role of Interfacial Energy and Specific Interactions on the Behavior of Poly(propylene glycol) Derivatives under 2D Confinement

Agnieszka Talik,<sup>\*,†,‡,§</sup> Magdalena Tarnacka,<sup>†,‡,§</sup> Iwona Grudzka-Flak,<sup>†,‡</sup> Paulina Maksym,<sup>†,‡,§</sup> Monika Geppert-Rybczynska,<sup>§</sup> Kamila Wolnica,<sup>†,‡</sup> Ewa Kaminska,<sup>||</sup> Kamil Kaminski,<sup>\*,†</sup> and Marian Paluch<sup>†,‡</sup>

<sup>†</sup>Institute of Physics, University of Silesia, 75 Pułku Piechoty 1, 41-500 Chorzów, Poland

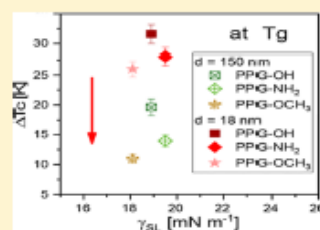
<sup>‡</sup>Silesian Center of Education and Interdisciplinary Research, University of Silesia, 75 Pułku Piechoty 1A, 41-500 Chorzów, Poland

<sup>§</sup>Institute of Chemistry, University of Silesia, Szkolna 9, 40-006 Katowice, Poland

<sup>||</sup>Department of Pharmacognosy and Phytochemistry, Medical University of Silesia in Katowice, School of Pharmacy with the Division of Laboratory Medicine in Sosnowiec, Jagiellońska 4, 41-200 Sosnowiec, Poland

**ABSTRACT:** The effect of the chemical modification of poly(propylene glycol) (PPG) end groups on the molecular dynamics under 2D confinement and the polymer/matrix interactions (including interfacial energies) was investigated by a combination of differential scanning calorimetry (DSC), broadband dielectric spectroscopy (BDS), surface tension and contact angle measurements. The replacement of –OH groups in native PPG allowed to modify the interactions with the hydroxyl groups attached to the pore walls of nanoporous aluminum oxide (AAO) membranes of various pore diameter. It was found that the observed reduction in the glass transition temperature ( $T_g$ ) of the core polymers correlates well with a general trend (the higher the solid–liquid interfacial tension,  $\gamma_{sl}$ , the lower  $T_{g,confined}$ ) reported earlier. Moreover, we demonstrated that although the interfacial solid–liquid energy

seems to be almost the same for each studied herein material, a clear change in the crossover temperature ( $T_c$ ), related to the vitrification of the polymers adsorbed to the pore walls, is noted. Interestingly, the shift in  $T_c$  with respect to the glass transition temperature of the bulk polymer scales well according to the decreasing ability in the formation of H bonds in the order PPG–OH  $\rightarrow$  PPG–NH<sub>2</sub>  $\rightarrow$  PPG–OCH<sub>3</sub> for the constant  $\gamma_{sl}$ . One can add that no such effect is found for the glass transition of the core polymers, where a similar shift of the  $T_g$  was recorded. This finding has been discussed in the context of various sensitivity of the studied materials to the density fluctuations, equilibration phenomena occurring below  $T_c$ , etc. We believe that our finding will help in a better understanding of an interplay between interfacial and core molecules and contribute significantly to the discussion on the impact of interfacial interactions on the molecular dynamics of polymers under 2D confinement.



### INTRODUCTION

Soft matter under nanoscale confinement often reveals different behavior with respect to the bulk materials. Generally, the enhancement of molecular dynamics and the shift in the phase transition temperatures,<sup>1–15</sup> which is usually discussed as a counterbalance of a few factors (finite size effects, interface, and free volume), is observed. Nevertheless, recent studies have highlighted the important role of the properties of interface on the overall behavior of the nanomaterials.<sup>16–19</sup>

As reported for the polymer thin films (1D confinement), generally strong interactions between polymer and substrate, i.e., by hydrogen bonding, seem to highly restrict the mobility of confined materials, leading to an increase in  $T_g$  while the application of nonattractive substrates (for example, gold) results in a decrease of  $T_g$ .<sup>20</sup> A similar scenario was observed for the poly(methyl methacrylate) (PMMA) deposited on the polar substrate, where the increase of  $T_g$  with decreasing film thickness was reported.<sup>21</sup> However, this kind of behavior is not a rule. In this context one can recall polystyrene (PS) films,

where no such correlation was noted. Interestingly,  $T_g$  of the polystyrene thin films decreased with the film thickness, independently of the applied substrate.<sup>21</sup>

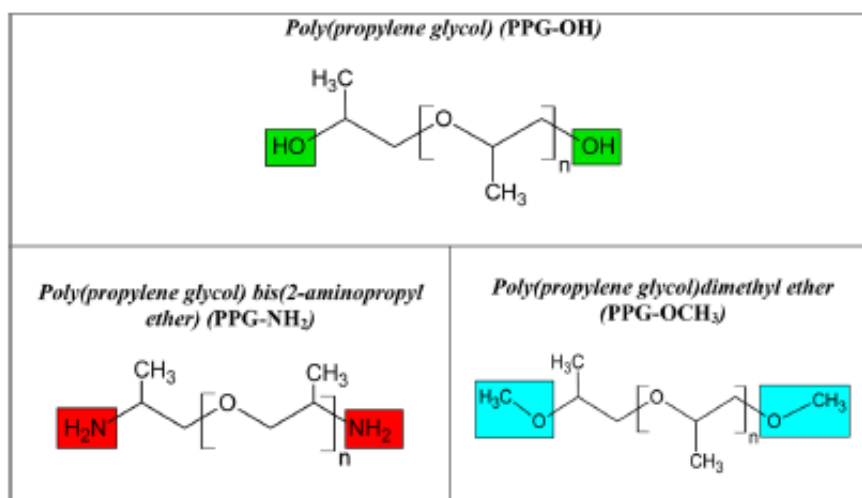
It is also worth mentioning that the molecular dynamics simulations indicated that the  $T_g$  of ultrathin polymer films increases with increasing interfacial energy,  $\gamma_{sl}$ , independently of the chemistry of the polymer film for a constant film thickness.<sup>22,23</sup> That clearly indicates that in fact the strength of interactions plays an important role in the direction and magnitude of the shift of the glass transition temperature.<sup>24</sup> However, herein, one has to also refer to the recent studies that clearly demonstrated that deviation from  $T_{g,bulk}$  can have a finite lifetime.<sup>16,25–27</sup> As reported for the thin polymer films, in some cases, the prolonged annealing allows recovering bulk properties. This equilibration at time scale much longer than reptation

Received: April 5, 2018

Revised: May 31, 2018

Published: June 18, 2018

Table 1. Chemical Structures of Examined PPG–OH and Its Derivatives



time (often identified as segmental relaxation times) leads to the perturbation of polymer density at the interface and the increase in the number of irreversible adsorbed chains.<sup>17–19,28</sup>

Thus, one can mention that the changes in  $T_g$  might be related not only to the film thickness, properties of the substrate, and strength of interactions, but also to the processes occurring at the interface.

Along with the comprehensive studies on the dynamics of polymers deposited as thin films there are also parallel investigations carried out for the macromolecules incorporated into porous materials of varying pore diameter (so-called 2D confinement). One can add that for this kind of confinement generally a depression of the glass transition temperature with respect to the bulk sample is noted. Recently, Alexandris et al. postulated that in contrast to the polymers deposited on the substrate an increase of the interfacial energy leads to a decrease of  $T_g$  for the macromolecules incorporated into porous materials.<sup>29</sup>

In order to explore more deeply the idea proposed in ref 29, we have studied a molecular dynamics of the chemically modified poly(propylene glycol) (PPG) (terminal OH groups were replaced by  $\text{NH}_2$  and  $\text{OCH}_3$  functional groups) of molecular weight  $M_n = 4000$  g/mol incorporated into nanoporous aluminum oxide (AAO) membranes of various pore diameter,  $d$ , varying in the range of 18–150 nm. One can add that a clear advantage of our studies is a fact that all measurements were carried out on one well-defined polymer, having the same backbone, characterized by the constant  $M_n$ , dispersity, and modified intermolecular interactions (achieved by the modification of terminal functional group) to probe the impact of interfacial (solid–liquid) energy as well as specific interactions on the segmental, chain dynamics and drop in the glass transition temperature of the investigated materials. Our data were discussed in the view of recent report by Alexandris et al.,<sup>29</sup> who found a close relationship between  $\gamma_{SL}$  and  $T_g$  in various kinds of macromolecules (see Table 1).

One can recall, that poly(propylene glycols), as well as poly(*cis*-isoprene) (PI), are the type A polymers characterized by a dipole moment arranged parallel to the chain backbone, which is manifested by an additional relaxation process (so-called normal mode).<sup>30</sup> Thus, information about segmental

(local) and chain (global) dynamics can be obtained directly from the dielectric measurements. Our recent studies on the native PPG incorporated into AAO templates indicated that segmental and normal mode processes become faster with the increasing geometrical constrain resulting in the reduction of  $T_g$ .<sup>31</sup> On the other hand, in the case of PI incorporated into AAO membranes, the spatial restriction did not affect the glass transition temperature, while the chain dynamics under confinement was found to be retarded when compared to the bulk sample, dependent on the pore size.<sup>7</sup> Therefore, quite different behavior with respect to the confined PPG was reported. Consequently, from this simple comparison it seems to be clear that the variation in the specific interactions between host material and both types of polymers must determine their behavior.

## ■ EXPERIMENTAL SECTION

**Materials.** Poly(propylene glycol) (PPG–OH) and Poly(propylene glycol bis(2-aminopropyl ether) (PPG– $\text{NH}_2$ ) with purity higher than 98% were supplied by Sigma-Aldrich. Iodomethane (>99%, Sigma-Aldrich) was used as received. All other solvents were applied without purification. The chemical structures are presented in Table 1. For clarity, PPG of  $M_n = 4000$  g/mol has a degree of polymerization ( $n$ ) equal to 68. The nanoporous aluminum oxide membranes used in this study (supplied from Synkera Co.) are composed of uniaxial channels (open from both sides) with well-defined pore diameter. Details concerning porosity, pore distribution, etc., can be found at the Web page of the producer.<sup>32</sup>

**Samples Preparation.** Prior to filling, AAO membranes were dried in an oven at 423 K under vacuum to remove any volatile impurities from the nanochannels. After cooling, they were placed in PPG. Then, the whole system was maintained at  $T = 343$  K in a vacuum ( $10^{-2}$  bar) for 24 h to let both compounds flow into the nanocavities. After completing the infiltration process, the surface of AAO membrane was dried, and the excess sample on the surface was removed by use of a paper towel. In the experiment, we used membranes with different pore diameters: 150, 73, 35, and 18 nm.

**Methods. Synthesis of PPG– $\text{OCH}_3$ .** The mixture of 10 g (2.5 mmol) of hydroxyl-functionalized PPG and 0.24 g (6 mmol, 2.4 equiv) of NaH (60% in mineral oil) was stirred under an inert gas atmosphere for 24 h in a two-neck bottom flask equipped with magnetic stirrer and rubber septum. Then  $\text{CH}_3\text{I}$  was added dropwise and stirring was continued for an additional 24 h. After that the reaction was terminated by adding 40 mL of methanol. The postreaction mixture

was purified by ultrafiltration followed by evaporation of the volatile fractions. The residue was dissolved in dichloromethane, and the organic solution was washed with water (three times) and next dried over  $\text{MgSO}_4$ . PPG-OCH<sub>3</sub> was received as a pale-yellow oil with 92% yield. The product of the reaction was confirmed by IR spectra (see Figure 1).

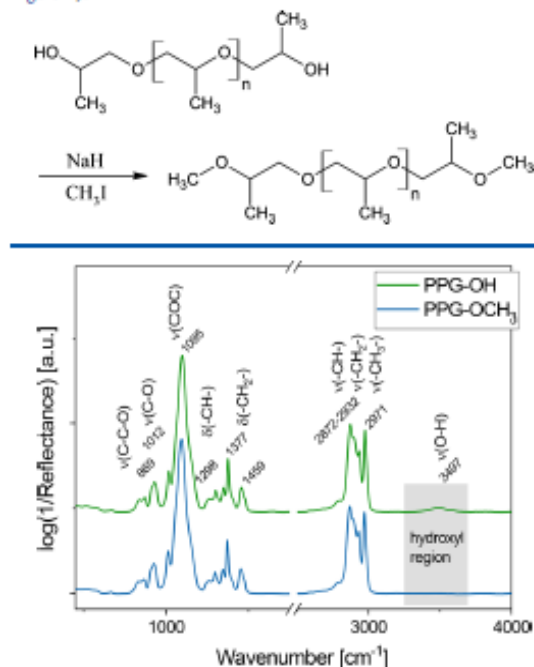


**Figure 1.** IR spectra collected before and after the synthesis of PPG-OCH<sub>3</sub>.

**Fourier Transform Infrared (FTIR) Spectroscopy.** FTIR measurements were carried out using the Agilent Cary 640 FTIR spectrometer equipped with a standard source and DTGS Peltier-cooled detector. The spectra have been collected using GladiATR diamond accessory in the 450–4000  $\text{cm}^{-1}$  range. All spectra were recorded by accumulation of 16 scans with a spectral resolution of 4  $\text{cm}^{-1}$ . Infrared data were preprocessed by baseline correction as well as water vapor and carbon dioxide removal using Grams Software Package.

Additionally, FTIR measurements have been carried out for PPG-OH and PPG-OCH<sub>3</sub> samples in order to identify the presence of -OH groups in the measured system. Here, both spectra (see Figure 1) are dominated by few marker bands described in the literature.<sup>33</sup> Therefore, one can detect bands located at  $\sim 869$ ,  $\sim 1012$ , and  $\sim 1095$   $\text{cm}^{-1}$  which are associated with the stretching vibrations of  $\nu(\text{C}-\text{C}-\text{O})$ ,  $\nu(\text{C}-\text{O})$ , and  $\nu(\text{COC})$  moieties, respectively. The other group of vibrations can be found at  $\sim 1298$  and  $\sim 1377$ – $1459$   $\text{cm}^{-1}$  as well as  $\sim 2872$ – $2932$  and  $\sim 2971$   $\text{cm}^{-1}$  originating from the deformation vibration of -CH- and -CH<sub>2</sub>- units in polymer backbone as well as stretching vibration of  $\nu(-\text{CH})$ ,  $\nu(-\text{CH}_2)$ , and  $\nu(-\text{CH}_3)$  groups, respectively. In addition, at  $\sim 3497$   $\text{cm}^{-1}$  a broad band with low intensity assigned to the stretching vibration of O-H group is also seen in PPG-OH. In turn, the PPG-OCH<sub>3</sub> spectrum is characterized by the similar band arrangement with the exception of this one observed in the hydroxyl region. That means that all hydroxyl units have been replaced by the -OCH<sub>3</sub> moiety.

**Broadband Dielectric Spectroscopy (BDS).** Isobaric measurements of the complex dielectric permittivity  $\epsilon^*(\omega) = \epsilon'(\omega) - i\epsilon''(\omega)$  were carried out using the Novocontrol Alpha dielectric spectrometer over the frequency range from  $10^{-2}$  to  $10^6$  Hz at ambient pressure. The temperature stability controlled by the Quatro Cryosystem using nitrogen gas cryostat was better than 0.1 K. Dielectric measurements of bulk PPG's were performed in a parallel-plate cell (diameter: 10

mm; gap: 0.1 mm) immediately after preparation of the amorphous sample. AAO membranes filled with PPG's were also placed in a similar capacitor (diameter: 10 mm; membrane thickness: 0.005 mm).<sup>34,35</sup> Nevertheless, the confined samples are a heterogeneous dielectric consisting of a matrix and an investigated compound. Because the applied electric field is parallel to the long pore axes, the equivalent circuit consists of two capacitors in parallel composed of  $\epsilon^*_{\text{polymer}}$  and  $\epsilon^*_{\text{AAO}}$ . Thus, the measured total impedance is related to the individual values through  $1/Z^*_c = 1/Z^*_{\text{polymer}} + 1/Z^*_{\text{AAO}}$ . It should be added that dielectric measurements on empty membranes were also carried out to evaluate the contribution of AAO, which turned out to be negligible. Dielectric measurements were performed in the temperature range 188–243 K for bulk and confined systems.

**Differential Scanning Calorimetry (DSC).** Calorimetric measurements were carried out using a Mettler-Toledo DSC apparatus (Mettler-Toledo International, Inc., Greifensee, Switzerland) equipped with a liquid nitrogen cooling accessory and an HSS8 ceramic sensor (heat flux sensor with 120 thermocouples). Temperature and enthalpy calibrations were performed by using indium and zinc standards. Measurements were carried out on bulk and the crushed membranes filled with PPG. The samples were contained in sealed crucibles, with a heating rate of 10 K/min over a temperature range from 160 to 300 K.

**Surface Tension and Contact Angle Measurements.** Surface tension  $\gamma$  (using pendant drop method with a Drop Shape Analysis Software) and contact angle  $\theta$  were measured with the DSA 100S Krüss tensiometer, GmbH, Germany. More detailed descriptions of instrumental and the experimental procedures have been described previously.<sup>34,37</sup> In this work, the surface tension of a series of PPG derivatives was measured in the temperature range 288.2–338.2 K, with a step of 10 K. Because of very high viscosity of examined PPGs some surface tensions were measured from 298.2 K. At given temperature the measuring procedure for each substance has been repeated several times. The temperature measurements uncertainty for surface tension experiment was  $\pm 0.1$  K, whereas for contact angle it was around  $\pm 0.5$  K. The uncertainty of surface tension is on the level  $\pm 0.1$  mN  $\text{m}^{-1}$ , but in our case the standard deviation of the mean value (from all points) was below this value. The density necessary for the surface tension calculations was measured with an Anton Paar DMA 5000 M densimeter with the uncertainty not greater than 0.001  $\text{g cm}^{-3}$ .

The contact angle of each material deposited on the aluminum oxide was measured in a thermostated chamber at  $T = 298$  K. The mean value of this parameter was obtained as the average of several dozen independent measurements. Precision of this measurements was  $0.01^\circ$ , but estimated uncertainty was between  $0.5^\circ$  and  $1.0^\circ$ . For the investigated substances as well as for the test liquids the time dependence for contact angle was registered. First attempts showed that after 60 s the drop placed on the solid material has a constant shape with a constant contact angle value. Thus, the contact angles for PPGs were registered for 2–3 min.

## RESULTS AND DISCUSSION

**Characterization of Bulk Materials.** As a first step of our investigations, we characterized the properties of the examined bulk systems. The DSC thermograms of bulk PPGs are given in Figure 2a. As illustrated, all DSC curves display one endothermic process located approximately at  $T = 202$  K, independently of the PPG end group. Values of  $T_g$  are added to the description of Figure 2a and listed in Table 2. Data for native PPG (label herein as PPG-OH) were taken from ref 31. As presented, no significant difference in calorimetric  $T_g$  between studied PPG derivatives is noted, and the glass transition temperature reaches  $T_g = 201$ – $203$  K for all bulk materials.

Furthermore, we performed BDS measurements and the representative dielectric spectra collected for the bulk PPG-OCH<sub>3</sub> are presented in Figure 2b. As observed, all samples revealed the presence of three relaxation processes: (i) the dc

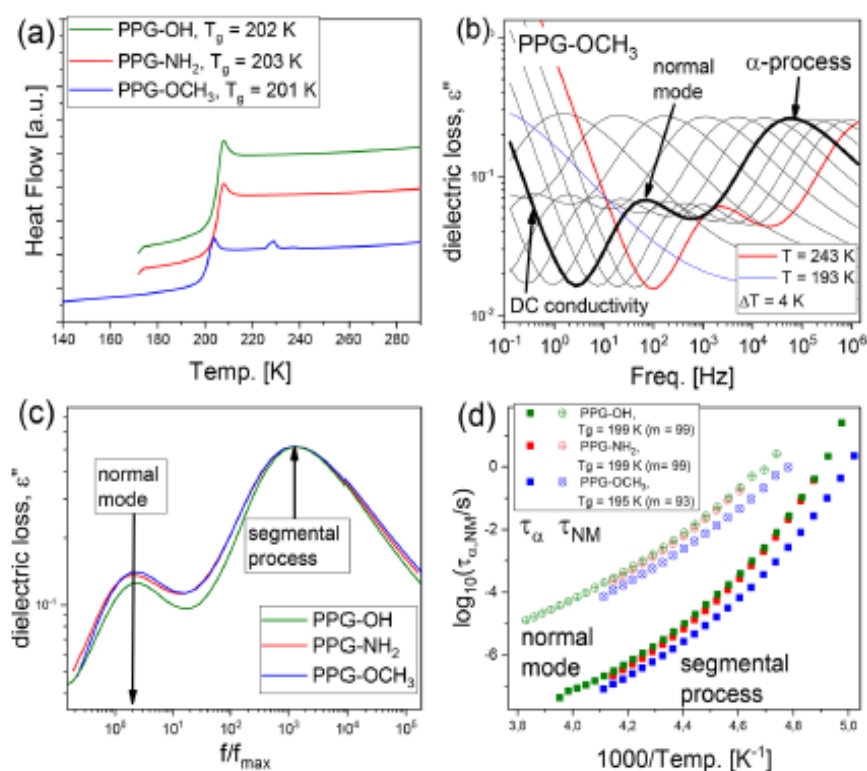


Figure 2. (a) DSC thermograms of bulk PPGs. (b) Dielectric loss spectra measured for bulk PPG-OCH<sub>3</sub>. (c) Comparison of the shape of the segmental relaxation measured for all bulk samples. (d) Temperature dependence of the relaxation times plotted for all examined bulk PPG materials. Data for PPG-OH were taken from ref 31.

Table 2. Values of  $T_g$ s and  $T_c$  Obtained for Bulk and Confined Samples from Calorimetric and Dielectric Measurements<sup>a</sup>

sample	DSC measurements				dielectric measurements			
	$T_{g1} \pm 2$ [K]	$T_{g2} \pm 2$ [K]	$\Delta C_{p1}$ [J/(g K)]	$\Delta C_{p2}$ [J/(g K)]	$T_c \pm 2$ K	$T_{g,confined}$ [K] for $\log \tau_a = 2$	$\Delta T_c$ [K]	$\Delta T_g$ [K]
PPG-OH								
bulk		202		0.67		199 ( $m = 99$ )		
150 nm	195.3	218.8	0.50	0.57	219	192.5	196	-6.9
73 nm	190.4	225.3	0.40	0.48	224	189.7	246	-9.7
35 nm	188.1	230.3	0.31	0.35	229	184.2	296	-15.2
18 nm	185.9	231.9	0.25	0.30	231	179.6	316	-19.8
PPG-NH <sub>2</sub>								
bulk		203		0.67		199 ( $m = 99$ )		
150 nm	195	219	0.37	0.28	213	193	14	-6
73 nm	190	225	0.31	0.18	219	185	20	-14
35 nm	188	230	0.11	0.49	223	181	24	-18
18 nm	186	232	0.25	0.48	227	180	28	-19
PPG-OCH <sub>3</sub>								
bulk		201		0.62		195 ( $m = 93$ )		
150 nm	192	213	0.77	0.71	206	187	11	-8
73 nm	191	219	0.79	0.63	215	184	20	-11
35 nm	189	222	0.54	0.36	217	184	22	-11
18 nm	185	231	0.79	0.72	221	177	26	-18

<sup>a</sup>Data for PPG-OH incorporated into AAO templates were taken from ref 31.

conductivity connected to the charge transport and located at the lowest frequencies, (ii) the normal mode reflecting the process connected to the global chain dynamics and fluctuations of the end-to-end vector of the chain, and (iii) the segmental ( $\alpha$ ) relaxation at the highest frequencies,

assigned to the cooperative motions of segments, which is considered to be responsible for the liquid-to-glass transition. Data for the PPG-OH were taken from ref 31. Additionally, as expected, the distribution of the relaxation times is not affected by the terminal modification of PPG, and the shape of the  $\alpha$ -

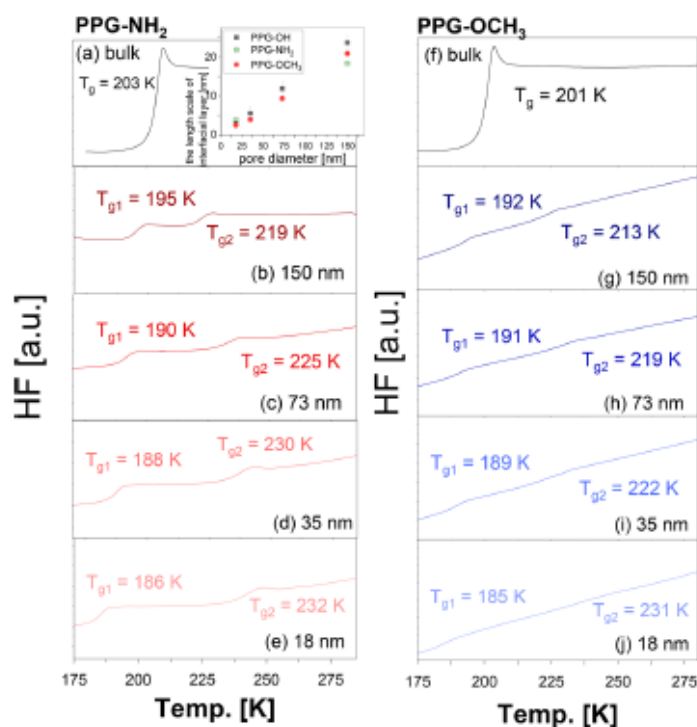


**Figure 3.** DSC thermograms of bulk and confined PPG-NH<sub>2</sub> (a–e) and PPG-OCH<sub>3</sub> (f–j). Note that bulk data were added for better data presentation and to highlight that confined  $T_g$ s are located below and above bulk  $T_g$ . Data for native PPG incorporated into AAO templates were taken from ref 31. As an inset in panel (a), the length scale of interfacial layer of polymers attached to the surface of alumina nanochannels is plotted vs pore diameter.

process is identical for all samples (see Figure 2c). The same scenario can be also observed in the case of the normal mode, which has similar shape and position in the experimental window.

The obtained loss spectra were further analyzed using the superposition of two Havriliak–Negami (HN) functions with an additional term describing the dc conductivity:<sup>38</sup>

$$\epsilon(\omega)^{\prime\prime} = \frac{\sigma_{dc}}{\epsilon_0 \omega} + \text{Im} \sum_{i=1}^2 \left( \epsilon_{\infty} + \frac{\Delta \epsilon_i}{[1 + (i\omega\tau_i)^{\alpha}]^{\beta}} \right) \quad (1)$$

where  $\alpha$  and  $\beta$  are the shape parameters representing the symmetric and asymmetric broadening of given relaxation peaks,  $\Delta \epsilon$  is the dielectric relaxation strength,  $\tau_{HN}$  is the HN relaxation time,  $\epsilon_0$  is the vacuum permittivity, and  $\omega$  is an angular frequency ( $\omega = 2\pi f$ ). Then, relaxation times of segmental,  $\tau_{\omega}$ , and normal mode,  $\tau_{NM}$ , processes were estimated from  $\tau_{HN}$  using the formula from ref 39. Temperature dependences of the calculated relaxation times are shown in Figure 2d. In order to estimate the values of  $T_g$ , presented data were fitted to the Vogel–Fulcher–Tamman (VFT) equation:

$$\tau_{\alpha} = \tau_{\infty} \exp\left(\frac{D_T T_0}{T - T_0}\right) \quad (2)$$

where  $\tau_{\infty}$  is the relaxation time at finite temperature,  $T_0$  is the temperature, where  $\tau$  goes to infinity, and  $D_T$  is the fragility parameter. The calculated values of the glass transition

temperature, defined as a temperature, where  $\tau_{\alpha}(T_g) = 100$  s, are indicated in Figure 2d and Table 2. Note that the obtained values of  $T_g$  are in a very good agreement with those reported in the literature for PPG-OH and PPG-NH<sub>2</sub>.<sup>45</sup> As presented, no difference in the molecular dynamics between both polymers can be detected. Thus, one can conclude that the modification of the terminal groups has small impact on the dynamical properties of both materials. On the other hand, in the case of PPG-OCH<sub>3</sub>, some deviation in  $\tau_{\alpha}$  and  $\tau_{NM}$  as well as a small reduction of  $T_g$  can be detected (see blue points in Figure 2d). Moreover, it should be highlighted that the difference in  $T_g$  estimated from BDS and DSC data for PPG-OCH<sub>3</sub> is the highest ( $\Delta T = 6$  K), although this difference is still acceptable. Interestingly, the relatively small chemical modification (the replacement of the end group) has a measurable impact on the molecular dynamics of examined materials. This difference can be also observed in the fragility (or steepness index,  $m$ ), which has been calculated accordingly to the following equation:<sup>40</sup>

$$m = \left. \frac{d \log \tau_{\alpha}}{d(T_g/T)} \right|_{T=T_g} \quad (3)$$

The estimated values of  $m$  were added to Figure 2d. As presented, the highest ( $m = 99$ ) and the lowest ( $m = 93$ ) values of  $m$  were obtained for PPG-OH (as well as PPG-NH<sub>2</sub>) and PPG-OCH<sub>3</sub>, respectively. One can recall that the  $m$  parameter

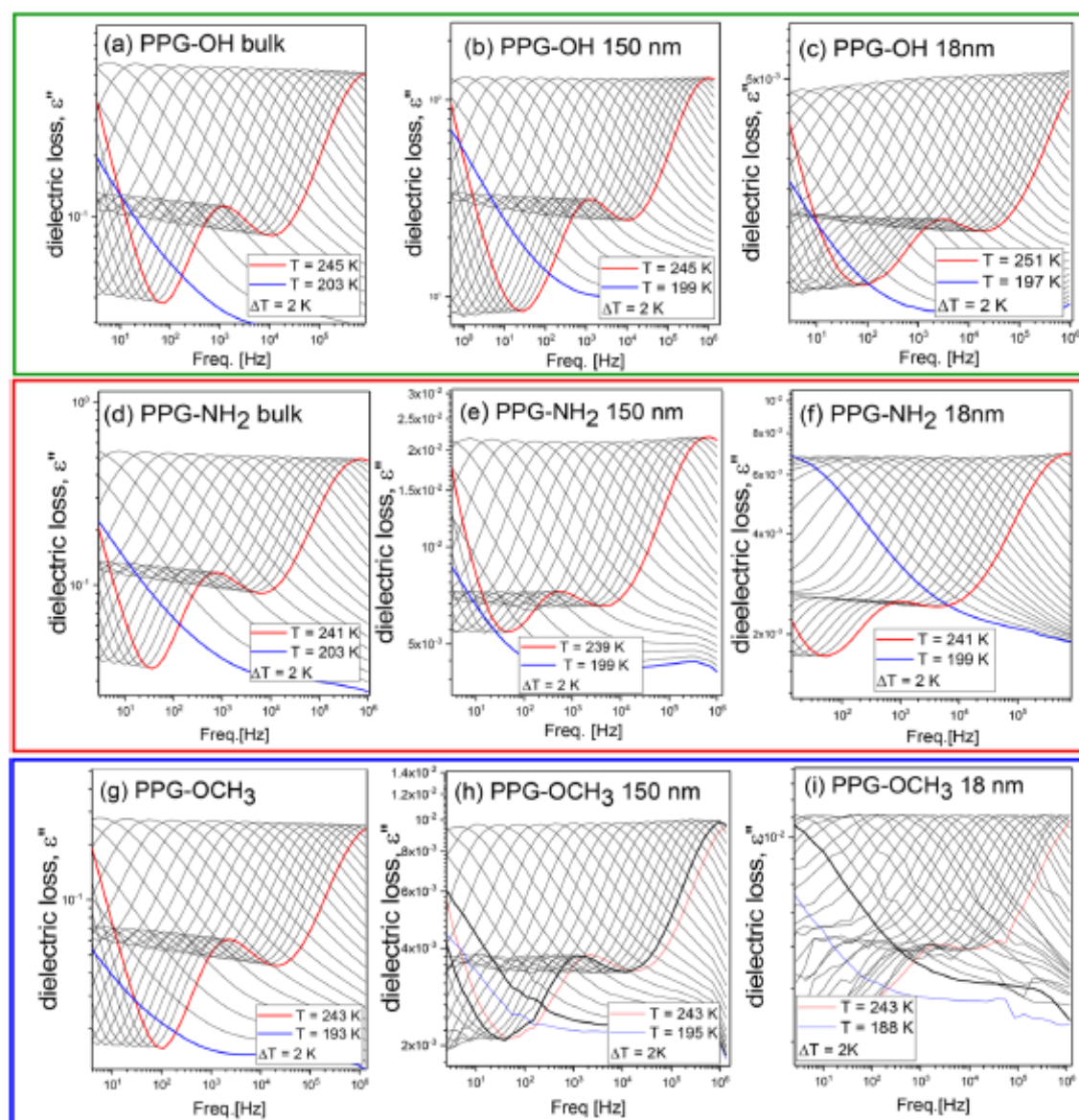


**Figure 4.** Dielectric loss spectra measured for the bulk PPG-OH (a), PPG-NH<sub>2</sub> (d), and PPG-OCH<sub>3</sub> (g) and polymers confined in AAO membranes of two pore sizes 150 nm (b, e, h) and 18 nm (c, f, i). Data for PPG-OH were taken from ref 31.

describes the sensitivity of the  $\alpha$ -relaxation to the temperature changes. It is worth adding that in the case of polymers this parameter is affected by the symmetry of the monomer, the presence of bulky pendant groups, tacticity, stereogeometry, and packing density.<sup>41–44</sup> Thus, the observed decrease of the fragility seems to be due to some variation in intermolecular interactions caused by the modification of PPG terminal groups. Note that the ability of hydrogen bonding in the examined polymers seems to decrease in the following manner: PPG-OH  $\rightarrow$  PPG-NH<sub>2</sub>  $\rightarrow$  PPG-OCH<sub>3</sub>. Interestingly, the elimination of the ability of H bond formation in the latter polymer is still manifested as a visible difference in temperature dependencies of the segmental and chain relaxation processes

with respect to the former two materials. One can add that the same fragility was obtained for both PPG-OH and PPG-NH<sub>2</sub> (where  $m = 99$ ), indicating very similar behavior. Nevertheless, it should be mentioned that accordingly to the literature, the fragility of PPG-OH and PPG-NH<sub>2</sub> strongly depends on  $M_n$  due to the decreasing role of the H bonds with increasing chain length.<sup>45</sup> As expected, both PPG-OH and PPG-NH<sub>2</sub> are characterized by the comparable  $T_g$  and dynamics of segmental and chain relaxation processes.

**Confined Systems.** Next, all examined PPGs were incorporated into AAO membranes of pore sizes varying in the range  $d = 18$ – $150$  nm (see *Experimental Section*). The representative thermograms of confined PPGs obtained during



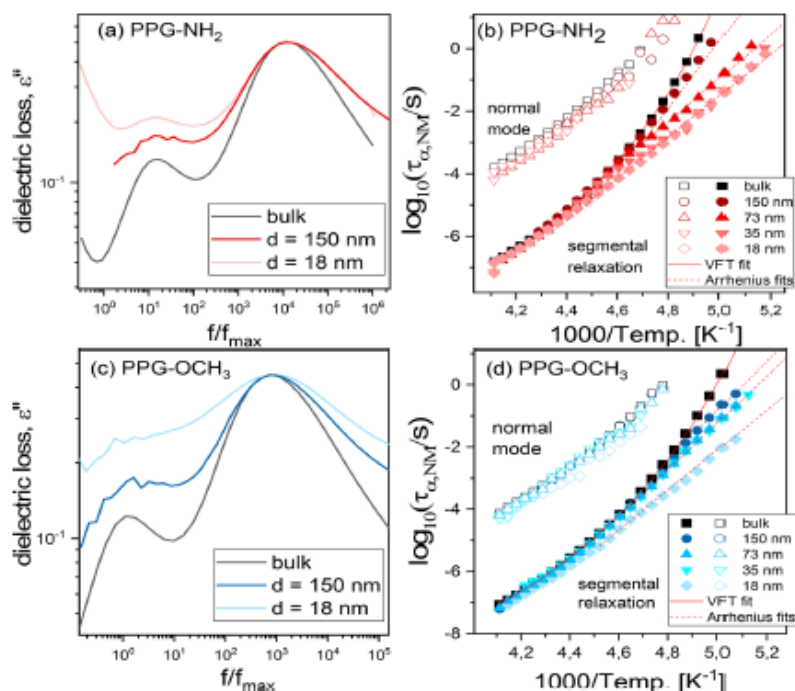


**Figure 5.** (a, c) Comparison of the segmental relaxation shape recorded for the bulk and confined PPG derivatives (PPG-NH<sub>2</sub> and PPG-OCH<sub>3</sub>) incorporated in two pore sizes  $d = 18$  nm and  $d = 150$  nm. (b, d) Relaxation map for the indicated bulk and confined systems.

heating are displayed in Figure 3. It can be noticed that spatially restricted systems exhibit two endothermic processes, reflecting a double glass transitions phenomenon occurring below and above the  $T_g$  of the bulk material. One can recall that according to the two-layer model, this double  $T_g$ s phenomenon is related to the two fractions of molecules/polymers of different dynamics. Consequently, we can distinguish (i) surface fraction associated with the polymers attached at the interface of pore walls, characterized by the  $T_g$  higher than the bulk ( $T_{g2}$ ), and (ii) the core macromolecules located in the center of the nanoporous channels, characterized by the  $T_g$  lower than the bulk ( $T_{g1}$ ).<sup>46</sup> It should be mentioned that the presence of double  $T_g$ s is widely reported in the literature for the low and high molecular weight glass-formers, including polymers incorporated into nanoporous templates.<sup>47,55,53,59</sup> Values of both  $T_g$ s together with the heat capacity jumps for the both detected endothermic transitions are listed in Table 2. As one can see,  $T_{g1}$  decreases with the reduction of the pore size, while the  $T_{g2}$  increases with the increasing confinement. It means that the difference between both  $T_g$ s ( $T_{g2}$  and  $T_{g1}$ ) increases with a decreasing pore diameter. The largest difference can be found for PPGs incorporated into AAO templates of  $d = 18$  nm, independently on the PPG terminal moieties. One can add that the values of both  $T_g$ s determined from DSC data differ slightly for the studied PPGs. Data for the PPG-OH incorporated into AAO templates were taken from ref 31.

Next, in order to explore the impact of modification of PPG terminal groups and to probe interfacial interactions between host and guest material, the length scale of interfacial layer,  $\zeta$ , of

polymers attached to the surface of alumina nanochannels was estimated accordingly to the following equation:<sup>47</sup>

$$\zeta = \frac{d}{2} \left[ 1 - \left( \frac{\Delta C_{p,1}}{\Delta C_{p,1} + \Delta C_{p,2}} \right)^{1/2} \right] \quad (4)$$

where  $d$  is the pore diameter and  $\Delta C_{p,1}$  and  $\Delta C_{p,2}$  are the changes of the heat capacity at  $T_{g1}$  and  $T_{g2}$ , respectively. Note that the application of eq 4 requires the following assumptions: (i) the volume of the material in the surface layer is proportional to the step change of its heat capacity, (ii) the density of the incorporated material does not change along the pore radius, and finally (iii) the shape of the pore is cylindrical. Values of the heat capacity jumps for the both detected endothermic transitions are listed in Table 2, while the pore diameter dependence of the interfacial layer thickness is shown as an inset in Figure 3a. Data for PPG-OH incorporated into AAO templates were taken from ref 31. As illustrated, the interfacial layer increases with the decreasing degree of confinement (the growth of  $d$ ) and reveals no significant end group dependence, when we take into account error bars in the estimation of this parameter. One can add that the calculated  $\zeta$  are comparable to those reported for PMMA (where  $\zeta \sim 14$  nm for  $d = 80$  nm pores)<sup>48</sup> and salol (where  $\zeta \sim 15$  nm for  $d = 100$  nm pores)<sup>49</sup> incorporated into AAO templates. At the first sight, it is well seen that the estimated  $\zeta$ 's seem to be quite large with respect to those determined for the polymers deposited on flat substrates. In these cases, many authors observed the

formation of the so-called irreversibly adsorbed layer (IAL), which was around 4–5 nm even in the thick samples. Therefore, there is a discrepancy between IAL and interfacial layer determined for the both geometrical constraints. To understand that one can remind that IAL can be estimated directly with large precision using well established and reliable methods. On the other hand, for the polymers incorporated in pores, the length scale of the adsorbed material can be calculated indirectly from the heat capacity jumps at the two glass transition temperatures. Therefore, one can suppose that except of the polymers strongly attached to the pore walls, also more loosely packed macromolecules of slower dynamics might contribute to the higher glass transition temperature. Moreover, there are also additional interactions between adsorbed PPG's and hydroxyl moieties, which may additionally affect the heat capacity jumps at the high glass transition temperature. Finally, it should be mentioned that upon calorimetric studies the samples were cooled and heated with the rate 10 K/min, which might successively affect sorption and desorption processes as well as exchange between adsorbed and core macromolecules. Furthermore, the estimated interfacial layer can be significantly overestimated with respect to IAL calculated for the polymers deposited as thin films on flat substrates.

Complementary to the calorimetric studies, we also performed BDS measurements. Dielectric loss spectra for various confined PPGs are shown in Figure 4. Again, one can distinguish three processes: the dc conductivity, normal mode, and segmental relaxation. Note that sometimes an additional process (so-called interfacial) reflecting reorientational motions of the molecules strongly interacting with pore walls can be also detected in confined systems.<sup>50,51</sup> Although, it is not a rule and is not the case for the studied herein materials. Additionally, a significant broadening of both processes (segmental relaxation and normal mode) with increasing confinement for all PPGs independently on the terminal units (see Figure 5a,c) was observed. Accordingly to the literature, this effect can be discussed in the context of (i) an increased length scale of heterogeneity,<sup>31</sup> (ii) a variation in the population and the degree of dynamic coupling of the formed clusters under confinement,<sup>49</sup> and/or (iii) the strong interactions between the interfacial and core polymers and AAO membrane. It should be added that a similar broadening of the distribution of the segmental and chain relaxation times with decreasing pore size was also observed for the native PPG and PI incorporated into AAO templates. Note that for the latter compound the low-frequency slope was reported to be lower than unity, indicating the retardation of the chain dynamics.<sup>7,31</sup> However, herein, we have found the pronounced enhancement of the dynamics (segmental and normal mode) close to  $T_g$  for all PPGs, independently of the end groups. One can add that studies on PI deposited on doped silicon substrate showed no impact of the film thickness on the dynamics of segmental process. On the other hand, the chain dynamics was observed to be significantly enhanced with respect to the bulk samples for the higher molecular weight polymers.<sup>52</sup>

Further analysis of the loss spectra with the use of the superposition of two HN functions with the conductivity term allows to plot relaxation times of the bulk PPGs and samples measured under confinement versus inverse of temperature (see Figure 5b,d). Data for the bulk systems were added for a better clarity of the presentation. As presented, in the high temperature range there is no difference between bulk and confined systems. However, further decreasing of temperature

revealed a pronounced deviation in  $\tau_\alpha$  of confined PPGs at some specific temperature (labeled as the crossover temperature,  $T_c$ ), independently of the terminal moieties. One can add that the same scenario was also observed in the case of the native PPG incorporated into AAO templates.<sup>31</sup> Values of  $T_c$  are listed in Table 2. It can be seen that  $T_c$  strongly depends on the pore diameter of the applied membranes. In fact, the smaller  $d$ , the higher  $T_c$ . Note that the same behavior was also reported in the case of  $T_{g2}$ . By the comparison of the obtained data, one can find a good agreement between  $T_c$  (estimated from BDS) and  $T_{g2}$  (determined from DSC). The discrepancies can be related to the difference in the cooling rate in DSC and dielectric measurements, which surely affected sorption–desorption processes and density packing at the interface. Therefore, the deviation in  $\tau_\alpha(T)$  of the confined PPGs observed at  $T_c$  can be related to the vitrification of the polymers adsorbed on the pore walls. Moreover, although BDS and DSC techniques probe different types of molecular motions, one can see that both of them can be successfully used to follow and detect the glass transition of the interfacial macromolecules. Interestingly, a similar deviation at  $T_c$  occurs also in  $\tau_{NM}$  of the examined nanosystems; but here, the effect is much less pronounced due to a different time scale of both processes. One can recall that the observed variation in the relaxation times due to the vitrification of the polymers adsorbed on the pore walls is commonly reported for the low and high molecular weight glass-forming liquids under 2D confinement.<sup>31,49,53</sup> Note that recent studies on the liquids incorporated into porous templates have indicated that below  $T_c$  (corresponding to the freezing out of the adsorbed layer) the free volume of the system remains constant (within experimental uncertainty).<sup>54</sup> At those conditions, the system enters isochoric/isodensity conditions governed by the negative pressure.<sup>55–58</sup>

In order to determine the values of  $T_g$  under confinement, temperature dependences of the segmental relaxation times were fitted by a combinations of VFT and Arrhenius equations. Note that at high temperatures (above  $T_c$ ) the examined  $\tau_\alpha(T)$  dependences follow VFT scenario, while below  $T_c$ , a change from VFT to the Arrhenius-like behavior can be seen. Thus, to describe the obtained data correctly in the wide range of temperature, we used two functions. The Arrhenius equation was used as follows:

$$\tau_\alpha = \tau_\infty \exp\left(\frac{\Delta E}{k_B T}\right) \quad (5)$$

where  $k_B$  is Boltzmann constant and  $\Delta E$  is the activation energy. Obtained values of the glass transition temperature (where  $\tau_\alpha(T_g) = 100$  s) of the confined PPGs are indicated in Table 2. As shown, an increasing degree of confinement results in a significant reduction of  $T_g$  for all studied PPGs. The lowest  $T_g$  was determined for the PPGs confined into the smallest pores ( $d = 18$  nm), independently of the terminal moieties (see Table 2). Again, a good agreement between  $T_{g1}$  and  $T_g$  estimated from the DSC and dielectric data was obtained (see Table 2).

To explore the impact of the intermolecular interactions on the molecular dynamics in the examined PPGs under confinement, we analyzed the difference between  $T_c$  and  $T_{g, bulk}$  labeled as  $\Delta T_c$  (where  $\Delta T_c = T_c - T_{g, bulk}$ ). Values of  $\Delta T_c$  plotted as a function of the pore diameter are presented in Figure 6a. As illustrated,  $\Delta T_c$  increases with the pore size and

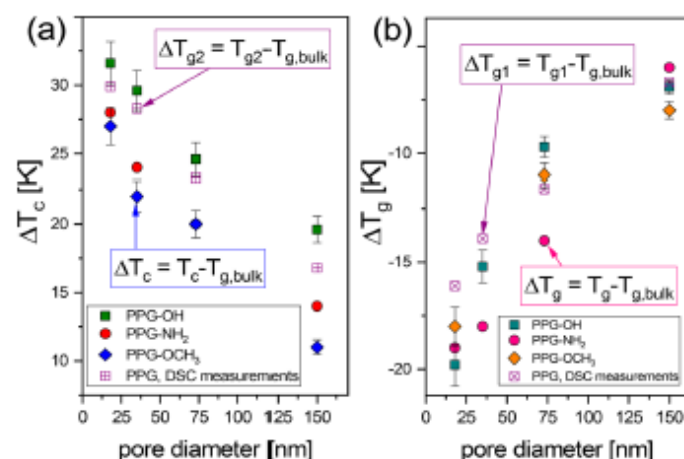


**Figure 6.** Deviation in  $T_c$  (a) and  $T_g$  (b) when compared to the glass transition temperature of the bulk material. Data for PPG–OH incorporated into AAO templates were taken from ref 31.

strongly depends on the examined PPG terminal units, where  $\Delta T_c$  decreases in the following order: PPG–OH  $\rightarrow$  PPG–NH<sub>2</sub>  $\rightarrow$  PPG–OCH<sub>3</sub> and seems to correspond quite well to the ability of H bonds formation (even though we take into account error bars around 2 K). In this context, one can assume that the deviation in  $\tau_c(T)$  dependences and  $\Delta T_c$  might be related to the variation in the interaction with the AAO templates surface (including H bonds) due to the modification of PPG end group. One could expect that the stronger interplay between material and pore walls, the higher  $\Delta T_c$  of the polymer. On the other hand, no such direct correlation can be deduced from the analysis of the  $\Delta T_{g1}$  (where  $\Delta T_{g1} = T_{g1} - T_{g,bulk}$ ) estimated from DSC as well as dielectric data (see Figure 6a). In this case,  $\Delta T_{g2}$  varies only slightly and is comparable for all studied polymers incorporated in pores of varying diameters.

**Interfacial Energy.** To get better insight and quantify the role of the surface interactions on the overall behavior of the confined PPGs, we carried out additional measurements of surface tension,  $\gamma_L$ , and contact angle,  $\theta$ . These parameters enabled us to calculate the interfacial energy (the solid–liquid interfacial tension,  $\gamma_{SL}$ ) and explore how it changes with the terminal modification of PPG. The values of  $\gamma_L$  and  $\theta$  obtained for the all examined PPGs are listed in Table 3. As presented, the lowest and the highest contact angle was observed for PPG–OH and PPG–OCH<sub>3</sub>, respectively. One can see that the

value of  $\theta$  increases in the same manner as it was observed previously in the case of decreasing  $\Delta T_c$ , which was assigned to a lowering ability of the formation of H bonds. As one can recall, contact angle provides a measure of wettability; thus, the better spreading out of a liquid drop on the examined surface, the smaller  $\theta$ . In this context, one can assume the presence of strong solid–liquid interactions, which decrease in the following order: PPG–OH  $\rightarrow$  PPG–NH<sub>2</sub>  $\rightarrow$  PPG–OCH<sub>3</sub>. Note that  $\theta$  of water is lower than 90°, indicating hydrophilic surface. On the other hand, no correlation between  $\gamma_L$  and PPG terminal group can be observed. In fact,  $\gamma_L$  is similar for the all examined PPGs.

Accordingly to Young's equation, a contact angle is related to solid surface energy (or solid–air interfacial tension,  $\gamma_S$ ),  $\gamma_{SL}$ , and  $\gamma_L$  in the following way:

$$\gamma_{SL} = \gamma_S - \gamma_L \cos \theta \quad (6)$$

As above-mentioned, both variables  $\gamma_L$  and  $\theta$  can be obtained directly from the measurements; thus, the only parameter required for further calculation is  $\gamma_S$ , which was estimated as follows. Note that the surface tension of a liquid (as well as any interfacial tension) is a sum of dispersive,  $d$ , and nondispersive components,  $nd$ :  $\gamma = \gamma^d + \gamma^{nd}$ ,<sup>59,60</sup> where the nondispersive contribution includes all parts of the interfacial tension resulting from nondispersion intermolecular interactions present in a liquid or solid phase, such as hydrogen bonds and base–acid interactions. When the work of adhesion is:

$$W_a = \gamma_L + \gamma_S - \gamma_{SL} \quad (7)$$

and assuming that:

$$W_a = 2(\sqrt{\gamma_S^d \gamma_L^d} + \sqrt{\gamma_S^{nd} \gamma_L^{nd}}) \quad (8)$$

the solid surface energy can be calculated with dispersive and nondispersive components accordingly to the following relation:

$$\frac{\gamma_L(1 + \cos \theta)}{2\sqrt{\gamma_L^d}} = \sqrt{\gamma_L^{nd}} \sqrt{\frac{\gamma_L^{nd}}{\gamma_L^d} \sqrt{\gamma_S^d}} \quad (9)$$

**Table 3.** Contact Angle at 298 K, Surface Tension of Samples (PPGs and Test Liquids) at 298 K, and Solid–Liquid Interfacial Tension of PPGs at 298 K and at  $T_g$  (from Table 2)<sup>a</sup>

sample	$\theta$ [deg]	$\gamma_L$ [mN m <sup>-1</sup> ]	$\gamma_{SL}$ at 298 K [mN m <sup>-1</sup> ]	$\gamma_{SL}$ at $T_g$ [mN m <sup>-1</sup> ]
PPG–OH	8.35	32.2	27.2	18.9
PPG–NH <sub>2</sub>	10	31.9	27.5	19.5
PPG–OCH <sub>3</sub>	14.0	31.6	27.9	18.1
water	45	71.7		
ethylene glycol	40.1	47.1		

<sup>a</sup>Surface tension for water and ethylene glycol were taken from ref 37.

For that purpose, some standard liquids, i.e., water and ethylene glycol, characterized by different distribution in dispersive and nondispersive contributions to surface tension, must be used. As reported in the literature, the dispersive and nondispersive parts of the surface tensions for water and ethylene glycol are as follows:  $\gamma^d = 21.8 \times 10^{-3} \text{ N m}^{-1}$ ,  $\gamma^{nd} = 51.0 \times 10^{-3} \text{ N m}^{-1}$  and  $\gamma^d = 29 \times 10^{-3} \text{ N m}^{-1}$ ,  $\gamma^{nd} = 17.4 \times 10^{-3} \text{ N m}^{-1}$ , respectively.<sup>29,61</sup> However, ethylene glycol is a much more dispersive liquid than water, what should give a reliable results of the surface energy applying the procedure proposed by Fowkes<sup>59</sup> and others.<sup>37,61–64</sup> Note that the purely dispersive solvents, such as i.e. bromobenzene or diiodomethane, could not be applied due to completely spreading out on the alumina surface. After all, the solid surface energy of alumina was estimated as  $\gamma_s = 58.97 \times 10^{-3} \text{ N m}^{-1}$  with a predominating nondispersive part  $\gamma^{nd} = 55.6 \times 10^{-3} \text{ N m}^{-1}$ . Therefore, having all the required data, we were able to estimate from Young's equation the values of the solid–liquid interfacial tension at 298 K and at  $T_g$  which are given in Table 3. Note that for calculation of  $\gamma_{SL}$  at  $T_g$  the surface tension was extrapolated using the temperature dependence of  $\gamma_l$  constructed from the values presented in Table 4, whereas  $\gamma_s$  and  $\cos \theta$  were assumed

**Table 4. Surface Tension of PPG Derivatives Determined in the Temperature Range 288–333 K**

temp [K]	$\gamma_l$ [mN m <sup>-1</sup> ]		
	PPG–OH	PPG–NH <sub>2</sub>	PPG–OCH <sub>3</sub>
288.2	32.96	32.73	
298.2	32.16	31.92	31.59
308.2	31.26	31.08	30.55
318.2	30.42	30.27	29.52
328.2	29.61	29.46	28.57
333.2			27.47

to be constant within a broad temperature range.<sup>29</sup> Interestingly, no difference in  $\gamma_{SL}$  between the examined PPGs can be observed, and despite previous dissimilarities,  $\gamma_{SL}$  of PPG–OH and PPG–OCH<sub>3</sub> reaches comparable value  $\gamma_{SL} \sim 27 \text{ mN m}^{-1}$  at 298 K (see Table 3). However, one can recall that recent work by Alexandris and co-workers<sup>29</sup> indicated that there is a correlation between  $\gamma_{SL}$  and the reduction of the glass

temperature of the confined systems with respect to the bulk. It was generalized that the higher  $\gamma_{SL}$ , the lower  $T_{g,confined}$ .

Thus, in order to examine this relationship in the case of modified PPG, we plotted the dependence of  $\Delta T_c$  and  $\Delta T_g$  versus interfacial energy at  $T_{g,bulk}$  for two pore diameters:  $d = 18 \text{ nm}$  and  $d = 150 \text{ nm}$ , as presented in Figure 7. It should be mentioned that previously only the dependence of  $\Delta T_g$  on  $\gamma_{SL}$  has been examined. However, herein, we also explored how the  $T_c$ , the glass transition temperature of the polymers attached to the interface, which should be directly related to the interfacial interactions, changes with  $\gamma_{SL}$ . Note that  $\Delta T_c = T_c - T_{g,bulk}$  while  $\Delta T_g = T_{g,bulk} - T_{g,confined}$ . Although  $\gamma_{SL}$  seems to be similar in all examined PPG's, a clear trend in variation of  $\Delta T_c(\gamma_{SL})$  can be noted (see arrows in Figure 7). As illustrated,  $\Delta T_c$  changes according to the decreasing ability in the formation of H bonds in the following order: PPG–OH  $\rightarrow$  PPG–NH<sub>2</sub>  $\rightarrow$  PPG–OCH<sub>3</sub> for the constant  $\gamma_{SL}$ . This simple relationship indicates that except of the interfacial energy also some strong specific interactions, such as H bonds or ionic, must be also taken into account to predict the variation of the glass transition temperature of the adsorbed polymers. On the other hand, a closer inspection of the data presented in Figure 7b showed that the  $T_g$  of the core macromolecules remains similar (within experimental uncertainty) in each studied herein PPG when plotted versus  $\gamma_{SL}$ . In addition, we also added our data to those reported in ref 29 in Figure 8. As can be observed, there is almost perfect agreement with the general trend reported by Alexandris et al.<sup>29</sup> Thus, according to the above, it is assumed that the stronger surface interactions, the lower  $T_g$ . Nevertheless, one has to remember that many theoretical and experimental studies on the polymers under 1D confinement reported the opposite effects. Accordingly to those works, strong surface interactions, including specific interactions (hydrogen bonding), have been suggested to reduce the interfacial mobility in molecular glasses and polymers leading to the higher  $T_g$ .<sup>53,65</sup> Interestingly, a similar finding, manifested in the shift of the  $T_c$  to the higher temperatures due to increasing strength of the specific interactions, was reported herein. Therefore, we believe that the observed depression of  $T_g$  should be interpreted as a consequence of the enhancement of  $\Delta T_c$  caused by the variation in the interfacial energy or formation of the specific interactions between host and guest molecules/

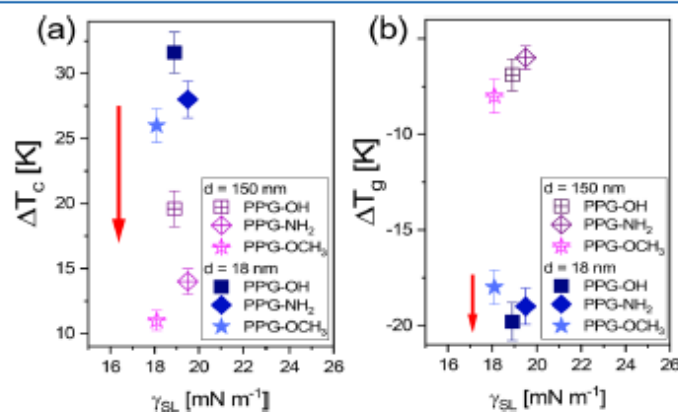


**Figure 7.** Dependence of  $\Delta T_c$  and  $\Delta T_g$  vs solid–liquid interfacial tension at  $T_{g,bulk}$  for all investigated PPGs incorporated in pores of indicated diameter:  $d = 18 \text{ nm}$  and  $d = 150 \text{ nm}$ .

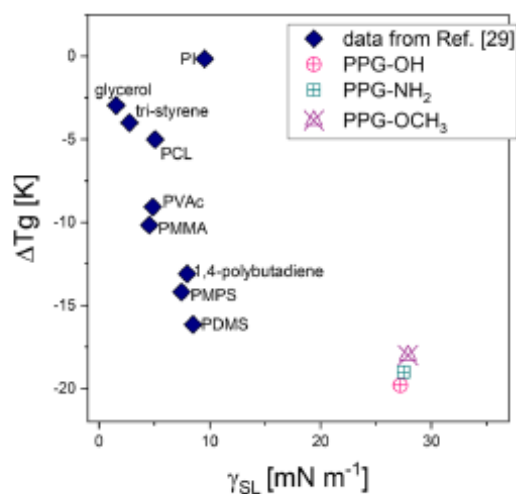


Figure 8.  $\Delta T_g$  for PPG's incorporated into nanochannels of  $d=18$  nm plotted versus  $\gamma_{SL}$  at 298K. Additional data obtained for polymers confined in pores in varying diameter (where  $25 \text{ nm} < d < 65 \text{ nm}$ ) were taken from ref 29.

polymers. Although, as discussed in the literature, also stiffness and roughness of the interface<sup>66–68</sup> have an impact on the glass transition temperature of the core polymers.

Having all that said one should also address an important issue. As it is well presented herein and in other papers the drop in the glass transition temperature of the core polymers is well correlated to the increase in  $T_c$  that raises with decreasing pore size in each studied herein chemically modified PPG. Therefore, one could expect that there will be also a similar trend, i.e., the higher glass transition temperature of the adsorbed polymers, the larger drop in  $T_g$  of the core macromolecules in the investigated materials. On the other hand, as discussed above, there is no such clear relationship. To explain that one can remind that there are several factors contributing to the determination of the glass transition temperature of the core polymers. First, it should be reminded that  $T_{g,confined}$  was estimated for the experimental data extrapolated to  $\tau_\alpha(T_g) = 100$  s. Second, as shown by some of us below the crossover temperature there is always physical equilibration manifested by the continuous shift of the segmental process to the lower frequencies in both low molecular weight glass-formers and nonmodified PPG. Third, the change in  $\tau_\alpha(T)$  at  $T_c$  strictly depends on the sensitivity of the segmental relaxation to the density fluctuation.<sup>56</sup> Finally, also thermal history and cooling rate have tremendous impact on the vitrification of the core molecules/polymers. Therefore, all these factors contribute more or less to the experimental finding that there is no direct correlation between increase in  $T_c$  and drop in  $T_g$  in the investigated PPG's.

## CONCLUSIONS

In this study, we examined the behavior of modified PPG derivatives, where the terminated groups  $-OH$  were replaced by the following structures:  $-NH_2$  and  $-OCH_3$ . Such relatively small chemical modification allowed to modify the interactions with the  $-OH$  groups attached to the walls of applied AAO templates and indicated the impact of both surface and specific interactions on the properties of the confined systems. As

observed, the glass transition temperature of the polymers attached to the pore walls increases with the ability of H bonds formation in the following order:  $PPG-OH \rightarrow PPG-NH_2 \rightarrow PPG-OCH_3$ . In this context, it should be noted that all these polymers are characterized by very similar interfacial energy with the alumina. On the other hand, no such relationship is observed in the case of the  $T_g$  of the core macromolecules. Moreover, one can note that the reduction in  $T_g$  of the investigated PPG's correlates well with an increase in  $\gamma_{SL}$ , as reported for various polymers confined in nanoporous alumina templates. Although, we have related the observed depression of  $T_g$  to the variation in the glass transition temperature of the interfacial layer ( $\Delta T_c$ ). However, there are also other factors, such as time scale of the physical equilibration taking place below  $T_c$ , thermal history of the sample, sensitivity of the segmental relaxation to the density fluctuations, roughness, and stiffness of the surface that may contribute to the glass transition temperature of the core polymers. We believe that these data will contribute significantly to the discussion on the impact of interfacial interactions on the molecular dynamics of polymers under 2D confinement.

## AUTHOR INFORMATION

### Corresponding Authors

\*(A.T.) E-mail: agnieszka.talik@smcebi.edu.pl.

\*(K.K.) E-mail: kamil.kaminski@us.edu.pl; kamil.kaminski@smcebi.edu.pl.

### ORCID

Agnieszka Talik: 0000-0001-7940-6967

Magdalena Tarnacka: 0000-0002-9444-3114

Paulina Maksym: 0000-0002-8506-7102

### Notes

The authors declare no competing financial interest.

## ACKNOWLEDGMENTS

K.K., K.W. and P.M. are thankful for financial support from the Polish National Science Centre (Dec. no. 2015/17/B/ST3/01195).

## REFERENCES

- (1) Forrest, J. A.; Dalnoki-Veress, K.; Stevens, J. R.; Dutcher, J. R. Effect of Free Surfaces on the Glass Transition Temperature of Thin Polymer Films. *Phys. Rev. Lett.* **1996**, *77*, 2002.
- (2) Ellison, C. J.; Torkelson, J. M. The Distribution of Glass-Transition Temperatures in Nanoscopically Confined Glass Formers. *Nat. Mater.* **2003**, *2*, 695.
- (3) Blaszczyk-Lezak, I.; Hernandez, M.; Mijangos, C. One Dimensional PMMA Nanofibers from AAO Templates. Evidence of Confinement Effects by Dielectric and Raman Analysis. *Macromolecules* **2013**, *46*, 4995–5002.
- (4) Duran, H.; Gitsas, A.; Floudas, G.; Mondeshki, M.; Steinhart, M.; Knoll, W. Poly( $\gamma$ -benzyl-L-glutamate) Peptides Confined to Nanoporous Alumina: Pore Diameter Dependence of Self-Assembly and Segmental Dynamics. *Macromolecules* **2009**, *42*, 2881–2885.
- (5) Krut'eva, M.; Wischniewski, A.; Monkenbusch, M.; Willner, L.; Maiz, J.; Mijangos, C.; Arbe, A.; Colmenero, J.; Radulescu, A.; Holderer, O.; Ohl, M.; Richter, D. Effect of Nanoconfinement on Polymer Dynamics: Surface Layers and Interphases. *Phys. Rev. Lett.* **2013**, *110*, 119901.
- (6) Sergeev, A.; Chen, D.; Lee, D. H.; Russell, T. P. Segmental Dynamics of Polymers During Capillary Flow into Nanopores. *Soft Matter* **2010**, *6*, 1111–1113.

- (7) Alexandris, S.; Sakellariou, G.; Steinhart, M.; Floudas, G. Dynamics of Unentangled *cis*-1,4-Polyisoprene Confined to Nanoporous Alumina. *Macromolecules* **2014**, *47*, 3895–3900.
- (8) Schonhals, A.; Rittig, F.; Karger, J. Self-diffusion of Poly(propylene Glycol) in Nanoporous Glasses Studied by Pulsed Field Gradient NMR: A Study of Molecular Dynamics and Surface Interactions. *J. Chem. Phys.* **2010**, *133*, 094903.
- (9) Petychakis, L.; Floudas, G.; Fleischer, G. Chain Dynamics of Polyisoprene Confined in Porous Media. A Dielectric Spectroscopy Study. *Europhys. Lett.* **1997**, *40*, 685.
- (10) Schonhals, A.; Goering, H.; Schick, Ch.; Frick, B.; Zorn, R. Glassy Dynamics of Polymers Confined to Nanoporous Glasses Revealed by Relaxational and Scattering Experiments. *Eur. Phys. J. E: Soft Matter Biol. Phys.* **2003**, *12*, 173.
- (11) Ellison, C. J.; Ryszowski, R. L.; Fredin, N. J.; Torkelson, J. M. Dramatic Reduction of the Effect of Nanoconfinement on the Glass Transition of Polymer Films via Addition of Small-molecule Diluent. *Phys. Rev. Lett.* **2004**, *92*, 095702.
- (12) Keddie, J. L.; Jones, R. A. L.; Cory, R. A. Size-dependent Depression of the Glass Transition Temperature in Polymer Films. *Europhys. Lett.* **1994**, *27*, 59.
- (13) Yang, C.; Onitsuka, R.; Takahashi, I. Confinement Effects on Glass Transition Temperature, Transition Breadth, and Linear Expansivity: an Ultrashort X-ray Reflectivity Study on Supported Ultrathin Polystyrene Films. *Eur. Phys. J. E: Soft Matter Biol. Phys.* **2013**, *36*, 1–8.
- (14) Fakhrabi, Z.; Sharp, J. S.; Forrest, J. A. Effect of Sample Preparation on the Glass-transition of Thin Polystyrene Films. *J. Polym. Sci., Part B: Polym. Phys.* **2004**, *42*, 4503–4507.
- (15) Lu, H.; Chen, W.; Russell, T. P. Relaxation of Thin Films of Polystyrene Floating on Ionic Liquid Surface. *Macromolecules* **2009**, *42*, 9111–9117.
- (16) Napolitano, S.; Wubbenhorst, M. The Lifetime of the Deviations from Bulk Behaviour in Polymers Confined at the Nanoscale. *Nat. Commun.* **2011**, *2*, 260.
- (17) Napolitano, S.; Lupascu, V.; Wubbenhorst, M. Temperature Dependence of the Deviations from Bulk Behavior in Ultrathin Polymer Films. *Macromolecules* **2008**, *41*, 1061–1063.
- (18) Napolitano, S.; Rotella, C.; Wubbenhorst, M. Can Thickness and Interfacial Interactions Unvocally Determine the Behavior of Polymers Confined at the Nanoscale? *ACS Macro Lett.* **2012**, *1*, 1189–1193.
- (19) Rotella, C.; Napolitano, S.; Vandendriessche, S.; Valev, V. K.; Verbiest, T.; Larkowska, M.; Kucharski, S.; Wubbenhorst, M. Adsorption Kinetics of Ultrathin Polymer Films in the Melt Probed by Dielectric Spectroscopy and Second-Harmonic Generation. *Langmuir* **2011**, *27*, 13533.
- (20) Keddie, J. L.; Jones, R. A. L.; Cory, R. A. Interface and Surface Effects on the Glass-Transition Temperature in Polymer-Films. *Faraday Discuss.* **1994**, *98*, 219–230.
- (21) Fryer, D. S.; Nealey, P. F.; de Pablo, J. J. Scaling of T<sub>g</sub> and Reaction Rate with Film Thickness in Photoresist: A Thermal Probe Study. *J. Vac. Sci. Technol., B: Microelectron. Process. Phenom.* **2000**, *18*, 3376.
- (22) Fryer, D. S.; Peters, R. D.; Kim, E. J.; Tomaszewski, J. E.; de Pablo, J. J.; Nealey, P. F.; White, C. C.; Wu, W.-L. Dependence of the Glass Transition Temperature of Polymer Films on Interfacial Energy and Thickness. *Macromolecules* **2001**, *34*, 5627–5634.
- (23) Lang, R. J.; Merling, W. L.; Simmons, D. S. Combined Dependence of Nanoconfined T<sub>g</sub> on Interfacial Energy and Softness of Confinement. *ACS Macro Lett.* **2014**, *3*, 758–762.
- (24) Torres, J. A.; Nealey, P. F.; de Pablo, J. J. de Pablo, J. J. Molecular Simulation of Ultrathin Polymeric Films near the Glass Transition. *Phys. Rev. Lett.* **2000**, *85*, 3221.
- (25) Napolitano, S.; Glynos, E.; Tito, N. B. Glass Transition of Polymers in Bulk, Confined Geometries, and Near Interfaces. *Rep. Prog. Phys.* **2017**, *80*, 036602.
- (26) Napolitano, S.; Sferazza, M. How Irreversible Adsorption Affects Interfacial Properties of Polymers. *Adv. Colloid Interface Sci.* **2017**, *247*, 172–177.
- (27) Perez-de-Eulate, N. G.; Sferazza, M.; Cangialosi, D.; Napolitano, S. Irreversible Adsorption Erases the Free Surface Effect on the T<sub>g</sub> of Supported Films of Poly(4-*tert*-butylstyrene). *ACS Macro Lett.* **2017**, *6*, 354–358.
- (28) Panagopoulou, A.; Napolitano, S. Irreversible Adsorption Governs the Equilibration of Thin Polymer Films. *Phys. Rev. Lett.* **2017**, *119*, 097801.
- (29) Alexandris, S.; Papadopoulos, P.; Sakellariou, G.; Steinhart, M.; Butt, H.-J.; Floudas, G. Interfacial Energy and Glass Temperature of Polymers Confined to Nanoporous Alumina. *Macromolecules* **2016**, *49*, 7400–7414.
- (30) Stockmayer, W. H. Dielectric Dispersion in Solutions of Flexible Polymers. *Pure Appl. Chem.* **1967**, *15*, 539–554.
- (31) Tarnacka, M.; Kaminski, K.; Mapesa, E. U.; Kaminska, E.; Paluch, M. Studies on the Temperature and Time Induced Variation in the Segmental and Chain Dynamics in Poly(propylene glycol) Confined at the Nanoscale. *Macromolecules* **2016**, *49*, 6678–6686.
- (32) <http://www.synkerainc.com/products-services/unikeraceramic-membranes/uniker-a-standard>.
- (33) *Infrared and Raman Characteristic Group Frequencies: Tables and Charts*, 3rd ed.; Socrates, G., Ed.; Wiley: 2004.
- (34) Jacob, C.; Sangoro, J. R.; Papadopoulos, P.; Schubert, T.; Naumov, S.; Valiullin, R.; Karger, J.; Kremer, F. Charge Transport and Diffusion of Ionic Liquids in Nanoporous Silica Membranes. *Phys. Chem. Chem. Phys.* **2010**, *12*, 13798.
- (35) Kipnusu, W. K.; Kossack, W.; Jacob, C.; Jasiurkowska, M.; Sangoro, J.; Kremer, F. Molecular Order and Dynamics of Tris-(2ethylhexyl)phosphate Confined in Uni-Directional Nanopores. *Z. Phys. Chem.* **2012**, *226*, 797.
- (36) Wandschneider, A.; Lehmann, J. K.; Heintz, A. Surface Tension and Density of Pure Ionic Liquids and Some Binary Mixtures with 1-propanol and 1-butanol. *J. Chem. Eng. Data* **2008**, *53*, 596–599.
- (37) Feder-Kubis, J.; Geppert-Rybczyńska, M.; Musiał, M.; Talić, E.; Guzik, A. Exploring the Surface Activity of a Homologues Series of Functionalized Ionic Liquids with a Natural Chiral Substituent: (–)-Menthhol in a Cation. *Colloids Surf., A* **2017**, *529*, 725–732.
- (38) Havriliak, S.; Negami, S. A Complex Plane Analysis of  $\alpha$ -dispersions in Some Polymer Systems. *J. Polym. Sci., Part C: Polym. Symp.* **1966**, *14*, 99–117.
- (39) Kremer, F.; Schonhals, A. *Broadband Dielectric Spectroscopy*; Springer: Berlin, 2003.
- (40) Angell, C. A. Entropy and Fragility in Supercooling Liquids. *J. Res. Natl. Inst. Stand. Technol.* **1997**, *102*, 171–185.
- (41) Ngai, K. L.; Roland, C. M. Chemical Structure and Intermolecular Cooperativity: Dielectric Relaxation Results. *Macromolecules* **1993**, *26*, 6824–6830.
- (42) Zheng, Q.; Durben, D. J.; Wolf, G. H.; Angell, C. A. Liquids at Large Negative Pressures: Water at the Homogeneous Nucleation Limit. *Science* **1991**, *254*, 829–83.
- (43) Debenedetti, P. G.; Stillinger, F. H. Supercooled Liquids and the Glass Transition. *Nature* **2001**, *410*, 259–267.
- (44) Dudowicz, J.; Freed, K. F.; Douglas, J. F. The Glass Transition Temperature of Polymer Melts. *J. Phys. Chem. B* **2005**, *109*, 21285–21292.
- (45) Kaminski, K.; Kipnusu, W. K.; Adrjanowicz, K.; Mapesa, E. U.; Jacob, C.; Jasiurkowska, M.; Włodarczyk, P.; Grzybowska, K.; Paluch, M.; Kremer, F. Comparative Study on the Molecular Dynamics of a Series of Polypropylene Glycols. *Macromolecules* **2013**, *46*, 1973–1980.
- (46) Pissis, P.; Kyritsis, A.; Daoulaki, D.; Barut, G.; Pelster, R.; Nimitz, G. Dielectric Studies of Glass Transition in Confined Propylene Glycol. *J. Phys.: Condens. Matter* **1998**, *10*, 6205–6227.
- (47) Park, J.-Y.; McKenna, G. B. Size and Confinement Effects on the Glass Transition Behavior of Polystyrene/*o*-Terphenyl Polymer Solutions. *Phys. Rev. B: Condens. Matter Mater. Phys.* **2000**, *61*, 6667.

- (48) Li, L. L.; Zhou, D. S.; Huang, D. H.; Xue, G. Double Glass Transition Temperatures of Poly(methyl methacrylate) Confined in Alumina Nanotube Templates. *Macromolecules* **2014**, *47*, 297–303.
- (49) Adrjanowicz, K.; Kolodziejczyk, K.; Kipnusu, W. K.; Tarnacka, M.; Mapesa, E. U.; Kaminska, E.; Pawlus, S.; Kaminski, K.; Paluch, M. Decoupling Between the Interfacial and Core Molecular Dynamics of Salol in 2D Confinement. *J. Phys. Chem. C* **2015**, *119*, 14366–14374.
- (50) He, F.; Wang, L.-L.; Richert, R. Dynamics of Supercooled Liquids in the Vicinity of Soft and Hard Interfaces. *Phys. Rev. B: Condens. Matter Mater. Phys.* **2005**, *71*, 144205.
- (51) Richert, R. Dynamics of Nanoconfined Supercooled Liquids. *Annu. Rev. Phys. Chem.* **2011**, *62*, 65–84.
- (52) Mapesa, E. U.; Popp, L.; Kipnusu, W. K.; Tress, M.; Kremer, F. Molecular Dynamics in 1- and 2-D Confinement as Studied for the Case of Poly(*Cis*-1,4-Isoprene). *Soft Mater.* **2014**, *12*, S22–S30.
- (53) Tarnacka, M.; Kaminska, E.; Kaminski, K.; Roland, C. M.; Paluch, M. Interplay between Core and Interfacial Mobility and its Impact on the Measured Glass Transition. Dielectric and Calorimetric Studies. *J. Phys. Chem. C* **2016**, *120*, 7373–7380.
- (54) Kipnusu, W. K.; Elsayed, M.; Kossack, W.; Pawlus, S.; Adrjanowicz, K.; Tress, M.; Mapesa, E. U.; Krause-Rehberg, R.; Kaminski, K.; Kremer, F. Confinement for More Space: a Larger Free Volume and Enhanced Glassy Dynamics of 2-ethyl-1-hexanol in Nanopores. *J. Phys. Chem. Lett.* **2015**, *6*, 3708–3712.
- (55) Kipnusu, W. K.; Elsayed, M.; Krause-Rehberg, R.; Kremer, F. Glassy Dynamics of Polymethylphenylsiloxane in One- and Two-dimensional Nanometric Confinement—A Comparison. *J. Chem. Phys.* **2017**, *146*, 203302.
- (56) Adrjanowicz, K.; Kaminski, K.; Koperwas, K.; Paluch, M. Negative Pressure Vitrification of the Isochorically Confined Liquid in Nanopores. *Phys. Rev. Lett.* **2015**, *115*, 265702.
- (57) Tarnacka, M.; Kipnusu, W. K.; Kaminska, E.; Pawlus, S.; Kaminski, K.; Paluch, M. The peculiar Behavior of Molecular Dynamics of Glass-forming Liquid Confined in the Native Porous Materials - The Role of Negative Pressure. *Phys. Chem. Chem. Phys.* **2016**, *18*, 23709–23714.
- (58) Soklarz, G.; Adrjanowicz, K.; Tarnacka, M.; Piontek, J.; Paluch, M. Confinement-Induced Changes in the Glassy Dynamics and Crystallization Behavior of Supercooled Fenofibrate. *J. Phys. Chem. C* **2018**, *122*, 1384–1395.
- (59) Fowkes, F. M. Attractive forces and interfaces. *Ind. Eng. Chem.* **1964**, *56*, 40–52.
- (60) Jańczuk, B.; Białopiotrowicz, T.; Zdziennicka, A. Some Remarks on the Components of the Liquid Surface Free Energy. *J. Colloid Interface Sci.* **1999**, *211*, 96–103.
- (61) Vicente, C. M. S.; André, P. S.; Ferreira, R. A. S. Simple Measurement of Surface Free Energy Using a Web Cam. *Rev. Bras. Ensino Fis.* **2012**, *34*, 3312.
- (62) Hejda, F.; Solař, P.; Kousal, J. Surface Free Energy Determination by Contact Angle Measurements – A Comparison of Various Approaches. *WDS'10 Proceedings of Contributed Papers, Part III*, 25–30, 2010.
- (63) Kalin, M.; Polajnar, M. The Correlation Between the Surface Energy, the Contact Angle and the Spreading Parameter, and Their Relevance for the Wetting Behavior of DLC with Lubricating Oils. *Tribol. Int.* **2013**, *66*, 225–233.
- (64) Kalin, M.; Polajnar, M. The Wetting of Steel, DLC Coatings, Ceramics and Polymers with Oils and Water: The Importance and Correlations of Surface Energy, Surface Tension, Contact Angle and Spreading. *Appl. Surf. Sci.* **2014**, *293*, 97–108.
- (65) Laventure, A.; Gujral, A.; Lebel, O.; Pellerin, C.; Ediger, M. D. Influence of Hydrogen Bonding on the Kinetic Stability of Vapor-Deposited Glasses of Triazine Derivatives. *J. Phys. Chem. B* **2017**, *121*, 2350–2358.
- (66) Mirigian, S.; Schweizer, K. S. Influence of Chemistry, Interfacial Width, and Non-Isothermal Conditions on Spatially Heterogeneous Activated Relaxation and Elasticity in Glass-Forming Free Standing Films. *J. Chem. Phys.* **2017**, *146*, 203301.
- (67) Lang, R. J.; Merling, W. L.; Simmons, D. S. Combined Dependence of Nanoconfined T<sub>g</sub> on Interfacial Energy and Softness of Confinement. *ACS Macro Lett.* **2014**, *3*, 758.
- (68) Baglay, R. R.; Roth, C. B. Local Glass Transition Temperature T<sub>g</sub>(z) of Polystyrene Next to Different Polymers: Hard vs. Soft Confinement. *J. Chem. Phys.* **2017**, *146*, 203307.

## **A2. Impact of the Interfacial Energy and Density Fluctuation on the Shift of the Glass-Transition Temperature of Liquids Confined in Pores.**

Autorzy: A. Talik, M. Tarnacka, M. Geppert-Rybczynska, A. Minecka, E. Kaminska, K. Kaminski, M. Paluch.

Referencja: J. Phys. Chem. C 2019, 123, 5549–5556

DOI: 10.1021/acs.jpcc.8b12551

Impact Factor czasopisma z roku opublikowania pracy: 4.189

Liczba punktów ministerialnych MNiSW czasopisma (2019): 140

Mój udział w pracy polegał na: przeglądzie literaturowym, zaplanowaniu eksperymentu, przygotowaniu próbek- substancji litych oraz infiltrowanych do nanoporowatych membran, wykonaniu pomiarów dielektrycznych a następnie analizie otrzymanych wyników oraz ich dyskusji, wykonaniu rysunków, uczestniczeniu w dyskusji wyników oraz tworzeniu manuskryptu a także w formułowaniu odpowiedzi na uwagi recenzentów.



# Impact of the Interfacial Energy and Density Fluctuations on the Shift of the Glass-Transition Temperature of Liquids Confined in Pores

Agnieszka Talik,<sup>\*,†,‡</sup> Magdalena Tarnacka,<sup>†,‡</sup> Monika Geppert-Rybczynska,<sup>§</sup> Aldona Minecka,<sup>||</sup> Ewa Kaminska,<sup>||</sup> Kamil Kaminski,<sup>\*,†,‡</sup> and Marian Paluch<sup>†,‡</sup>

<sup>†</sup>Institute of Physics and <sup>‡</sup>Silesian Center of Education and Interdisciplinary Research, University of Silesia, 75 Pułku Piechoty 1A, 41-500 Chorzow, Poland

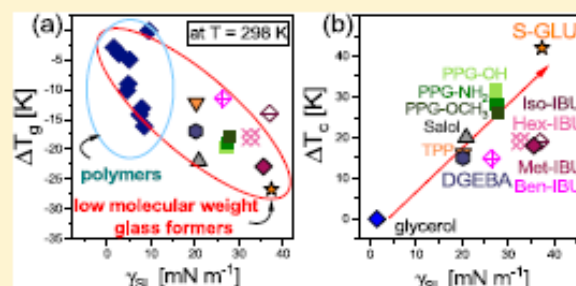
<sup>§</sup>Institute of Chemistry, University of Silesia, Szkolna 9, 40-006 Katowice, Poland

<sup>||</sup>Department of Pharmacognosy and Phytochemistry, School of Pharmacy with the Division of Laboratory Medicine in Sosnowiec, Medical University of Silesia in Katowice, Jagiellonska 4, 41-200 Sosnowiec, Poland

## Supporting Information

**ABSTRACT:** The behavior of the low- and high-molecular weight glass formers confined in nanoporous templates remains an unsolved puzzle despite the intensive long-term studies in this matter. Special effort is taken to understand the enhancement of segmental or structural dynamics and the depression of the glass-transition temperatures,  $T_g$ s in materials infiltrated in pores of the nanometric size. In this paper, we have analyzed dielectric, calorimetric, and contact angle data collected for various systems to determine which factors are responsible for these effects. It turned out that with increasing interfacial energy, molecules attached to the pore walls (interfacial layer) vitrify at higher temperatures.

Moreover, the dynamics of core molecules starts to deviate from bulk-like behavior. Therefore, a greater depression of the glass-transition temperature,  $T_g$ , of this fraction of molecules is noted. Also, it was found that the sensitivity of structural dynamics to the density fluctuations, quantified by the pressure coefficient of the glass-transition temperature,  $dT_g/dp$ , is another useful parameter to predict the shift of the glass-transition temperature of the confined glass formers. The results presented herein emphasize the great importance of surface effects, which play a primary role in a unified description of the impact of the nanometric spatial restriction on the dynamics of confined materials.



## 1. INTRODUCTION

Intensive studies carried out over the last 20 years allowed to better understand the impact of various kinds of nanometrical spatial confinement on the molecular dynamics and evolution of the glass transition in the high (polymers) and low molecular-weight glass formers. As already established, the behavior of the soft matter under confinement seems to be governed by a few factors, that is, finite size, interfacial interactions (together with the processes occurring at the interface<sup>1</sup>), surface properties (including roughness and polarity of the template/substrate), free volume,<sup>2,3</sup> conformational changes,<sup>4–7</sup> negative pressure effects,<sup>8,9</sup> and time.<sup>1,10,11</sup> Nevertheless, although many aspects of the nanometrical spatial restriction are already well-understood, the detailed molecular picture of this complex problem is still missing, and many following questions (i.e., how to predict more precisely the direction and magnitude of the shift of the glass-transition temperature, the variation in the segmental/structural relaxation process? Or if there is any link between the behavior

of the materials deposited as thin films or incorporated into porous matrices?) are yet to be addressed.

It has been shown that the direction and magnitude of the shift in  $T_g$  for the polymer deposited as thin films (defined herein as one-dimensional confinement, 1D) strictly depend on the intermolecular potential<sup>12</sup> and the interfacial energy,  $\gamma_{SL}$ ,<sup>13,14</sup> between the material and the substrate. The increase in both parameters leads to a rise of the  $T_g$  of the deposited macromolecules, independently on the chemistry of the polymer films of the same thickness. It is worthwhile to add those specific intermolecular interactions, such as H-bonds, having a strong impact on the lowering mobility of the interfacial layer and increase of the glass-transition temperature. On the other hand, for macromolecules and low-molecular-weight glass formers infiltrated into nanopores of varying diameters, generally, a completely different behavior

Received: December 30, 2018

Revised: February 13, 2019

Published: February 13, 2019

(depression of the  $T_g$ ) is observed.<sup>4,15,16</sup> One can recall that many various theories and ideas have been applied to address this phenomenon more carefully. In this context, one can mention about the concept of negative pressure in nanocavities that develops during cooling<sup>9</sup> or the role of the dynamical heterogeneities that do not grow because of geometry restriction posed by the pores, and so forth.<sup>8</sup> Nevertheless, recently Alexandris et al.<sup>15</sup> have postulated that the depression of the  $T_g$  of the materials confined in the porous templates is governed by the interfacial energy. Surprisingly, in contrast to polymers deposited as thin films, they reported that the increase of  $\gamma_{SL}$  leads to a reduction in  $T_g$ .<sup>9,15,17</sup> Therefore, a different pattern of behavior in the shift of  $T_g$  between the materials deposited as thin films and infiltrated into the porous matrix with respect to the variation in the interfacial energy seems to be a puzzle. In this context, one should ask: what is the reason for that? The answer to this question is of great importance for finding a unified description of the impact of 1D and 2D confinement on the dynamics of spatially restricted materials.

To fulfill this significant gap in our understanding of the above-mentioned issue, we have examined twelve various low- and high-molecular-weight glass formers, from which we have chosen three systems: glycerol, hexyl-2-[4-(2-methylpropyl)phenyl]propanoate (Hex-IBU), and bisphenol-A diglycidyl ether (DGEBA), as representative examples of markedly different behavior under spatial restriction imposed by alumina (AAO) nanoporous templates of pore size  $d = 18$  nm. The application of dielectric spectroscopy and differential scanning calorimetry (DSC), together with the surface tension and contact angle measurements, enabled us to follow the difference in the molecular dynamics of all investigated nanomaterials because of their different macroscopic properties (especially their interfacial energy,  $\gamma_{SL}$ ). The variation in the glass-transition temperatures of all materials plotted versus their  $\gamma_{SL}$  was compared with the literature data, indicating a fundamental relationship giving an opportunity to predict the behavior of the soft matter under 2D confinement. In addition, we have shown that besides the interfacial energy also the sensitivity of the structural process to the density fluctuations plays an important role in better understanding the behavior of the confined liquids. We believe that the obtained data enable us to explain many results, often considered as contradictory, that is, no deviation in the temperature dependence of the structural relaxation times and the lack of the two glass-transition phenomena reported for some materials under 2D spatial restriction.

## 2. EXPERIMENTAL SECTION

**2.1. Materials.** Glycerol, bisphenol-A diglycidyl ether (DGEBA), phenyl salicylate (salol), and triphenyl phosphite (TPP) with purity higher than 98% were supplied by Sigma-Aldrich. 1,2,3,4,6-penta-*O*-(trimethylsilyl)- $\alpha$ -D-glucopyranose (S-GLU) (the mixture of  $\alpha$ - and  $\beta$ -anomers) was synthesized for this paper, according to the procedure presented in ref 18. The purity of the sample was greater than 99%. Methyl, isopropyl, hexyl, and benzyl esters of ibuprofen (Met-IBU, methyl-2-[4-(2-methylpropyl)phenyl]propanoate; Iso-IBU, propane-2-yl 2-[4-(2-methylpropyl)phenyl]propanoate; Hex-IBU, hexyl-2-[4-(2-methylpropyl)phenyl]propanoate; and Ben-IBU, benzyl-2-[4-(2-methylpropyl)phenyl]propanoate) of greater than 98% purities were synthesized according to the procedure reported in ref 19. The chemical structures of all

examined compounds are presented in the Supporting Information (Figure S1). The nanoporous aluminum oxide membranes used in this study (supplied from Synkera Co and InRedox) are composed of uniaxial channels (open from both sides) with well-defined pore diameter (Figure S1).

**2.2. Sample Preparation.** Before filling, AAO membranes were dried in an oven at  $T = 423$  K in a vacuum ( $10^{-2}$  bar) for  $t = 24$  h to remove any volatile impurities from the nanochannels. After cooling, they were placed in liquid samples. Then, the whole system was maintained at  $T = 298$  K in a vacuum ( $10^{-2}$  bar) for  $t = 6$  h to let compounds flow into the nanocavities. After completing the infiltration process, the surface of the AAO membrane was dried, and the excess sample from the surface was removed by the use of a metal blade and paper towel. In the experiment, we used the membranes of pore diameter,  $d = 18$  nm.

**2.3. Methods.** **2.3.1. Broadband Dielectric Spectroscopy.** Isobaric measurements of the complex dielectric permittivity,  $\epsilon^*(\omega) = \epsilon'(\omega) - i\epsilon''(\omega)$ , were carried out using the Novocontrol Alpha dielectric spectrometer over the frequency range from  $10^{-2}$  to  $10^6$  Hz at ambient pressure. The temperature stability controlled by Quatro Cryosystem using nitrogen gas cryostat was better than 0.1 K. Dielectric measurements of bulk samples were performed in a parallel-plate cell (diameter: 10 mm, gap: 0.1 mm) immediately after the preparation of liquid samples. AAO membranes filled with investigated materials were also placed in a similar capacitor (diameter: 10 mm, membrane thickness: 0.05 mm).<sup>20,21</sup> Nevertheless, confined samples are heterogeneous dielectrics composed of a matrix and an investigated compound. Because the applied electric field is parallel to the long pore axes, the equivalent circuit consists of two capacitors in parallel composed of  $\epsilon_{\text{compound}}^*$  and  $\epsilon_{\text{AAO}}^*$ . Thus, the measured total impedance is related to the individual values through  $1/Z_c^* = 1/Z_{\text{compound}}^* + 1/Z_{\text{AAO}}^*$ . It should be added that dielectric measurements on empty membranes were also carried out to evaluate the contribution of AAO, which turned out to be negligible to the recorded data. Dielectric measurements were performed in the temperature range  $T = 171$ – $293$  K for the bulk and confined systems.

**2.3.2. Differential Scanning Calorimetry.** Calorimetric measurements were carried out using a Mettler-Toledo DSC apparatus (Mettler-Toledo International, Inc., Greifensee, Switzerland) equipped with a liquid nitrogen cooling accessory and an HSS8 ceramic sensor (heat flux sensor with 120 thermocouples). Temperature and enthalpy calibrations were performed by using indium and zinc standards. Measurements were carried out on bulk and the crushed membranes filled with the examined compounds. The samples were contained in sealed crucibles, with a heating rate of 10 K/min, over a temperature range from 140 to 300 K.

**2.3.3. Surface Tension and Contact Angle Measurements.** The surface tension of liquids  $\gamma_L$  (pendant-drop method) and contact angle  $\theta$  were measured with the DSA 100S Krüss Tensiometer, GmbH Germany. The description of the instrument and procedures has been presented previously.<sup>22,23</sup> The measuring procedure at 298.2 K for all substances has been repeated dozen or more times. The temperature measurements uncertainty was  $\pm 0.1$  K, whereas the uncertainty of surface tension was  $\pm 0.1$  mN·m<sup>-1</sup>. Density,  $\rho$ , required for the surface tension experiment was measured with an Anton Paar DMA 5000M densimeter with the uncertainty not worse than 0.0001 g·cm<sup>-3</sup>.

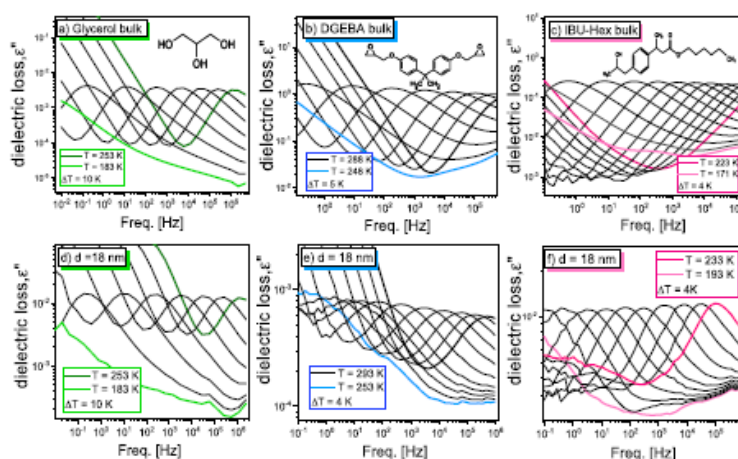


Figure 1. Dielectric spectra of bulk and confined systems measured above their glass-transition temperatures. Black and d color curves correspond to the data taken at different temperatures. As insets, the chemical structures of investigated compounds are presented.

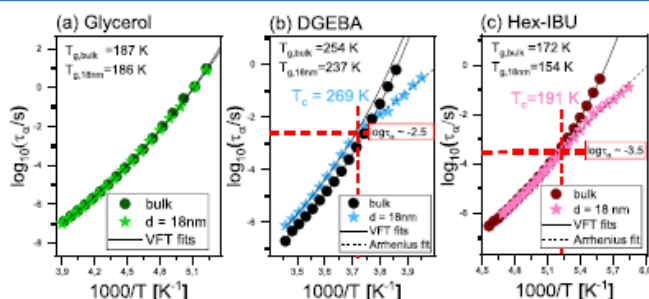


Figure 2. Temperature dependences of structural relaxation times for indicated samples. Black solid and dashed lines are the best fits using VFT and Arrhenius equations, respectively.

The contact angle on the aluminum oxide was registered in a thermostated chamber at  $T = 298$  K as the average of several independent measurements during minimum 2–3 min (for drops with constant shape and constant contact angle value). The uncertainty of temperature measurements was  $\pm 0.5$  K, the precision of contact angle measurements was  $0.01^\circ$ , and the estimated uncertainty was  $\pm 1.5^\circ$ .

### 3. RESULTS AND DISCUSSION

Dielectric spectra of three representative bulk and confined systems collected above  $T_g$  are presented in Figure 1. Note that the data for DGEBA (bulk and confined) and Hex-IBU (bulk) were taken from refs 24 and 19, respectively. It should be mentioned that all dielectric measurements were performed using the same protocol, where samples were quenched and measured on heating. As shown, all spectra reveal the presence of the dc conductivity at the lowest frequencies, related to the charge transport, and the structural relaxation ( $\alpha$ -process) at higher frequencies, reflecting the cooperative motions of the

whole molecules and responsible for the liquid-to-glass transition.

To get more detailed information into the dynamics of the examined bulk and confined samples, collected loss spectra were analyzed with the use of the Havriliak–Negami (HN) function<sup>25</sup> with an additional conductivity term

$$\epsilon''(\omega) = \frac{\epsilon_{dc}}{\epsilon_0 \omega} + \epsilon_\infty + \frac{\Delta\epsilon_1}{[1 + (i\omega\tau_{HN})^\alpha]^\beta} \quad (1)$$

where  $\alpha$  and  $\beta$  are the shape parameters representing the symmetric and asymmetric broadening of the given relaxation peaks,  $\Delta\epsilon$  is the dielectric relaxation strength,  $\tau_{HN}$  is the HN relaxation time,  $\epsilon_0$  is the vacuum permittivity, and  $\omega$  is an angular frequency ( $\omega = 2\pi f$ ). Note that the relaxation times of structural,  $\tau_\alpha$  process were estimated from  $\tau_{HN}$  according to the equation given in ref 26.

The determined structural relaxation times for the bulk and confined materials plotted versus the inverse temperature are

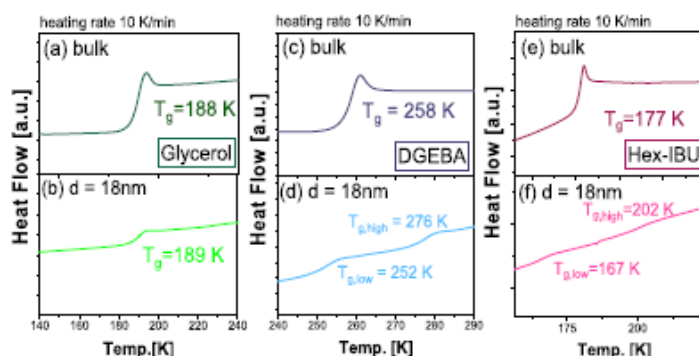


Figure 3. DSC thermograms obtained for the bulk and confined systems.

shown in Figure 2. As observed, the temperature evolutions of the structural relaxation times differ significantly from each other. In the case of confined glycerol,  $\tau_a(T)$  dependence remains bulk-like, whereas for Hex-IBU and DGEBA incorporated in alumina pores, the structural relaxation times start to deviate from the macroscopic sample at some specific crossover temperatures. For this paper, we label this temperature as  $T_c$ . Because of this experimental finding, the relaxation times obtained for the latter systems were fitted by a combination of the Vogel–Fulcher–Tammann (VFT) and Arrhenius equations. Above  $T_c$ , the VFT equation was applied

$$\tau_a = \tau_\infty \exp\left(\frac{D_T T_0}{T - T_0}\right) \quad (2)$$

where  $\tau_\infty$  is the relaxation time at finite temperature,  $T_0$  is the value of temperature, where  $\tau$  goes to infinity,  $D_T$  is the fragility parameter; whereas below  $T_c$  the Arrhenius equation was used

$$\tau_a = \tau_\infty \exp\left(\frac{E_a}{k_B T}\right) \quad (3)$$

where  $k_B$  is the Boltzmann constant and  $E_a$  is the activation energy. Note that in the case of confined systems, the VFT equation was used only for an accurate determination of a point (temperature), at which the slope changes; whereas  $T_g$ s of confined compounds were estimated from the extrapolation of the Arrhenius fits.

It should be stressed that the bulk-like behavior of confined glycerol in the whole examined range of temperature (see Figure 2a) is consistent with the previous reports showing a similar behavior of this compound infiltrated into pores made of different materials and various diameters.<sup>27–29</sup> On the other hand, the dynamics of confined DGEBA is retarded at high temperatures (Figure 2b), whereas confined Hex-IBU reveals bulk-like properties well above  $T_c$ , see Figure 2c. Moreover, as noted above, there is a change from the VFT to the Arrhenius-like behavior in  $\tau_a(T)$ -dependence of DGEBA and Hex-IBU confined in AAO templates. This change in the structural dynamics occurs at some specific temperature condition,  $T_c$  (see Figure 2b,c). Numerous dielectric and calorimetric studies reported in the literature indicated that this phenomenon is strictly related to the vitrification of the interfacial layer.<sup>6,17,28,30</sup> Moreover, this experimental observation is consistent with a simple model proposed by Park and

McKenna<sup>31</sup> and Arndt et al.<sup>32</sup> (the so-called “two-layer model”) that describes the heterogeneity of the materials confined in nanoporous matrices. According to this simple approach, there are two fractions of molecules, characterized by different mobility and  $T_g$ : (i) those attached to the surface of applied nanochannels (interfacial layer), interacting with the surface of the walls of alumina pores and characterized by the higher  $T_g$  than the bulk sample, and (ii) those located at the center of the nanochannels (described as a “core” set) of the  $T_g$  lower than the macroscale compound. Although, it should be mentioned that Arndt et al.<sup>32</sup> suggested that the discrepancy between  $\tau_a(T)$  dependence of the bulk and confined samples may be related to the exchange process between interfacial and core molecules as well. Consequently, the enhanced dynamics detected in Hex-IBU and DGEBA might be assigned to the variation in the packing density at the interface. Interestingly, in ref 32, authors also provided an explanation of the presence or absence of the relaxation process of the interfacial layer in loss spectra measured for the confined liquids. They postulated that it is because of the interplay between the time scale of the exchange process and the experiment. If the exchange between core and interfacial molecules is slow with respect to the time of experiments, two relaxation processes can be detected. In the opposite situation, only one dominant structural process is expected. Nevertheless, it should also be added that in contrast to our calorimetric data, Arndt et al.<sup>32</sup> reported only a single glass-transition temperature for each sample confined in the silica pores they have measured.

Additionally, one can note that the change from the VFT to the Arrhenius-like behavior in  $\tau_a(T)$  dependence of DGEBA and Hex-IBU confined in AAO templates occurs at different structural relaxation times,  $\log_{10} \tau_a(T_c) \approx -2.5$  and  $\log_{10} \tau_a(T_c) \approx -3.5$  for the former and the latter sample, respectively. It means that most likely the glass-transition temperature of the interfacial layer increases more in Hex-IBU with respect to DGEBA.

Next, we determined the values of both: the glass transition of the core molecules,  $T_g$  and the interfacial fraction,  $T_c$ <sup>33</sup> from the dielectric data. It should be mentioned that the  $T_c$  was identified as a temperature where  $\tau_a(T)$  of the confined liquids starts to deviate from the bulk behavior. On the other hand, the  $T_g$  was defined as the temperature at which  $\tau_a = 100$  s. The obtained values of  $T_g$ s and  $T_c$ s are added to Figure 2. As presented, the  $T_g$  decreases with confinement or remains bulk-

like (glycerol), whereas  $T_c$  increases with decreasing pore size, as usually reported for the materials incorporated in pores.

On the basis of the data presented in Figure 2, one can notice a quite peculiar behavior of the glycerol under confinement for which  $\tau_\alpha(T)$  remains bulk-like in the whole range of temperatures. Consequently, the  $T_g$  of the confined compound matches perfectly the one determined for the bulk sample. In one of our previous papers, we claimed that it is due to the weak sensitivity of the structural dynamics to the density variation, which can be easily quantified by the ratio of the activation enthalpy at constant volume and constant pressure ( $E_v/E_p$  ratio).<sup>8</sup> Briefly,  $E_v/E_p$  ratio varies in the range of 0–1, where both limiting values imply that the dynamics are governed by either volume ( $E_v/E_p = 0$ ) or temperature ( $E_v/E_p = 1$ ) fluctuations.<sup>34</sup> It was shown that the lower  $E_v/E_p$  ratio, the more pronounced variation in  $\tau_\alpha(T)$ -dependence at  $T_c$  is expected.<sup>8</sup> Because the structural dynamics of glycerol is characterized by the pretty high  $E_v/E_p = 0.94$ ,<sup>35</sup> no confinement effect should be observed under spatial restriction conditions.<sup>8</sup> Therefore, the unique behavior of glycerol infiltrated in AAO membranes of  $d = 18$  nm might be related to the fact that structural relaxation is predominantly a thermally activated process. Alternatively, one can hypothesize that glycerol might be very weakly attached to the pore surface, forming an interfacial layer of similar dynamics to the core molecules. However, this scenario seems to be controversial if one takes into account that this polyalcohol has three hydroxyl units that may form H-bonds with alumina. Anyway, to verify this hypothesis, we performed comprehensive calorimetry measurements on the bulk glycerol, and the sample infiltrated into alumina pores of  $d = 18$  nm.

Interestingly, the obtained thermograms revealed that the confined glycerol, similar to the bulk material, displays only one glass-transition temperature. On the other hand, for DGEBA and Hex-IBU incorporated into AAO templates, two  $T_g$ s can be detected, see Figure 3. It is worthwhile to add that there is a quite good correspondence between the low and the high glass-transition temperature and  $T_g$  and  $T_c$  estimated from dielectric data. That simply means that the  $T_c$  and the  $T_g$  are, in fact, related to the vitrification of the interfacial layer and core molecules, respectively. Some discrepancies between both characteristic temperatures are probably because of different cooling rates applied during dielectric and calorimetric studies.

Presented herein are the results that seem to be quite surprising considering the chemical structure of the investigated compounds. One can note that DGEBA and Hex-IBU do not have any OH units capable of forming as strong H-bonds as glycerol (see the insets in Figure 1). Nevertheless, there is a clear additional high glass-transition temperature indicating the vitrification of the interfacial layer for the confined DGEBA and Hex-IBU. Interestingly in the case of the polyalcohol, such a scenario does not occur. The lack of the second glass-transition temperature in the confined glycerol does not mean that the interfacial layer is not formed. One may suppose that in this particular case, both fractions of the molecules (core and interfacial) have similar dynamics and glass-transition temperatures (Table 1).

To get a better insight into this issue, we performed further surface tension,  $\gamma_L$ , and contact angle,  $\theta$ , measurements allowing the calculation of the interfacial energy,  $\gamma_{SL}$ ; see the Supporting Information. These kind of measurements enabled us to measure the strength of interactions between the host (alumina) and confined compounds. One can add that

**Table 1.** Values of  $T_g$ s and  $T_c$ s Obtained for the Confined Samples from Calorimetric and Dielectric Measurements

sample	BDS measurements		DSC measurements	
	$T_c$ [K]	$T_g$ [K] for $\log_{10} \tau_\alpha = 2$	$T_{g,low}$ [K]	$T_{g,high}$ [K]
		Glycerol		
bulk		187		188
18 nm		186		189
		DGEBA		
bulk		254		258
18 nm	269	237	252	276
		Hex-IBU		
bulk		172		177
18 nm	191	154	167	202

generally in literature, another approach based on the functionalization/silanization of the native pores is applied to elucidate host–guest interactions and its impact on the molecular dynamics of confined samples. This issue has been explored intensively by Kremer's group.<sup>6,20,21</sup> They found quite a strong impact of the pore functionality on the behavior of liquids infiltrated into nanochannels. On the other hand, determination of the interfacial energy allows the strength of interactions between the porous material and infiltrated liquids to be quantified more precisely and makes more general conclusions. It is also worthwhile to add that the contact angle, surface tension, and interfacial energy were calculated for the liquid samples measured at  $T = 298$  K. Apart from glycerol, DGEBA, and Hex-IBU, we have also examined nine other materials infiltrated within AAO templates and plotted the difference between the glass-transition temperature of the bulk material ( $T_{g,bulk}$ ) and  $T_g$  of the core molecules ( $T_g$ ), where  $\Delta T_g = T_g - T_{g,bulk}$  versus  $\gamma_{SL}$  together with the literature data measured for polymers and some low molecular glass formers taken from ref 15 (see Figure 4a). Note that for this purpose, we used only  $T_g$ s determined from the dielectric data for the materials incorporated into nanopores of the smallest diameter ( $d = 18$  nm), having the same thermal history (measured on heating after cooling the samples below  $T_g$ ). As presented, all points follow the general trend reported before for the materials incorporated into porous templates.<sup>15</sup> However, at first sight, two different dependences: the first for macromolecules and the second for the low-molecular weight-glass formers, marked by blue and red circles, respectively, can be observed.

Moreover, we would like to draw the attention of the reader to one very important issue that explains the presence or absence of the two glass-transition phenomena reported for many liquids infiltrated into porous templates. As can be observed, glycerol is characterized by the extremely low interfacial energy,  $\gamma_{SL} = 1.5$  mN·m<sup>-1</sup>, whereas  $\gamma_{SL}$  of the two other compounds is equal to 20 and 33 mN·m<sup>-1</sup> for DGEBA<sup>24</sup> and Hex-IBU, respectively. Moreover, one can also note that glycerol is characterized by the relatively high contact angle,  $\theta = 63^\circ$ , and surface tension,  $\gamma_L = 60$  mN·m<sup>-1</sup>, whereas in the case of other materials, we determined the following values of these parameters:  $\theta = 35^\circ$  and  $\gamma_L = 47.41$  mN·m<sup>-1</sup>, as well as  $\theta = 7^\circ$  and  $\gamma_L = 26.5$  mN·m<sup>-1</sup> for DGEBA and Hex-IBU, respectively (see Table S1). This simple comparison enabled us to certify that in contrast to the latter systems, glycerol weakly wets and interacts with alumina. Therefore, it seems that the observed behavior might be used further to explain the absence of the second high glass-transition temperature for the

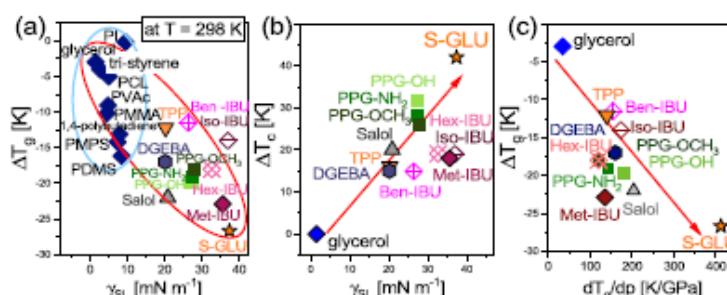


**Figure 4.** Panels (a,b): interfacial energy dependences of  $\Delta T_g$  (a) and  $\Delta T_c$  (b) for various low- and high-molecular-weight compounds. Panel (c): dependence of  $\Delta T_g$  vs the pressure coefficient of the glass-transition temperature ( $dT_g/dp$ ). Blue data were taken from ref 15, whereas those for PPGs, DGEBA, salol, and TPP were taken from refs. 1,7,24,30,4 respectively. For details concerning the following steps of the analysis together with the description of applied techniques, please see the Supporting Information.

confined polyalcohol. Consequently, we might conclude that good wettability and strong interactions between host and guest materials are important parameters that are responsible for the formation of the stable interfacial layer of reduced mobility.

For a better understanding of the correlation between  $\Delta T_g$  and  $\gamma_{SL}$  found in Figure 4a, we also examined the changes in  $T_c$  assigned to the vitrification of the interfacial layer with respect to the glass-transition temperature of the bulk material (where  $\Delta T_c = T_c - T_{g,bulk}$ ) as a function of the interfacial energy, see Figure 4b. As shown, the experimental points follow the linear trend. We found that the higher the  $\gamma_{SL}$ , the higher the  $\Delta T_c$ , which seems to correspond very well with the data collected for the thin polymer films, where the strong interactions increase the  $T_g$ . In this context, one can suppose that with increasing value of the surface tension between the liquid and the matrix, an additional very effective constraint, leading to a decrease in configurational entropy, is imposed on the molecules attached to the pore walls. This effect is equivalent to the situation as if a smaller volume was available to the molecules of the liquid. Both of these factors contribute to the rise in the glass-transition temperature of the interfacial layer.

Moreover, a direct comparison of the data shown in Figure 4a,b enabled us to formulate a more fundamental conclusion. In the case of the samples characterized by the low interfacial energy, no departure from the VFT behavior and the lack of the double glass-transition phenomenon are expected. Moreover, the reported changes in the molecular dynamics of the confined systems (mainly polymers) seem to be because of finite size effects enforcing the changes in the molecular or chain conformations, density fluctuations, and so forth. On the other hand, for compounds characterized by the higher  $\gamma_{SL}$  (in our case, low-molecular-weight materials), structural relaxation times determined for the confined samples start to deviate from the ones obtained for the bulk samples because of the vitrification of the interfacial molecules at  $T_c$ . The stronger the interactions with the matrix, the  $T_c$  generally shifts to higher temperatures. That agrees with the data reported in Figure 2, where the deviation of the  $\tau_a(T)$  dependence from the bulk behavior also shifts in the same way for the confined DGEBA and Hex-IBU. Consequently, the  $T_g$  of the materials incorporated into porous templates decreases with increasing  $\gamma_{SL}$ . This effect is in some way similar to that described by

Stevenson et al.,<sup>36</sup> who showed that dynamics near the surface of glasses is much faster with respect to the bulk sample.

However, as shown in Figure 4a, this rule is not always satisfied because we can easily find systems characterized by the same interfacial energy and much different depression of the glass-transition temperature under confinement. To explain this experimental finding, we also decided to consider the sensitivity of the structural process to the density fluctuations, which can be quantified by the pressure coefficient of the glass-transition temperature,  $dT_g/dp$  (see Supporting Information). For that purpose, we either collected the values of  $dT_g/dp$  from the literature or determined this parameter from the high-pressure measurements performed on the bulk samples; see the Supporting Information. As shown in Figure 4c, the depression of the glass transition of the confined liquids correlates quite well with the  $dT_g/dp$  ratio. In fact, when we take into account this parameter, one can easily explain various depression of the  $T_g$  for materials characterized by similar interfacial energy. This relationship can be illustrated by comparing two sets of data: (1) collected for 1,2,3,4,6-penta-*O*-(trimethylsilyl)-*D*-glucopyranose (S-GLU,  $\gamma_{SL} \approx 37 \text{ mN}\cdot\text{m}^{-1}$ ) and isopropyl derivative of ibuprofen (Iso-IBU,  $\gamma_{SL} \approx 37 \text{ mN}\cdot\text{m}^{-1}$ ) and (2) obtained for DGEBA ( $\gamma_{SL} \approx 20 \text{ mN}\cdot\text{m}^{-1}$ ),<sup>24</sup> phenyl salicylate (salol,  $\gamma_{SL} \approx 20 \text{ mN}\cdot\text{m}^{-1}$ ), and TPP ( $\gamma_{SL} \approx 20 \text{ mN}\cdot\text{m}^{-1}$ ). Each group has comparable/constant  $\gamma_{SL}$ , whereas the  $dT_g/dp$  ratio differs significantly. One can see that with the higher pressure coefficient of the glass-transition temperature (that means the higher sensitivity of the structural process to the density fluctuations/density packing), the greater depression of the  $T_g$  for the materials incorporated into the nanoporous matrix is detected. Therefore, besides the wettability, surface tension, and interfacial energy, also  $dT_g/dp$  must be considered to understand better the variation of the molecular dynamics of the liquids infiltrated into nanoporous templates.

#### 4. CONCLUSIONS

In conclusion, we have examined 12 various low- and high-molecular-weight glass formers, characterized by different molecular dynamics and behavior under geometrical constraint conditions using dielectric spectroscopy and Differential Scanning Calorimetry. These studies were also combined with the contact angle measurements that enabled us to get insights into the wettability and strength of interactions between host and guest materials. Variation in the molecular dynamics of the confined compounds turned out to be directly

correlated with the interfacial energy. As observed,  $T_g$  of the materials incorporated into pores decreases with increasing  $\gamma_{SL}$ , because of the rise of the glass-transition temperature of the interfacial molecules attached to the walls of alumina. Surprisingly, for the materials characterized by very low values of  $\gamma_{SL}$  (i.e., glycerol), no confinement effects nor double glass-transition phenomenon were detected. This indicates that there might be some threshold value of  $\gamma_{SL}$ , below which the surface interactions are too weak to induce these effects. Moreover, we noted that the degree of depression of the  $T_g$  of the confined liquids depends on the  $dT_g/dp$  ratio calculated from the high-pressure measurements of the bulk samples. By plotting our data together with the literature ones, it was found that the knowledge about the interfacial energy and the pressure coefficient of the  $T_g$  gives us relatively easy and reliable opportunity to estimate the direction and magnitude of the variation in the vitrification temperature of the liquids confined in pores. We believe that the presented herein data are of fundamental interest in the context of a proper interpretation of many, often discussed as contradictory results, and emphasize the impact of surface interactions and density fluctuations on the behavior of the spatially restricted materials.

## ■ ASSOCIATED CONTENT

### Supporting Information

The Supporting Information is available free of charge on the ACS Publications website at DOI: 10.1021/acs.jpcc.8b12551.

Description of surface tension and contact angle measurements and the determination of the pressure sensitivity of the structural relaxation,  $dT_g/dp$  (PDF)

## ■ AUTHOR INFORMATION

### Corresponding Authors

\*E-mail: agnieszka.talik@smcebi.edu.pl (A.T.).

\*E-mail: kamil.kaminski@us.edu.pl, kamil.kaminski@smcebi.edu.pl (K.K.).

### ORCID

Agnieszka Talik: 0000-0001-7940-6967

Magdalena Tarnacka: 0000-0002-9444-3114

Aldona Minecka: 0000-0001-5603-032X

Ewa Kaminska: 0000-0001-9725-8654

Kamil Kaminski: 0000-0002-5871-0203

### Notes

The authors declare no competing financial interest.

## ■ ACKNOWLEDGMENTS

K.K. is thankful for the financial support from the Polish National Science Centre within the OPUS project (Dec. no 2015/17/B/ST3/01195). M.T. is thankful for the financial support from the Foundation for Polish Science (FNP).

## ■ REFERENCES

- (1) Napolitano, S.; Wubbenhorst, M. The Lifetime of the Deviations From Bulk Behavior in Polymers Confined at the Nanoscale. *Nat. Commun.* **2011**, *2*, 260.
- (2) Napolitano, S.; Rotella, C.; Wubbenhorst, M. Can Thickness and Interfacial Interactions Univocally Determine the Behavior of Polymers Confined at the Nanoscale? *ACS Macro Lett.* **2012**, *1*, 1189–1193.
- (3) White, R. P.; Lipson, J. E. G. Connecting Pressure-Dependent Dynamics to Dynamics under Confinement: The Cooperative Free

Volume Model Applied to Poly(4-chlorostyrene) Bulk and Thin Films. *Macromolecules* **2018**, *51*, 7924–7941.

(4) Tarnacka, M.; Kaminska, E.; Kaminski, K.; Roland, C. M.; Paluch, M. Interplay between Core and Interfacial Mobility and its Impact on the Measured Glass Transition. Dielectric and Calorimetric Studies. *J. Phys. Chem. C* **2016**, *120*, 7373–7380.

(5) Minecka, A.; Kaminska, E.; Tarnacka, M.; Talik, A.; Grudzka-Flak, I.; Wolnica, K.; Dulski, M.; Kaminski, K.; Paluch, M. Conformational Changes Underlying Variation in the Structural Dynamics of the Materials Confined at the Nanometric Scale. *Phys. Chem. Chem. Phys.* **2018**, *20*, 30200–30208.

(6) Jasiurkowska-Delaporte, M.; Kossack, W.; Kipnusu, W. K.; Sangoro, J. R.; Iacob, C.; Kremer, F. Glassy Dynamics of Two Poly(ethylene glycol) Derivatives in the Bulk and in Nanometric Confinement as Reflected in its Inter- and Intra-molecular Interactions. *J. Chem. Phys.* **2018**, *149*, 064501.

(7) Gin, P.; Jiang, N.; Liang, Ch.; Taniguchi, T.; Akgun, B.; Satija, S. K.; Endoh, M. K.; Koga, T. Revealed Architectures of Adsorbed Polymer Chains at Solid-Polymer Melt Interfaces. *Phys. Rev. Lett.* **2012**, *109*, 265501.

(8) Adrjanowicz, K.; Kaminski, K.; Koperwas, K.; Paluch, M. Negative Pressure Vitrification of the Isochorically Confined Liquid in Nanopores. *Phys. Rev. Lett.* **2015**, *115*, 265702.

(9) Tarnacka, M.; Kipnusu, W. K.; Kaminska, E.; Pawlus, S.; Kaminski, K.; Paluch, M. The Peculiar Behavior of Molecular Dynamics of Glass-forming Liquid Confined in the Native Porous Materials – the Role of Negative Pressure. *Phys. Chem. Chem. Phys.* **2016**, *18*, 23709–23714.

(10) Napolitano, S.; Capponi, S.; Vanroy, B. Glassy Dynamics of Soft Matter under 1D Confinement: How Irreversible Adsorption Affects Molecular Packing, Mobility Gradients and Orientational Polarization in Thin Films. *Eur. Phys. J. E* **2013**, *36*, 61.

(11) Tarnacka, M.; Madejczyk, O.; Kaminski, K.; Paluch, M. Time and Temperature as Key Parameters Controlling Dynamics and Properties of Spatially Restricted Polymers. *Macromolecules* **2017**, *50*, 5188–5193.

(12) Torres, J. A.; Nealey, P. F.; de Pablo, J. J. Molecular Simulation of Ultrathin Polymeric Films near the Glass Transition. *Phys. Rev. Lett.* **2000**, *85*, 3221–3224.

(13) Fryer, D. S.; Peters, R. D.; Kim, E. J.; Tomaszewski, J. E.; de Pablo, J. J.; Nealey, P. F.; White, C. C.; Wu, W.-L. Dependence of the Glass Transition Temperature of Polymer Films on Interfacial Energy and Thickness. *Macromolecules* **2001**, *34*, 5627–5634.

(14) Lang, R. J.; Merling, W. L.; Simmons, D. S. Combined Dependence of Nanoconfined Tg on Interfacial Energy and Softness of Confinement. *ACS Macro Lett* **2014**, *3*, 758–762.

(15) Alexandris, S.; Papadopoulos, P.; Sakellariou, G.; Steinhart, M.; Butt, H.-J.; Floudas, G. Interfacial Energy and Glass Temperature of Polymers Confined to Nanoporous Alumina. *Macromolecules* **2016**, *49*, 7400–7414.

(16) Zhang, C.; Li, L.; Wang, X.; Xue, G. Stabilization of Poly(methyl methacrylate) Nanofibers with Core–Shell Structures Confined in AAO Templates by the Balance between Geometric Curvature, Interfacial Interactions, and Cooling Rate. *Macromolecules* **2017**, *50*, 1599–1609.

(17) Talik, A.; Tarnacka, M.; Grudzka-Flak, I.; Maksym, P.; Geppert-Rybczynska, M.; Kaminska, E.; Kaminski, K.; Paluch, M. The Role of Interfacial Energy and Specific Interactions on the Behavior of Poly(propylene glycol) Derivatives under 2D Confinement. *Macromolecules* **2018**, *51*, 4840–4852.

(18) Minecka, A.; Kaminska, E.; Tarnacka, M.; Dzienia, A.; Madejczyk, O.; Waliko, P.; Kasprzycka, A.; Kamiński, K.; Paluch, M. High Pressure Studies on Structural and Secondary Relaxation Dynamics in Silyl Derivative of Glucose. *J. Chem. Phys.* **2017**, *147*, 064502.

(19) Minecka, A.; Kaminska, E.; Heczko, D.; Tarnacka, M.; Grudzka-Flak, I.; Bartoszek, M.; Zięba, A.; Wrzalik, R.; Śmieszek-Lindert, W. E.; Dulski, M.; et al. Studying Molecular Dynamics of the

Slow, Structural and Secondary Relaxation Processes in Series of Substituted Ibuprofens. *J. Chem. Phys.* **2018**, *148*, 224505.

(20) Iacob, C.; Sangoro, J. R.; Papadopoulos, P.; Schubert, T.; Naumov, S.; Valiullin, R.; Kärger, J.; Kremer, F. Charge Transport and Diffusion of Ionic Liquids in Nanoporous Silica Membranes. *Phys. Chem. Chem. Phys.* **2010**, *12*, 13798–13803.

(21) Kipnusu, W. K.; Kossack, W.; Iacob, C.; Jasiurkowska, M.; Rume Sangoro, J.; Kremer, F. Molecular Order and Dynamics of Tris(2ethylhexyl)phosphate Confined in Uni-Directional Nanopores. *Z. Phys. Chem.* **2012**, *226*, 797–805.

(22) Wandschneider, A.; Lehmann, J. K.; Heintz, A. Surface Tension and Density of Pure Ionic Liquids and Some Binary Mixtures with 1-propanol and 1-butanol. *J. Chem. Eng. Data* **2008**, *53*, 596–599.

(23) Feder-Kubis, J.; Geppert-Rybczyńska, M.; Musiał, M.; Talić, E.; Guzik, A. Exploring the Surface Activity of a Homologues Series of Functionalized Ionic Liquids with a Natural Chiral Substituent: (–)-Menthol in a Cation. *Colloids Surf., A* **2017**, *529*, 725–732.

(24) Tamacka, M.; Dulski, M.; Geppert-Rybczyńska, M.; Talić, A.; Kamińska, E.; Kamiński, K.; Paluch, M. Variation in the Molecular Dynamics of DGEBA Confined Within AAO Templates Above and Below the Glass Transition Temperature. *J. Phys. Chem. C* **2018**, *122*, 28033–28044.

(25) Havriliak, S.; Negami, S. A complex Plane Analysis of  $\alpha$ -dispersions in Some Polymer Systems. *J. Polym. Sci., Part C: Polym. Symp.* **2007**, *14*, 99–117.

(26) Kremer, F.; Schönhals, A. *Broadband Dielectric Spectroscopy*; Springer: Berlin, 2003.

(27) Brás, A. R.; Merino, E. G.; Neves, P. D.; Fonseca, I. M.; Dionísio, M.; Schönhals, A.; Correia, N. T. Amorphous Ibuprofen Confined in Nanostructured Silica Materials: A Dynamical Approach. *J. Phys. Chem. C* **2011**, *115*, 4616–4623.

(28) Kipnusu, W. K.; Elsayed, M.; Kossack, W.; Pawlus, S.; Adrjanowicz, K.; Tress, M.; Mapesa, E. U.; Krause-Rehberg, R.; Kamiński, K.; Kremer, F. Confinement for More Space: A Larger Free Volume and Enhanced Glassy Dynamics of 2-Ethyl-1-hexanol in Nanopores. *J. Phys. Chem. Lett.* **2015**, *6*, 3708–3712.

(29) Brás, A. R.; Fonseca, I. M.; Dionísio, M.; Schönhals, A.; Affouard, F.; Correia, N. T. Influence of Nanoscale Confinement on the Molecular Mobility of Ibuprofen. *J. Phys. Chem. C* **2014**, *118*, 13857–13868.

(30) Adrjanowicz, K.; Kolodziejczyk, K.; Kipnusu, W. K.; Tamacka, M.; Mapesa, E. U.; Kamińska, E.; Pawlus, S.; Kamiński, K.; Paluch, M. Decoupling between the Interfacial and Core Molecular Dynamics of Salol in 2D Confinement. *J. Phys. Chem. C* **2015**, *119*, 14366–14374.

(31) Park, J.-Y.; McKenna, G. B. Size and Confinement Effects on the Glass Transition Behavior of Polystyrene/*O*-terphenyl Polymer Solutions. *Phys. Rev. B: Condens. Matter Mater. Phys.* **2000**, *61*, 6667–6676.

(32) Arndt, M.; Stannarius, R.; Gorbatschow, W.; Kremer, F. Dielectric Investigations of the Dynamic Glass Transition in Nanopores. *Phys. Rev. E: Stat. Phys., Plasmas, Fluids, Relat. Interdiscip. Top.* **1996**, *54*, 5377–5390.

(33) Stöckel, F.; Fischer, E. W.; Richert, R. Dynamics of Glass-Forming Liquids. II. Detailed Comparison of Dielectric Relaxation, DC-conductivity, and Viscosity Data. *J. Chem. Phys.* **1996**, *104*, 2043–2055.

(34) Casalini, R.; Roland, C. M. Thermodynamical Scaling of the Glass Transition Dynamics. *Phys. Rev. E: Stat., Nonlinear, Soft Matter Phys.* **2004**, *69*, 062501.

(35) Roland, C. M.; Hensel-Bielowka, S.; Paluch, M.; Casalini, R. Supercooled Dynamics of Glass-Forming Liquids and Polymers under Hydrostatic Pressure. *Rep. Prog. Phys.* **2005**, *68*, 1405–1478.

(36) Stevenson, J. D.; Wolynes, P. G. On the Surface of Glasses. *J. Chem. Phys.* **2008**, *129*, 234514.



**A3.The influence of the nanocurvature on the surface interactions and molecular dynamics of model liquid confined in cylindrical pores**

Autorzy: A. Talik, M. Tarnacka, M. Wojtyniak, E. Kaminska, K. Kaminski, M. Paluch.

Referencja: Journal of Molecular Liquids 298 (2020) 111973

DOI: 10.1016/j.molliq.2019.111973

Impact Factor czasopisma z roku opublikowania pracy: 5.065

Liczba punktów ministerialnych MNiSW czasopisma (2019): 100

Mój udział w pracy polegał na: przeglądzie literaturowym, przygotowaniu materiału do badań, wykonaniu pomiarów dielektrycznych oraz uczestniczeniu w pomiarach AFM, analizie i przedstawieniu otrzymanych danych eksperymentalnych, dyskusji wyników. Współudział w redagowaniu treści manuskryptu oraz formułowanie odpowiedzi na uwagi recenzentów.



## The influence of the nanocurvature on the surface interactions and molecular dynamics of model liquid confined in cylindrical pores

Agnieszka Tali<sup>a,b,\*</sup>, Magdalena Tarnacka<sup>a,b</sup>, Marcin Wojtyniak<sup>a,b</sup>, Ewa Kaminska<sup>c</sup>, Kamil Kaminski<sup>a,b,\*\*</sup>, Marian Paluch<sup>a,b</sup>

<sup>a</sup> Institute of Physics, University of Silesia in Katowice, 75 Pułku Piechoty 1, 41-500, Chorzów, Poland

<sup>b</sup> Silesian Center of Education and Interdisciplinary Research, University of Silesia in Katowice, 75 Pułku Piechoty 1A, 41-500, Chorzów, Poland

<sup>c</sup> Department of Pharmacognosy and Phytochemistry, Faculty of Pharmaceutical Sciences in Sosnowiec, Medical University of Silesia Katowice, Poland



### ARTICLE INFO

#### Article history:

Received 14 July 2019

Received in revised form 19 September 2019

Accepted 18 October 2019

Available online 23 October 2019

#### Keywords:

Tolman length

Glass transition temperature

Finite size

Surface effects

Surface tension

Interfacial energy

### ABSTRACT

Currently, a great effort is put on the understanding of the effect of the nanometrical constraint on the dynamics of the soft materials. Recent studies by Alexandris et al. [*Macromolecules*, **2016**, 49, 7400–7414] and some of us [*J. Phys. Chem. C*, **2019**, 123, 5549–5556] revealed that the enhancement of the molecular mobility and depression in the glass transition of various low and high molecular weight glass formers infiltrated into Anodic Aluminum Oxide (AAO) templates strongly correlates with the strength of the interfacial interactions between the materials and the porous medium. However, in those investigations, one very important and fundamental aspect related to the variation in the wettability, the surface tension as well as the interfacial energy due to surface curvature has been completely overlooked. Herein, we have performed systematic and unique Atomic Force Microscopy (AFM) measurements on the model glass-forming liquid, glycerol (GLY), incorporated into porous AAO membranes of varying pore diameter. It was found that with increasing degree of confinement, the adhesion force between GLY and AFM tip decreases significantly. It seems that as indicated by the Tolman relation, the interfacial tension of the confined GLY drops leading to a better wetting of polyalcohol within the smallest pores. Interestingly, for this particular system (confined within templates of  $d = 10$  nm), a complementary Differential Scanning Calorimetry (DSC) investigations revealed the presence of the two glass transition temperatures upon heating runs. This indicated that the enhancement of the interactions between alumina and alcohol leads to the formation of the interfacial layer that vitrifies at higher temperature ( $T_{g,interfacial}$ ) than the bulk material. Interestingly, the observed double  $T_g$ s appeared only on heating. Moreover, different thermal protocols revealed the variation of the heat capacity jump corresponding to the glass transition temperature of the interfacial layer upon the annealing experiments, indicating the ongoing desorption process. In addition, it was also found that the structural dynamics of GLY incorporated within  $d = 10$  nm starts to deviate below  $T_{g,interfacial}$  from the behavior of the non-confined sample. Reported data are the first experimental evidence on the correlation between variation of the surface interactions with the substrate's curvature and enhancement of the dynamics of the confined liquids. Thus, a better understanding of the dynamics of confined soft matter, especially the relation between the finite size and surface interactions can be gained.

© 2019 Published by Elsevier B.V.

### 1. Introduction

The liquid-to-glass transition remains one of the most explored and still unsolved phenomena of condensed soft matter for the last half-century. Although many theoretical and experimental investigations

focusing on the role of free volume, entropy, cooperativity, spatial heterogeneity have been carried out, no consensus on the nature and origin of the glass transition has been achieved yet [1–3].

An interesting and promising approach allowing to verify current concepts of the glass transition, especially the ones related to the dynamical heterogeneities and free volume, is studying the behavior of supercooled liquids confined at the nanoscale. However, due to the perturbation in density and intermolecular interactions introduced by substrate or nanoporous template, the understanding of basic physical properties as well as dynamics of soft matter at such conditions becomes a complex and challenging task. Generally, the variation in mobility and glass transition temperature,  $T_g$ , is considered as being

\* Corresponding author. Institute of Physics, University of Silesia in Katowice, 75 Pułku Piechoty 1, 41-500, Chorzów, Poland.

\*\* Corresponding author. Institute of Physics, University of Silesia in Katowice, 75 Pułku Piechoty 1, 41-500, Chorzów, Poland.

E-mail addresses: [agnieszka.tali@smcebi.edu.pl](mailto:agnieszka.tali@smcebi.edu.pl) (A. Tali), [kamil.kaminski@us.edu.pl](mailto:kamil.kaminski@us.edu.pl), [kamil.kaminski@smcebi.edu.pl](mailto:kamil.kaminski@smcebi.edu.pl) (K. Kaminski).

related to the interplay between several factors, i.e., finite size, surface effects, free volume, substrate roughness, etc. [4,5]. Interestingly, for some substances under nanometrical confinement, the bifurcation of the relaxation times was observed [5,24,28,29,35], which was assigned to the double glass transition phenomenon related to the vitrification of the core and interfacial molecules, respectively. Moreover, it should be pointed out that recent studies have clearly highlighted the impact of surface interactions on the dynamics of materials infiltrated in porous membranes [4,6]. Interestingly, an increasing interfacial energy,  $\gamma_{SL}$ , leads to a depression of  $T_g$  of confined systems when compared to the bulk samples [4]. However, it should be mentioned that, in fact, the reduction of the  $T_g$  results from the increase of the glass transition temperature of the interfacial molecules attached to the pore walls,  $T_{g,interfacial}$ , with increasing  $\gamma_{SL}$  [5,6], what is consistent with the data reported for the polymers deposited as thin films [7,8].

At this point, one can emphasize that generally,  $\gamma_{SL}$  is evaluated for the materials deposited on planar surfaces; while in the case of cylindrical nanocavities, the infiltrated liquids wet/interact with surfaces curved to the nanometric scale. As discussed in the literature, there are fundamental differences in wetting planar and curved surfaces. Just to mention that the interface curvature inhibits the first order wetting transition observed for planar surfaces [9]. In this context, the behavior of soft matter near the curved interface seems to be somewhat different, since most likely the interfacial energy, the surface tension and density could be affected by the curvature [10]. This issue was well addressed by Gibbs [11], who has shown that the surface tension,  $\gamma_L$ , gets a function of curvature  $1/R$  of the interphase boundary if the surface of a liquid is curved [11]. Furthermore, this approach was developed by Tolman [12–15], leading to the following expression linking the variation of the surface tension with the interface curvature:

$$\gamma_L(R) = \gamma_L \left( 1 - \frac{2\delta}{R} \right) \quad (1)$$

where  $R$  is a liquid drop radius,  $\gamma_L(R)$  and  $\gamma_L$  are the surface tension of curved and planar surfaces, respectively [15]. The relationship mentioned above indicates the presence of an additional parameter called the Tolman length,  $\delta$ , describing a curvature dependence of the surface tension. This new variable, of the order of  $\delta \approx 0.3$  nm, defines a distance between equimolar surface,  $R_e$ , and the surface of tension,  $R_s$ , where  $\delta = R_e - R_s$ . According to Eq. (1), the surface tension deviates significantly from its planar value, when the droplet radius has a nanometrical size or is of the order of  $\delta$ . However, surprisingly, both theoretical and experimental studies have also shown that  $\gamma_L$  starts to deviate from its planar value for the curvatures even smaller than Tolman length, i.e., in the case of liquids confined within mesoporous templates (pore size,  $d = 2$ – $50$  nm) [15,48,49] and references therein. Therefore, a decrease in pore diameter, related to the increasing interfacial curvature, could have a strong impact on the interfacial tension, wetting properties of the confined liquids as well as the interfacial energy [16–19]. Furthermore, the variation in molecular dynamics of materials incorporated within pores of nanometric diameters can be directly related to the change in surface interactions induced by the curvature of the interface. This aspect seems to be important in the context of the value of  $\gamma_{SL}$  (quantifying the strength of the interfacial interactions) in cylindrical pores, which could be significantly changed when compared to the ones calculated for a planar surface. One can remind that the interfacial energy, the surface tension and the contact angle are connected to each other via the Young equation ( $\gamma_S L = \gamma_S - \gamma_L \cos \theta$ , where  $\theta$  is the contact angle and  $\gamma_S$  is the surface energy) [20,21].

In this paper, we have examined the behavior of low-molecular-weight glass former, glycerol (GLY), incorporated into anodic aluminum oxide (AAO) templates of various pore size,  $d = 10$ – $150$  nm, to explore the combination of the surface interactions and finite size effects on the behavior of this polyalcohol. One can recall that except one study by Uhl et al. [22], no difference between the behavior of bulk sample

and glycerol incorporated within silica [23] and alumina membranes [24–26] has been reported so far. Interestingly, in Ref. [22], it was shown that change in dynamics of GLY confined within zeolitic imidazolate frameworks (ZIF-8 and ZIF-11 of  $d = 1.2$ – $1.5$  nm) is connected to the freezing cooperativity length scale [4,27]. This interpretation was in line with the one proposed by Arndt et al. [28] to explain deviation in the structural dynamics of model liquid (salol) incorporated into porous glass, and Fischer et al. [29] for glycerol confined in MOFs (metal-organic framework) systems.

Herein, we have shown that the approach relying on the connection between the depression of the glass transition temperatures of the liquids incorporated into porous AAO and their interfacial energies, surface tensions, as proposed by Alexandris et al. [4] and further verified by some of us [5,6] must be modified. Performed AFM measurements indicated that as predicted by Tolman, the wettability, the surface tension and the interfacial energy of model liquid glycerol vary with the increasing curvature (decrease of pore diameter). Therefore, a unique experimental approach to probe the impact of nano curvature on the basic properties of the liquids wetting curved surface has appeared. It should also be pointed out that due to an enhancement in wettability of the polyalcohol in the smallest AAO pores ( $d = 10$  nm), a double glass transition phenomenon was observed. Interestingly, below the high glass transition temperature,  $T_{g,interfacial}$ , the structural dynamics of the confined glycerol started to deviate from the bulk sample.

## 2. Experimental section

### 2.1. Materials

Glycerol (GLY) with the purity greater than 99.9% was supplied by Sigma-Aldrich and used as received. As a constrain medium, we used the commercially available anodic aluminum oxide (AAO) membranes (InRedox, USA) composed of uniaxial channels (open from both sides) parallel to each other of well-defined pore diameter,  $d$ . In the experiment, we used membranes of various pore diameters,  $d = 10, 18, 80$  and  $150$  nm. The template's thickness is  $50 \mu\text{m}$ , whereas the membrane's diameter is  $13$  mm. The chemical structure of GLY and the scheme of applied AAO templates are presented in Fig. 1.

### 2.2. Samples preparation

As first, the applied AAO templates were dried in an oven at  $T = 423$  K under a vacuum ( $10^{-2}$  bar) for at least  $t = 24$  h to remove any volatile impurities from the nanochannels. After cooling, they were used as a constraint medium. For that purpose, AAO templates were placed in a small glass flask containing GLY. The whole system was maintained at  $T = 298$  K in a vacuum ( $10^{-2}$  bar) for  $t = 1$  h to let all compounds flow into the nanocavities. Samples were finally annealed at  $T = 353$  K under a vacuum ( $10^{-2}$  bar) for  $t = 1$  h and weighted after that. The complete filling was obtained by a series of repeated infiltration procedure until the weight of the templates before and after was constant. After completing the infiltration process, the surface of the AAO membrane was dried, and the excess sample on the surface was removed by the use of a metal blade and a paper towel. The same procedure was applied to all studied pore sizes.

### 2.3. Methods

#### 2.3.1. Broadband Dielectric Spectroscopy (BDS)

Isobanic measurements of the complex dielectric permittivity  $\epsilon^*(\omega) = \epsilon'(\omega) - i\epsilon''(\omega)$  were performed using the Novocontrol Alpha dielectric spectrometer over the frequency range from  $10^{-2}$  to  $10^6$  Hz at ambient pressure. The temperature stability controlled by Quatro Cryosystem using nitrogen gas cryostat was better than  $0.1$  K. Dielectric measurements of the bulk sample were carried out in a parallel-plate cell (diameter:  $10$  mm, gap:  $0.1$  mm). AAO membranes filled with GLY were

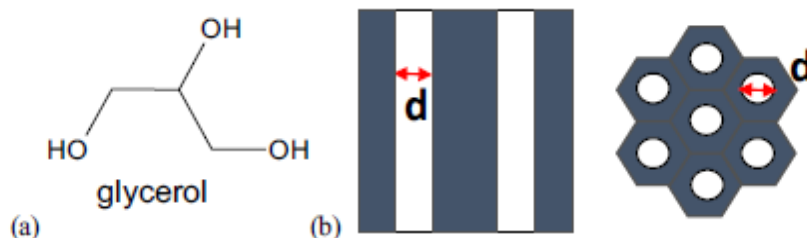


Fig. 1. The chemical structure of glycerol (a) and the applied AAO templates (b).

placed in a capacitor (diameter: 10 mm, membrane thickness: 0.05 mm). Nevertheless, confined samples are heterogeneous dielectrics, composed of a matrix and an investigated compound. Because the applied electric field is parallel to the long pore axes, the equivalent circuit consists of two capacitors in parallel composed of  $\epsilon^*_{\text{compound}}$  and  $\epsilon^*_{\text{AAO}}$ . Thus, the measured total impedance is related to the individual values through  $1/Z^*_c = 1/Z^*_{\text{compound}} + 1/Z^*_{\text{AAO}}$ . It should be added that dielectric measurements on empty membranes were also performed to evaluate the contribution of AAO, which turned out to be negligible to the recorded data. Dielectric measurements were carried out in the temperature range  $T = 253 - 183$  K for the bulk and confined systems. The measured dielectric spectra were corrected according to the method presented in Ref. [4].

### 2.3.2. Differential Scanning Calorimetry (DSC)

Calorimetric measurements were carried out using a Mettler-Toledo DSC apparatus (Mettler-Toledo International, Inc., Greifensee, Switzerland) equipped with a liquid nitrogen cooling accessory and an HSS8 ceramic sensor (heat flux sensor with 120 thermocouples). Temperature and enthalpy calibrations were investigated using indium and zinc standards, while the heat capacity,  $C_p$ , calibration was performed using a sapphire disc. Measurements of the bulk sample were performed for sealed alumina crucible filled with glycerol, which was measured over a wide temperature range from 170 K to room temperature with heating rate equals to 10 K/min. In the case of confined systems, the filled membranes were crushed to fix the measurement alumina crucibles. For annealing experiments, samples were quenched deep below  $T_g$  of bulk material ( $T_g = 188$  K), heated to the given annealing temperature ( $T_{\text{anneal}} = 213 - 236$  K) and then measured as a function of time. Immediately after the annealing, samples were cooled and scanned with a heating rate of 10 K/min over a temperature range from 160 K to 300 K.

### 2.3.3. Atomic Force Microscopy (AFM)

Surface topography and mechanical parameters (adhesion) were measured using NanoWizard®3 BioScience (JPK Instruments, Berlin, Germany) AFM. Images were acquired using rectangular Si cantilevers with stiffness equal to 1.8 N/m and the resonant frequency close to 75 kHz. After the placing crushed templates in the crucibles, they were sealed and measured at the same conditions as in the case of measurements of the bulk sample. Each measurement was repeated three times. The tip radius was less than 1 nm (super sharp tip with diamond-like carbon spike from BudgetSensors). Statistical analysis and mechanical parameters were estimated using JPK software and Gwyddion package [30].

## 3. Results and discussion

At the beginning of this investigation, dielectric measurements of bulk and confined GLY were carrying out, and the obtained dielectric loss spectra are presented in Fig. 2. All investigated materials were measured upon slow cooling from  $T = 253$  K to the temperatures below  $T_g$  of the bulk material,  $T = 183$  K.

As illustrated, all spectra revealed the existence of the two relaxation processes, the structural ( $\alpha$ ) relaxation located at high-frequency range, and dc conductivity, at lower

frequencies. The dc conductivity is connected to the charge transport of ionic impurities, while the  $\alpha$ -relaxation is related to the cooperative motions of molecules and viscous flow that is considered to be responsible for the liquid-to-glass transition. It is also worthwhile to add that we did not detect any additional relaxation process connected to the motions of the material adsorbed to the pore walls, so-called interfacial layer, usually reported for the liquids infiltrated into pores [23,28,31,32]. This is consistent with the data published by Arndt et al. [23] for glycerol infiltrated into silica porous templates. Authors discussed the lack of evidence of an additional process in terms of the difference in the time scale of the experiment and the exchange between core and interfacial molecules.

Thus, at first glance, there are no differences in the collected spectra between a bulk sample and GLY infiltrated into AAO pores. However, a simple comparison of the  $\alpha$ -loss peaks measured for each sample, characterized by the same structural relaxation times ( $\tau_{\alpha} \approx \text{const.}$ ), revealed a detectable variation in their width or FWHM (full-width-half-maxima) with the pore size of AAO (see insets to Fig. 2). For the pore diameters of  $d = 80$  nm and  $d = 150$  nm, the shape of the  $\alpha$ -process remains bulk-like, while the distribution of relaxation times broadens, when the pore size drops below  $d = 18$  nm (see inset to Fig. 2(c)). One can mention that the observed phenomenon, i.e., the variation in the distribution of the structural relaxation times with reducing pore diameter is rather a universal feature of the liquids infiltrated into porous templates [5,25]. It is often discussed in terms of the increasing length-scale heterogeneity under confinement that is induced by the substrate [33,34]. One can also hypothesize that this effect can be related to the increasing strength of the interactions between the studied polyalcohol and porous matrix due to the variation in the wettability, the surface tension and the interfacial energy induced by increasing surface curvature in pores of the lowest diameters [35].

To get a deeper insight into the dynamics of GLY confined into AAO templates, we analyzed collected data with the use of Havriliak-Negami (HN) function with an additional conductivity term [36] (see Eq. (2)):

$$\frac{\epsilon(\omega) - \sigma_0 \epsilon_0}{\epsilon_0 \omega + \Delta\epsilon} = \frac{c_0 \omega + \Delta\epsilon}{[1 + (\omega \tau_{\text{HN}})^{\alpha_{\text{HN}}}]^{\beta_{\text{HN}}}} \quad (2)$$

where:  $\alpha_{\text{HN}}$  and  $\beta_{\text{HN}}$  are the shape parameters representing the symmetric and asymmetric broadening of given relaxation peaks,  $\Delta\epsilon$  is the dielectric relaxation strength,  $c_0$  is the vacuum permittivity,  $\omega$  is an angular frequency ( $\omega = 2\pi f$ ), and  $\tau_{\text{HN}}$  is the HN relaxation time. Using a well-known protocol, the structural relaxation times,  $\tau_{\alpha}$ , were estimated from  $\tau_{\text{HN}}$  [37]. Furthermore, the glass transition temperature,  $T_g$ , was estimated by fitting the temperature dependences of  $\tau_{\alpha}$  using the Vogel-Fulcher-Tammann (VFT) equation [38] (see Eq. (3)):

$$\tau_{\alpha} = \tau_{\infty} \exp\left(\frac{D_T T_0}{T - T_0}\right) \quad (3)$$

where:  $T_0$  is the temperature, where  $\tau$  goes to infinity,  $\tau_{\infty}$  is the relaxation time at finite temperature, and  $D_T$  is the fragility parameter. Structural relaxation times plotted vs. reciprocal temperature for each investigated sample are presented in Fig. 3.

As can be seen, the structural dynamics in the studied polyalcohol incorporated into AAO templates of  $d = 18 - 150$  nm is bulk-like in the whole studied temperature range. Interestingly, a slightly different scenario was detected for the material infiltrated into AAO pores of the smallest diameter,  $d = 10$  nm. In this particular case, at some specific temperature ( $T_{g(\text{interfacial})}$ ), a small deviation of  $\tau_{\alpha}(T)$  from that measured for the bulk sample is noted. It should be mentioned that to estimate  $T_{g(\text{interfacial})}$  from the presented data accurately, the temperature dependences of the structural relaxation times were analyzed using a method proposed by Sichel [39] from the following equation:

$$S = \left(\frac{d \ln \tau_{\alpha}}{dT}\right)^{(-0.5)} \quad (4)$$

where  $S$  is the Stickelö pentor. The temperature dependence of  $S$  is presented as an inset in Fig. 3(c). As shown, there is a clear change in the slope of  $S(T)$  at  $T_{g(\text{interfacial})} \approx 243$  K for the glycerol confined at the alumina pores of the lowest diameter,  $d = 10$  nm; while in case of the bulk sample and other confined samples, no similar scenario was found. One can add that a comparable situation has been recently reported for GLY incorporated into zeolitic imidazolate frameworks of very small size ( $d = 1.16$  and  $d = 1.46$  nm)

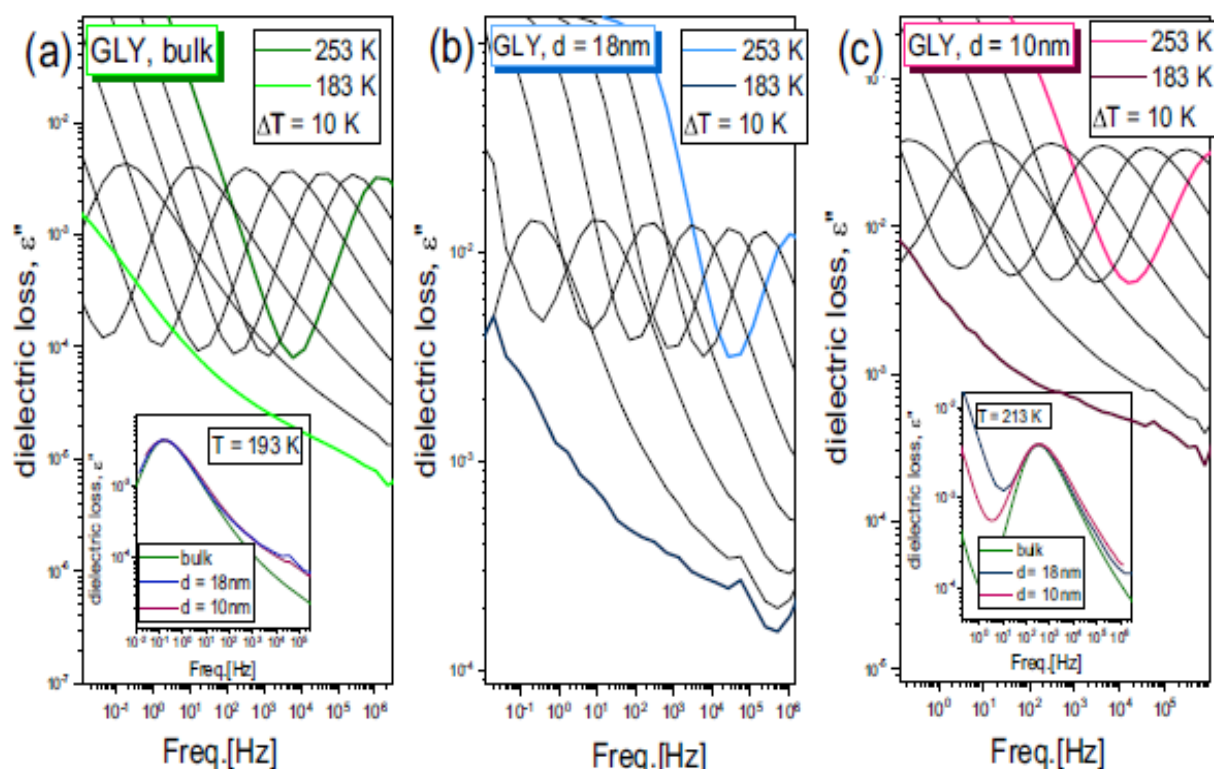


Fig. 2. Dielectric loss spectra of bulk (a) and confined (b,c) glycerol measured above  $T_g$ . As insets, the shape of the structural relaxation peak measured at  $T = 193$  K (a) and  $T = 213$  K (c). Note that the measured spectra were shifted vertically to superpose at the maximum. Data for GLY infiltrated within  $d = 18$  nm were taken from Ref. [6].

[22]. This behavior was related to the freezing of dynamical heterogeneities, that cannot build up upon cooling due to the geometrical restriction. The discussed interpretation is in line with that proposed by Arndt et al. [23] for salol infiltrated into porous silica. Nevertheless, recently it has been shown that the deviation in  $\tau_\alpha(T)$  for the confined samples with respect to the bulk materials can also be related to the vitrification of the interfacial molecules/polymers [5,40,41]. At these conditions, due to the density fluctuations, dynamics of the core molecules varies, and the system can be considered as being under isochoric conditions [24]. Moreover, it was also found that the scale of the deviation of  $\tau_\alpha$  measured

for the liquid incorporated into pores with respect to the bulk samples depends on the sensitivity of the structural relaxation process to the density fluctuation, quantified by the ratio of isochoric and isobaric activation barriers ( $E_v/E_p$ ) [24] or pressure coefficient of the glass transition temperature ( $dT_g/dp$ ) [6]. Therefore, since the structural dynamics of GLY is barely affected by the density variation (high  $E_v/E_p = 0.94$  [42] and low  $dT_g/dp = 35\text{--}40$  K/GPa [43,44]), only a slight change of the  $\tau_\alpha(T)$  of the confined polyalcohol is expected, if the vitrification of the interfacial layer underlies this phenomenon [45]. In this context, it is worthwhile to stress that we have calculated  $E_v/E_p = 0.96$  from both

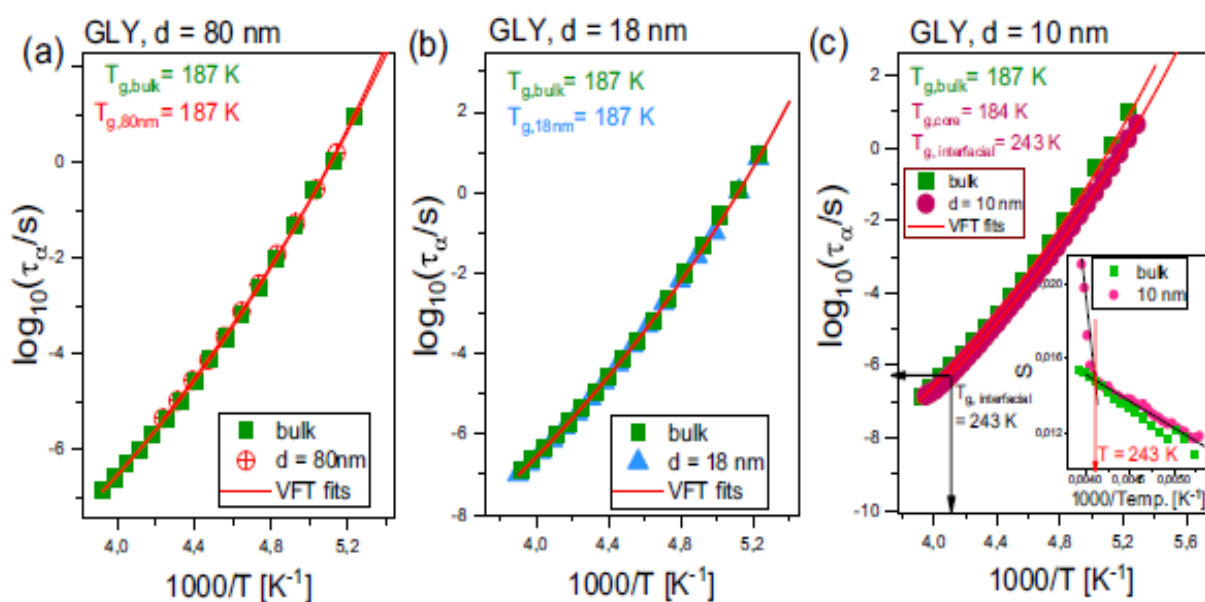


Fig. 3. Structural relaxation times plotted versus inverse temperature for bulk and confined glycerol. Note that the data for GLY infiltrated within  $d = 80$  and  $d = 18$  nm were taken from Ref. [24] and Ref. [6]. Red solid lines are the best VFT fits. As inset in panel (c), Söckel ( $S$ ) plot of  $\alpha$ -relaxation times for bulk and confined glycerol within  $d = 10$  nm.

the temperature dependencies of the structural relaxation times obtained for the bulk glycerol and the sample confined in pores of  $d = 10$  nm at  $T_{g,interf,24} = 243$  K that was determined from the Stückel analysis. Interestingly, the calculated ratio is very close to that given in the literature [42], suggesting a close relationship between the vitrification of the interfacial layer and a change in the structural dynamics of glycerol. However, to verify this hypothesis further studies with the use of Differential Scanning Calorimetry (DSC) were performed.

Representative thermograms obtained upon heating of the bulk GLY and polyalcohol confined into AAO pores of varying diameters are presented in Fig. 4. It can be observed that there is only one endothermic heat capacity jump related to the vitrification of bulk polyalcohol and material infiltrated into AAO pores of the larger diameter  $d = 18$  nm (see Fig. 4 (a,b)). In fact, the glass transition temperatures of these systems are comparable. On the other hand, a completely different situation is noted for GLY infiltrated into pores of  $d = 10$  nm. In this case, unexpectedly, an additional endothermic event related to the glass transition phenomenon is observed at much higher temperatures. Consequently, two glass transitions located below and above  $T_g$  of the bulk glycerol (Fig. 4 (c)) are detected for this system. Accordingly to a very simple approach proposed by Park and McKenna (so-called "two-layer model") [46], the observed two glass transitions are connected to the vitrification of the two different fractions of molecules: (i) core (placed in the center of nanochannels) and (ii) interfacial (molecules adsorbed on the porous walls), which vitrify at different temperature when compared to the bulk liquid [46]. However, it should be mentioned herein that  $T_{g,high}$  is generally not observed upon cooling of the polyalcohol (please see Fig. S1 in SI). In fact, very recent studies by Polididis et al. [47] on entangled *cis*-1,4-polyisoprene confined within AAO templates clearly demonstrated that the additional glass transition is a conditional event and depends on the thermal history of the sample and sorption/desorption processes taking place at the pore walls. Interestingly, it was observed only when the spatially restricted system is cooled below  $T_{g,low}$ . This experimental observation allowed authors [47] to hypothesize that  $T_{g,low}$  is in fact a spinodal temperature. However, this concept, although quite interesting, requires further experimental investigations and confirmations. Nevertheless, it should also be emphasized that the lower and higher glass transition temperatures,  $T_{g,low}$  and  $T_{g,high}$ , determined from DSC heating measurements were assigned to the  $T_g$ 's of core and interfacial layer, respectively. Interestingly, the glass transition temperature of the interfacial layer obtained from the calorimetric ( $T_{g,high} \approx 236$  K) data agrees more less with the temperature  $T_{g,interf,local} \approx 243$  K where  $\tau_{\alpha}(T)$  starts to deviate from the bulk behavior. Such a good correspondence between both temperatures estimated from the two independent measurements indicated that the change in the structural dynamics of glycerol confined within  $d = 10$  nm pores is directly related to the vitrification of the interfacial layer.

In addition to the standard DSC measurements described above, we have carried out series of annealing experiments at different temperatures to check the impact of the thermal history on the behavior of the both glass transition temperatures detected for GLY confined in the smallest pores ( $d = 10$  nm). As shown in the thermograms presented in Fig. S1 in SI file, a clear decrease in the intensity of  $T_{g,high}$  was noted. This effect is most likely connected to the desorption processes occurring upon time dependent studies. Moreover, it is also worthwhile to stress that both vitrification temperatures ( $T_{g,low}$  and  $T_{g,high}$ ) remained constant, within the experimental uncertainty. It is

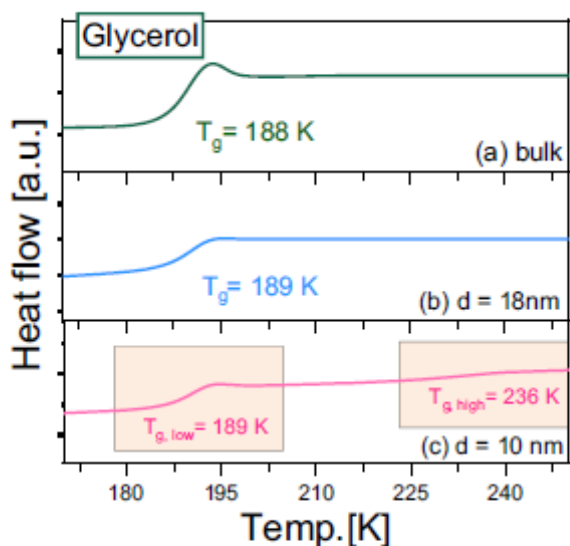


Fig. 4. DSC thermograms obtained for the bulk (a) and confined glycerol (b,c) upon heating. Calorimetric data obtained during the cooling scans for all studied systems and after the annealing experiments of GLY within AAO templates of  $d = 10$  nm are presented in Fig. S1 in SI file.

quite expected, since there was only 1 K difference between  $T_{g,low}$  and the one measured for the bulk material.

Hence, one can claim that the presence or absence of the two glass transition phenomenon in GLY incorporated into AAO pores of different diameters is as an unexpected as an intriguing finding. One can remind that the presence of a single glass transition in the sample incorporated into AAO pores of larger pore diameter ( $d = 18$ – $150$  nm) has been recently also rationalized considering the pretty low wettability,  $\theta = 63^\circ$ , high interfacial tension,  $\gamma_L = 60$  mN m $^{-1}$ , and low interfacial energy,  $\gamma_{SL} = 1.5$  mN m $^{-1}$ , between alumina and glycerol [4,6]. It was concluded, that the surface interactions between the studied GLY and applied AAO membranes are probably too weak to form strongly bonded interfacial layer. Consequently, the bulk-like dynamics of confined GLY is observed. Hence, at this point, one should ask the question, what is the reason for the peculiar behavior of examined alcohol infiltrated into AAO pores of the smallest diameter ( $d = 10$  nm)? Why did we detect the two glass transition temperatures for this sample? Does a decrease in pore size (an increase in the curvature of applied nanochannels) play any role in the observed effect?

To get a deeper insight into this issue, one can recall the equation formulated by Tolman and mentioned in the introduction. According to this approach, the surface tension,  $\gamma_c$ , of a liquid on the curved surface decreases with respect to the one determined for the planar interface (see Eq. (1)). Although this effect is more expected for a curvature close to the Tolman length, that is around  $\delta = 0.3$  nm [17], there are both experimental and theoretical works showing that some deviation in surface tension can be already noted for smaller curvatures [15,48,49]. Consequently, some measurable effects may be expected for glycerol confined in the pores of much larger diameter than the Tolman length. To verify this hypothesis, we have carried out final measurements with the use of the AFM technique. Herein, it is worthwhile to point out that these investigations were performed along the cross-section of both the empty and filled with the polyalcohol membranes.

The AFM technique can be directly implemented for the measurement of the adhesion force between the sample and the cantilever tip [50]. In order to do that, the tip is brought into contact with the sample at a constant velocity until the maximum load is obtained. Afterwards, the movement is reversed, and the sample and the tip are separated. However, due to the interaction between the tip and the surface, a certain force has to be applied to separate them again. This force is described as the adhesion force in our experiments and it can be defined as the total force that is exerted by a liquid (GLY) on the AFM tip. This force depends on several parameters. However, the most important one is a linear function of the liquid's surface tension  $\gamma_L$  [51]. Thus, by measuring a number of force-curves in a raster, one can generate an adhesion map. This map can be further analyzed and compared to the sample topography. The typical result of AFM topography and adhesion force map for a representative sample of GLY infiltrated within membranes of  $d = 10$  nm is presented in Fig. 5. AFM data collected for GLY infiltrated into higher pore size,  $d = 120$  nm and 20 nm, are presented in Fig. S2 in SI.

The further analysis is consisted of gathering data from several images and compiling it into a histogram of adhesion force values. Those histograms were fitted and separated into different components – the adhesion values coming from the native empty AAO template and other components related to the adhesion force of GLY confined in the nanochannels. Thus, to avoid considering other tip-surface related parameters (contact size, tip material etc.), we decided to analyze only the difference between adhesion force of GLY within nanochannels and the adhesion force of the empty AAO templates. The result of this operation is plotted as a function of the pore diameter, please see Fig. 5(e). As shown, although there are quite large error bars in the estimation of the adhesion force, it decreases systematically with the pore diameter. That indicates that the surface tension of the glycerol decreases with the increasing curvature (lowering pore diameter) as predicted by Tolman [12–14]. Consequently, in AAO pores of  $d = 10$  nm, one can expect better wettability and higher interfacial energy that leads to the formation of more strongly attached interfacial layer that vitrifies at higher temperatures with respect to the bulk polyalcohol. Furthermore, at this condition, the dynamics of the confined glycerol starts to deviate from the macroscale liquid.

#### 4. Conclusions

As predicted by the Tolman relation, the surface tension,  $\gamma_c$ , of a liquid on the curved surface decreases with respect to the one determined for the planar interface. Although this effect is more expected for a curvature close to the Tolman length of the order of  $\delta = 0.3$  nm [17], some deviation in surface tension can be already noted even for smaller curvatures [15,48,49]. To experimentally investigate the above relation, we have performed unique AFM measurements on the glycerol incorporated into AAO membranes of varying pore sizes,  $d = 10$ – $150$  nm. These investigations seem to indicate that with decreasing pore diameter, the wettability of this alcohol is enhanced. Thus, a new experimental approach to probe the fundamental properties of the liquids wetting curved surfaces appeared. As observed, an increase in the wettability and the interfacial energy between host and guest materials in the smallest AAO pores ( $d = 10$  nm) lead to the formation of the interfacial layer attached to the walls. As a consequence, a double glass transition phenomenon connected to the vitrification of the core and interfacial

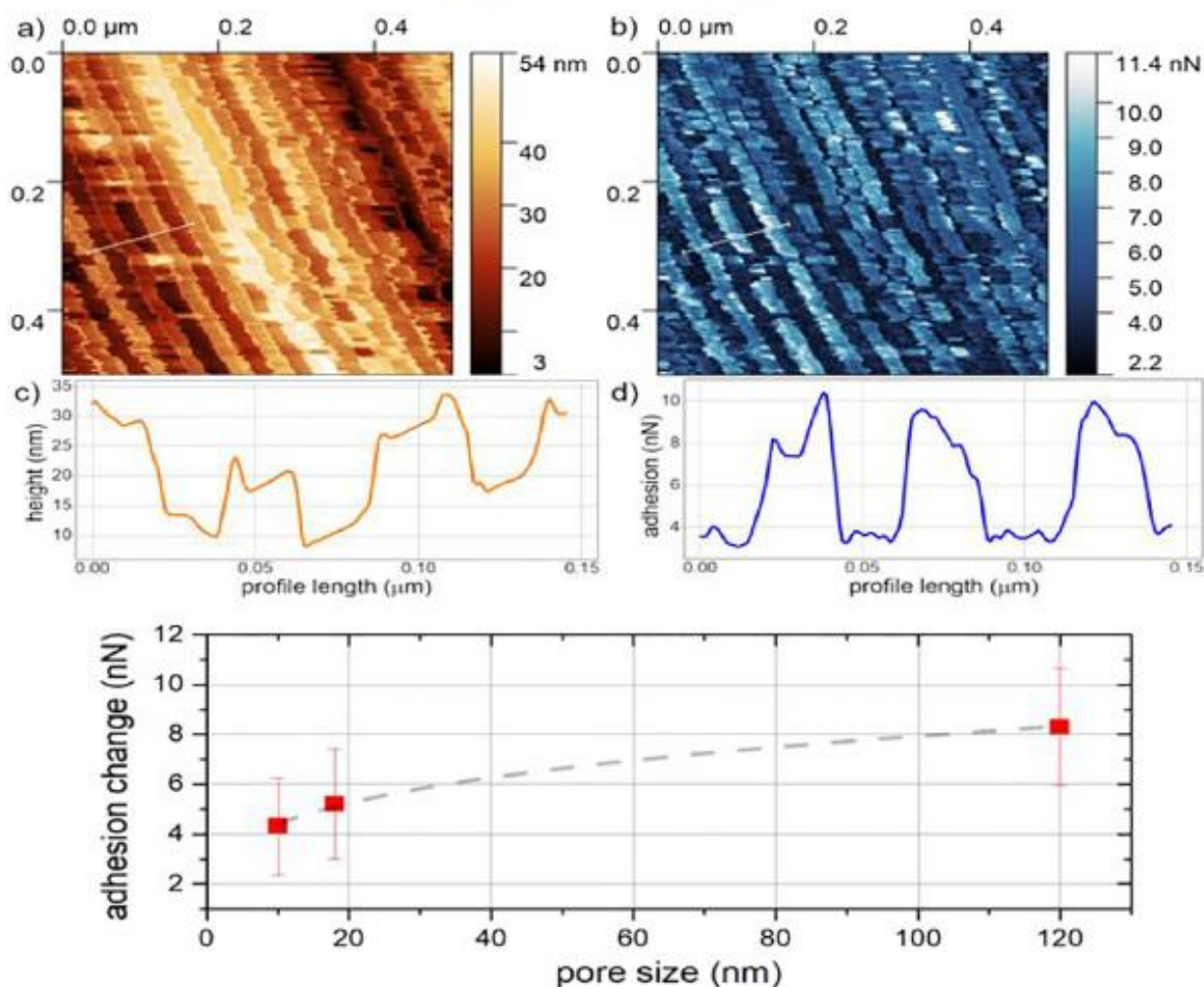


Fig. 5. AFM topography (a) and adhesion force map (b) obtained on the cross-section of the AAO membrane showing open pores ( $d = 10$  nm) filled with GLY. One can notice higher (brighter) regions at the adhesion force maps which correlate with darker (nanochannels) regions at topography. The profiles in the (c) and (d) image corresponding to the marked white line in the topography and adhesion force map, respectively. The difference between adhesion force of the GLY in nanochannels and the adhesion force of the uncoated AAO template plotted as a function of an AAO pore size measured by the AFM (e). The dotted lines are only the guide for an eye. AFM data collected for GLY infiltrated into higher pore size,  $d = 120$  nm and 20 nm, are presented in Fig. S2 in SI.

molecules was observed in thermograms collected upon heating samples. Additional annealing experiments have clearly indicated that the intensity of the higher  $T_g$  related to the vitrification of the interfacial layer decreases with time. It may suggest the ongoing desorption processes taking place at the interface. In addition, it was found that below the high glass transition temperature,  $T_{g,interfacial}$ , the structural dynamics of the confined polyalcohol started to deviate from the bulk material. The close correlation between all these experimental findings indicated that for a deeper understanding of the dynamics of the confined liquids and depression of the glass transition temperature, a variation in the wettability, the surface tension and the interfacial energy with the surface curvature must be taken into account. Finally, our data unquestionably have demonstrated that it is very difficult to separate the impact of finite size effects from the surface ones since both seem to be directly entangled.

#### Declaration of competing interest

The authors declare no competing financial interests.

#### Acknowledgments

KK is thankful for financial support from the Polish National Science Centre within the OPUS project (Dec. no 2015/17/B/ST3/01195). M.T. is thankful for financial support from the Foundation for Polish Science (FNP).

#### Appendix A. Supplementary data

Supplementary data to this article can be found online at <https://doi.org/10.1016/j.molliq.2019.111973>.

#### References

- [1] R. Busseler, R. Lefort, M. Guendouz, B. Frick, O. Merdrignac-Conanec, D. Morineau, Molecular dynamics of glycerol and glycerol-trehalose bioprotectant solutions nanoconfined in porous silicon, *J. Chem. Phys.* 130 (2009) 214502, <https://doi.org/10.1063/1.3147222>.

- [2] M. Alcoutlabi, G.J. McKenna, Effects of confinement on material behaviour at the nanometre size scale, *J. Phys. Condens. Matter* 17 (2005) <https://doi.org/10.1088/0953-8984/17/15/R01R461-R52>.
- [3] F. Kremer, A. Schönhalz, *Broadband Dielectric Spectroscopy*, Springer, Berlin, 2003.
- [4] S. Alexandris, P. Papadopoulos, G. Sakellariou, M. Steinhart, H.-J. Butt, G. Floudas, Interfacial energy and glass transition of polymers confined to nanoporous alumina, *Macromolecules* 49 (2016) 7400–7414, <https://doi.org/10.1021/acs.macromol.6b01484>.
- [5] A. Talić, M. Tarnacka, I. Gładzka-Flak, P. Malosyn, M. Geppert-Rybczyńska, E. Kamińska, K. Kamiński, M. Paluch, The role of interfacial energy and specific interactions on the behavior of poly(propylene glycol) derivatives under 2D confinement, *Macromolecules* 51 (13) (2018) 4840–4852, <https://doi.org/10.1021/acs.macromol.8b00658>.
- [6] A. Talić, M. Tarnacka, M. Geppert-Rybczyńska, A. Minecka, E. Kamińska, K. Kamiński, M. Paluch, Impact of the interfacial energy and density fluctuations on the shift of the glass-transition temperature of liquids confined in pores, *J. Phys. Chem. C* 123 (9) (2019) 5549–5556, <https://doi.org/10.1021/acs.jpcc.8b12551>.
- [7] D.S. Fryer, R.D. Peters, E.J. Kim, J.L. Tomaszewski, J.J. de Pablo, P.F. Nealey, C.C. White, W.L. Wu, Dependence of the glass transition temperature of polymer films on interfacial energy and thickness, *Macromolecules* 34 (2001) 5627–5634, <https://doi.org/10.1021/ma001932q>.
- [8] R.J. Lang, W.L. Merling, D.S. Simmons, Combined dependence of nanoconfined  $T_g$  on interfacial energy and softness of confinement, *ACS Macro Lett.* 3 (2014) 758–762, <https://doi.org/10.1021/acs.macromol.5b00361v>.
- [9] A. Aasen, E.M. Blokhuys, Ø. Wilhelmsen, Tolman lengths and rigidity constants of multicomponent fluids: fundamental theory and numerical examples, *J. Chem. Phys.* 148 (2018) 204702, <https://doi.org/10.1063/1.5026747>.
- [10] V.D. Nguyen, F.C. Schoemaker, E.M. Blokhuys, P. Schall, Measurement of the curvature-dependent surface tension in nucleating colloidal liquids, *Phys. Rev. Lett.* 121 (2018) 246102, <https://doi.org/10.1103/PhysRevLett.121.246102>.
- [11] W. Gibbs, *Collected Works*, vol. 1, Longmans Green and Company, New York, 1928, 219.
- [12] R.C. Tolman, Consideration of the Gibbs theory of surface tension, *J. Chem. Phys.* 16 (1948) 758, <https://doi.org/10.1063/1.1746894>.
- [13] R.C. Tolman, The effect of droplet size on surface tension, *J. Chem. Phys.* 333 (1949) <https://doi.org/10.1063/1.1747247>.
- [14] R.C. Tolman, The superficial density of matter at a liquid-vapor boundary, *J. Chem. Phys.* 17 (1949) 118, <https://doi.org/10.1063/1.1747204>.
- [15] E.M. Blokhuys, J. Kuipers, Thermodynamic expressions for the Tolman length, *J. Chem. Phys.* 124 (2006) 074701, <https://doi.org/10.1063/1.2167642>.
- [16] S. Kim, D. Kim, J. Kim, S. An, W. Jhe, Direct evidence for curvature-dependent surface tension in capillary condensation: kelvin equation at molecular scale, *Phys. Rev. X* 8 (2018), 041046, <https://doi.org/10.1103/PhysRevX.8.041046>.
- [17] Sergey V. Stepanov, Vsevolod M. Byakov, Olga P. Stepanova, The determination of microscopic surface tension of liquids with a curved interphase boundary by means of positron spectroscopy, *Russ. J. Phys. Chem.* 74 (2000) 565–577.
- [18] D. Kashchiev, Determining the curvature dependence of surface tension, *J. Chem. Phys.* 118 (2003) 9081, <https://doi.org/10.1063/1.1576218>.
- [19] Ø. Wilhelmsen, D. Bedeaux, D. Reguera, Communication: Tolman length and rigidity constants of water and their role in nucleation, *J. Chem. Phys.* 142 (2015) 171103, <https://doi.org/10.1063/1.4919689>.
- [20] T. Young, An essay on the cohesion of fluids, *Philos. Trans. R. Soc. Lond.* 95 (1805) 65–87, <https://doi.org/10.1098/rstl.1805.0005>.
- [21] F.M. Fowkes, Attractive forces and interfaces, *Ind. Eng. Chem.* 56 (1964) 40–52, <https://doi.org/10.1021/ie50660a008>.
- [22] M. Uhl, J.K.H. Fischer, P. Sippel, H. Burzen, P. Lunkenheimer, D. Volkmer, A. Loidl, Glycerol confined in zeolitic imidazolate frameworks: the temperature-dependent cooperativity length scale of glassy freezing, *J. Chem. Phys.* 150 (2019), 024504, <https://doi.org/10.1063/1.5080334>.
- [23] M. Arndt, R. Stammarius, W. Gorbatschow, F. Kremer, Dielectric investigations of the dynamic glass transition in nanopores, *Phys. Rev. E* 54 (1996) 5377, <https://doi.org/10.1103/PhysRevE.54.5377>.
- [24] K. Adrjanowicz, K. Kamiński, K. Koperwas, M. Paluch, Negative pressure vitrification of the isochorically confined liquid in nanopores, *Phys. Rev. Lett.* 115 (2015) 265702, <https://doi.org/10.1103/PhysRevLett.115.265702>.
- [25] W. Zheng, S.L. Simon, Confinement effects on the glass transition of hydrogen bonded liquids, *J. Chem. Phys.* 127 (2007) 194501, <https://doi.org/10.1063/1.2793787>.
- [26] W. Gorbatschow, M. Arndt, R. Stammarius, F. Kremer, Dynamics of H-bonded liquids confined to nanopores, *Europhys. Lett.* 35 (1996) 719, <https://doi.org/10.1209/epl/1996-00175-8>.
- [27] Y. He, J. Mi, C. Zhong, Surface tension and Tolman length of spherical particulate in contact with fluid, *J. Phys. Chem. B* 112 (2008) 7251–7256, <https://doi.org/10.1021/jp711692j>.
- [28] M. Arndt, R. Stammarius, H. Groothues, E. Hempel, F. Kremer, Length scale of cooperativity in the dynamic glass transition, *Phys. Rev. Lett.* 79 (1997) 2077, <https://doi.org/10.1103/PhysRevLett.79.2077>.
- [29] J.K.H. Fischer, P. Sippel, D. Denysenko, P. Lunkenheimer, D. Volkmer, A. Loidl, Metal-organic frameworks as host materials of confined supercooled liquids, *J. Chem. Phys.* 143 (2015) 154505, <https://doi.org/10.1063/1.4933308>.
- [30] D. Necas, P. Klapetek, Gwyddion: an open-source software for SPM data analysis, *Cent. Eur. J. Phys.* 10 (2012) 181–188, <https://doi.org/10.2478/s11534-011-0096-2>.
- [31] F. He, L.-L. Wang, R. Richert, Dynamics of Supercooled liquids in the vicinity of soft and hard interfaces, *Phys. Rev. B* 71 (14) (2005) 144205, <https://doi.org/10.1103/PhysRevB.71.144205>.
- [32] R. Richert, Dynamics of nanoconfined supercooled liquids, *Annu. Rev. Phys. Chem.* 62 (2011) 65–84, <https://doi.org/10.1146/annurev-physchem-082210-103343>.
- [33] J. Schuller, Yu. B. Melnichenko, R. Richert, E.W. Fischer, Dielectric studies of the glass transition in porous media, *Phys. Rev. Lett.* 73 (1994) 2224, <https://doi.org/10.1103/PhysRevLett.73.2224>.
- [34] F. Kremer, *Dynamics in Geometrical Confinement*, Springer, 2014.
- [35] M. Tarnacka, K. Kamiński, E.L. Mapeša, E. Kamińska, M. Paluch, Studies on the temperature and time induced variation in the segmental and chain dynamics in poly(propylene glycol) confined at the nanoscale, *Macromolecules* 49 (17) (2016) 6678–6686, <https://doi.org/10.1021/acs.macromol.6b01237>.
- [36] S. Havriliak, S.A. Negami, Complex plane analysis of  $\alpha$ -dispersions in some polymer systems, *J. Polym. Sci. Part C Polym. Symp.* 14 (1966) 99–117, <https://doi.org/10.1002/polc.5070140111>.
- [37] F. Kremer, A. Schönhalz, *Dielectric Relaxation Spectroscopy: Fundamentals and Applications*, Springer, Berlin, 2003.
- [38] H. Vogel, Das temperaturabhängigkeitsgesetz der Viskosität von Flüssigkeiten, *J. Phys. Z.* 22 (1921) 645–646.
- [39] F. Stöckel, E.W. Fischer, R. Richert, Dynamics of glass-forming liquids. I. Temperature-derivative analysis of dielectric relaxation data, *J. Chem. Phys.* 102 (1995) 6251, <https://doi.org/10.1063/1.469071>.
- [40] K. Adrjanowicz, K. Kolodziejczyk, W.K. Kipnusu, M. Tarnacka, E.L. Mapeša, E. Kamińska, S. Pawlus, K. Kamiński, M. Paluch, Decoupling between the interfacial and core molecular dynamics of salol in 2D confinement, *J. Phys. Chem. C* 119 (2015) 14366–14374, <https://doi.org/10.1021/acs.jpcc.5b01391>.
- [41] M. Tarnacka, E. Kamińska, K. Kamiński, C.M. Roland, M. Paluch, Interplay between Core and Interfacial Mobility and Its Impact on the Measured Glass Transition: Dielectric and Calorimetric Studies, *J. Phys. Chem. C* 120 (2016) 7373–7380, <https://doi.org/10.1021/acs.jpcc.5b12745>.
- [42] C.M. Roland, S. Hensel-Bielowka, M. Paluch, R. Casalini, Supercooled dynamics of glass-forming liquids and polymers under Hydrostatic pressure, *Rep. Prog. Phys.* 68 (2005) 1405–1478, <https://doi.org/10.1088/0034-4885/68/6/R03>.
- [43] J.M. O'Reilly, The effect of pressure on glass temperature and dielectric relaxation time of polyvinyl acetate, *J. Polym. Sci.* 57 (1962) 429–444, <https://doi.org/10.1002/pol.19621205716534>.
- [44] M. Paluch, R. Casalini, S. Hensel-Bielowka, C.M. Roland, Effect of pressure on the crystallization in glycerol and xylitol, *J. Chem. Phys.* 116 (2002) 9839, <https://doi.org/10.1063/1.1473652>.
- [45] W.K. Kipnusu, M. Elsayed, R. Krause-Rehberg, F. Kremer, Glassy dynamics of polymethylphenylsiloxane in one- and two-dimensional nanometric confinement—a comparison, *J. Chem. Phys.* 146 (2017) 203302, <https://doi.org/10.1063/1.4974767>.
- [46] J.-Y. Park, G.J. McKenna, Size and confinement effects on the glass transition behavior of polystyrene/o-terphenyl polymer solutions, *Phys. Rev. B Condens. Matter Phys.* 61 (2000) 6667, <https://doi.org/10.1103/PhysRevB.61.6667>.
- [47] Ch. Politidis, S. Alexandris, G. Sakellariou, M. Steinhart, G. Floudas, Dynamics of entangled cis-1,4-polyisoprene confined to nanoporous alumina, *Macromolecules* 52 (2019) 4185–4195, <https://doi.org/10.1021/acs.macromol.9b00523>.
- [48] A.E. Nielsen, S. Sarig, Homogeneous nucleation of droplets and interfacial tension in the liquid system methanol-water-tribromomethane, *J. Cryst. Growth* 8 (1971) [https://doi.org/10.1016/0022-0248\(71\)90014-5](https://doi.org/10.1016/0022-0248(71)90014-5).
- [49] V.B. Fenelonov, G.G. Kodenyov, V.G. Kostrovsky, On the dependence of surface tension of liquids on the curvature of the liquid-vapor interface, *J. Phys. Chem. B* 105 (2001) 1050–1055, <https://doi.org/10.1021/jp9929972>.
- [50] Y. Martin, C.C. Williams, H.K. Wickramasinghe, Atomic force microscope-force mapping and profiling on a sub-100-Å scale, *J. Appl. Phys.* 61 (1987) <https://doi.org/10.1063/1.3388074723-472>.
- [51] P.M. McGuiggan, J.S. Wallace, Maximum force technique for the measurement of the surface tension of a small droplet by AFM, *J. Adhes.* 82 (2006) 997–1011, <https://doi.org/10.1080/00218460600876225>.



#### **A4.Are hydrogen supramolecular structures being suppressed upon nanoscale confinement? The case of monohydroxy alcohols**

Autorzy: A. Talik, M. Tarnacka, M. Geppert-Rybczyńska, B. Hachuła, R. Bernat, A. Chrzanowska, K. Kaminski, M. Paluch.

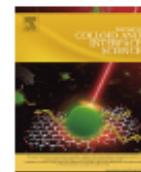
Referencja: Journal of Colloid and Interface Science 576 (2020) 217–229

DOI: 10.1016/j.jcis.2020.04.084

Impact Factor czasopisma z roku opublikowania pracy: 7.489

Liczba punktów ministerialnych MNiSW czasopisma (2019): 100

Mój udział w pracy polegał na: przeglądzie literaturowym, zaplanowaniu oraz koordynowaniu eksperymentu, przygotowaniu próbek, wykonaniu pomiarów a następnie analizie otrzymanych danych, przygotowaniu rysunków oraz dyskusji otrzymanych wyników, oraz przygotowaniu manuskryptu a także formułowaniu odpowiedzi na uwagi recenzentów.



## Are hydrogen supramolecular structures being suppressed upon nanoscale confinement? The case of monohydroxy alcohols



Agnieszka Talik<sup>a,b,\*</sup>, Magdalena Tarnacka<sup>a,b</sup>, Monika Geppert-Rybczyńska<sup>c</sup>, Barbara Hachuła<sup>c</sup>, Roksana Bernat<sup>c</sup>, Agnieszka Chrzanowska<sup>d</sup>, Kamil Kaminski<sup>a,b,\*</sup>, Marian Paluch<sup>a,b</sup>

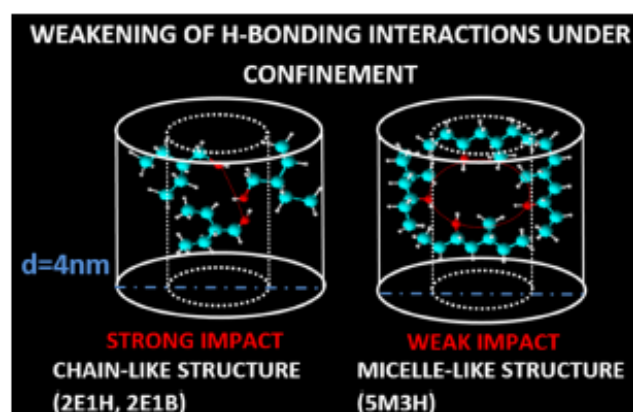
<sup>a</sup>Institute of Physics, University of Silesia in Katowice, 75 Pułku Piechoty 1, 41-500 Chorzów, Poland

<sup>b</sup>Silesian Center of Education and Interdisciplinary Research, University of Silesia in Katowice, 75 Pułku Piechoty 1A, 41-500 Chorzów, Poland

<sup>c</sup>Institute of Chemistry, University of Silesia in Katowice, Szkolna 9, 40-006 Katowice, Poland

<sup>d</sup>Department of Physical Chemistry, Institute of Chemical Sciences, Faculty of Chemistry, Maria Curie-Skłodowska University in Lublin, M. Curie-Skłodowska Sq. 3, 20-031, Lublin, Poland

### GRAPHICAL ABSTRACT



### ARTICLE INFO

#### Article history:

Received 29 December 2019

Revised 15 April 2020

Accepted 20 April 2020

Available online 4 May 2020

#### Keywords:

Monohydroxy alcohols

Surface effects

Confinement

Surface tension

Interfacial energy

Self-assembly

Hydrogen bonds

### ABSTRACT

In this paper, the molecular dynamics, H-bonding pattern and wettability of the primary and secondary monohydroxyalcohols, 2-ethyl-1-hexanol (2E1H), 2-ethyl-1-butanol (2E1B) and 5-methyl-3-heptanol (5M3H) infiltrated into native and functionalized silica and alumina pores having pore diameters,  $d = 4\text{ nm}$  and  $d = 10\text{ nm}$ , have been studied with the use of Broadband Dielectric (BDS) and Fourier Transform InfraRed (FTIR) spectroscopies, as well as contact angle measurements. We found significant differences in the behavior of alcohols forming chain- (2E1H, 2E1B) or micelle-like (5M3H) supramolecular structures despite of their similarities in the wettability and interfacial energy. It turned out that nanoassociates as well as H-bonds are more or less affected by the confinement dependently on the chemical structure and alcohol order. Moreover, a peculiar behavior of the self-assemblies at the interface was noted in the latter material (5M3H). Finally, it was found that irrespectively to the sample, type of pores, functionalization, the temperature evolution of Debye relaxation times,  $\tau_D$ , of the confined systems deviates from the bulk behavior always at similar  $\tau_D$  due to vitrification of the interfacial layer. This

\* Corresponding authors at: Institute of Physics, University of Silesia in Katowice, 75 Pułku Piechoty 1, 41-500 Chorzów, Poland.

E-mail addresses: [agnieszka.talik@smcebi.edu.pl](mailto:agnieszka.talik@smcebi.edu.pl) (A. Talik), [kamil.kaminski@us.edu.pl](mailto:kamil.kaminski@us.edu.pl), [kamil.kaminski@smcebi.edu.pl](mailto:kamil.kaminski@smcebi.edu.pl) (K. Kaminski).

<https://doi.org/10.1016/j.jcis.2020.04.084>

0021-9797/© 2020 Elsevier Inc. All rights reserved.

## 1. Introduction

Intra- and intermolecular hydrogen bonds (H-bonds), although relatively weak (~20 kJ/mol), determine physicochemical properties of many glass-forming liquids [1–4]. Moreover, they have also a tremendous influence on the progress of various chemical (e.g., isomerizations [5]), biological (e.g., keeping the structure of proteins) and physical (e.g., phase transitions, specific heat capacity) processes. However, despite intensive studies, there is still a lack of detailed description of H-bonds, self-association phenomenon, and behavior of these specific interactions at various external conditions, i.e., high pressure or spatial geometrical confinement [6,7].

Important insights on the behavior of H-bonds offered a systematic and comprehensive study on monohydroxy alcohols (monoalcohols), by means of broadband dielectric spectroscopy [1,7–10]. Interestingly, in dielectric loss spectra of these systems, besides of commonly observed structural process responsible for the vitrification, also an additional slower Debye (*D*) relaxation related to the mobility of supramolecular self-assemblies is detected [11,12]. As shown, the amplitude of this mode depends on the position of the hydroxyl group. Briefly, if the –OH moiety is located at the terminal (i.e., 2-ethyl-1-hexanol, 2E1H) or secondary or tertiary carbon atoms (i.e., 5-methyl-3-heptanol, 5M3H), *D*-relaxation is visible either as a process of higher or smaller amplitude, respectively [10,13,23]. By monitoring the dielectric strength, relaxation times of *D*-mode ( $\tau_D$ ), or its time scale separation from the structural relaxation, we can gain indirect insights into the population and behavior of H-bonds and morphology of associates. A change in these parameters can be used to explain the impact of solvent, high electric field, and compression on the population/strength of these specific interactions as well as the architecture of the supramolecular structures [10,14]. In this context, it is worthwhile to stress that high-pressure studies on 2E1H revealed that at low-pressure range ( $p < 0.53$  GPa), the number of hydrogen bonds remains constant, while further compression leads to the reduction of the size and number of chain-like supramolecular structures [23]. The modification within the H-bonding pattern was also manifested by the variation within the scaling exponent,  $\gamma$ , material constant connected to the repulsive part of the intermolecular potential [15], and the isobaric fragility parameter,  $m_p$ . As shown, the  $m_p$  was constant below the threshold value  $p = 0.53$  GPa, whereas it increased at higher pressure due to a decrease in the H-bonds population. Interestingly, a similar scenario was found for the other hydrogen-bonded materials [15,23].

The other way to effectively influence on the population of the hydrogen-bonds is the application of the nanometrical spatial restriction [16,17]. As shown, the pre-peak, strictly related to the presence of the supramolecular structures ordered on the medium range scale, detected in diffractograms obtained from neutron scattering experiments for the bulk *tert*-butanol [18], is completely suppressed for the alcohol confined within mesoporous silica. This simply means that the internal ordering is no longer preferred at such conditions [18]. Moreover, dielectric data obtained for 2E1H incorporated into silica porous glass [16] revealed a decrease of the amplitude of the Debye process under confinement with respect to the bulk sample. It was interpreted as the change in the degree of association of the alcohol [19]. In fact, it was shown that the size of the chain-like associates is almost twice lower with respect to those formed in the non-restricted material. A similar

effect was reported for 2E1H confined within the surface of the collagen matrix [19], where the dynamics of both structural and Debye relaxations were strongly dependent on the alcohol concentration. It was well demonstrated that with an increase in the degree of dilution, the Debye process gets broader and becomes nonexponential [19]. At the same time, the relative strength of the structural process increased as a consequence of a breakup of the supramolecular structure, eventually reaching the limit of a non-associated liquid. The change in the H-bonding pattern under confinement affected also kinetics and progress of the physical processes. The best illustration of that is the crystallization of water. In this particular case, the change in the pore diameter influenced the character of crystallization (homo vs. hetero) as well as affected the ice structure (from hexagonal to cubic) due to increasing interactions with the pore walls. Interestingly, it was shown that in a porous matrix characterized by a pore diameter  $d < 2.6$  nm, stable crystals are not created [16,19,20]. Moreover, for salol, a weakly H-bonded compound, incorporated into AAO pores, two various polymorphic forms differing significantly in the thermodynamic stability were obtained by a simple change in the diameter of nanochannels [21].

In this paper, we examined the role of H-bonds on the behavior of three monoalcohols having the different location of the hydroxyl group (–OH): 2-ethyl-1-hexanol (2E1H), 2-ethyl-1-butanol (2E1B) and 5-methyl-3-heptanol (5M3H, see Fig. 1). The various position of the hydroxyl group results in a formation of different supramolecular structures, either ring- or chain-like [1], and affects the amplitude of the Debye process [6,10,22,23,24]. The selected materials were infiltrated into alumina porous template (of  $d = 10$  nm) as well as in both hydrophilic (native) and hydrophobic (silanized) silica pores (of  $d = 4$  nm), and measured using two experimental techniques: Broadband Dielectric (BDS) and Infrared (IR) spectroscopies. The main aim of our studies was to elucidate the impact of the interfacial hydrogen interactions on the behavior of confined substances, especially the formation of the supramolecular structure at the interfaces. It should be pointed out that the former technique gives insights into the molecular dynamics of the studied materials, whereas the latter one is dedicated to studying the strength of H-bonds structures. Therefore, a quite interesting perspective to evaluate the impact of the spatial restriction on the dynamics of alcohols having tendencies to form supramolecular structures of different architecture as well as a change in the H-bonding pattern appeared.

## 2. Experimental section

### 2.1. Materials

2-Ethyl-1-butanol (2E1B), 2-ethyl-1-hexanol (2E1H) and 5-methyl-3-heptanol (5M3H) having purity higher than 99%, were supplied by Sigma-Aldrich. Their chemical structures are presented in Fig. 1. The nanoporous aluminum oxide (AAO) membranes used in this study (supplied from InRedox) are composed of uniaxial channels (open from both sides) with well-defined pore diameter. The nanoporous silica membranes were prepared by electrochemical etching of silicon wafers and subsequent thermal oxidation. In the experiment, we used both alumina membranes characterized by pore diameter  $d = 10$  nm and silica templates (native and sila-

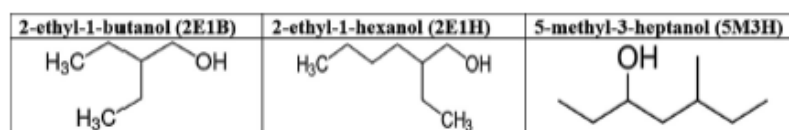


Fig. 1. The chemical structure of the three investigated monoalcohols.

nized) of  $d = 4$  nm [16,25,26]. Details concerning the applied nanoporous matrices are presented in the SI file.

## 2.2. Samples preparation

Before filling, AAO and silica membranes were dried in an oven at  $T = 423$  K under vacuum to remove any volatile impurities from the nanochannels. After cooling, they were immersed with alcohol. Then, the whole system was maintained in a vacuum ( $10^{-2}$  bar), where the nanopores were filled by capillary wetting. After completing the infiltration process, the surface of AAO and silica membranes were dried, and the excess sample on the surface was removed by use of the paper towel. The complete filling was obtained by weighing the templates before and after each infiltration to constant mass. In the experiment, we used membranes of various pore diameters,  $d = 4$  nm (silica), and  $d = 10$  nm (alumina). The pore diameters of freshly prepared silica templates were confirmed by SEM and complementary low-temperature nitrogen adsorption/desorption isotherms measurements (see SI).

## 3. Methods

### 3.1. Broadband dielectric spectroscopy (BDS)

Isobaric measurements of the complex dielectric permittivity  $\epsilon^*(\omega) = \epsilon'(\omega) - i\epsilon''(\omega)$  were carried out using the Novocontrol Alpha dielectric spectrometer over the frequency range from  $10^{-1}$  to  $10^6$  Hz at ambient pressure. The temperature stability controlled by Quatro Cryosystem using nitrogen gas cryostat was better than 0.1 K. Dielectric measurements of bulk monohydroxy alcohols were performed in a parallel-plate cell (diameter: 10 mm, gap: 0.1 mm). AAO and silica membranes filled with 2E1B, 2E1H, and 5M3H were also placed in a similar capacitor (diameter: 5 mm and 10 mm) [25,26]. Nevertheless, the confined samples are a heterogeneous dielectric consisting of a matrix and an investigated compound. Because the applied electric field is parallel to the long pore axes, the equivalent circuit consists of two capacitors in parallel composed of  $\epsilon_{\text{compound}}^*$  and  $\epsilon_{\text{matrix}}^*$ . Thus, the measured total impedance is related to the individual values through  $1/Z^* = 1/Z_{\text{compound}}^* + 1/Z_{\text{matrix}}^*$ . It should be added that dielectric measurements on empty membranes were also carried out to evaluate the contribution of AAO, and silica which turned out to be negligible.

### 3.2. IR spectroscopy

FTIR spectra of the bulk and confined samples were recorded on a Nicolet iSSO FTIR spectrometer (Thermo Scientific) in the region of  $4000$ – $1300$   $\text{cm}^{-1}$  by averaging 32 scans with a spectral resolution of  $4$   $\text{cm}^{-1}$ . The bands located below  $1300$   $\text{cm}^{-1}$  are not taken into account due to the absorption of  $\text{CaF}_2$  windows (below  $800$   $\text{cm}^{-1}$ ) and the detector saturation in the region of Si–O stretching vibrations. The spectra were measured at room temperature ( $T = 293$  K), at the glass transition temperature of bulk ( $T_{g, \text{bulk}}$ ), and interfacial molecules of confined alcohols ( $T_{g, \text{interfacial}}$ ) determined from BDS measurements. To record FTIR spectra at

low temperatures, a liquid nitrogen-cooled Linkam THMS 600 stage (the temperature accuracy of  $\pm 0.1$  °C) was adapted to the Nicolet spectrometer.

### 3.3. Surface tension and contact angle measurements

The surface tension of liquids  $\gamma_L$  (pendant drop method) and contact angle  $\theta$  were measured with the DSA 100S Krüss Tensiometer, GmbH Germany. The description of the instrument and procedures has been presented previously [27,28]. The measuring procedure at  $T = 298.2$  K for all substances has been repeated dozen or more times. The temperature measurements uncertainty was  $\pm 0.1$  K. The precision of contact angle measurements was  $0.01^\circ$ , and the estimated uncertainty was  $\pm 1.5^\circ$ , whereas the uncertainty of surface tension was  $\pm 0.1$   $\text{mN}\cdot\text{m}^{-1}$ . Density,  $\rho$ , required for the surface tension experiment was measured with an Anton Paar DMA 5000 M densimeter with the uncertainty not worse than  $0.0001$   $\text{g}\cdot\text{cm}^{-3}$ . For the surface energy estimation of native and silanized silica some of the following liquids were considered: water, ethylene glycol, diiodomethane and glycerol. The dispersive and non-dispersive part in the surface tension for these substances were taken from Ref. [48]. The procedure for surface energy calculations has been also previously reported in Ref. [44]. The calculated surface energy for native silica was  $67.6$   $\text{mJ}/\text{m}^2$  with dominant non-dispersive part equal  $66.6$   $\text{mJ}/\text{m}^2$ . For silanized surface respective value was  $25.3$   $\text{mJ}/\text{m}^2$  with as expected dominant, dispersive component  $22.8$   $\text{mJ}/\text{m}^2$ .

## 4. Results and discussion

Representative dielectric loss spectra measured for the bulk monohydroxy alcohols: 2-ethyl-1-butanol (2E1B), 2-ethyl-1-hexanol (2E1H, data were taken from Ref. [16]), and 5-methyl-3-heptanol (5M3H), and samples infiltrated into silica ( $d = 4$  nm) and alumina pores ( $d = 10$  nm) are shown in Fig. 2, and in Fig. S3 in Supporting Information (SI) file. In each case, one can detect the following processes: (i) *dc*-conductivity related with the charge transport, (ii) prominent Debye process strictly connected with the H-bonds formation and (iii) a weakly separated structural,  $\alpha$  relaxation at a higher frequency, related to the glass-transition phenomenon (Fig. 2(a, d)). For the confined alcohols, an additional process located at the lower frequency side of the Debye relaxation can be noted in the presented data (Fig. 2(b, e)). One can suppose that this additional mobility might be a Maxwell-Wagner relaxation that is generally detected in the loss spectra collected for the heterogeneous composite materials. In fact, a presence of this particular process might be connected to the sample character that is composed of solid alumina or silica membranes and liquid, incomplete pore filling, or eventual crystallization of the alcohols at the pore walls. However, it should be noted that the majority of studies performed up to date revealed that crystallization is strongly suppressed for the systems infiltrated into pores of diameter close to the critical radius of the nuclei ( $r = 2$ – $3$  nm). In this context, one can recall extensive studies on the water that crystallize in bulk while in pores, this process is being continuously suppressed due to lowering pore diameter [29]. The same situation

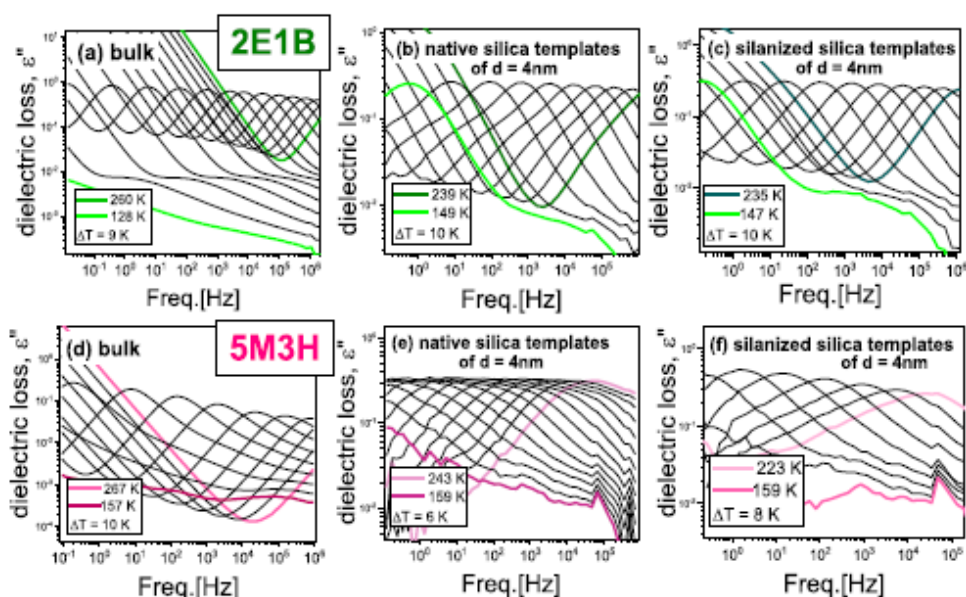


Fig. 2. Representative dielectric loss spectra of bulk and confined monohydroxy alcohols measured upon slow cooling. For 2E1H, spectra were represented in Ref. [16].

was observed for fenofibrate and salol confined in alumina nanoporous templates [30,31]. Moreover, considering literature data published for the spatially restricted samples, this additional process might also be related to the motions of the molecules adsorbed to the pore walls, so-called interfacial relaxation process [32,33]. To verify both hypotheses, we functionalized/silanized the surface of the silica templates with the use of methoxytrimethylsilane to make it more hydrophobic [34]. As shown for all compounds, this additional slow process is completely or partially suppressed after silanization, indicating that it can be assigned to the dynamics of molecules strongly interacting with the pore walls indeed (Fig. 2(c)). This effect is well illustrated in Fig. 3, where the loss spectra measured for the bulk and confined samples characterized by the same relaxation times of the Debye process,  $\tau_D$ , were superposed (representative loss spectra were arbitrarily shifted vertically to superpose at maximum). As shown in Fig. 3, the interfacial process observed for the primary alcohols vanishes

completely, while in the case of the secondary 5M3H, it is still detectable, although not as a separated peak. Moreover, it was also found that dependently on the sample, the shape, and intensity of the interfacial process change. Herein, it should also be commented that the Maxwell-Wagner relaxation was detected in the loss spectra measured at a higher temperature range for the alcohols confined in silica and alumina pores (data not shown).

Data presented in Fig. 3 also revealed that, surprisingly, there is no interfacial process connected to the reorientation of the adsorbed molecules for the alcohols infiltrated into alumina membranes ( $d = 10$  nm). To explain this experimental observation, one can suppose that there are different interactions of the confined alcohols with alumina and silica surface of the pore walls. To address this issue and quantify the strength of the surface interactions, as well as their impact on the presence/absence of the interfacial process, additional contact angle,  $\theta$ , and surface tension,  $\gamma_s$ , measurement (Table 1) were performed. Note, that the interfacial

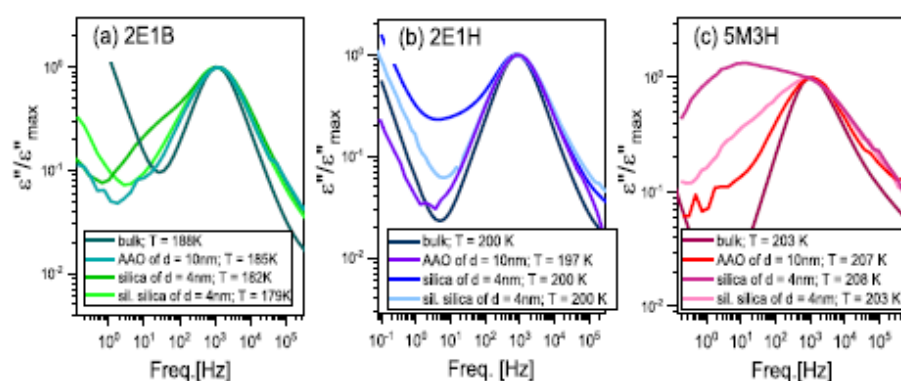


Fig. 3. Comparison of the shape of Debye loss peaks obtained for bulk and confined monohydroxy alcohols. The presented spectra were normalized with respect to the maximum of dielectric loss ( $\epsilon''_{max}$ ).

**Table 1**  
Contact angle ( $\theta$ ), surface tension ( $\gamma_L$ ), and the interfacial energy ( $\gamma_{SL}$ ) of indicated substances at  $T = 298$  K.

samples	Alumina surface			Native silica			Silanized silica		
	$\theta$ [°]	$\gamma_L$ [mN m <sup>-1</sup> ]	$\gamma_{SL}$ [mN m <sup>-1</sup> ]	$\theta$ [°]	$\gamma_L$ [mN m <sup>-1</sup> ]	$\gamma_{SL}$ [mN m <sup>-1</sup> ]	$\theta$ [°]	$\gamma_L$ [mN m <sup>-1</sup> ]	$\gamma_{SL}$ [mN m <sup>-1</sup> ]
2E1B	1.5	25.09	33.9	8.5	25.09	42.8	21.5	25.09	2.0
2E1H	1.3	25.65	33.3	12.7	25.65	42.6	25.6	25.65	2.2
5M3H	5.3	22.7	36.4	0	22.7	44.9	4.7	22.7	2.7

energy,  $\gamma_{SL}$ , was estimated from the surface tension and the contact angle accordingly to the Young equation ( $\gamma_{SL} = \gamma_S - \gamma_L \cos \theta$ , where  $\gamma_S$  is the surface energy) [35,36]. It was found that all investigated systems are characterized by the comparable surface tension  $\gamma_L$  and interfacial energies  $\gamma_{SL}$  (34–45 mJ/m<sup>2</sup>) independently to the structure and surface. Moreover, each investigated alcohol wets alumina and silica very well since the measured contact angles lie within the range  $\theta \sim 2$ – $10^\circ$  (see Table 1). Interestingly, the situation has changed after the silanization of SiO<sub>2</sub> surface. In this particular case, the contact angle determined for 2E1B and 2E1H increased from  $\theta \sim 10^\circ$  (native) to  $\theta \sim 25^\circ$  (silanized), while that measured for 5M3H remained almost unchanged ( $\theta \sim 0^\circ$  vs.  $\theta \sim 5^\circ$ ). What is more, due to the low energy of the silanized surface, we obtained very low interfacial energies ( $\gamma_{SL} \sim 2$ ) for the considered systems. This quite peculiar finding indicates that there is a strong change in the character of interactions between alcohol and functionalized silica at the interface. Following work by Fowkes et al. [37,38], one can suppose that strong dispersion forces between host and guest materials dominate in the silanized pores, see Table 1. As discussed above, the investigated samples wet alumina and silica surfaces very well, and the silanization of the silica surface does not change the wettability of the alcohols as dramatically as one can expect. Contrary, 5M3H wets all studied surfaces very well (including the silanized silica). Thus, an evident broadening of the low-frequency side of a Debye process due to pore silanization might be considered as a manifestation of the heterogeneous dynamics of the supramolecular structures at the interface connected to the presence of still relatively strong surface dispersive interactions. In this context, it is worthwhile to stress that in the case of 2E1B and 2E1H, the silanization of templates resulted in complete suppression of the interfacial process in the dielectric spectra, which is consistent to the data published for the other confined liquids [25,39]. The peculiar behavior of 5M3H might be connected to its enhanced tendency to form micelle-like supramolecular structures that are more amphiphilic with respect to the chain-like associates created by the primary alcohols. Therefore, considering the results of contact angle measurements discussed above, one can suppose that an appearance/absence of the interfacial process in the loss spectra of alcohols incorporated within alumina or silica pores is not related to the change in wettability and interfacial energy. It might be connected to the different packing, layering of the supramolecular structures, and distribution of the dipole moments at the interface. Alternatively, this effect might also be assigned to the lowering pore diameter that has an impact on the rate of exchange between core and interfacial molecules with respect to the time scale of the experiment, as discussed in Ref. [40]. However, it should be noted that for 2E1H incorporated into silica pores of  $d = 8$  nm (comparable to  $d = 10$  nm of alumina membranes), an interfacial process was clearly observed in the loss spectra [16]. Therefore to address this problem in more detail, further studies are required.

Additionally, loss spectra presented in Fig. 3 demonstrated, that the observed prominent Debye process of the core molecules is getting broader for each sample with lowering pore diameter when compared to the bulk sample while, the structural relaxation is still weak and not well-resolved as a separated peak in the loss spectra, see Fig. 3.

Taking advantage of the loss spectra measured for the confined materials, we investigated in more detail the molecular dynamics of the molecules/self-assemblies located in the center of pores and those attached to the interface. As a first, we studied a ratio between the relaxation times of the Debye and interfacial process,  $\tau_D/\tau_{INT}$  (Fig. 4(a)) providing direct information about the difference in the time scale of the dynamics of supramolecular nanoassociates in both locations. Note that the relaxation times were determined from the fitting analysis of the obtained dielectric loss spectra with the use of two or three Havriliak-Negami (HN) function with an additional dc-conductivity term [41]:

$$\varepsilon''(\omega) = \frac{\sigma_{dc}}{\varepsilon_0 \omega} + \text{Im} \sum_{i=1}^2 \left( \varepsilon_{\infty} + \frac{\Delta \varepsilon_i}{1 + (i\omega\tau_i)^\alpha \beta_i} \right), \quad (1)$$

where  $\alpha$  and  $\beta$  - the shape parameters representing the symmetric and asymmetric broadening of given relaxation peaks,  $\varepsilon_0$  is the vacuum permittivity,  $\Delta \varepsilon$  is the dielectric relaxation strength,  $\omega$  is an angular frequency ( $\omega = 2\pi f$ ). As illustrated in Fig. 4(a), there is a difference in the time scale between  $\tau_D$  and  $\tau_{INT}$  for primary and secondary alcohols at higher temperatures. In fact, in this regime,  $\tau_D/\tau_{INT}$  ratio is the lowest for 5M3H indicating the largest separation between relaxation times of the supramolecular structures at the interface and in the core location. Nevertheless, when approaching the glass transition temperature,  $T_g$ ,  $\tau_D/\tau_{INT}$  reach comparable values for all substances. Similar deviation in the behavior of secondary alcohol with respect to the other systems is noted when we analyze the ratio between the dielectric relaxation strengths of Debye and interfacial process,  $\Delta \varepsilon_D/\Delta \varepsilon_{INT}$ , see Fig. 4(b). Interestingly in contrast to 2E1B and 2E1H, the  $\Delta \varepsilon_D/\Delta \varepsilon_{INT}$  ratio of confined 5M3H is the lowest, since the amplitude of the interfacial process in this particular system is even greater than that of Debye mode of the core molecules. The observed difference between the behavior of 2E1H and 2E1B with respect to 5M3H infiltrated to the pores must be connected to the chemical structure of the studied substances and the architecture of the formed supramolecular structures. In this context, it is worthwhile to remind, that in the primary alcohols chain-like structures are preferred, while in 5M3H molecules are mostly arranged as cyclic/ring associates having amphiphilic character [7]. To understand in more detail these data, one can recall paper by Ghoufi et al. [42] who studied structural and dynamical behavior of *tert*-butanol (a system capable of forming ring/cyclic clusters just like 5M3H) infiltrated within native and silanized silica pores of the average pore diameter  $d = 2.4$  nm. Authors have shown that independently of the functionalization, the mean size of the nanoaggregates (4 molecules) is not affected by the spatial restriction. Moreover, it was claimed, that along with the significant increase in the density (about 78%) also enhanced anisotropy in the layering and permittivity of the material in the proximity of the interface was reported. Taking into account this finding, one can suppose that large dielectric strength of the interfacial process in 5M3H is related to both densifications of the supramolecular structures or specific layering near the interface leading to the increase of the parallel component of the dielectric permittivity ( $\varepsilon_{||}$ ) with respect to the perpendicular one ( $\varepsilon_{\perp}$ ). Alternatively, we can also consider that due to the interactions with the surface, some cyclic micelle-like structures are being opened

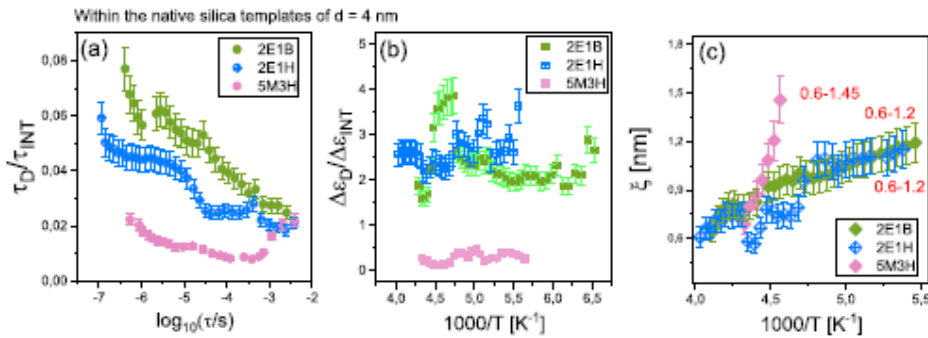


Fig. 4. (a) Ratio of the Debye and interfacial relaxation times  $\tau_D/\tau_{INT}$  calculated for native pores plotted as a function of Debye relaxation time, (b) and (c) temperature evolution of  $\Delta\epsilon_D/\Delta\epsilon_{INT}$  ratio, as well as thickness of adsorbed layer in native hydrophilic pores together with error bars, is presented, respectively. Error bars show the standard deviation for  $n = 6$ .

and transformed into linear associates contributing to an additional increase of the dielectric strength of the interfacial process. Additionally, it should be commented that the broad distribution of the relaxation times of the interfacial process in 5M3H might also be related to the fact that non intuitively, this compound adsorbs to the native silica pores via  $\text{CH}_3$  moiety [42]. It is due to the fact that alcohol molecules prefer the formation of intermolecular H-bonds than the ones with the matrix. Therefore, there are very weak hydrogen bonds of the strength comparable to the dispersive interactions between supramolecular structures of micelle-like geometry and silica pore walls [1,43,44].

Due to the presence of a prominent interfacial process observed in the loss spectra of alcohols confined in native silica pores, it was also possible to estimate the approximate thickness of the adsorbed layer,  $\xi$ , accordingly to the relation proposed by Kipnusu et al. [16]:

$$\xi(T) = R_p \left[ 1 - \sqrt{\frac{\Delta\epsilon_m - \phi\Delta\epsilon_a}{\phi(\Delta\epsilon_b - \Delta\epsilon_a)}} \right], \quad (2)$$

where  $R_p$  is the average radius of the nanopores;  $\phi$  is the porosity;  $\epsilon_b, \epsilon_a$  are contributions of the bulk-like (core) and the adsorbed (interfacial) molecules. The temperature dependences of estimated  $\xi$  are presented in Fig. 4(c). As illustrated, the thickness of the interfacial layer differs dependently on the chemical structure of the studied compound. For 2E1B and 2E1H,  $\xi$  reaches a comparable value ( $\xi \sim 0.6\text{--}1.2$  nm), whereas, in the case of the confined 5M3H, it is a little higher when compared to the other systems ( $\xi \sim 0.6\text{--}1.45$  nm). One can assume, that a small difference in  $\xi$  might be again correlated with a different architecture of the formed supramolecular self-assemblies, and their different packing near the pore walls.

Since in the literature authors reported no, partial, or complete disruption of the H-bonded clusters in mono-hydroxy alcohols confined in silica pores of very low diameters ( $d \sim 1\text{--}4$  nm), we decided to address this issue relying on the collected dielectric data. For that purpose, we used the relation proposed by Gainau [45] who applied a model derived for the description of the dynamics of the type A-polymers characterized by a dipole moment arranged parallel to the chain backbone to calculate the number of molecules involved in the H-bonded supramolecular self-assemblies,  $N$ . This assumption leads to the following expression [45]:

$$\frac{\Delta\epsilon_D}{\Delta\epsilon_a} = \frac{\left(\frac{\mu_{\text{end-to-end}}}{\mu_{\perp}}\right)^2}{N} \approx 4N, \quad (3)$$

where  $\Delta\epsilon_D, \Delta\epsilon_a$  are dielectric strength of the Debye and structural relaxation process,  $\mu_{\text{end-to-end}} = N\mu$  and  $\mu_{\perp}$  is expected to be  $-\mu/2$ . Dipole moments of the investigated systems were calculated from DFT computations and are equaled to  $\mu \sim 1.5$  D. Temperature dependences of  $N$  are presented in Fig. 5. As shown in the case of 2E1B and 2E1H,  $N$  reaches values of  $N \sim 10\text{--}13$  and  $N \sim 7\text{--}8$  for the bulk samples, which agrees with the literature data [16,45]. However, interestingly, the number of H-bonded molecules decreases significantly under confinement, indicating the reduction in the chain length of the supramolecular structures in these systems. Note, that a comparable decrease of  $N$  with a lowering of pore size was previously reported by Kipnusu et al. [16] for 2E1H confined into silica pores. On the other, in the case of the secondary alcohol, 5M3H forming mainly micelle-like supramolecular structures,  $N$  parameter remains constant under confinement (within experimental uncertainty, see Fig. 5). What is more,  $N$  is not affected by the functionality (native vs. silanized) of the pores. This result is consistent with the data reported by Ghufi et al. [42] for *tert*-butanol confined within silica pores of  $d \sim 2\text{--}3$  nm. They have shown that the number of molecules was around  $N \sim 4$  independently on the studied system (bulk and confined within native and silanized pores). Therefore, from this simple comparison, it becomes clear that the spatial confinement affects the number of H-bonded molecules organized in a chain- or ring-like supramolecular structures in a completely different way. It is also worthwhile to stress that at first sight, data reported herein stay in contrast to the papers showing that supramolecular structures formed by alcohols cannot survive within pores of very low diameter  $d \sim 1\text{--}4$  nm [17,18]. Briefly, one can remind that Jansson et al. [17] discussed that self-assemblies formed by 2-ethyl-1-hexanol (2E1H), 2-ethyl-1-butanol (2E1B), and 2-methyl-1-butanol (2M1B) are destroyed in the samples confined within small (quasi-two-dimensional) Na-veemiculite clay and (quasi-one-dimensional) commercial zeolite-13X (of pore diameter  $d \sim 1$  nm). In some way, this assumption was confirmed in a paper by Morineau et al. [18], who found that there is no pre-peak in diffraction data obtained for *tert*-butanol infiltrated into MCM-41 molecular sieves ( $d \sim 2.4$  nm and  $d \sim 3.5$  nm). However, a lack of the pre-peak in diffractograms of the monohydroxy alcohols infiltrated into pores does not necessarily mean that self-assemblies are destroyed. It indicates that the medium-range ordering rather than the size of supramolecular structures are affected in the spatially restricted samples. On the other hand it must be emphasized that Ghufi et al. [42] have shown that for the alcohols forming micelle-like aggregates number of molecules in clusters is constant in cylindrical nanochannels, having pore diameter even lower than those used herein. Moreover,

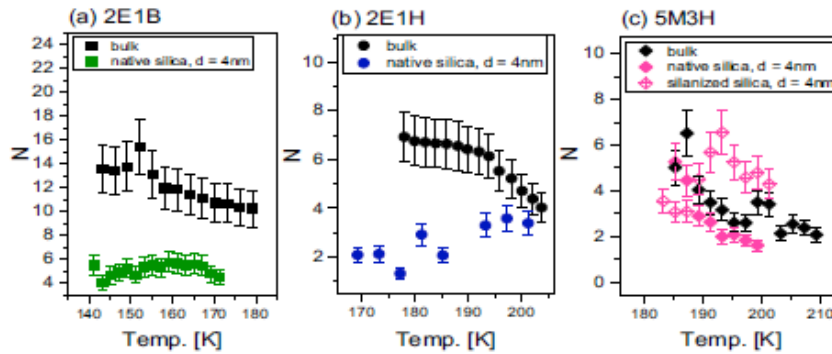


Fig. 5. The number of molecules involved in the supramolecular self-assemblies for the bulk materials and monohydroxy alcohols infiltrated into native and silanized (5M3H) pores, calculated from Eq. (3). Error bars show the standard deviation for  $n = 6$ .

it should be noted we have applied silica or alumina nanoporous membranes having 50  $\mu\text{m}$  long uniaxial pores of the average diameter  $d = 4$  nm and  $d = 10$  nm, respectively. Therefore, there is a lot of space along the pores to allow effective packing of the supramolecular structures in such systems.

In the next step, we compared the dynamics of the confined alcohols with respect to the bulk samples. Relaxation times,  $\tau$ , of all three processes (Debye, structural, and interfacial) determined for the bulk and spatially restricted materials plotted versus inverse temperature are shown in Fig. 6. Note that  $\tau$  was determined from the measured dielectric loss spectra from the fitting collected data by the superposition of the two or three Havriliak-Negami (HN) functions with an additional dc-conductivity term (Eq. (1)). As illustrated, the  $\tau(T)$ -dependence of both processes, Debye and structural, remains the same, within the experimental uncertainty, for all examined samples at high temperatures. However, at the low-temperature range, a pronounced crossover of the temperature evolution of the relaxation times from the VFT to the Arrhenius-like behavior at some temperature  $T_g^{\text{interfacial}}$  was detected independently to the chemical structure of alcohols and the nanoporous membrane, see Fig. 6. One can recall that according to the literature data published for various low- and high-molecular-weight liquids incorporated in pores, this effect is related to the vitrification of the interfacial layer [21,32,33,40]. Note that the performed studies reported to date revealed a good agreement between dielectric  $T_g^{\text{interfacial}}$  and the high glass transition of interfacial layer detected by complementary calorimetric measurements (where no crystallization was observed) [21,49,50]. Interestingly herein, the crossover in  $\tau_D(T)$  and  $\tau_\alpha(T)$ -dependences occurs at temperatures at which the relaxation times of the interfacial process reached  $\tau_{\text{INT}} \sim 1\text{--}10$  s. This confirms that the observed variation in dynamics of the Debye and structural processes is directly connected to the vitrification of the molecules attached to the pore walls [21] (Fig. 6(a–c)). One can add that a similar effect was also reported for a poly(propylene glycol) of  $M_n = 4000$  g/mol, a type-A macromolecule, where polymers adsorbed at the interface induced variation in the chain and segmental dynamics of the core material. What is more, similarly, as in the case of alcohol, the vitrification of the interfacial molecules had a much larger impact on the segmental relaxation than for the chain dynamics [46,47]. In addition, we also would like to draw the attention of the reader to the fact, that despite a change in chemical structure and architecture of the supramolecular structures in the studied materials, the temperature dependences of the Debye relaxation times of all confined samples deviate from

the bulk-like behavior at approximately the same  $\tau_D$  irrespectively of the applied porous template, see Fig. 6 and SI. One can mention, that this phenomenon might be related to the surface effects between alcohols and porous material which are comparable for all studied alcohols (comparable wettability, surface tensions as well as interfacial energies – Table 1) as discussed previously in the following Refs. [48–50]. Although, unexpectedly, we found that in the silanized silica pores, the deviation in the temperature evolution of the Debye relaxation times of the confined alcohol also occurs due to vitrification of the interfacial layer. Note that a change in the  $\tau_D(T)$  occurs at comparable Debye relaxation time, as in the case of the materials infiltrated in the non-modified silica pores despite the significant variation in the interfacial energies between native and silanized template and alcohol, see Fig. 6. Interestingly, very recently similar pattern of behavior has been reported by Tu et al. [51] for the ionic liquids incorporated into porous alumina membranes. In this particular case, the vitrification of the interfacial layer occurred at more less the same temperature independently on the functionalization (hydrophilic vs. hydrophobic) of the pore walls. To explain the extraordinary finding reported herein, one can refer to the work [42] on the behavior of *tert*-butanol confined in silica pores. Authors revealed that the mobility of the interfacial molecules/self-assemblies interacting with the native and silanized pore walls are slightly modified. Although the change in dynamics is not significant, it is due to the fact that independently on the pores functionalization, alcohol molecules prefer to form intermolecular H-bonds rather than with the template. Consequently, even in native pores, supramolecular structures adsorb at the interface *via*  $-\text{CH}_3$  moiety, while in the silanized ones, there are mainly strong dispersive interactions between host and guest molecules. Therefore even though there is a significant change in the interfacial energies, the specific interactions between template and alcohol are not so much different.

Additionally, one can mention that recent studies on the materials infiltrated into porous templates highlighted that apart from the surface interaction [48]; also the sensitivity of the structural process to the density fluctuations, *i.e.*, quantified by the pressure coefficient of the glass transition temperature,  $dT_g/dp$  [50], contributes to the deviation in dynamics of confined systems with respect to the bulk samples. As reported, the higher  $dT_g/dp$ , the greater deviation in  $\tau_\alpha(T)$ -dependence of the infiltrated materials from their bulk behavior, as well as the larger depression of  $T_g$  is expected. Interestingly, the studied alcohols are characterized by a comparable pressure coefficient of the glass transition temperature,  $dT_g/dp = 71$  K/GPa, and  $dT_g/dp = 85$  K/GPa for 2E1H [23]



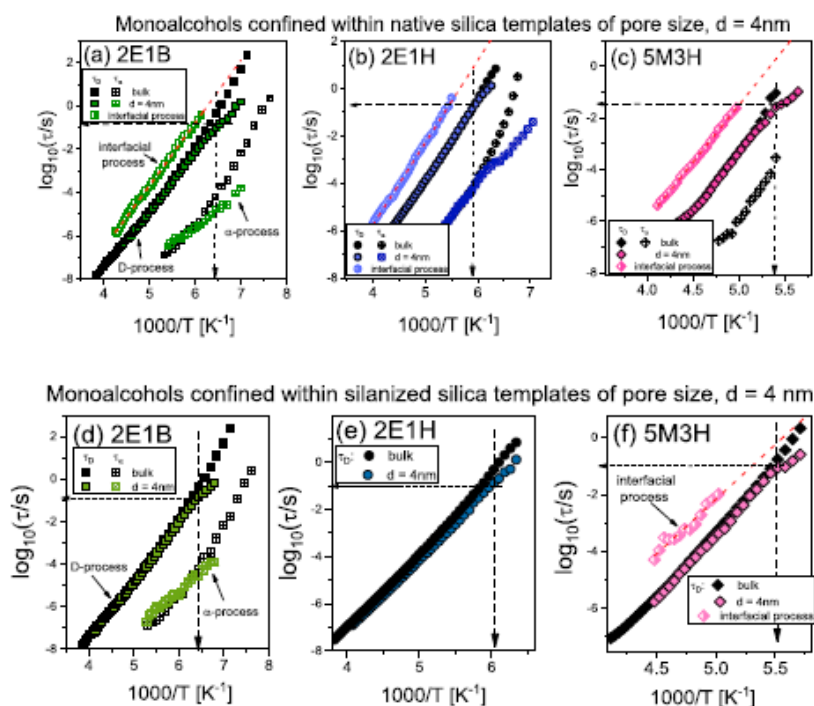


Fig. 6. Temperature dependences of Debye and structural relaxation times obtained for bulk materials and samples confined into native (a–c) and silanized (d–f) silica membranes.

and 5M3H [10], respectively. Therefore, one can suppose that a comparable deviation in  $\tau_D(T)$ -dependence for the confined alcohols might also be connected with their similar  $dT_g/dp$ , see Fig. 6.

To summarize this part, one can also discuss our data in the context of neutron or quasi-elastic neutron scattering (QENS) studies on the liquids confined in pores [52]. One of the most interesting objects of these investigations was water that has a strong tendency to self-association. Interestingly, these experiments, similarly to our dielectric data, revealed that there are two fractions of water that differ in mobility and density distribution. In the center of the pore (core molecules), the density is lower, more uniform, and water molecules move faster with respect to the ones attached to the pore walls. Additionally, from the QENS experiments, the authors calculated radial and axial components of the mean square displacement component of MSD (mean-squared displacement) that were much different [52]. They found that molecules attached to the pore walls are much more mobile along the pores. This finding might be used to explain different shapes (distribution of the relaxation times) of the interfacial processes of the investigated alcohols confined in silica pores. One can suppose that in the primary and secondary alcohols, there is a difference in the time scale of the uniaxial and radial mobility of the supramolecular structures attached to the surface. However, it is just a assumption since dielectric spectroscopy probe reorientational motions, while QENS experiments provided information about MSD. Although both parameters do not have to be necessarily coupled, the latter investigations have demonstrated that the degree of decoupling between translational and rotational dynamics is weakly affected by the pore

diameter. In addition from the analysis of the self-intermediate scattering function  $F(Q,t)$ , it was obtained there is a systematic increase in the relaxation times of the molecules attached to the walls with the lowering of pore size. One can stress, that these studies are consistent with the dielectric investigations reported for many liquids confined in alumina pores [43,49,50,53–55].

Having dynamical properties of the molecules confined within native and silanized silica pores discussed, we performed comprehensive infrared investigations. Just to mention that this technique can be successfully applied to monitor the dynamics of hydrogen-bonds due to the exceptional sensitivity to the changes in the geometry of proton-donor and proton-acceptor connected with the formation of these particular directional interactions. Briefly, one can stress that a correlation between the infrared X–H stretching frequency and the length of the X–H bond is well-known in the literature [56]. The formation of hydrogen-bonded molecular aggregates in bulk and confined alcohols was probed by monitoring the evolution of their –OH band in the FTIR spectra recorded at room temperature ( $T = 293$  K), at the glass transition temperature ( $T_g$ , bulk) and crossover temperature ( $T_g$ , interfacial), where  $\tau_D$  of the spatially restricted samples starts to deviate from the bulk behavior. Experimental results of FTIR measurements obtained for alcohol samples in the spectral range of 3800–2400  $\text{cm}^{-1}$  are shown in Fig. 7. However, since we were mainly interested in the studying dynamics of H-bonds, our attention was focused on the analysis of FTIR spectra in the limited frequency range connected to the stretching vibration of the hydroxyl moiety (3000–3600  $\text{cm}^{-1}$ ). A summary of the spectral parameters such

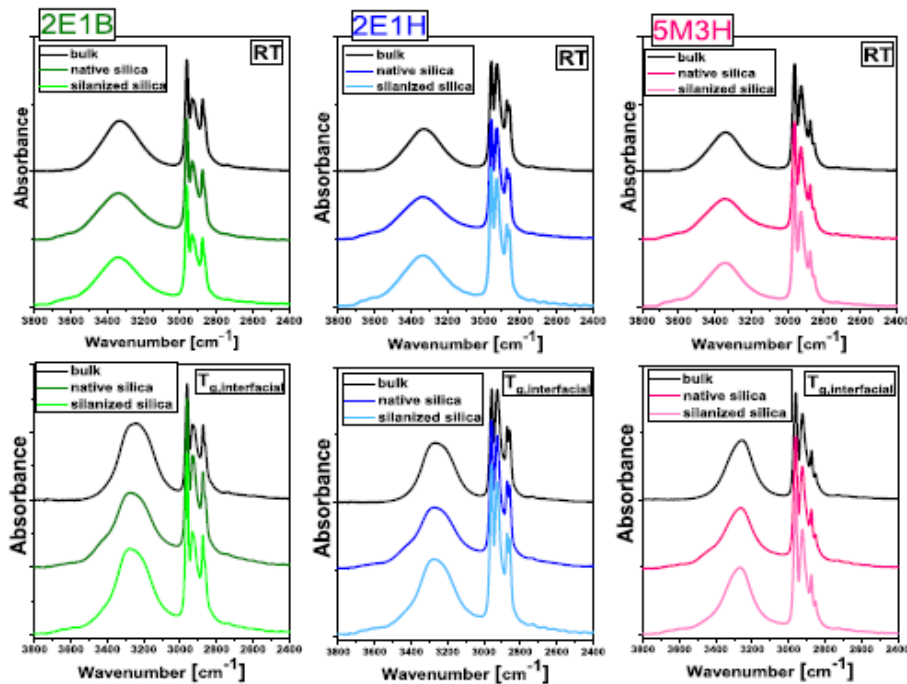


Fig. 7. The  $\nu_{\text{OH}}$  band of the bulk alcohols (and samples confined in native and silanized pores measured at room temperature (upper),  $T_{g, \text{bulk}}$  and at the  $T_{g, \text{interfacial}}$  where  $t_0$  of the spatially restricted samples starts to deviate from the bulk behavior (bottom) in the frequency range of 3800–2400  $\text{cm}^{-1}$ .

as peak frequencies, the half-bandwidths (the full-width-at-half-maximum, FWHM;  $\Delta\nu_{1/2}$ ), and the integral intensities,  $I$ , of the  $\text{—OH}$  bands for the bulk and confined alcohols are presented in Table 2.

The dominating feature of the IR spectra of alcohol is a broad band between 3700 and 3000  $\text{cm}^{-1}$  assigned to the hydrogen-bonded  $\text{—OH}$  groups. At room temperature, the  $\text{—OH}$  stretching vibrational bands of bulk samples are observed at 3331, 3330, and 3343  $\text{cm}^{-1}$  for 2E1B, 2E1H, and 5M3H, respectively. Thus, the  $\text{—OH}$  stretching frequencies of 2E1B and 2E1H are close to each other; while, 5M3H has larger the  $\nu_{\text{OH}}$  frequency value, indicating

weaker hydrogen bonds in this sample. Moreover, a very weak peak located at  $\sim 3630 \text{ cm}^{-1}$ , associated with the free  $\text{—OH}$  stretching vibration of alcohol molecules, is also detected in the IR spectra of all bulk systems. A lowering temperature induces a redshift of  $\text{O—H}$  stretch vibrations to 3236, 3270, and 3256  $\text{cm}^{-1}$  at  $T_g$  for 2E1B, 2E1H, and 5M3H, respectively. The largest redshift is observed for 2E1B (95  $\text{cm}^{-1}$ ) when compared to 2E1H (60  $\text{cm}^{-1}$ ) and 5M3H (87  $\text{cm}^{-1}$ ). Thus, the strength of hydrogen-bonded aggregates in bulk increases with decreasing temperature. It should be pointed out that the “non-H-bonded” alcohol molecules, characterized by the  $\text{O—H}$  vibration of frequency above 3600  $\text{cm}^{-1}$ ,

Table 2

The spectral parameters of the  $\nu_{\text{OH}}$  band of the bulk and samples confined in native and silanized silica pores at  $T = 293 \text{ K}$ , and at  $T_{g, \text{bulk}}$  and  $T_{g, \text{interfacial}}$ , where  $t_0$  of the spatially restricted samples starts to deviate from the bulk behavior.

Sample	Peak at 293 K [ $\text{cm}^{-1}$ ]	Peak at $T_{g, \text{interfacial}}$ [ $\text{cm}^{-1}$ ]	FWHM at 293 K [ $\text{cm}^{-1}$ ]	FWHM at $T_{g, \text{interfacial}}$ [ $\text{cm}^{-1}$ ]	Area at 293 K [a.u.]	Area at $T_{g, \text{interfacial}}$ [a.u.]
<b>Bulk materials</b>						
2E1B	3331	3236	234,6833	206,7919	83,266	112,916
2E1H	3330	3270	224,1861	195,2512	122,333	155,367
5M3H	3343	3256	203,7542	166,8354	114,844	166,330
<b>Confined within native silica templates of <math>d = 4 \text{ nm}</math></b>						
2E1B	3339	3277	255,7062	227,9866	176,054	190,586
2E1H	3330	3276	249,2337	225,7980	134,454	155,162
5M3H	3344	3263	232,4940	186,5649	140,738	168,815
<b>Confined within silanized silica templates of <math>d = 4 \text{ nm}</math></b>						
2E1B	3338	3277	252,0996	210,6249	216,539	243,119
2E1H	3331	3277	253,6326	212,4584	172,788	195,934
5M3H	3344	3256	227,9145	166,8483	154,343	196,454

do not appear in low-temperature regions, indicating that all molecules form associates. Moreover, a reduction in the half-bandwidth of the  $\nu_{\text{O-H}}$  band with both the elongation of the alcohol chain and a decrease of temperature is noted. Additionally, the integral intensities of the  $\nu_{\text{O-H}}$  bands of bulk alcohols increase with a reduction of temperature. These changes in spectral parameters suggest an increase in the strengths and the number of hydrogen bonds. Interestingly in the vicinity of  $T_g$ , the more homogeneous nature of these specific interactions in terms of their strength is noted.

The incorporation of primary alcohols to the native and silanized silica pores leads to the change in their H-bond network properties, which is manifested in the IR spectra as the blue-shift of the  $\nu_{\text{O-H}}$  peak frequency. Thus, at first sight, one can find that the strength of the hydrogen bonds in the confined alcohols is weaker with respect to the bulk systems [57]. The —OH stretching band of confined alcohols varies more significantly with respect to the bulk samples after decreasing temperature. 2E1B shows the largest blue-shift of the O—H stretching vibrations at temperatures, where a deviation in dynamics of Debye process is noted ( $41 \text{ cm}^{-1}$  for native vs.  $27 \text{ cm}^{-1}$  for silanized pores); while in the case of 2E1H, a weak blue-shift is observed ( $6 \text{ cm}^{-1}$  and  $7 \text{ cm}^{-1}$  for hydrophilic and hydrophobic pores). On the other hand, almost no blue-shift is observed for the OH stretching vibration of confined 5M3H. That means that the strength of H-bonds in micelle-like supramolecular structures is weakly affected by the silica pores at this condition. Moreover, the analysis of Table 2 shows that the  $\nu_{\text{OH}}$  bandwidth for alcohol increases in the following order: bulk samples  $\rightarrow$  alcohols infiltrated into silanized templates  $\rightarrow$  compounds confined within native pores. As shown, bulk primary alcohols are homogeneous in terms of the size of associates, while the confined compounds prefer to form a greater number of small species. In this context, it is worthwhile to stress that the  $\nu_{\text{OH}}$  band of confined alcohols consists of the two components of which the intense and broad one of lower frequency ( $\sim 3330\text{--}3340 \text{ cm}^{-1}$ ) is attributed to the fully H-bonded aggregates, whereas a shoulder at higher frequency  $\sim 3600 \text{ cm}^{-1}$  can be assigned to the non-H-bonded alcohol molecules, respectively (see Fig. S5 in SI). At lower temperature, the spectral profile of the —OH stretching band becomes even more complex, i.e., an additional shoulder at  $\sim 3450 \text{ cm}^{-1}$  appears. It is attributed to the weak hydrogen bonding interactions between the surface silanol (Si—OH) groups of the silica pores and O—H or possibly  $\text{CH}_3$  moieties of alcohol molecules, as discussed by Ghoufi et al. [42]. In the silanized silica pores, this shoulder is considerably less intense, although still detectable because there are mainly dispersive interactions between host and guest materials. A drop in temperature has a similar effect on the  $\nu_{\text{OH}}$  bands of the confined alcohols as in bulk samples. In both cases, a redshift of the O—H frequencies, along with the increase in the integral intensities and a decrease in the half-bandwidths of the bands connected to the stretching vibration of this moiety, is noted. Interestingly, the largest redshift is observed for the confined 5M3H ( $81 \text{ cm}^{-1}$  and  $88 \text{ cm}^{-1}$  for the native and silanized pores, respectively). On the other hand, in 2E1B ( $62 \text{ cm}^{-1}$  vs.  $61 \text{ cm}^{-1}$  for non-modified and functionalized pores, respectively) and 2E1H ( $54 \text{ cm}^{-1}$  for native and silanized pores, respectively), this effect is smaller. Moreover, 5M3H shows the largest percentage change in half-bandwidth and the integral intensity after decreasing temperature both in bulk and in pores.

Herein it is also worthwhile to compare our results with the ones obtained from the molecular dynamics (MD) simulations on water, a model associated liquid, confined in the silica pores of varying pore sizes. These investigations clearly showed that the silica surface perturbs the local structure and hydrogen bond dynamics of water [58–67]. Rovere and co-workers [62] found that in agreement with the QENS experiments discussed earlier; there is a heterogeneous distribution of the H-bonds throughout the pore.

In the layers located in the proximity of the interface, an orientational disorder, together with a reduction of the average number of H-bonds, was noted. On the other hand, in the central part of the pore (core water), the density and coordination number of water was the same as bulk sample [62]. Therefore similarly to the dielectric and QENS investigations, MD simulations considered the behavior of water in view of "core-shell" model, where the water molecules attached to the surface and those located in the middle part are characterized by distinctively different dynamics, physical properties and H-bonding pattern in silica pores of  $d = 2\text{--}20 \text{ nm}$  [67]. It should also be noted that the confinement effects on the water were also monitored through changes in the FTIR spectroscopic response. The analysis of vibrational bands detected in the  $\nu_{\text{OH}}$  stretching region ( $3200\text{--}3700 \text{ cm}^{-1}$ ) in terms of their origin and the local orientation of the water molecules has led to two contradictory interpretations. In the first approach, the various frequencies in the  $\nu_{\text{OH}}$  band of confined water were assigned to different water populations corresponding to water molecules with the coordination numbers from 1 to 4 [68–71]. In this case, the shift of the O—H stretching band from the lower to higher frequencies was interpreted as due to a decrease in the number of hydrogen bonds with surrounding water molecules [68,69]. To provide a quantitative evaluation of the observed changes, the O—H stretch region was fitted using at least 3 Gaussian curves, representing unique water populations, described as network water (NW), intermediate water (IW), and multimer water (MW) [68–70]. The first type of water molecules, NW, was assigned to strongly H-bonded water molecules having a coordination number close to four (centered around  $3310 \text{ cm}^{-1}$ ). The second type, IW (around  $3450 \text{ cm}^{-1}$ ), was ascribed to distorted H-bonded water molecules that may be located at the interface of the long-distance networks. The third component located around  $3590 \text{ cm}^{-1}$ , called MW water, corresponded to molecules that did not feature the kind of supermolecular connectivity of NW or IW, consisted of free monomers or as dimers, trimers. However, it should be emphasized that the contribution of silanol units from the matrix was not included in these considerations. Thus, in the other approach, Gupta et al. [71] interpreted FTIR spectra taking into account the orientation of water molecules with respect to the silanol group of the silica. They found that the band around  $\sim 1150 \text{ cm}^{-1}$  is closely related to the surface-bound water molecules, which confirmed that the presence of the polar —OH group on the hydroxylated silica surface provides adsorption sites for water with preferred orientations. Based on our FTIR spectra, we found that after the incorporation of alcohols into the silica pores, the band attributed to Si-OH groups at  $3744 \text{ cm}^{-1}$  disappeared and the intensities of the  $\nu_{\text{OH}}$  peak decreased (the absorbance of the  $\nu_{\text{OH}}$  band in confinement was not as intense as in bulk sample). Thus, our FTIR results also confirmed the formation of a hydrogen bond between the hydroxyl group of alcohols and the silanol groups of the silica pores. Taking into account the above-mentioned literature data on confined water, one can suppose, that change in the frequency of the —OH stretching vibration (shift towards larger wavenumbers) of alcohols confined in silica pores does not only represent weakening of the strength of H-bonds but may indicate the lower number of molecules in the nanoassociates as well. Just to stress that the greatest change in the shift of the stretching vibration of —OH moiety was noted for 2E1B for which a strong reduction in the length of chain-like structures was determined from the analysis of dielectric data. Much smaller effects were noted for the other alcohols infiltrated into silica pores. Finally, it should be noted that our FTIR spectra also confirmed the strong heterogeneous character of H-bonds in the confined systems. However, due to strong band overlap, it was hard to analyse them and correlate their behavior to the dynamics of interfacial and core alcohols monitored by means of dielectric spectroscopy.

## 5. Conclusions

Herein, we explored the behavior of bulk primary 2-ethyl-1-hexanol (2E1H) and 2-ethyl-1-butanol (2E1B) as well as secondary 5-methyl-3-heptanol (5M3H), capable of forming a supramolecular structure of different architecture and samples infiltrated within various nanoporous templates by means of dielectric and infrared spectroscopies, as well as contact angle measurements. For the alcohols incorporated into native silica pores, we observed a pronounced interfacial relaxation process connected to the reorientation of molecules absorbed at the interface. The analysis of the dynamical properties, including the ratio of relaxation times and dielectric strength of the interfacial process and Debye relaxation of the core molecules allowed to find out, that primary alcohols behave different with respect to the secondary one. The analysis of the dielectric data indicated that a number of molecules in chain-like structures in 2E1H and 2E1B confined in native and silanized silica pores are significantly reduced; while in 5M3H, it remains constant. Interestingly, despite a variation in the contact angle and interfacial energies, it was found that change in the temperature evolution of Debye relaxation times for the alcohols infiltrated into hydrophilic and hydrophobic silica as well as alumina pores occurs at similar  $\tau_D$  with respect to the bulk samples. To explain this peculiar finding, we considered two explanations. One based on the data published earlier by Ghoufi et al. [42] who shown that there is a small change in dynamics of the molecules interacting with the native and silanized pores; while the second one relies on the comparison of the pressure coefficient of the glass transition temperatures that were fairly the same for the studied alcohols. As a final point, it was shown that H-bonds generally become weaker under confinement, and there is large heterogeneity in the distribution of the strength of these particular interactions in pores. It should be noted that the impact of the spatial restriction is more pronounced for the hydrogen-bonds in primary alcohols, while in the secondary ones, this effect is not as significant. Interestingly, this result agrees with the outcome of dielectric investigations. Presented herein data is the first attempt to correlate the impact of nanospatial confinement on the H-bonding pattern, dynamics, and wettability of the self-assembly samples having tendencies to form supramolecular clusters of various architecture. Therefore, we believe that combined studies offer a deeper understanding of the processes taking place at the interface and general behavior of associating liquids in pores of varying diameter and functionality.

## ORCID authorship contribution statement

**Agnieszka Talik:** Methodology, Investigation, Formal analysis, Visualization. **Magdalena Tarnacka:** Methodology, Conceptualization, Resources, Funding acquisition. **Monika Geppert-Rybczyńska:** Investigation. **Barbara Hachula:** Investigation, Formal analysis. **Roksana Bernat:** Investigation, Visualization. **Agnieszka Chrzanowska:** Investigation, Visualization. **Kamil Kamiński:** Methodology, Conceptualization, Resources, Supervision, Funding acquisition. **Marian Paluch:** Resources, Supervision.

## Declaration of Competing Interest

The authors declare that they have no known competing financial interests or personal relationships that could have appeared to influence the work reported in this paper.

## Acknowledgment

K.K. is thankful for financial support from the Polish National Science Centre within the OPUS 9 project (Dec no. 2015/17/B/

ST3/01/195). M.T. acknowledges funding from the Polish National Science Centre within the OPUS project (Dec. no 2019/33/B/ST3/00500).

## Notes

The authors declare no competing financial interests.

## Appendix A. Supplementary material

Supplementary data to this article can be found online at <https://doi.org/10.1016/j.jcis.2020.04.084>.

## References

- [1] L.P. Singh, R. Richert, Watching hydrogen-bonded structures in an alcohol convert from rings to chains, *Phys. Rev. Lett.* 109 (2012) 167802, <https://doi.org/10.1103/PhysRevLett.109.167802>.
- [2] R. Böhmer, C. Gainaru, R. Richert, Structure and dynamics of monohydroxy alcohols—Milestones towards their microscopic understanding, 100 years after Debye, *Phys. Rep.* 545 (2014) 125–195, <https://doi.org/10.1016/j.physrep.2014.07.005>.
- [3] N. Lou, Y. Wang, X. Li, H. Li, P. Wang, C. Westdort, A.P. Sokolov, H. Xiong, Dielectric relaxation and rheological behavior of supramolecular polymeric liquid, *Macromolecules* 46 (2013) 3160–3166, <https://doi.org/10.1021/jm400088w>.
- [4] M. Preuß, C. Gainaru, T. Hecksher, S. Bauer, J.C. Dyre, R. Richert, R. Böhmer, Experimental studies of Debye-like process and structural relaxation in mixtures of 2-ethyl-1-hexanol and 2-ethyl-1-hexyl bromide, *J. Chem. Phys.* 137 (2012) 144502, <https://doi.org/10.1063/1.4755754>.
- [5] A. Minecka, E. Kamińska, D. Heczko, K. Jurkiewicz, K. Wolnica, M. Dulski, B. Hachula, W. Pisarski, M. Tarnacka, A. Talik, K. Kamiński, M. Paluch, Studying structural and local dynamics in model H-bonded active ingredient - Curcumin in the supercooled and glassy states at various thermodynamic conditions, *Eur. J. Pharm. Sci.* 135 (2019) 38–50, <https://doi.org/10.1016/j.ejps.2019.05.005>.
- [6] S. Bauer, K. Burlafinger, C. Gainaru, P. Lunkenheimer, W. Hiller, A. Loidl, R. Böhmer, Debye relaxation and 250 K anomaly in glass forming monohydroxy alcohols, *J. Chem. Phys.* 138 (2013) 094505, <https://doi.org/10.1063/1.4793469>.
- [7] C. Gainaru, M. Wikarek, S. Pawlus, M. Paluch, R. Figuli, M. Wilhelm, T. Hecksher, B. Jakobsen, J.C. Dyre, R. Böhmer, Oscillatory shear and high-pressure dielectric study of 5-methyl-3-heptanol, *Colloid Polym Sci* 292 (2014) 1913–1921, <https://doi.org/10.1007/s00396-014-3274-0>.
- [8] G.P. Johari, W. Dannhauser, Viscosity of isomeric octyl alcohols as a function of temperature and pressure, *J. Chem. Phys.* 51 (1969) 1626, <https://doi.org/10.1063/1.1672223>.
- [9] K. Adrjanowicz, B. Jakobsen, T. Hecksher, K. Kamiński, M. Dulski, M. Paluch, K. Niss, Slow supramolecular mode in amine and thiol derivatives of 2-ethyl-1-hexanol revealed by combined dielectric and shear-mechanical studies, *J. Chem. Phys.* 143 (2015) 181102, <https://doi.org/10.1063/1.4935510>.
- [10] S. Pawlus, M. Wikarek, C. Gainaru, M. Paluch, R. Böhmer, How do high pressures change the Debye process of 4-methyl-3-heptanol?, *J. Chem. Phys.* 139 (2013) 064501, <https://doi.org/10.1063/1.4816364>.
- [11] F.X. Hassion, R.H. Cole, Dielectric Properties Of Liquid Ethanol And 2-Propanol, *J. Chem. Phys.* 23 (1955) 1756, <https://doi.org/10.1063/1.1740575>.
- [12] C. Hansen, F. Stöckel, T. Berger, R. Richert, E.W. Fischer, Dynamics of glass-forming liquids. III. Comparing the dielectric  $\alpha$ - and  $\beta$ -relaxation of 1-propanol and *o*-terphenyl, *J. Chem. Phys.* 107 (1997) 1086, <https://doi.org/10.1063/1.474456>.
- [13] T. Hecksher, Communication: linking the dielectric Debye process in monoalcohols to density fluctuations, *J. Chem. Phys.* 144 (2016) 161103, <https://doi.org/10.1063/1.4947470>.
- [14] S. Pawlus, M. Paluch, M. Nagaraj, J.K. Vij, Effect of high hydrostatic pressure on the dielectric relaxation in a non-crystallizable monohydroxy alcohol in its supercooled liquid and glassy states, *J. Chem. Phys.* 135 (2011) 084507, <https://doi.org/10.1063/1.3626027>.
- [15] S. Pawlus, M. Paluch, A. Grzybowski, Communication: The modynamic scaling of the Debye process in primary alcohols, *J. Chem. Phys.* 134 (2011) 041103, <https://doi.org/10.1063/1.3540636>.
- [16] W.K. Kipnusu, M. Elsayed, W. Kossack, S. Pawlus, K. Adrjanowicz, M. Tress, E.U. Mapeza, R. Krause-Rehberg, K. Kamiński, F. Kremer, Confinement for more space: a larger free volume and enhanced glassy dynamics of 2-ethyl-1-hexanol in nanopores, *J. Phys. Chem. Lett.* 6 (2015) 3708–3712, <https://doi.org/10.1021/acs.jpclett.5b01533>.
- [17] H. Jansson, J. Swenson, The slow dielectric Debye relaxation of monoalcohols in confined geometries, *J. Chem. Phys.* 134 (2011) 104504, <https://doi.org/10.1063/1.3563630>.
- [18] D. Morineau, C.A. Simionescu, Does molecular self-association survive in nanochannels?, *J. Phys. Chem. Lett.* 1 (2010) 1155–1159, <https://doi.org/10.1021/jz100132d>.

- [19] C. Gainaru, S. Schildmann, R. Böhmer, Surface and confinement effects on the dielectric relaxation of a monohydroxy alcohol, *J. Chem. Phys.* 135 (2011) 174510, <https://doi.org/10.1063/1.3655356>.
- [20] T. El Goresy, R. Böhmer, Diluting the hydrogen bonds in viscous solutions of *n*-butanol with *n*-bromobutane: a dielectric study, *J. Chem. Phys.* 128 (2008) 154520, <https://doi.org/10.1063/1.2903403>.
- [21] K. Adrjanowicz, K. Kolodziejczyk, W.K. Kiprusu, M. Tarnacka, E.U. Mapeša, E. Kamińska, S. Pawlus, K. Kamiński, M. Paluch, Decoupling between the interfacial and core molecular dynamics of Salol in 2D confinement, *J. Phys. Chem. C* 119 (25) (2015) 14366–14374, <https://doi.org/10.1021/acs.jpcc.5b01391>.
- [22] G.P. Johari, O.E. Kalinowskaya, J.K. Vij, Effects of induced steric hindrance on the dielectric behavior and H bonding in the supercooled liquid and vitreous alcohol, *J. Chem. Phys.* 114 (2001) 4634, <https://doi.org/10.1063/1.1346635>.
- [23] D. Fragiadakis, C.M. Roland, R. Casalini, Insights on the origin of the Debye process in monoalcohols from dielectric spectroscopy under extreme pressure conditions, *J. Chem. Phys.* 132 (2010) 144505, <https://doi.org/10.1063/1.3374820>.
- [24] A. Reiser, G. Kasper, C. Gainaru, R. Böhmer, Communications: High-pressure dielectric scaling study of a monohydroxy alcohol, *J. Chem. Phys.* 132 (2010) 181101, <https://doi.org/10.1063/1.3421555>.
- [25] C. Jacob, J.R. Sangoro, P. Papadopoulos, T. Schubert, S. Naumov, R. Valiulin, J. Karger, F. Kremer, Charge transport and diffusion of ionic liquids in nanoporous silica membranes, *Phys. Chem. Chem. Phys.* 12 (2010) 13798, <https://doi.org/10.1039/d004546h>.
- [26] W.K. Kiprusu, W. Kossack, C. Jacob, M. Jasiurkowska, J. Sangoro, F. Kremer, Molecular order and dynamics of tris(2-ethylhexyl)phosphate confined in unidirectional nanopores, *Z. Phys. Chem.* 226 (2012) 797, <https://doi.org/10.1524/zpch.2012.0287>.
- [27] A. Wandschneider, J.K. Lehmann, A. Heintz, Surface tension and density of pure ionic liquids and some binary mixtures with 1-propanol and 1-butanol, *J. Chem. Eng. Data* 53 (2008) 596–599, <https://doi.org/10.1021/jc700621d>.
- [28] J. Fedler-Kubis, M. Geppert-Rybczyńska, M. Musiał, E. Talik, A. Guzik, Exploring the surface activity of a homologous series of functionalized ionic liquids with a natural chiral substituent: (–)-menthol in a cation, *Colloids Surf. A Physicochem. Eng. Asp.* 529 (2017) 725–732, <https://doi.org/10.1016/j.colsurfa.2017.06.040>.
- [29] Y. Yao, V. Pella, W. Huang, K.A.J. Zhang, K. Landfester, H.-J. Butt, M. Vogel, G. Floudas, Crystallization and dynamics of water confined in model mesoporous silica particles: two ice nuclei and two fractions of water, *Langmuir* 35 (2019) 5890–5901, <https://doi.org/10.1021/acs.langmuir.9b00496>.
- [30] G. Szklarski, K. Adrjanowicz, M. Tarnacka, J. Piótecki, M. Paluch, Confinement-induced changes in the glassy dynamics and crystallization behavior of supercooled fenofibrate, *J. Phys. Chem. C* 122 (2) (2018) 1384–1395, <https://doi.org/10.1021/acs.jpcc.7b10946>.
- [31] K. Kolodziejczyk, M. Tarnacka, E. Kamińska, M. Dulski, K. Kamiński, M. Paluch, Crystallization kinetics under confinement. Manipulation of the crystalline form of salol by varying pore diameter, *Cryst. Growth Des.* 16 (3) (2016) 1218–1227, <https://doi.org/10.1021/acs.cgd.5b01181>.
- [32] F. He, L.-J. Wang, R. Richert, Dynamics of supercooled liquids in the vicinity of soft and hard interfaces, *Phys. Rev. B* 71 (2005) 144205, <https://doi.org/10.1103/PhysRevB.71.144205>.
- [33] R. Richert, Dynamics of nanoconfined supercooled liquids, *Annu. Rev. Phys. Chem.* 62 (2011) 65–84, <https://doi.org/10.1146/annurev-physchem-032210-103343>.
- [34] S.D. Bhagat, C.-S. Oh, Y.-H. Kim, Y.-S. Ahn, J.-G. Ye, Methyltrimethoxysilane based monolithic silica aerogels via ambient pressure drying, *Microporous Mesoporous Mater.* 100 (1–3) (2007) 350–355, <https://doi.org/10.1016/j.micromeso.2006.10.026>.
- [35] T. Young, An essay on the cohesion of fluids, *Philos. Trans. R. Soc. Lond.* 95 (1805) 65–87, <https://doi.org/10.1098/rstl.1805.0005>.
- [36] F.M. Fowkes, Attractive forces and interfaces, *Ind. Eng. Chem.* 56 (1964) 40–52, <https://doi.org/10.1021/ie50660a008>.
- [37] F.M. Fowkes, Determination of interfacial tensions, contact angles, and dispersion forces in surfaces by assuming additivity of intermolecular interactions in surfaces, *J. Phys. Chem.* 66 (1962) 382, <https://doi.org/10.1021/j100808a524>.
- [38] F.M. Fowkes, Attractive forces at interfaces, *J. Ind. Eng. Chem.* 56 (1964) 40–52, <https://doi.org/10.1021/ie50660a008>.
- [39] F. Kremer, Dynamics in geometrical confinement, 2014.
- [40] M. Arndt, R. Stannarius, W. Gorbatschow, F. Kremer, Dielectric investigations of the dynamic glass transition in nanopores, *Phys. Rev. E* 54 (1996) 5377, <https://doi.org/10.1103/PhysRevE.54.5377>.
- [41] S. Havriliak, S. Negami, A complex plane analysis of  $\alpha$ -dispersions in some polymer systems, *J. Polym. Sci. Part C Polym. Symp.* 14 (1966) 99–117, <https://doi.org/10.1002/polc.5070140111>.
- [42] A. Ghoufi, I. Hureau, D. Morineau, R. Renou, A. Szymczyk, Confinement of tert-butanol nanoclusters in hydrophilic and hydrophobic silica nanopores, *J. Phys. Chem. C* 117 (2013) 15203–15212, <https://doi.org/10.1021/jp404702j>.
- [43] M. Tarnacka, O. Madejczyk, M. Dulski, P. Malszym, K. Kamiński, M. Paluch, Is there a liquid-liquid phase transition in confined triphenyl phosphite?, *J. Phys. Chem. C* 121 (35) (2017) 19442–19450, <https://doi.org/10.1021/acs.jpcc.7b05336>.
- [44] M. Tarnacka, M. Dulski, M. Geppert-Rybczyńska, A. Talik, E. Kamińska, K. Kamiński, M. Paluch, Variation in the molecular dynamics of DGEBA confined within AAO templates above and below the glass-transition temperature, *J. Phys. Chem. C* 122 (49) (2018) 28033–28044, <https://doi.org/10.1021/acs.jpcc.8b07522>.
- [45] C. Gainaru, R. Meier, S. Schildmann, C. Lederle, W. Hiller, E.A. Rössler, R. Böhmer, Nuclear-magnetic-resonance measurements reveal the origin of the Debye process in monohydroxy alcohols, *Phys. Rev. Lett.* 105 (2010) 258303, <https://doi.org/10.1103/PhysRevLett.105.258303>.
- [46] A. Schönhalz, R. Stanga, Broadband dielectric study of anomalous diffusion in a poly(propylene glycol) melt confined to nanopores, *J. Chem. Phys.* 108 (1998) 5130, <https://doi.org/10.1063/1.475918>.
- [47] W.H. Stockmayer, Dielectric dispersion in solutions of flexible polymers, *Pure Appl. Chem.* 15 (1967) 539–554, <https://doi.org/10.1351/pac196715030539>.
- [48] S. Alexandris, P. Papadopoulos, G. Sakellariou, M. Steinhart, H.-J. Butt, G. Floudas, Interfacial energy and glass temperature of polymers confined to nanoporous alumina, *Macromolecules* 49 (2016) 7400–7414, <https://doi.org/10.1021/acs.macromol.6b01484>.
- [49] A. Talik, M. Tarnacka, I. Gładzka-Flak, P. Malszym, M. Geppert-Rybczyńska, K. Wolnica, E. Kamińska, K. Kamiński, M. Paluch, The role of interfacial energy and specific interactions on the behavior of poly(propylene glycols) derivatives under 2D confinement, *Macromolecules* 51 (13) (2018) 4840–4852, <https://doi.org/10.1021/acs.macromol.8b00658>.
- [50] A. Talik, M. Tarnacka, M. Geppert-Rybczyńska, A. Minecka, E. Kamińska, K. Kamiński, M. Paluch, Impact of the interfacial energy and density fluctuations on the shift of the glass transition temperature of the liquids confined in pores, *J. Phys. Chem. C* 123 (9) (2019) 5549–5556, <https://doi.org/10.1021/acs.jpcc.8b12551>.
- [51] W. Tu, K. Chut, G. Szklarski, L. Laskowski, K. Grzybowski, M. Paluch, K. Adrjanowicz, Dynamics of pyrrolidinium-based ionic liquids under confinement. II. The effects of pore size, inner surface and cationic alkyl chain length, *J. Phys. Chem. C* (2019), <https://doi.org/10.1021/acs.jpcc.9b0461>.
- [52] N. Kuon, A.A. Milischuk, B.M. Ladanyi, E. Flenner, Self-intermediate scattering function analysis of supercooled water confined in hydrophilic silica nanopores, *J. Chem. Phys.* 146 (21) (2017), <https://doi.org/10.1063/1.4984764>.
- [53] M. Tarnacka, K. Kamiński, E.U. Mapeša, E. Kamińska, M. Paluch, Studies on the temperature and time induced variation in the segmental and chain dynamics in poly(propylene glycol) confined at the nanoscale, *Macromolecules* 49 (17) (2016) 6678–6686, <https://doi.org/10.1021/acs.macromol.6b01237>.
- [54] M. Tarnacka, O. Madejczyk, K. Kamiński, M. Paluch, Time and temperature as key parameters controlling dynamics and properties of spatially restricted polymers, *Macromolecules* 50 (13) (2017) 5188–5193, <https://doi.org/10.1021/acs.macromol.7b00616>.
- [55] A. Talik, M. Tarnacka, M. Wojtyński, E. Kamińska, K. Kamiński, M. Paluch, The influence of the nanocurvature on the surface interactions and molecular dynamics of model liquid confined in cylindrical pores, *J. Mol. Liq.* 111973 (2019), <https://doi.org/10.1016/j.molliq.2019.11.1973>.
- [56] G.A. Jeffrey, *An Introduction to Hydrogen Bonding*, vol. 32, Oxford University Press, New York, 1997. DOI: 10.1021/ja9756331.
- [57] Ch.-H. Wang, P. Bai, J.L. Siepmann, A.E. Clark, Deconstructing hydrogen-bond networks in confined nanoporous materials: implications for alcohol-water separation, *J. Phys. Chem. C* 118 (34) (2014) 19723–19732, <https://doi.org/10.1021/jp502867v>.
- [58] E. Spohr, C. Hartnig, P. Gallo, M. Rovere, Water in porous glasses a computer simulation study, *J. Mol. Liq.* 80 (2–3) (1999) 165–178, [https://doi.org/10.1016/S0167-7328\(99\)80066-3](https://doi.org/10.1016/S0167-7328(99)80066-3).
- [59] P. Gallo, M. Rovere, Molecular dynamics study of the glass transition in confined water, *J. Phys. 10 (P7) (2000) 203–206*, <https://doi.org/10.1051/jp4:2000740>.
- [60] P. Gallo, M. Rovere, E. Spohr, Glass transition and layering effects in confined water: a computer simulation study, *J. Chem. Phys.* 113 (24) (2000) 11324–11335, <https://doi.org/10.1063/1.1328073>.
- [61] S.H. Lee, P.J. Rossky, A comparison of the structure and dynamics of liquid water at hydrophobic and hydrophilic surfaces – a molecular-dynamics simulation study, *J. Chem. Phys.* 100 (4) (1994) 3334–3345, <https://doi.org/10.1063/1.466425>.
- [62] M. Rovere, M.A. Ricci, D. Vellati, F. Bruni, A molecular dynamics simulation of water confined in a cylindrical SiO<sub>2</sub> pore, *J. Chem. Phys.* 108 (23) (1998) 9859–9867, <https://doi.org/10.1063/1.476424>.
- [63] P. Raiteri, A. Laio, M. Parrinello, Correlations among hydrogen bonds in liquid water, *Phys. Rev. Lett.* 93 (8) (2004), <https://doi.org/10.1103/PhysRevLett.93.087801>, pp. 087801–1–087801–4.
- [64] Q. Zhang, K.-Y. Chan, N. Quirke, Quirke Nicholas Molecular dynamics simulation of water confined in a nanopore of amorphous silica, *Mol. Simul.* 35 (15) (2009) 1215–1223, <https://doi.org/10.1080/08927020903116029>.
- [65] C. Wang, H. Lu, Z. Wang, P. Xiu, B. Zhou, G. Zuo, R. Wan, J. Hu, H. Fang, Stable liquid water droplet on a water monolayer formed at room temperature on ionic model substrates, *Phys. Rev. Lett.* 103 (2009) 137801, <https://doi.org/10.1103/PhysRevLett.103.137801>.
- [66] S.M. Mutsaers, A. Kirch, J.M. de Almeida, V.M. Sanchez, C.R. Miranda, Molecular dynamics simulations of water confined in calcite slit pores: an NMR spin relaxation and hydrogen bond analysis, *J. Phys. Chem. C* 121 (12) (2017) 6674–6684, <https://doi.org/10.1021/acs.jpcc.6b12412>.
- [67] L.C. Bourg, C.I. Steefel, Molecular dynamics simulations of water structure and diffusion in silica nanopores, *J. Phys. Chem. C* 116 (21) (2012) 11566–11564, <https://doi.org/10.1021/jp301299a>.

- [68] J.-B. Brubach, A. Mermet, A. Filabozzi, A. Gershel, P. Roy, Signatures of the hydrogen bonding in the infrared bands of water, *J. Chem. Phys.* 122 (18) (2005) 184509, <https://doi.org/10.1063/1.1894929>.
- [69] S. Le Caër, S. Pin, S. Esnouf, Q. Raffy, J.Ph. Renault, J.-B. Brubach, G. Creff, P. Roy, A trapped water network in nanoporous material: the role of interfaces, *Phys. Chem. Chem. Phys.* 13 (2011) 17658–17666, <https://doi.org/10.1039/c1cp21980d>.
- [70] A.W. Knight, N.G. Kalugin, E. Coker, A.G. Ilgen, Water properties under nanoscale confinement, *Sci. Rep.* 9 (1) (2019) 8246, <https://doi.org/10.1038/s41598-019-44651-z>.
- [71] P.K. Gupta, M. Meuwly, Dynamics and vibrational spectroscopy of water at hydroxylated silica surfaces, *Faraday Discuss.* 167 (2013) 329, <https://doi.org/10.1039/c3fd00096f>.

## **A5. Impact of Confinement on the Dynamics and H-Bonding Pattern in Low-Molecular Weight Poly(propylene glycols)**

Autorzy: A. Talik, M. Tarnacka, M. Geppert-Rybczyńska, B. Hachuła, K. Kaminski, M. Paluch.

Referencja: J. Phys. Chem. C 2020, 124, 17607–17621

DOI: 10.1021/acs.jpcc.0c04062

Impact Factor czasopisma z roku opublikowania pracy: 4.189

Liczba punktów ministerialnych MNiSW czasopisma (2019): 140

Mój udział w pracy polegał na: przeglądzie literaturowym, uczestniczeniu w formułowaniu hipotezy badawczej, przygotowaniu próbek do badań, wykonaniu pomiarów dielektrycznych a następnie analizie otrzymanych wyników, przygotowaniu rysunków oraz opisie wyników. Uczestnictwo w przygotowaniu manuskryptu oraz w formułowaniu odpowiedzi na uwagi recenzentów.

# Impact of Confinement on the Dynamics and H-Bonding Pattern in Low-Molecular Weight Poly(propylene glycols)

Agnieszka Talik,\* Magdalena Tamacka,\* Monika Geppert-Rybczyńska, Barbara Hachula,\* Kamil Kaminski, and Marian Paluch

Cite This: *J. Phys. Chem. C* 2020, 124, 17607–17621

Read Online

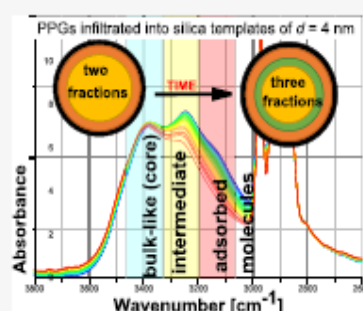
ACCESS |

Metrics & More

Article Recommendations

Supporting Information

**ABSTRACT:** Herein, we explored thermal properties, dynamics, wettability, and H-bonding pattern in various poly(propylene glycols) (PPG) of  $M_n = 400$  g/mol confined into two types of nanoporous templates: silica ( $d = 4$  nm) and alumina ( $d = 18$  nm). Unexpectedly, it was found that the mobility of the interfacial layer and the depression of the glass transition temperature weakly depend on the pore size, surface functionalization, and wettability. However, interestingly, we have reported strengthening of the hydrogen bonds in samples confined in silica pores. Further, the unique annealing experiments on PPG-OH with the use of Fourier transform infrared spectroscopy revealed the reorganization of oligomers close to the interface and the formation of three distinct fractions, interfacial, intermediate, and bulk-like, in the infiltrated samples. These experiments might shed new light on the variation of the segmental/structural relaxation times due to annealing of materials of different molecular weights infiltrated into pores or deposited in the form of a thin layer.



## 1. INTRODUCTION

The behavior of soft materials under nanoscale spatial restriction conditions became an attractive field of research over the past decades.<sup>1,2</sup> A special attention was focused on understanding in detail the molecular mechanisms governing the variation in the physicochemical properties of confined compounds.<sup>3,4</sup> Interestingly, as shown by numerous theoretical and experimental studies, these fluctuations arise mostly because of the competition of three major effects: surface interactions, finite size, and free volume.<sup>5–8</sup>

In fact, most investigations carried out to date demonstrated that the deviation in the molecular dynamics and phase/glass transition temperatures of confined materials is directly correlated with the size reduction realized by the decrease in both thicknesses of thin films and the pore diameter,  $d$ , of porous templates.<sup>9</sup> What is important, the positronium annihilation measurements carried out for liquids infiltrated into porous templates revealed that along with the change in the diameter of the nanocavities, a strong fluctuation in the free volume is noted.<sup>10–12</sup> At this point, it is worth quoting recent work by White and Lipson, who derived the cooperative free volume (CFV) model to describe general temperature and free volume-dependent structural relaxation behavior<sup>10–12</sup> of the bulk and confined materials. Briefly, one can stress that in this model, a group of molecules cooperate to obtain enough space for a rearrangement, and hence, the number of cooperating particles is inversely proportional to the free volume. This model was applied by Napolitano *et al.*<sup>13</sup> to explain enhanced dynamics of poly(4-chlorostyrene) and poly(2-vinylpyridine),

prepared in a form of thin layers on the substrates differing in roughness. Moreover, recently, the CFV approach was used to describe segmental and chain dynamics of amino-terminated poly(propylene glycol) (PPG-NH<sub>2</sub>) confined into native and slanted silica pores.<sup>6</sup> In this context, it is worthwhile to stress that a weak/negligible variation of the free volume below temperature connected to the vitrification of the interfacial molecules served as a base to formulate hypothesis that negative pressure controls dynamics of liquids confined in pores.<sup>8,14–16</sup>

Along with the development of the concepts relying on the variation in the finite size and free volume, an increasing number of papers highlighted the impact of the surface effects, as a dominant factor governing behavior of confined liquids. Especially, an increasing attention was paid lately to the processes occurring at the interface,<sup>17–19</sup> surface interactions,<sup>20,21</sup> and roughness.<sup>13,22</sup> One can recall that there were successful attempts to predict the direction and the magnitude of the confinement effect for various glass formers both deposited as thin films<sup>20,23,24</sup> and infiltrated within alumina [anodic aluminum oxide (AAO)] membranes<sup>21,25</sup> based on the

Received: May 6, 2020

Revised: July 7, 2020

Published: July 9, 2020





interfacial energy,  $\gamma_{\text{SL}}$ . As shown, the higher  $\gamma_{\text{SL}}$ , the greater deviation from the bulk behavior is expected.<sup>21,25</sup>

Nevertheless, it should be noted that although finite size and surface effects on the dynamics of nanospacially confined liquids are very often considered separately, recent works indicated some kind of entanglement between them. In this context, it is worthwhile to remind recent atomic force microscopy measurements performed for glycerol incorporated within alumina membranes of  $d = 10$  nm,<sup>26</sup> demonstrating that surface tension and most likely interfacial tension  $\gamma_{\text{SL}}$  varies with the surface curvature of applied nanochannels.<sup>27–29</sup> Moreover, a close correlation between both effects is also well illustrated in the case of the dielectric studies on PPG infiltrated within controlled porous glasses of various pore diameters ( $d = 2.5–20$  nm).<sup>30–32</sup> As shown, the glass transition temperature,  $T_g$ , of infiltrated PPG revealed a nonlinear (parabolic) dependence, where the rise of  $T_g$  noted for smaller pore diameter ( $d < 3$  nm) was discussed in terms of the adsorption effects overcoming the confinement one. On the other hand, in the case of various PPG derivatives within silica pores characterized by a little larger pore sizes ( $d = 4–8$  nm),<sup>5,56</sup> a linear reduction of  $T_g$  with increasing degree of confinement was observed for both native and silanized templates. This might indicate that the impact of the surface effects should be often discussed together with the finite size (especially the pore curvatures) which might induce changes in the surface interactions and also should be taken into account to predict the behavior of the confined liquids.<sup>33–36</sup>

In this article, we probe the counterbalance between the confinement and surface effects on the chemically modified poly(propylene glycols) (PPG) derivatives of molecular weight  $M_n = 400$  g/mol incorporated into silica (native and silanized) and alumina (AAO) membranes of various pore diameters ( $d = 4$  nm and  $d = 18$  nm) measured using dielectric and infrared (IR) spectroscopy as well as differential scanning calorimetry (DSC). These investigations allowed to get insight into the variation in wettability, dynamics, and H-bonded pattern in the spatially restricted samples infiltrated into both kind of membranes.

## 2. MATERIALS AND METHODS

**2.1. Materials.** Poly(propylene glycol) (PPG-OH) and poly(propylene glycol) bis(2-aminopropyl ether) (PPG-NH<sub>2</sub>) of  $M_n = 400$  g/mol with purity higher than 98% were supplied by Sigma-Aldrich. The nanoporous alumina oxide membranes used in this study (supplied from InRedox) are composed of uniaxial channels (open from both sides) with well-defined pore diameter,  $d \sim 18 \pm 2$  nm, thickness  $\sim 50 \pm 2$   $\mu\text{m}$ , and porosity  $\sim 12 \pm 2\%$ . Details concerning pore density, distribution, and so forth can be found on the Webpage of the producer.<sup>37</sup> The preparation of native and functionalized silica templates are presented in the Supporting Information file. Finally, it should be mentioned that density of the confined materials is assumed to be approximately the same as the bulk material at room temperature (RT).

**2.2. Methods.** **2.2.1. Broadband Dielectric Spectroscopy (BDS).** Isochronic measurements of the complex dielectric permittivity  $\epsilon^*(\omega) = \epsilon'(\omega) - i\epsilon''(\omega)$  were carried out using the Novocontrol Alpha dielectric spectrometer over the frequency range from  $10^{-1}$  Hz to  $10^6$  Hz at ambient pressure. The temperature uncertainty controlled by Quatro Cryosystem using the nitrogen gas cryostat was better than 0.1 K. Dielectric measurements of native silica and silanized membranes (of  $d =$

4 nm) filled with PPG-OH, PPG-NH<sub>2</sub>, and PPG-OCH<sub>3</sub> were placed between stainless steel plates having 5 mm diameter. Moreover, dielectric measurements on empty membranes were also carried out to evaluate their contribution which turned out to be negligible, to the measured loss spectra (see Figure S1 in the Supporting Information file).

**2.2.2. Differential Scanning Calorimetry.** Calorimetric measurements were carried out using a Mettler-Toledo DSC apparatus (Mettler-Toledo International, Inc., Greifensee, Switzerland) equipped with a liquid nitrogen cooling accessory and an HSS8 ceramic sensor. Temperature and enthalpy calibrations were investigated using indium and zinc standards, and the heat capacity,  $C_p$ , calibration was performed using a sapphire disc. After placing crushed templates in the aluminum crucibles, they were sealed and measured over a wide temperature range with cooling and heating rates equal to 10 K/min. Each experiment was repeated three times. In addition, measurements on empty membranes were carried out (please see Figure S1 in the Supporting Information file). It was found that in the range of the studied temperature, there is no change in heat flow, indicating no contribution from the silica and alumina to the heat capacity jumps detected for the membranes filled with studied PPGs.

**2.2.3. Fourier Transform Infrared Spectroscopy (FTIR).** The Nicolet iSS0 FTIR spectrometer (Thermo Scientific) was used to measure the FTIR spectra of the bulk and the confined PPGs samples. FTIR spectra were recorded in the  $4000–1300$   $\text{cm}^{-1}$  frequency region with a spectral resolution of  $4$   $\text{cm}^{-1}$ . The limited spectral range resulted from the detector saturation in the region of Si–O and Al–O stretching vibrations. Each spectrum was obtained by averaging 32 scans. The measurements were carried at RT (293 K) and glass transition temperature ( $T_g$ ) determined from the BDS measurements. The low-temperature IR spectra were obtained by using a liquid nitrogen-cooled Linkam THMS 600 stage (the temperature accuracy of  $\pm 0.1$  °C), which was adapted to the Nicolet spectrometer. The measurements were performed at a cooling rate of  $10$  °C/min in a nitrogen atmosphere. The time-dependent IR spectra were measured at equal intervals, that is, every 1 min after the temperature stabilization at  $T = 183$  K. The FTIR spectra of native, silanized silica, and alumina membranes were measured and are presented in Figure S1. The –OH stretching band decomposition was performed using the MagicPlot 2.9.3 software (MagicPlot Systems, LLC). The band occurring between  $3050$  and  $3950$   $\text{cm}^{-1}$  was decomposed with the use of several Gaussian functions adjusting the intensity and the width of the fitting curves. The two wavelength intervals at  $\approx 2400–2500$  and  $3050–3950$   $\text{cm}^{-1}$  (excluding the spectral region of the CH stretching band) were used for fitting. All spectral parameters were left free during the fitting procedure. The “best fit” was considered when the statistical parameter  $R$  was the lowest. One can stress that although the amount of –OH groups on silica surface can vary with the surface preparation method,<sup>38</sup> the peak position connected to the vibration of this moiety is located at  $\nu_{\text{Si-OH}} \sim 3748$   $\text{cm}^{-1}$ . Interestingly, at this region, we did not observe any contribution from the PPG infiltrated into pores. Thus, there is no need to consider the influence of Si–OH groups from the silica membrane during the deconvolution process. In the case of alumina templates, the maximum of the OH band is found at  $3640$   $\text{cm}^{-1}$  in the range of weak H-bonded bulk-like PPG-OH molecules. However, the analysis of the OH vibration in this frequency regime does not affect a discussion

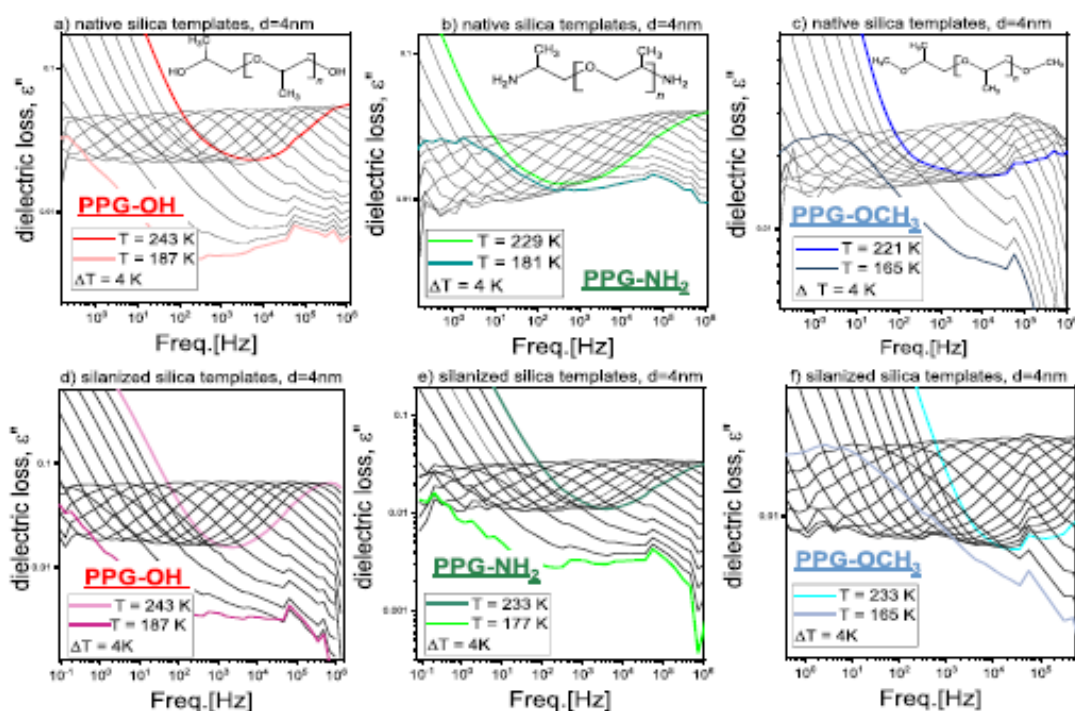


**Figure 1.** Dielectric loss spectra for various PPG derivatives confined into native (a–c) and silanized (d–f) silica templates of  $d = 4$  nm, measured above  $T_g$ . Black and color curves correspond to the different temperatures. The chemical structures of investigated substances are presented as insets (a–c).

about existence of three different layers of PPG-OH infiltrated in silica and alumina native pores. The CH band components were also excluded from the decomposition of the OH band as the fitting of a poorly resolved broad OH band with multiple component is always subject to a large error. Thus, fitting even more bands (*i.e.*, the CH signals) can only worsen the final deconvolution result.

**2.2.4. Surface Tension and Contact Angle Measurements.** The surface tension of liquids  $\gamma_L$  (pendant drop method) and contact angle  $\theta$  were measured with the DSA 100S Krüss Tensiometer, GmbH Germany. The description of the instrument and procedures has been presented previously.<sup>39,40</sup> The measuring procedure at  $T = 298.2$  K for all substances has been repeated dozen or more times. The temperature measurement uncertainty was  $\pm 0.1$  K. The precision of contact angle measurements was  $0.01^\circ$ , and the estimated uncertainty was  $\pm 1.5^\circ$ , whereas the uncertainty of surface tension was  $\pm 0.1$  mN·m<sup>-1</sup>. Density,  $\rho$ , required for the surface tension experiment was measured with an Anton Paar DMA 5000M densimeter with the uncertainty not worse than  $0.0001$  g·cm<sup>-3</sup>. For the surface energy estimation of native and silanized silica, some of the following liquids were considered: water, ethylene glycol, diiodomethane, and glycerol. The dispersive and nondispersive part in the surface tension for these substances were taken from ref 21. The calculated surface energy for native silica was  $67.6$  mJ/m<sup>2</sup> with the dominant nondispersive part equaling  $66.6$  mJ/m<sup>2</sup>. For the silanized surface, the respective value was  $25.3$  mJ/m<sup>2</sup> with the as-expected dominant and the dispersive component was  $22.8$  mJ/m<sup>2</sup>.

### 3. RESULTS AND DISCUSSION

Dielectric loss spectra of studied poly(propylene) glycols (PPG) terminated by three different groups, –OH, –NH<sub>2</sub>, and –OCH<sub>3</sub>, incorporated into native and silanized silica templates (of  $d = 4$  nm) are shown in Figure 1. Note that dielectric spectra for bulk substances, taken from ref 41, are presented in the Supporting Information file. In all cases, dielectric data revealed the presence of the dc conductivity related to the charge transport and the segmental ( $\alpha$ ) relaxation at higher frequencies reflecting the cooperative motions of the molecules and responsible for the liquid-to-glass transition. Herein, one can stress that because of low molecular weight,  $M_n < 1000$  g/mol, of studied PPG,<sup>16,25</sup> the additional mobility related to the fluctuations of the end-to-end vector of the chain ends called usually as the normal mode process cannot be observed (see Figure 1).

One can also mention that often for the materials confined within silica membranes, the appearance of the interfacial process, reflecting reorientational motions of the polymers adsorbed at the surface of the pore walls, are widely reported. Interestingly, this specific relaxation is not observed in the case of studied PPG, independently to the applied porous matrix and functionalization (see Figure 1). This finding agrees with the data published by Amdt *et al.*,<sup>1</sup> who studied salol and glycerol, differing in the number of hydroxyl units, infiltrated in silica pores of  $d = 4$ – $8$  nm. They found that while a reorientation of the adsorbed molecules can be detected for the former system (salol with one –OH group), it is not visible for the latter alcohol (glycerol with three –OH moieties). It was proposed to link this experimental observation to the balance between timescales of the exchange process between

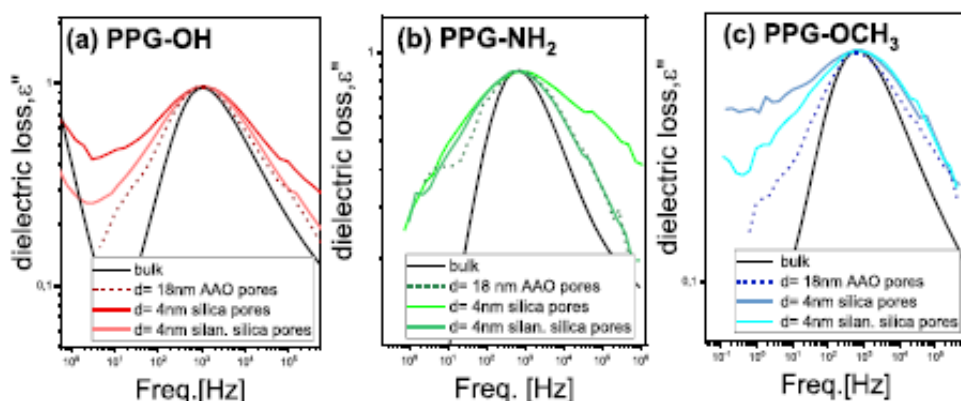


Figure 2. Segmental  $\alpha$ -loss peaks collected at comparable  $\tau_{\alpha}$  for bulk and confined PPG-OH (a), PPG-NH<sub>2</sub> (b), and PPG-OCH<sub>3</sub> (c). Data for PPG derivatives confined within AAO membranes of  $d = 18$  nm were taken from ref 41.

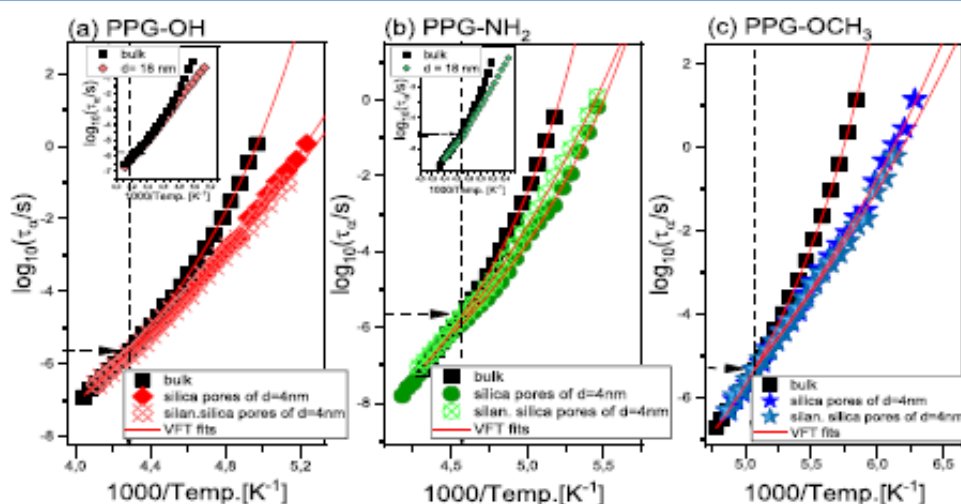


Figure 3. Structural relaxation times plotted vs inverse temperature for all studied PPG derivatives infiltrated into silica and alumina templates. Red solid lines are the best fits to the VFT equations (eq 2). Data for PPG derivatives confined within AAO membranes of  $d = 18$  nm were taken from ref 41.

core and interfacial molecules and experiments.<sup>1</sup> Note that if the exchange between both fractions is either fast or slow with respect to the time of the experiments, the interfacial process can be detected or not in the loss spectra respectively. However, we suppose that this phenomenon might be also somehow related to the number of hydroxyl units within the sample. Once the number of this particular moieties is equal to unity, the interfacial process is well visible as a separate loss peak, while in the case of materials with two or more  $-OH$  groups (*i.e.*, glycerol or PPG-OH), this mode vanishes. This pattern of behavior is similar to what was previously found in the case of bulk alcohols, where for monohydroxy alcohols, an additional Debye relaxation (related to the formation of the hydrogen bonding supramolecular structure) is observed; while in polyalcohols, there is no trace of this kind of mobility in the collected dielectric spectra.<sup>26</sup> Nevertheless to explain if there is any relationship between the appearance of the Debye process in monohydroxyalcohols and interfacial process in liquids confined in pores, further studies are required.

In Figure 2,  $\alpha$ -loss peaks of the bulk and confined samples were superimposed at the constant segmental relaxation times,

$\tau_{\alpha}$ , for all investigated compounds. As shown, the shape of the  $\alpha$ -loss peaks significantly broadens with increasing confinement because of the increased dynamical heterogeneity induced by the additional interactions with the pore walls.<sup>15,42</sup> However, it should be pointed out that the  $\alpha$ -loss peak of PPGs within the functionalized (silanized) silica templates is, interestingly, narrower than the one recorded for PPG infiltrated into native silica. In general, this might suggest a change in the surface interactions between hydrophobic (silanized) and hydrophilic (native) templates. Note that the broader  $\alpha$ -loss peaks within native templates might also be a result of the dynamical perturbation introduced by stronger interactions between the substrate and adsorbed molecules. It is worth mentioning that similar observations were made for other low and high molecular weight samples infiltrated in pores.<sup>1,25,31,42</sup>

To explore in more detail, the molecular dynamics of confined materials and collected dielectric spectra were analyzed using Havriliak–Negami (HN) function with the conductivity term<sup>43</sup>

Table 1. Values of the Glass Transition Temperatures, Changes in Heat Capacity, and Thickness of the Interfacial Layer Calculated for Bulk and Confined Systems Collected from Calorimetric and Dielectric Measurements<sup>a</sup>

	$T_{g,core}$ [K]	$T_{g,interfacial}$ [K]	$\Delta T_{g,core}$ [K]	$\Delta T_{g,interfacial}$ [K]	$T_{g,core}$ [K]	$T_{g,ic}$ [K]	$\Delta C_{p,core}$ [J/g K]	$\Delta C_{p,ic}$ [J/g K]	$\xi$ [nm]
PPG-OH									
bulk	196				199				
native SiO <sub>2</sub>	183	231	-13	35	185	226	0.393	0.651	0.9
silanized SiO <sub>2</sub>	179	230	-17	34	190	221	0.284	0.335	0.52
PPG-NH <sub>2</sub>									
bulk	187				193				
native SiO <sub>2</sub>	176	221	-11	34	178	222	0.413	0.945	0.89
silanized SiO <sub>2</sub>	176	217	-11	30	184	217	0.327	0.278	0.37
PPG-OCH <sub>3</sub>									
bulk	169				173				
native SiO <sub>2</sub>	156	197	-13	28	159	187	0.171	0.353	0.86
silanized SiO <sub>2</sub>	154	197	-15	28	163	190	0.215	0.423	0.97

<sup>a</sup>Data for bulk PPG derivatives taken from ref 41.

$$\epsilon(\omega)^* = \frac{\epsilon_{ic}}{\epsilon_0 \omega} + \frac{\Delta \epsilon}{[1 + (i\omega\tau_{HN})^{\alpha_{HN}}]^{\beta_{HN}}} \quad (1)$$

where  $\alpha_{HN}$  and  $\beta_{HN}$  are the shape parameters representing the symmetric and asymmetric broadening of given relaxation peaks,  $\Delta \epsilon$  is the dielectric relaxation strength,  $\tau_{HN}$  is the HN relaxation time,  $\epsilon_0$  is the vacuum permittivity, and  $\omega$  is an angular frequency ( $\omega = 2\pi f$ ). Note that  $\tau_a$  was estimated from  $\tau_{HN}$  accordingly to the equation given in ref 44. Determined segmental relaxation times were plotted as a function of inverse temperature and shown in Figure 3. As illustrated, the  $\tau_a(T)$ -dependences of all confined PPG is a bulk-like at a high-temperature region. However, below the temperatures denoted as  $T_{g,interfacial}$ , they start to deviate from the bulk behavior irrespectively of the sample and porous template. As widely reported, this phenomenon is related to the vitrification of the materials adsorbed to the pore walls.<sup>1,6,15,45</sup> In this context, one can mention about “two-layer” or “core-shell” models often used to discuss/interpret results of molecular dynamics simulations or quasi-elastic neutron scattering investigations.<sup>46</sup> In view of these simplified approaches, liquids infiltrated in pores are considered as consisted of the molecules located in the center of the pores (“core”) and adsorbed to the walls (“interfacial”). They are characterized by different densities and mobilities because of additional interactions with the solid substrate.<sup>1,60</sup>

Analysis of the data presented in Figure 3 unexpectedly revealed that the bifurcation of  $\tau_a(T)$ -dependences of the confined PPGs occurs at similar  $\tau_a$  ( $\log \tau_a \sim -5.5$ ) independently to the terminal groups, applied porous template, and functionalization (silanized or native). It is worth adding that the deviation of  $\tau_a(T)$ -dependences of PPGs infiltrated into alumina templates also occurs at comparable  $\tau_a$ , the same as in the case of material confined in silica pores (see insets of Figure 3a,b). Note that data for PPG derivatives within AAO membranes of  $d = 18$  nm were taken from ref 41. In this context, it should be mentioned that the similar finding has been recently reported for a primary and secondary monohydroxy alcohols incorporated within alumina and silica pores. It was shown that the temperature dependences of the Debye relaxation times,  $\tau_D$  (reflecting the mobility of supramolecular self-assemblies<sup>47,48</sup>), deviate from the bulk-like behavior at approximately the same  $\tau_D$  irrespectively of the porous template, chemical structure, and architecture of the supramolecular structures formed in the studied systems.<sup>49</sup>

Moreover, recently Tu *et al.*<sup>50</sup> found the same scenario in ionic liquids confined in the native and functionalized alumina pores. This indicates that the change in the porous template, hydrophobicity, or hydrophilicity of the pore surface does not affect segmental dynamics of the interfacial layer to much because the bifurcation of  $\tau_a(T)$ -dependences of the core PPGs occurs at similar  $\tau_a$  ( $\log \tau_a \sim -5.5$ ). Interestingly, this agrees with the molecular dynamics simulations showing that although functionalization of the pore walls influences on the dynamics of the interfacial molecules, this effect is not significant.<sup>51</sup>

To estimate the glass transition temperature,  $T_g$ , obtained, data presented in Figure 3 were fitted using the Vogel–Fulcher–Tamman (VFT) equation<sup>52–54</sup>

$$\tau_a = \tau_\infty \exp\left(\frac{D_T T_0}{T - T_0}\right) \quad (2)$$

where  $\tau_\infty$  is the relaxation time at finite temperature,  $D_T$  is the fragility parameter, and  $T_0$  is the temperature, where  $\tau$  goes to infinity. It should be mentioned that the two VFT functions were applied for the confined systems because of the observed deviation in the slope of  $\tau_a(T)$ -dependences. The first one (high temperature VFT) was used only for an accurate determination of a point (temperature), at which the slope changes (related to the vitrification of the interfacial layer and denoted as  $T_{g,interfacial}$ ), while, the glass transition temperatures of the confined samples (in this case of the core polymers,  $T_{g,core}$ ) were estimated from the second, low-temperature VFT fits. The values of all calculated glass transition temperatures are listed in Table 1. Note that  $T_{g,core}$  is defined as a temperature at which  $\tau_a = 100$  s. As observed, irrespectively of the terminal group and applied template, estimated values of  $T_{g,interfacial}$  are comparable. Moreover, the same scenario can also be observed in the case of  $T_{g,core}$  (within the experimental uncertainty). This implies that the performed surface modification (silanization) along with the variation in the porous matrix and pore diameter have for some reason a marginal impact on the segmental dynamics of infiltrated PPG derivatives. This observation seems to be quite surprising taking into account that to date, a simple silanization of silica, leading to a prominent change of the polarity, specific interactions (H-bonds), hydrophilicity, and hydrophobicity, generally induced difference in the behavior of materials incorporated within native and functionalized templates.<sup>30–32</sup>

To better understand reported findings, we further measured contact angles  $\theta$ , and surface tensions  $\gamma_L$ , and calculated the interfacial tension,  $\gamma_{SL}$ , prior and after surface modification.<sup>55,56</sup> The estimated values of contact angles and surface tensions for all studied materials and surfaces are listed in Table 2. As

**Table 2.** Contact Angles ( $\theta$ ), Surface Tension ( $\gamma_L$ ), and Interfacial energy ( $\gamma_{SL}$ ) Estimated at RT  $T = 298$  K for All Investigated Systems<sup>a</sup>

sample	$\theta$ [deg]	$\gamma_L$ [mN·m <sup>-1</sup> ]	$\gamma_{SL}$ [mN·m <sup>-1</sup> ]
Alumina Surface			
PPG-OH	6.2	32.4	26.7
PPG-NH <sub>2</sub>	5.4	31.6	27.6
PPG-OCH <sub>3</sub>	6.0	22.8	36.3
Silica Native Surface			
PPG-OH	26.3	32.4	38.5
PPG-NH <sub>2</sub>	24.7	31.6	38.9
PPG-OCH <sub>3</sub>	5.8	22.8	4.5
Silica-Silanized Surface			
PPG-OH	37.9	32.4	-0.2
PPG-NH <sub>2</sub>	28.7	31.6	-2.3
PPG-OCH <sub>3</sub>	7.4	22.8	2.8

<sup>a</sup>Data for the alumina surface were taken from ref 41.

observed, the contact angles of investigated samples change significantly depending on their chemical structure and type of matrices. Both PPG-OH and PPG-NH<sub>2</sub> are characterized by comparable contact angles on native silica surface ( $\theta \sim 25^\circ$ ), which indicates good wettability. However, their  $\theta$  increases because of surface modification even up to  $\theta \sim 37^\circ$  for PPG-OH on the silanized silica surface. The increase of  $\theta$  suggests, in fact, the reduction of wettability on the modified interface with respect to the native one, more likely because of the strong change in the interactions between host and guest materials. In this context, one can also add that in the case of the alumina surface, the contact angle of both PPG-OH and PPG-NH<sub>2</sub> is extremely low ( $\theta \sim 6^\circ$  indicates they wet this surface perfectly). On the other hand, PPG-OCH<sub>3</sub> surprisingly seems to wet all surface in a similar manner as its contact angle remains comparable for all surfaces ( $\theta \sim 6\text{--}7^\circ$ ).

Next, we estimated interfacial energy,  $\gamma_{SL}$ , according to the Young equation ( $\gamma_{SL} = \gamma_S - \gamma_L \cos \theta$ , where  $\gamma_S$  is the surface energy).<sup>55</sup> Calculated values of  $\gamma_{SL}$  are listed in Table 2. Interestingly, for the silanized matrices, we noted low values of interfacial energies for all examined compounds. This indicates a clear change in the interfacial interactions between materials and functionalized silica in the vicinity of the pore walls, where the dispersive interactions prevail.<sup>56,57</sup> In this context, one can recall studies on the thin films that revealed that the higher value of  $\gamma_{SL}$ , the greater deviation from the bulk behavior because of the reduced mobility at the interface.<sup>20,23,24</sup> This approach was further applied to the porous materials by Alexandris *et al.*<sup>21</sup> for several polymers infiltrated within AAO membranes.<sup>21,58</sup> As shown, the increase of the difference between the glass transition temperature,  $T_g$ , of the bulk and confined samples,  $\Delta T_g$ , enlarges with the rise of the interfacial tension. This relationship was well quantified by the systematic measurements of the wettability, allowing us to calculate the interfacial energy,  $\gamma_{SL}$ , and  $T_g$  of the spatially restricted polymers.<sup>21,25</sup> Further studies indicated that higher  $\gamma_{SL}$  implies reduced mobility of the interfacial layers that consequently leads to greater depression of  $T_{g,core}$  in pores.<sup>25</sup>

In Figure 4, we have plotted the estimated values of  $\gamma_{SL}$  versus  $\Delta T_{g,core}$  and  $\Delta T_{g,interfacial}$  calculated for PPGs infiltrated

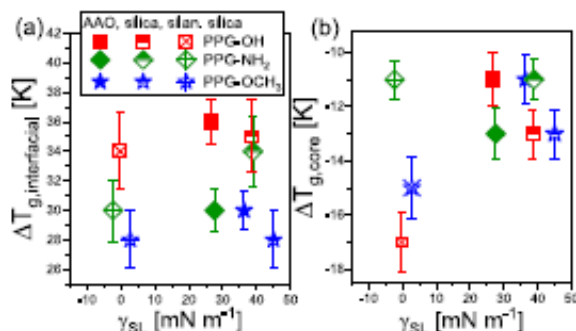


**Figure 4.**  $\Delta T_{g,interfacial}$  (a) and  $\Delta T_{g,core}$  (b) calculated from dielectric data, plotted as a function of the interfacial energy for studied PPG derivatives incorporated into AAO (of  $d = 18$  nm) and native and silanized silica (of  $d = 4$  nm) pores. Data for PPGs confined within AAO membranes of  $d = 18$  nm were taken from ref 41.

into alumina ( $d = 18$  nm) and silica ( $d = 4$  nm) templates. Note that  $\Delta T_{g,core}$  is the difference between  $T_{g,core}$  and  $T_g$  of bulk ( $\Delta T_{g,core} = T_{g,core} - T_g$ ), while  $\Delta T_{g,interfacial}$  is the discrepancy between  $T_{g,interfacial}$  and  $T_g$  of bulk ( $\Delta T_{g,interfacial} = T_{g,interfacial} - T_g$ ). As shown in Figure 4, both  $\Delta T_{g,core}$  and  $\Delta T_{g,interfacial}$  of all investigated PPG incorporated in porous matrices are similar (within experimental uncertainty). Surprisingly, despite a clear variation in wettability, interfacial energy and pore size ( $d = 18$  nm vs  $d = 4$  nm), no differences between studied systems infiltrated within alumina and silica templates can be observed. In this context, one can remind that recent studies on various PPG derivatives infiltrated into AAO membranes revealed that  $\gamma_{SL}$  weakly depends on both their terminal groups and molecular weight,  $M_n$ , whereas  $\Delta T_{g,interfacial}$  changes with both these factors.<sup>59</sup> The finding discussed above clearly indicates that although the interfacial tension is a very useful parameter to predict depression of the glass transition temperature of the polymers infiltrated into porous media, it is not sufficient to understand the complex dynamics of such heterogeneous systems. Therefore, the contribution of other factors, possibly related to the variation in the density packing and roughness of the pore walls must be considered as well.

In the next step, we have performed additional DSC measurements to support/confirm results of dielectric investigations. Thermograms recorded for all studied PPG derivatives incorporated within silica templates are presented in Figure 5. As illustrated, all samples exhibit the presence of the two endothermic processes, related to the vitrification of the interfacial (denoted as  $T_{g,interfacial}$ ) and “core” (labeled as  $T_{g,core}$ ) molecules located above and below  $T_g$  of the bulk material, respectively (so-called the double glass-transition phenomenon).<sup>42,60,61</sup> It should be pointed out that even for PPGs infiltrated into silanized silica templates characterized by the extremely low value of the interfacial energy, ( $\gamma_{SL} \sim 2$  mN·m<sup>-1</sup>), double glass transition was detected. The value of  $T_{g,interfacial}$  and  $T_{g,core}$  obtained from DSC measurements for confined materials and also  $T_g$  of the bulk samples were added to Table 1. Although, there are some discrepancies between the value of  $T_g$  determined from calorimetric and dielectric measurements, which can be due to the difference in the

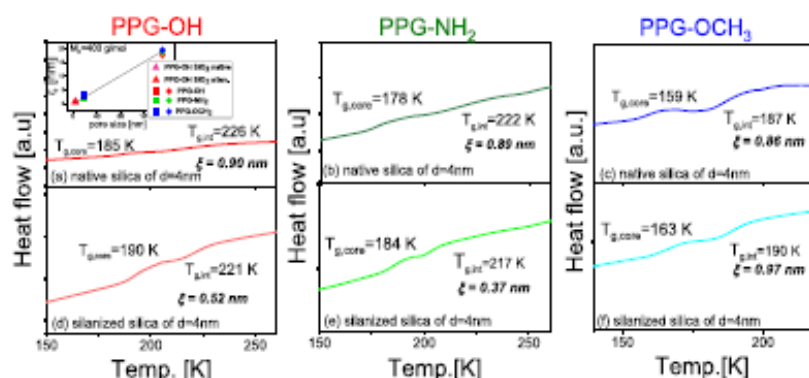


Figure 5. DSC thermograms together with the estimated length scale of the interfacial layer,  $\xi$  (eq 3), obtained for PPGs incorporated into both native and silanized silica templates; as the inset, the length scale of interfacial layer ( $\xi$ ) plotted vs pore diameter for PPG-OH, PPG-NH<sub>2</sub>, PPG-OCH<sub>3</sub> confined into AAO ( $d = 150, 18 \text{ nm}$ ) and SiO<sub>2</sub> ( $d = 4 \text{ nm}$ , native and silanized) membranes.

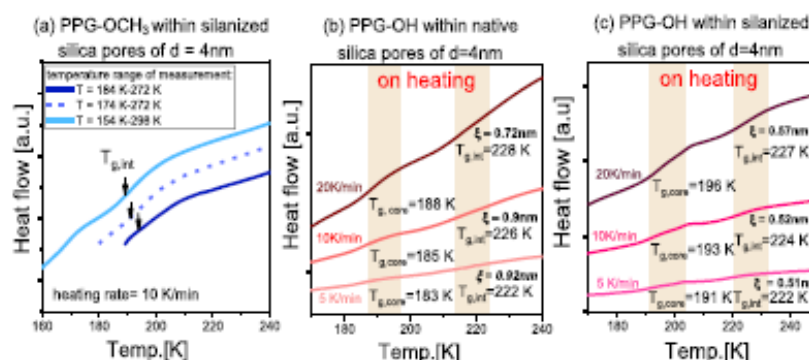


Figure 6. DSC thermograms obtained for confined systems: (a) thermal history of PPG-OCH<sub>3</sub> confined into  $d = 4 \text{ nm}$  of silanized silica pores and examined for selected temperatures above  $T_{g,core}$ , at constant heating rate = 10 K/min; (b,c) heating traces obtained for PPG-OH confined into native and silanized silica pores following different cooling rates (5–20 K/min).

heating/cooling rate applied in both methods<sup>41</sup> they are similar.

Furthermore, we also determined the length scale of the interfacial layer,  $\xi$ , which also can be obtained directly from DSC measurements<sup>60</sup>

$$\xi = \frac{d}{2} \left[ 1 - \left( \frac{\Delta C_{p,interfacial}}{\Delta C_{p,interfacial} + \Delta C_{p,core}} \right)^{1/2} \right] \quad (3)$$

where  $d$  is the pore diameter;  $\Delta C_{p,core}$  and  $\Delta C_{p,interfacial}$  are the changes of the heat capacity at  $T_{g,core}$  and  $T_{g,interfacial}$ . Note that the application of eq 3 requires the following assumptions: (i) the volume of the material in the surface layer is proportional to the step change of its heat capacity, (ii) the density of the incorporated material does not change along the pore radius, and (iii) the shape of the pore is cylindrical. The values of the heat capacity and calculated thickness of the interfacial layer are listed in Table 1 and Figure 5. As observed, the estimated  $\xi$  reaches similar values for all PPGs when infiltrated into native silica membranes (within experimental uncertainty), which are comparable to those ones reported earlier for 2E1H<sup>8</sup> or for monohydroxy alcohols,<sup>49</sup> where the value of  $\xi$  oscillated around  $\sim 1 \text{ nm}$ . However, after the silanization,  $\xi$  decreases for PPG-OH and PPG-NH<sub>2</sub> because of change in the interfacial interaction (i.e., suppression of H-bonds). In contrast, in the

case of PPG-OCH<sub>3</sub>, the length scale of the interfacial layer increases after the surface modification, most likely due to increased surface-dispersive interactions.<sup>56,57</sup> One can add that according to the literature,  $\xi$  varies dependently to the type and strength of interactions, including hydrogen bonds.<sup>1</sup> It is also worthwhile to add that  $\xi$  of low-molecular-weight PPG incorporated within the alumina templates of  $d = 18\text{--}150 \text{ nm}$  increases with the pore size but was relatively independent to the terminal end-groups of studied oligomers. In addition, we compared and plotted the thickness of the interfacial layer estimated for the PPG oligomer infiltrated into pores, made of silica and alumina having different pore sizes; please see the inset in Figure 5. Data for PPG infiltrated in AAO were taken from ref 41. This graph clearly illustrates that there is a linear relationship between thickness of the interfacial layer and pore diameter,  $d$ , which indicates some entanglement between both parameters. Moreover, it is worthwhile to stress that the interfacial layer estimated from calorimetry for the samples infiltrated into larger pores barely agree with those calculated for the thin films. In this particular case,  $\xi$  is around  $\sim 2\text{--}3 \text{ nm}$  and weakly depends on the film thickness.<sup>62</sup> Hence, one can state that the interfacial layer determined from calorimetry for the infiltrated systems is related to the length scale obeying molecules/polymers of much slower dynamics with respect to

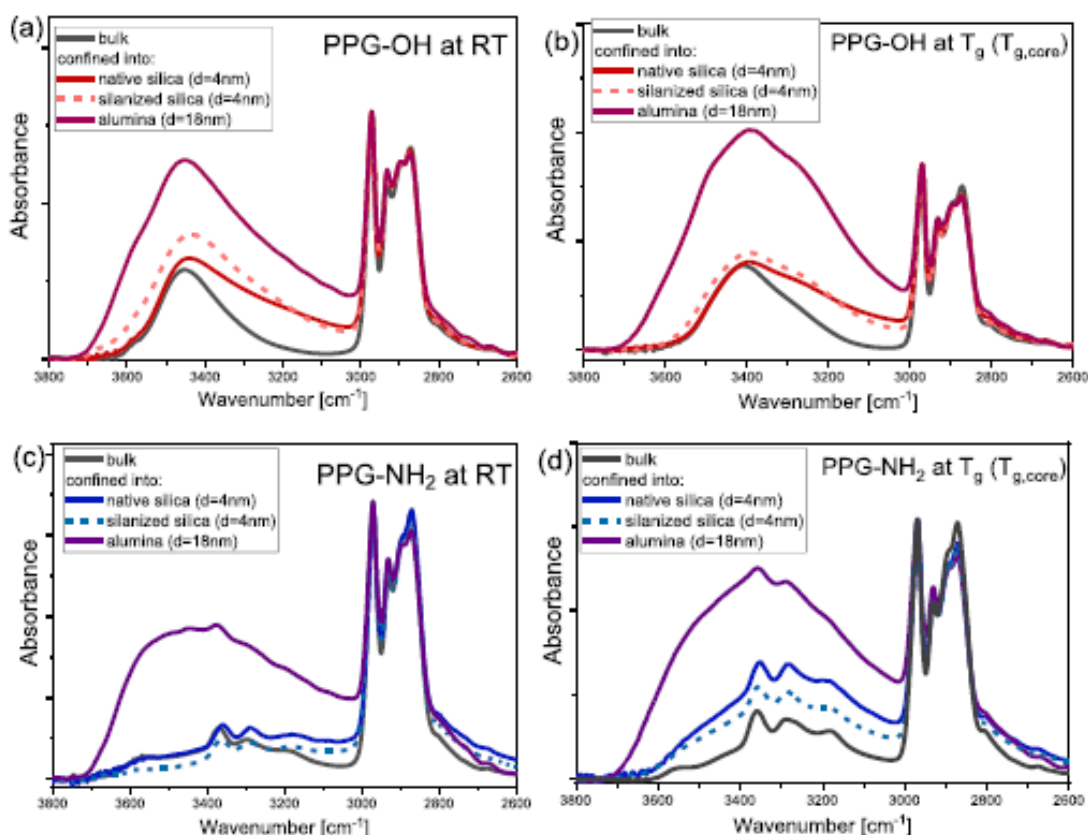


**Figure 7.** FTIR spectra of bulk (black) and confined PPG-OH (a,b) and PPG-NH<sub>2</sub> (c,d) measured in the  $\nu_{\text{O-H}}$  and the  $\nu_{\text{C-H}}$  vibration regions at RT (a,c) and at glass transition temperature (b,d). The spectra were normalized to the C-H absorption peak at around 2970 cm<sup>-1</sup>.

the core material because of the perturbation introduced by interactions with the substrate.

Taking advantage of the fact that both glass transition temperatures were well visible in the thermograms collected for the PPG confined in silica and alumina pores, we decided to find out whether this material will behave in a similar way as entangled *cis*-1,4-polyisoprene (PI) infiltrated in AAO membranes.<sup>58</sup> Just to mention that in this particular case, Politidis *et al* have demonstrated that  $T_{\text{g,interfacial}}$  is conditional and can be detected only for the samples cooled down below  $T_{\text{g,core}}$ ; this observation allowed them to hypothesize that  $T_{\text{g,core}}$  is a spinodal temperature. Therefore, as a subsequent point of our studies, we have performed additional calorimetric measurements using several temperature protocols to investigate the behavior of low-molecular-weight PPG derivatives infiltrated into silica templates of  $d = 4$  nm to check how does various thermal histories influence the existence of the double glass-transition phenomenon. For this purpose, we carried out three cooling scans followed by heating in accordance to the following protocols: (1) cooling down to 184 K (deep below  $T_{\text{g,core}}$ ), (2) cooling to 174 K (between both detected  $T_{\text{g}}$ s), and (3) again cooling down to 184 K. Representative DSC thermograms obtained for infiltrated PPG-OCH<sub>3</sub> are shown in Figure 6a. Interestingly, in contrast to the data reported in ref 58, a prominent  $T_{\text{g,interfacial}}$  appears in all registered thermograms questioning assignments of the low glass transition temperature as the spinodal temperature. To explain the discrepancy between results reported herein and the ones

presented in ref 58, one should consider (i) different molecular weights of studied polymers (we focused only on PPG of  $M_n = 400$  g/mol), (ii) various porous templates (characterized by different finite size and surface interactions), and (iii) significantly different wettabilities and interfacial tension of PI and PPG on the alumina and silica surfaces.

Furthermore, we also carried out a series of DSC measurements with different heating rates, 5–20 K/min. Selected thermograms recorded for PPG-OH incorporated within native and silanized templates of  $d = 4$  nm are presented in Figure 6b,c. As expected, both  $T_{\text{g}}$ s shift toward higher temperatures with the increasing heating rate. Additionally, we also observed that the length scale of the interfacial layer,  $\xi$ , increases with lowering the heating rate in the case of PPG-OH infiltrated into native silica templates (Figure 6b); whereas for PPG-OH within the silanized silica templates,  $\xi$  seems to remain constant independently to the applied heating rate (Figure 6c). This simple experiments indicated that although the dynamics of the interfacial layer is not so much different in the vicinity of the functionalized pore walls, the length scale of the molecules adsorbed to the pore walls is affected in a more significant way.

As a final point of our investigations, we have carried out additional FTIR measurements to gain information about the H-bonded pattern in the samples confined within silica and alumina nanopores. Figure 7 shows the comparison of FTIR spectra of bulk PPG-OH, PPG-NH<sub>2</sub>, and samples infiltrated in alumina and silica (native and functionalized) templates at RT

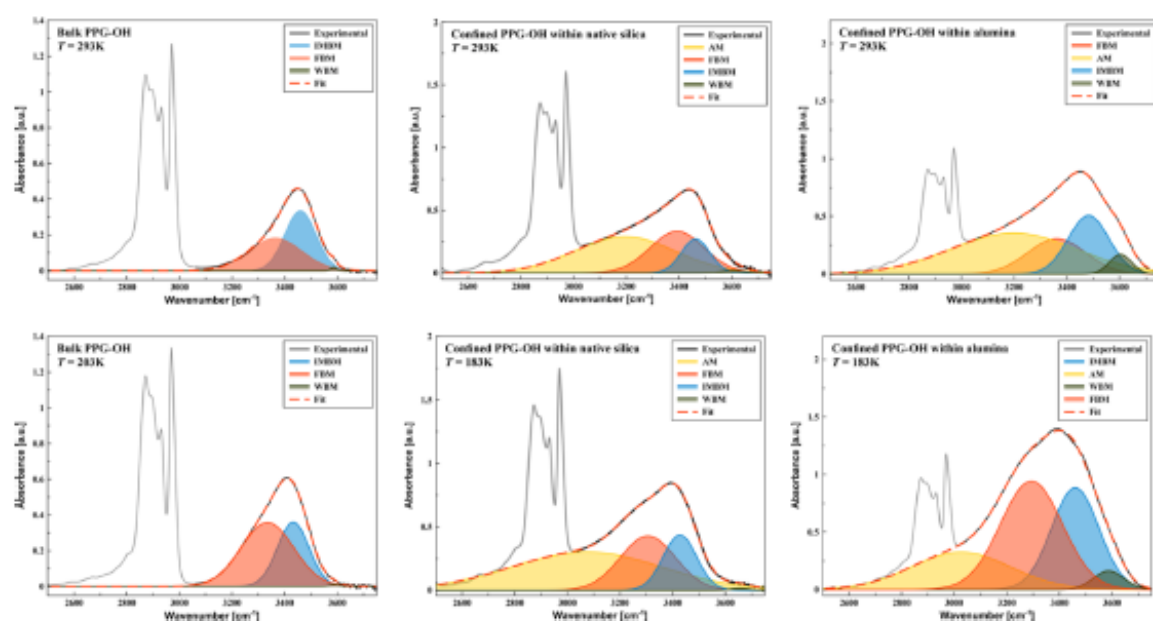


**Figure 8.** Decomposition of the  $\nu_{\text{OH}}$  band of bulk and confined PPG-OH in the frequency range of 2500 and 3750  $\text{cm}^{-1}$  in the temperatures of 293 K and  $T_g$ .

and  $T_g$  in the spectral region corresponding to the stretching vibration of the X–H and C–H moieties (3800–2600  $\text{cm}^{-1}$ ). It should be noted that the FTIR spectral data, especially obtained for alumina pores, were difficult to interpret because of additional strong contribution of the stretching vibrations of the –OH groups of the pore surface to the measured spectra.

An informative band for the analysis of hydrogen bond interactions is that connected to the X–H stretching vibrations of the proton donor groups (the  $\nu_{\text{X-H}}$ ). This spectral feature occurs in the range of 3700–3000  $\text{cm}^{-1}$  in the FTIR spectra of the studied systems. The band observed between 3000 and 2800  $\text{cm}^{-1}$  is responsible for the stretching vibrations of the C–H groups of the carbon skeleton. The position and frequency of the  $\nu_{\text{X-H}}$  bands for the bulk samples differ between PPG-OH and PPG-NH<sub>2</sub> (see Figure 7). At 293 K (room temperature, RT)  $\nu_{\text{O-H}}$  band of bulk PPG-OH occurs as a single broad peak located at 3453  $\text{cm}^{-1}$ , whereas the  $\nu_{\text{N-H}}$  band of PPG-NH<sub>2</sub> consists of three peaks at 3369, 3298, and 3201  $\text{cm}^{-1}$ . Thus, the H-bonds in both PPG derivatives are of medium strength. The different profiles of the  $\nu_{\text{X-H}}$  band of PPG-OH and PPG-NH<sub>2</sub> correspond to the various types of H-bonded aggregates. Note that it seems that the H-bonded oligomeric structures dominate in PPG-OH, while probably a more complex H-bonding network (the ring- or chain-like structures) can be formed in PPG-NH<sub>2</sub>. The spectral modifications of the X–H stretching bands of PPG-OH and PPG-NH<sub>2</sub> accompanying the temperature drop are consistent with the trend reported in the literature and discussed in the Supporting Information file.

In the next step, the FTIR approach was applied to investigate the effects of the nanoconfinement of PPG samples after their incorporation into different nanopore templates (silica and alumina). Representative spectra measured at different temperatures for the sample infiltrated in porous matrices are presented in Figures S4 and S5 in the Supporting

Information file. The interaction of PPGs molecules within silica or alumina membranes causes noticeable changes in their IR spectra that represent the change in the hydrogen-bonded pattern in the investigated systems. At RT, the IR spectra of the confined liquids exhibit a significant redshift of the  $\nu_{\text{X-H}}$  peak frequency values, relative to the bulk samples (Figure 7). This spectral effect is associated with the existence of stronger H-bonds in PPGs under nanoconfinement. Similar results are observed in IR spectra measured after the temperature drop. In detail, the larger redshift of the O–H stretching vibrations for PPG-OH molecules is observed for the native pores (14  $\text{cm}^{-1}$ ) compared to the silanized pores (11  $\text{cm}^{-1}$ ) or the alumina ones (12  $\text{cm}^{-1}$ ) at  $T_g$ . In the case of PPG-NH<sub>2</sub> the most intense peak of the  $\nu_{\text{N-H}}$  band at 3359  $\text{cm}^{-1}$  is shifted by 4  $\text{cm}^{-1}$  in native pores and 3  $\text{cm}^{-1}$  in silanized pores relative to the bulk at  $T_g$ . On the other hand, the  $\nu_{\text{N-H}}$  peak in alumina membranes shows the same position as that in the bulk. Thus, the PPG molecules within silanized silica pores exhibit the smallest spectral changes (*i.e.*, the redshift of the  $\nu_{\text{X-H}}$  peak frequency value) relative to other systems. This is because of the weaker interactions between the host and guest material. It is also observed that the  $\nu_{\text{X-H}}$  bands measured for the confined samples are much broader than those measured for the bulk materials. This indicates that PPG molecules also exhibit greater variability in the size of the H-bonded aggregates in a confined environment. In order to address this issue more carefully, we performed additional analysis relying on the deconvolution of the spectra measured in the 3000–3800  $\text{cm}^{-1}$  region for PPG-OH; please see Figures 8 and S6. This oligomer was selected and described in detail because it interacts the most with the native pores. To evaluate the contribution of specific components in this complex spectral regime, data collected for bulk and confined PPG-OH were fitted to the combination of several Gauss functions. The procedure of the fitting of the –OH stretching bands was



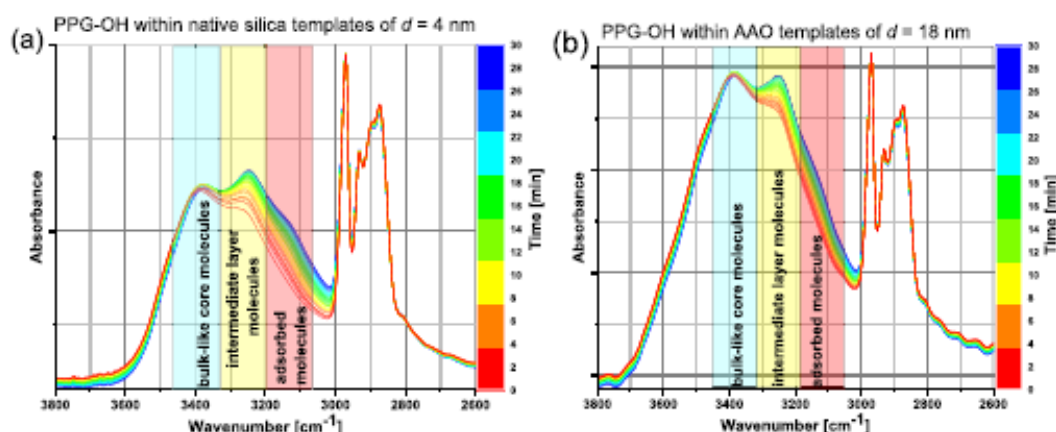


Figure 9. Time-dependent FTIR spectra of confined PPG-OH within the native silica (a) and alumina membranes (b) in the O–H and C–H stretching regions, recorded at 183 K over 30 min. The spectra were normalized to the C–H peak at around 2970  $\text{cm}^{-1}$ .

performed following the scheme reported for liquid water in refs.<sup>63,66</sup> This approach allows studying the hydrogen bonding interactions between surface silanol and PPG-OH at the interface. It is worthwhile to point out that H-bonds can be formed between PPG-OH molecules, silanol groups, and the host and guest material via the siloxane bridging oxygen group.

The bulk spectrum of PPG-OH in Figure 8 consists of the three Gaussian components assigned to vibration of the OH moiety in the (i) fully H-bonded bulk-like molecules (FBM, 3393–3259  $\text{cm}^{-1}$ ), (ii) intermediate (partially) H-bonded molecules (IMBM, 3482–3417  $\text{cm}^{-1}$ ), and (iii) weakly H-bonded molecules (WBM, 3619–3587  $\text{cm}^{-1}$ ). For the sample confined in pores, an additional Gaussian component is required to describe the FTIR spectra in the 3198–3026  $\text{cm}^{-1}$  region. This additional band is assigned to the  $\nu_{\text{OH}}$  in the molecules adsorbed (AM) at the interface. The comparison of the deconvoluted IR spectra in the –OH stretching vibration region for bulk and confined PPG-OH at RT and at  $T_g$  is shown in Figures 8 and S6 in the Supporting Information file. Figure S7 illustrates the temperature variations of the spectral parameters such as peak position and integrated areas obtained for each component (fraction of molecule) from the fitting IR spectra of bulk and confined PPG-OH to the superposition of several Gauss functions. All these parameters are also listed in Table S1. On the other hand in Table S2, the percentage areas of the deconvoluted profiles are shown, which give information on the different populations of H-bonded structural arrangements in PPG-OH. From the analysis of the results obtained at  $T_g$  (Table S1), one finds a redshift of the maximum of the all fractions of H-bonded oligomers in confined sample with respect to the bulk material. This indicates the enhancement of the H-bonding interactions under confinement. As shown in Figure 8, the largest peak area in bulk sample corresponds to the fully H-bonded PPG-OH molecules. On the other hand, quite a large variety of adsorption behavior of PPG-OH on the different pore walls is observed (Figures 8 and S6). In the native pores, the adsorption process is the most dominant because the AM component has the largest percentage in the OH band profile in selected temperatures. The silanized membranes exhibit similar behavior at higher temperatures; however, below 263 K, partially H-bonded PPG-OH structures predominate. In the case of alumina templates, the AM

component also dominates at 293K–233 K, whereas at low temperatures, the interactions between FBM are the strongest.

Next, the change in contribution of various Gaussian components to the overall spectrum upon temperature drops was monitored. As shown in Table S1, the positions of FBM and IMBM substructures are shifted to lower wavenumbers with decreasing temperature, indicating the strengthening of the interactions between “fully” and “partially” H-bonded PPG-OH molecules. On the contrary, the blueshift of the WBM components is observed because of the growth of the degree of association of PPG-OH at  $T_g$ . Simultaneously, the integrated area of the FBM and IMBM components increases and the WBM area decreases as the temperature is lowered indicating the growing organization of PPG-OH toward a fully H-bonded network. However, it should be pointed out that the FBM contribution in confined PPG-OH within the silanized silica templates exhibits opposite temperature effect, that is, it decreases with the lowering temperature. More detailed analysis based on the percentage contribution of the Gaussian component areas shows that in bulk PPG-OH, the FBM-type molecules are the dominating population, their proportion steadily increases from 48 to 62% as the temperature decreases from RT to  $T_g$ . Interestingly, in all-confined PPG-OH, the AM sub-band has the largest percentage at RT. As the temperature is lowered, the adsorption process is rather reduced in favor of the fully (alumina templates) and partially (silica and alumina templates) H-bonded interactions. The greatest effect of temperature on the adsorption process is observed for the alumina membrane in which the AM contribution decreases from 51 to 23%, while the FBM and IMBM populations increases 20–42 and 24–30%, respectively. Thus, the variations of the respective populations illustrate that for confined materials, the adsorbed PPG-OH molecules are always the dominating population at RT. At  $T_g$ , the interfacial H-bonded species are prevailing only in the native silica pores.

As a final point of our investigations, we have performed the time-dependent FTIR measurements on the PPG-OH confined into silica and alumina membranes to verify whether the annealing at  $T_{g,\text{core}}$  will influence on the H-bonding network. The analysis of these spectra in the  $\nu_{\text{O–H}}$  band region shows both changes in the shape of the band profile and its broadening as a function of time (Figure 9). The peak located around 3400  $\text{cm}^{-1}$ , originating from the bulk-like core

molecules, essentially shows no variation over time (the light blue area in Figure 9). Simultaneously the strong intensity growth of the sub-band at the lower wavenumber (approximately  $3250\text{ cm}^{-1}$ ) in both kind of pores (indicated as a light yellow area in Figure 9) was clearly detected. Interestingly, this band has been assigned herein to the vibration of the hydroxyl moiety in FBM. Moreover, IR spectra recorded during annealing also revealed appearance of the sub peak at  $\nu_{\text{OH}} \sim 3120\text{ cm}^{-1}$  connected to the adsorbed molecules. This band is probably because of the formation of the strongest H-bonds between PPG molecules and hydroxyl units attached to the silica and alumina templates (highlighted as light pink area in Figure 9). Growing intensity of the band observed at  $3250\text{ cm}^{-1}$  during annealing can be assigned to the formation of an intermediate layer of the molecules located between core and interfacial ones. However, because of overlapping of this band with that originating from the fraction of FBM of the bulk material, it was not possible to detect it in the FTIR spectra measured at different temperatures. Moreover, analysis of the position of the new band at  $3120\text{ cm}^{-1}$  indicated stronger interactions between the PPG-OH molecules and the silica surface with respect to the alumina. It is worthy to mention that this oligomer wets the alumina surface much better with respect to the silica one. Hence, it is a clear indication that enhanced wettability does not have to necessarily mean stronger interactions between host and guest material at least in the case of associating H-bonded liquids. Moreover, various strengths of the H-bonds between PPG and hydroxyl moieties attached to the silica and alumina pores suggest different chemical characters of this functional group that affects their different tendencies in formation of these specific interactions in both kinds of materials.

It must be also stressed that above discussed results obtained for confined PPGs differ from those obtained for water or alcohols infiltrated in nanoporous templates. For primary alcohols incorporated to the native and silanized silica pores, we have found that the strength of H-bonds in confined samples was weaker compared to those in bulk systems which was manifested in the IR spectra as the blueshift of the  $\nu_{\text{O-H}}$  peak frequency.<sup>49</sup> In the case of water confined in zeolites, the O-H bands were slightly redshifted with respect to bulk water, indicating, that under confinement, molecules are relatively strongly hydrogen-bonded.<sup>64</sup> Moreover, the IR spectra of water confined in controlled pore glasses proved that this fluid is perturbed on very large scales (more than 10 nm), even in pores of greater diameter ( $d = 55\text{ nm}$ ). The position of the connectivity band ( $\sim 150\text{ cm}^{-1}$ ) increased when the pore size decreased, suggesting stronger H-bonding interactions between neighboring water molecules. Additionally, an important decrease of the FWHM of the connectivity band was found for the spatially restricted sample (70%) which was related to a different orientation dynamics of water (up to 55 nm) as compared to bulk liquid.<sup>65</sup> Besides, Baum *et al.*<sup>66</sup> highlighted the predominant effect of the pore size, the kosmotropic properties and the surface ions excess on the dynamics, and the structure of water molecules in the pore and within the interfacial layer. The molecular dynamics simulations of the IR spectrum of isotopically dilute HOD in  $\text{D}_2\text{O}$  in 2.4 nm hydrophilic, amorphous silica pores<sup>67</sup> showed that -OH groups are involved in weaker H-bonds to the silica oxygen acceptors than to water, leading to blueshifts in their frequencies, although this spectral effect was not observed in the measured IR spectra. This fact was explained by the smaller

transition dipole moments of these -OH groups. Similar results were reported for HDO in  $\text{H}_2\text{O}$  in Aerosol-OT reverse micelles of varying sizes.<sup>68</sup> Although, in this case, the  $\nu_{\text{O-D}}$  bands exhibited a significant blueshift relative to the bulk liquid, indicating a weakening of hydrogen bonds between the OD groups because of the presence of the interface between the water pool and the surfactant headgroups.<sup>67,69</sup> Herein, it is also worth to mention about work by Zanotti *et al.* for water molecules in Vycor (a hydrophilic porous silica glass).<sup>70</sup> They have found the O-H stretching sub-band at  $3230\text{ cm}^{-1}$  that was interpreted as a result of the existence of a monolayer of water molecules H-bonded to the silanol (Si-OH) groups of the Vycor surface. The position of this peak revealed that the H-bonds in this system are significantly stronger than in bulk liquid water (around  $3400\text{ cm}^{-1}$ ). A further more detailed understanding of the molecular interactions of water confined in mesoporous silica was presented by Knight *et al.*<sup>71</sup> The authors fit the O-H stretch region using three Gaussian curves, representing unique water populations, described as network water (NW), intermediate water (IW), and multimer water (MW). However, these studies also showed a systematic blueshift in the IR peak locations of NW, IW, and MW in confined water. The authors suspected that water in pores is congregating around surface hydroxyl groups to form islands of highly coordinated localized regions. Hence, results of Knight *et al.* are similar to those reported herein.<sup>71</sup> However, it is worthwhile to point out that FTIR measurements on PPG confined in either silica or alumina membranes clearly revealed that although there are at least three fractions of molecules differing in the H-bond pattern in these conditions, the strength of these specific interactions is much stronger with respect to the bulk materials.

At the first sight, this experimental finding questions interpretation of the calorimetric data suggesting that there are two fractions of molecules differing in mobility and glass transition temperature discussed in terms of the "two-layer" (or "core-shell") model. However, it must be stressed that a change in the H-bonded pattern does not have to influence dynamics of confined systems to the extent allowing registration of the third glass transition temperature related to the vitrification of the intermediate layer. In this context, one can recall papers devoted to polymer thin films discussing the occurrence of the third (intermediate) layer.<sup>23</sup> As reported,  $T_g$  of ultrathin poly(methyl methacrylate) (PMMA) films depends on the type of applied substrates, that is, increasing for silicon oxide (polar surface) because of the hydrogen bonding and decreasing for the nonpolar surface, together with thickness reduction. It was observed that the dynamics and  $T_g$  of each layer differ from the corresponding bulk substances. This indicates that the nature of the interaction between materials and interface is one of the dominant factors in determining the glass-transition temperatures that strongly depends on the thickness of the film and the interfacial energy between the polymer and the substrate. Additionally, the formation of the third layer between the adsorbed layer and core volume was investigated for nanopores.<sup>72</sup> Using calorimetric measurements, it was revealed the existence of three  $T_g$ s for PMMA confined into AAO nanopores of  $d = 300\text{ nm}$ , where (i) molecules near interfaces (of  $T_g$  higher than for the bulk), (ii) molecules interacting at the center of nanopores ( $T_g$  lower than for the bulk), and (iii) fraction located between above-mentioned (characterized by intermediate  $T_g$  in a nonequilibrium state). Interestingly for PMMA restricted

into  $d = 80$  nm of AAO, only double  $T_g$ s was noted.<sup>61</sup> Generally, the formation of the third layer was considered as being strictly connected with the weakening of the interfacial effect between polymer matrices together with increasing pore diameter.<sup>23,72</sup> Besides, it was indicated that the existence of the third layer and also the shift of  $T_g$  strictly depends on the thermal history (heating/cooling rate, aging/annealing procedure) of the samples and might be strictly correlated with the exchange effects between the adsorbed layer, interlayer (two layers are trapped in a non-equilibrium state), and the core volume.<sup>23,72</sup> Note that recently, the presence of the additional interlayer under confinement was also reported for poly-(methylphenylsiloxane) infiltrated into AAO templates, where interestingly, the third  $T_g$  was also detected for small pore size,  $d = 18$  nm.<sup>73</sup>

One can also add that the resolving of the intermediate layer within the confined PPGs with time might, in fact, help us to understand better the reported recent shift of the segmental/structural relaxation process of various incorporated materials upon the annealing experiments performed at following temperature conditions,  $T_{g,interfacial} > T_{anneal} > T_{g,core}$ .<sup>62,74,75</sup> Note that at the studied range of temperatures, the examined systems are highly heterogeneous (the interfacial fraction of molecules is vitrified and the core ones are not). Briefly, as the annealing experiment proceeds, the shift of the  $\alpha$ -relaxation peak toward lower frequencies was observed<sup>74,75</sup> resulting in completely different  $\tau_\alpha(T)$ -dependences of confined materials with respect to the measurements performed prior to annealing (see Figure S8 in the Supporting Information file). As assumed, the density packing of core and interfacial molecules was out of equilibrium, which was recovered upon sample annealing. Consequently, the confined system moves from the one isochoric condition to the other, characterized by different densities and dynamics.<sup>15,41,76</sup> Nevertheless, as indicated by complementary FTIR measurements, the observed variation of structural/segmental dynamics might be also related to the variation of the H-bonding pattern or processes ongoing at the interface. It looks that during the annealing, there is a strong rearrangement of the interfacial layer leading to the formation of strong H-bonds between PPG and either silica or alumina pore walls. Moreover, the enhancement of these specific interactions is accompanied by the formation of the intermediate layer being in some distance from the pore walls.<sup>23,41,72</sup> Thus, in the annealed samples, we can clearly distinguish into three fractions, namely, interfacial, intermediate, and bulk-like fractions of molecules in the liquids infiltrated into pores.

#### 4. CONCLUSIONS

In this work, we investigated the behavior of three various poly(propylene glycol) derivatives of  $M_n = 400$  g/mol characterized by different abilities to form H-bonds and incorporated into alumina ( $d = 18$  nm) and silica (native and silanized of  $d = 4$  nm) templates. These studies enabled us to explore the impact of finite size and surface interactions on the overall behavior of substances in spatially restricted systems. The observed deviation of segmental relaxation times from the bulk-like behavior indicates that independently on the pore diameter and applied templates, they deviate at similar  $\tau_\alpha$ . Interestingly, we observed that although previous reports suggested that the shift in glass transition temperatures correlates with the interfacial energy and wettability, such relationship does not hold for PPGs infiltrated within alumina

( $d = 18$  nm) and native and functionalized silica ( $d = 4$  nm) templates. It indicates that besides the surface interactions and finite size (curvature), also other factors, that is, specific interactions, and density packing, possibly surface roughness, should also be taken into account when discussing the behavior of the confined liquid. Additionally, for the investigated PPGs, we observed that  $T_{g,inter}$  occurs even if  $T_{g,core}$  has not been reached before, which indicates that  $T_{g,core}$  is not a spinodal temperature. Finally, using FTIR spectroscopy, it was also revealed that the strength of hydrogen bond interactions between the incorporated material and interface differs dependently to the applied templates. Moreover, the time-dependent IR spectra recorded during annealing around the  $T_{g,core}$  revealed rearrangement in the interfacial layer leading to the formation of very strong H-bonds between PPG and alumina or silica pore walls. Consequently, this simple experiment allowed us to visualize and distinguish an intermediate layer (rarely reported in literature) between interfacial and bulk-like fraction of molecules. This completely new finding might shed new light and allow us to better understand the shift of the structural/segmental relaxation upon annealing below  $T_{g,interfacial}$ . It seems that variation in the H-bonds and density packing between molecules attached to the interface and the intermediate ones is responsible for this phenomenon.

#### ■ ASSOCIATED CONTENT

##### Supporting Information

The Supporting Information is available free of charge at <https://pubs.acs.org/doi/10.1021/acs.jpcc.0c04062>.

Preparation of porous silica templates, DSC thermograms, dielectric loss, and FTIR spectra of empty silica templates, nitrogen adsorption/desorption isotherms measured for native silica templates, dielectric loss spectra of bulk PPGs, dielectric loss spectra collected upon annealing of confined samples, FTIR spectra measured for bulk and confined PPGs, and their decomposition as well as temperature evolution (PDF)

#### ■ AUTHOR INFORMATION

##### Corresponding Authors

Agnieszka Talik – Institute of Physics and Silesian Center of Education and Interdisciplinary Research, University of Silesia in Katowice, 41-500 Chorzow, Poland; [orcid.org/0000-0001-7940-6967](https://orcid.org/0000-0001-7940-6967); Email: [agnieszka.talik@smcebi.edu.pl](mailto:agnieszka.talik@smcebi.edu.pl)

Magdalena Tarnacka – Institute of Physics and Silesian Center of Education and Interdisciplinary Research, University of Silesia in Katowice, 41-500 Chorzow, Poland; [orcid.org/0000-0002-9444-3114](https://orcid.org/0000-0002-9444-3114); Email: [magdalena.tarnacka@smcebi.edu.pl](mailto:magdalena.tarnacka@smcebi.edu.pl)

Barbara Hachuła – Institute of Chemistry, University of Silesia in Katowice, 40-006 Katowice, Poland; Email: [barbara.hachula@us.edu.pl](mailto:barbara.hachula@us.edu.pl)

##### Authors

Monika Geppert-Rybczyńska – Institute of Chemistry, University of Silesia in Katowice, 40-006 Katowice, Poland; [orcid.org/0000-0002-7112-9624](https://orcid.org/0000-0002-7112-9624)

Kamil Kaminski – Institute of Physics and Silesian Center of Education and Interdisciplinary Research, University of Silesia in Katowice, 41-500 Chorzow, Poland; [orcid.org/0000-0002-5871-0203](https://orcid.org/0000-0002-5871-0203)

Marian Paluch – Institute of Physics and Silesian Center of Education and Interdisciplinary Research, University of Silesia in Katowice, 41-500 Chorzow, Poland

Complete contact information is available at: <https://pubs.acs.org/10.1021/acs.jpcc.0c04062>

## Notes

The authors declare no competing financial interest.

## ACKNOWLEDGMENTS

M.T., M.P., and K.K. is thankful for financial support from the Polish National Science Centre within the OPUS project (Dec. no. 2019/33/B/ST3/00500).

## REFERENCES

- (1) Arndt, M.; Stannarius, R.; Gorbatschow, W.; Kremer, F. Dielectric investigations of the dynamic glass transition in nanopores. *Phys. Rev. E: Stat. Phys., Plasmas, Fluids, Relat. Interdiscip. Top.* **1996**, *54*, 5377–5390.
- (2) Suzuki, Y.; Duran, H.; Steinhart, M.; Butt, H.-J.; Floudas, G. Suppression of Poly(ethylene oxide) Crystallization in Diblock Copolymers of Poly(ethylene oxide)-*b*-poly(*ε*-caprolactone) Confined to Nanoporous Alumina. *Macromolecules* **2014**, *47*, 1793–1800.
- (3) Jasiurkowska-Delaporte, M.; Kossack, W.; Kipnusu, W. K.; Sangoro, J. R.; Iacob, C.; Kremer, F. Glassy dynamics of two poly(ethylene glycol) derivatives in the bulk and in nanometric confinement as reflected in its inter- and intra-molecular interactions. *J. Chem. Phys.* **2018**, *149*, 064501.
- (4) Iacob, C.; Sangoro, J. R.; Papadopoulos, P.; Schubert, T.; Naumov, S.; Valiullin, R.; Kärger, J.; Kremer, F. Charge transport and diffusion of ionic liquids in nanoporous silica membranes. *Phys. Chem. Chem. Phys.* **2010**, *12*, 13798–13803.
- (5) Kipnusu, W. K.; Elsayed, M.; Krause-Rehberg, R.; Kremer, F. Glassy dynamics of polymethylphenylsiloxane in one- and two-dimensional nanometric confinement—A comparison. *J. Chem. Phys.* **2017**, *146*, 203302.
- (6) Kipnusu, W. K.; Elmahdy, M. M.; Elsayed, M.; Krause-Rehberg, R.; Kremer, F. Counterbalance between Surface and Confinement Effects As Studied for Amino-Terminated Poly(propylene glycol) Constraint in Silica Nanopores. *Macromolecules* **2019**, *52*, 1864–1873.
- (7) Huwe, A.; Arndt, M.; Kremer, F.; Hagemmüller, C.; Behrens, P. Dielectric Investigations of the Molecular Dynamics of Propanediol in Mesoporous Silica Materials. *J. Chem. Phys.* **1997**, *107*, 9699.
- (8) Kipnusu, W. K.; Elsayed, M.; Kossack, W.; Pawlus, S.; Adrjanowicz, K.; Tress, M.; Mapesa, E. U.; Krause-Rehberg, R.; Kaminski, K.; Kremer, F. Confinement for More Space: A Larger Free Volume and Enhanced Glassy Dynamics of 2-ethyl-1-hexanol in Nanopores. *J. Phys. Chem. Lett.* **2015**, *6*, 3708–3712.
- (9) Wubbenhorst, M.; Lupascu, V. Glass Transition Effects in Ultra-Thin Polymer Films Studied by Dielectric Spectroscopy - Chain Confinement vs. Finite Size Effects. **2005**, *12th International Symposium on Electrets*, 2005.
- (10) White, R. P.; Lipson, J. E. G. Polymer Free Volume and Its Connection to the Glass Transition. *Macromolecules* **2016**, *49*, 3987–4007.
- (11) White, R. P.; Lipson, J. E. G. How Free Volume Does Influence the Dynamics of Glass Forming Liquids. *ACS Macro Lett.* **2017**, *6*, 529–534.
- (12) White, R. P.; Lipson, J. E. G. Connecting Pressure-Dependent Dynamics to Dynamics under Confinement: The Cooperative Free Volume Model Applied to Poly(4-chlorostyrene) Bulk and Thin Films. *Macromolecules* **2018**, *51*, 7924–7941.
- (13) Panagopoulou, A.; Rodriguez-Tinoco, C.; White, R. P.; Lipson, J. E. G.; Napolitano, S. Substrate Roughness Speeds Up Segmental Dynamics of Thin Polymer Films. *Phys. Rev. Lett.* **2020**, *124*, 027802.
- (14) Adrjanowicz, K.; Kaminski, K.; Koperwas, K.; Paluch, M. Negative Pressure Vitrification of the Isochorically Confined Liquid in Nanopores. *Phys. Rev. Lett.* **2015**, *115*, 265702.
- (15) Tarnacka, M.; Kipnusu, W. K.; Kaminska, E.; Pawlus, S.; Kaminski, K.; Paluch, M. The peculiar Behavior of Molecular Dynamics of Glass-forming Liquid Confined in the Native Porous Materials - The Role of Negative Pressure. *Phys. Chem. Chem. Phys.* **2016**, *18*, 23709–23714.
- (16) Szklarz, G.; Adrjanowicz, K.; Tarnacka, M.; Pionteck, J.; Paluch, M. Confinement-Induced Changes in the Glassy Dynamics and Crystallization Behavior of Supercooled Fenofibrate. *J. Phys. Chem. C* **2018**, *122*, 1384–1395.
- (17) Napolitano, S.; Rotella, C.; Wubbenhorst, M. Can Thickness and Interfacial Interactions Uniquely Determine the Behavior of Polymers Confined at the Nanoscale? *ACS Macro Lett.* **2012**, *1*, 1189–1193.
- (18) Napolitano, S.; Lupascu, V.; Wubbenhorst, M. Temperature dependence of the deviation from bulk behaviour in ultrathin polymer films. *Macromolecules* **2008**, *41*, 1061–1063.
- (19) Rotella, C.; Napolitano, S.; Vandendriessche, S.; Valev, V. K.; Verbiest, T.; Larkowska, M.; Kucharski, S.; Wubbenhorst, M. Adsorption Kinetics Of Ultrathin Polymer Films In The Melt Probed By Dielectric Spectroscopy And Second-Harmonic Generation. *Langmuir* **2011**, *27*, 13533.
- (20) Torres, J. A.; Nealey, P. F.; de Pablo, J. J. Molecular Simulation of Ultrathin Polymeric Films near the Glass Transition. *Phys. Rev. Lett.* **2000**, *85*, 3221–3224.
- (21) Alexandris, S.; Papadopoulos, P.; Sakellariou, G.; Steinhart, M.; Butt, H.-J.; Floudas, G. Interfacial Energy and Glass Temperature of Polymers Confined to Nanoporous Alumina. *Macromolecules* **2016**, *49*, 7400–7414.
- (22) Tarnacka, M.; Wojtyniak, M.; Brzózka, A.; Talik, A.; Hachula, B.; Kaminska, E.; Sulka, G.; Kaminski, K.; Paluch, M. The Unique Behavior of Poly(propylene glycols) Confined within Alumina Templates Having Nanostructured Interface. *Nano Lett.* Publication Date: June 19, 2020.
- (23) Fryer, D. S.; Peters, R. D.; Kim, E. J.; Tomaszewski, J. E.; de Pablo, J. J.; Nealey, P. F.; White, C. C.; Wu, W.-L. Dependence of the Glass Transition Temperature of Polymer Films on Interfacial Energy and Thickness. *Macromolecules* **2001**, *34*, 5627–5634.
- (24) Lang, R. J.; Merling, W. L.; Simmons, D. S. Combined Dependence of Nanoconfined Tg on Interfacial Energy and Softness of Confinement. *ACS Macro Lett.* **2014**, *3*, 758–762.
- (25) Talik, A.; Tarnacka, M.; Geppert-Rybczynska, M.; Minceka, A.; Kaminska, E.; Kaminski, K.; Paluch, M. Impact of the Interfacial Energy and Density Fluctuations on the Shift of the Glass-Transition Temperature of Liquids Confined in Pores. *J. Phys. Chem. C* **2019**, *123*, 5549–5556.
- (26) Talik, A.; Tarnacka, M.; Wojtyniak, M.; Kaminska, E.; Kaminski, K.; Paluch, M. The influence of the nanocurvature on the surface interactions and molecular dynamics of model liquid confined in cylindrical pores. *J. Mol. Liq.* **2020**, *298*, 111973.
- (27) Tolman, R. C. The Effect of Droplet Size on Surface Tension. *J. Chem. Phys.* **1949**, *17*, 333.
- (28) Tolman, R. C. The Superficial Density of Matter at a Liquid-Vapor Boundary. *J. Chem. Phys.* **1949**, *17*, 118.
- (29) Simavilla, D. N.; Huang, W.; Housmans, C.; Sferazza, M.; Napolitano, S. Taming the Strength of Interfacial Interactions via Nanoconfinement. *ACS Cent. Sci.* **2018**, *4*, 755–759.
- (30) Schönhals, A.; Goering, H.; Schick, Ch. Segmental and chain dynamics of polymers: from the bulk to the confined state. *J. Non-Cryst. Solids* **2002**, *305*, 140–149.
- (31) Schönhals, A.; Stauga, R. Dielectric Normal Mode Relaxation of Poly(propylene glycol) Melts in Confining Geometries. *J. Non-Cryst. Solids* **1998**, *235–237*, 450–456.
- (32) Schönhals, A.; Stauga, R. Broadband Dielectric Study of Anomalous Diffusion in a Poly(propylene glycol) Melt Confined to Nanopores. *J. Chem. Phys.* **1998**, *108*, 5130–5136.

- (33) Aasen, A.; Blokhuys, E. M.; Wilhelmsen, Ø. Tolman lengths and rigidity constants of multicomponent fluids: Fundamental theory and numerical examples. *J. Chem. Phys.* **2018**, *148*, 204702.
- (34) Gibbs, J. W. *The Collected Works*; Longmans Green and Company: New York, 1928; Vol. I, p 219.
- (35) Blokhuys, E. M.; Kuipers, J. Thermodynamic expressions for the Tolman length. *J. Chem. Phys.* **2006**, *124*, 074701.
- (36) Stepanov, S. V.; Byakov, V. M.; Stepanova, O. P. The Determination of Microscopic Surface Tension of Liquids with a Curved Interphase Boundary by Means of Positron Spectroscopy. *Russ. J. Phys. Chem.* **2000**, *74*, S65–S77.
- (37) <https://www.inredox.com>, accessed: 10.02.2020.
- (38) Ngo, D.; Liu, H.; Chen, Z.; Kaya, H.; Zimudzi, T. J.; Gin, S.; Mahadevan, T.; Du, J.; Kim, S. H. Hydrogen bonding interactions of H<sub>2</sub>O and SiOH on a bororoaluminosilicate glass corroded in aqueous solution. *npj Mater. Degrad.* **2020**, *4*, 1–14.
- (39) Wandschneider, A.; Lehmann, J. K.; Heintz, A. Surface Tension and Density of Pure Ionic Liquids and Some Binary Mixtures with 1-propanol and 1-butanol. *J. Chem. Eng. Data* **2008**, *53*, 596–599.
- (40) Feder-Kubis, J.; Geppert-Rybczyńska, M.; Musiał, M.; Talić, E.; Guzik, A. Exploring the Surface Activity of a Homologues Series of Functionalized Ionic Liquids with a Natural Chiral Substituent: (–)-Menthol in a Cation. *Colloid Surf., A* **2017**, *529*, 725–732.
- (41) Tamacka, M.; Talić, A.; Kamińska, E.; Geppert-Rybczyńska, M.; Kamiński, K.; Paluch, M. The Impact of Molecular Weight on the Behavior of Poly(propylene glycols) Derivatives Confined within Alumina Templates. *Macromolecules* **2019**, *52*, 3516–3529.
- (42) Alexandris, S.; Sakellariou, G.; Steinhart, M.; Floudas, G. Dynamics of Unentangled cis-1,4-Polyisoprene Confined to Nanoporous Alumina. *Macromolecules* **2014**, *47*, 3895–3900.
- (43) Havriliak, S.; Negami, S. A. Complex Plane Analysis of  $\alpha$ -dispersions in Some Polymer Systems. *J. Polym. Sci., Part C: Polym. Symp.* **1966**, *14*, 99–117.
- (44) Kremer, F.; Schönhals, A. *Broadband Dielectric Spectroscopy*; Springer: Berlin, 2003.
- (45) Arndt, M.; Stannarius, R.; Grootheus, H.; Hempel, E.; Kremer, F. Length Scale of Cooperativity in the Dynamic Glass Transition. *Phys. Rev. Lett.* **1997**, *79*, 2077.
- (46) Kuon, N.; Milischuk, A. A.; Ladanyi, B. M.; Flenner, E. Self-intermediate scattering function analysis of supercooled water confined in hydrophilic silica nanopores. *J. Chem. Phys.* **2017**, *146*, 214501.
- (47) Hassion, F. X.; Cole, R. H. Dielectric Properties of Liquid Ethanol and 2-Propanol. *J. Chem. Phys.* **1955**, *23*, 1756.
- (48) Hansen, C.; Stickel, F.; Berger, T.; Richert, R.; Fischer, E. W. Dynamics of glass-forming liquids. III. Comparing the dielectric  $\alpha$ - and  $\beta$ -relaxation of 1-propanol and o-terphenyl. *J. Chem. Phys.* **1997**, *107*, 1086.
- (49) Talić, A.; Tamacka, M.; Geppert-Rybczyńska, M.; Hachula, B.; Bernat, R.; Chranowska, A.; Kamiński, K.; Paluch, M. Are hydrogen supramolecular structures being suppressed upon nanoscale confinement? The case of monohydroxy alcohols. *J. Colloid Interface Sci.* **2020**, *576*, 217–229.
- (50) Tu, W.; Chat, K.; Szklarz, G.; Laskowski, L.; Grzybowska, K.; Paluch, M.; Richert, R.; Adrjanowicz, K. Dynamics of Pyrrolidinium-Based Ionic Liquids under Confinement. II. The Effects of Pore Size, Inner Surface, and Cationic Alkyl Chain Length. *J. Phys. Chem. C* **2020**, *124*, 5395–5408.
- (51) Kremer, F. *Dynamics in Geometrical Confinement*; Springer: Cham, Switzerland, 2014.
- (52) Vogel, H. Temperaturabhängigkeitgesetz der Viskosität von Flüssigkeiten. *Phys. Z.* **1921**, *22*, 645–646.
- (53) Fulcher, G. S. Analysis of Recent Measurements of the Viscosity of Glasses. *J. Am. Ceram. Soc.* **1925**, *8*, 339–355.
- (54) Tammann, G.; Hesse, W. Die Abhängigkeit der Viskosität von der Temperatur bei unterkühlten Flüssigkeiten. *Z. Anorg. Allg. Chem.* **1926**, *156*, 245–257.
- (55) Young, T. III. An essay on the cohesion of fluids. *Philos. Trans. R. Soc. London* **1805**, *95*, 65–87.
- (56) Fowkes, F. M. Attractive forces and interfaces. *Ind. Eng. Chem.* **1964**, *56*, 40–52.
- (57) Fowkes, F. M. Determination of interfacial tensions, contact angles, and dispersion forces in surfaces by assuming additivity of intermolecular interactions in surfaces. *J. Phys. Chem.* **1962**, *66*, 382.
- (58) Politidis, C.; Alexandris, S.; Sakellariou, G.; Steinhart, M.; Floudas, G. Dynamics of Entangled cis-1,4-Polyisoprene Confined to Nanoporous Alumina. *Macromolecules* **2019**, *52*, 4185–4195.
- (59) Talić, A.; Tamacka, M.; Grudka-Flak, L.; Maksym, P.; Geppert-Rybczyńska, M.; Wolnica, K.; Kamińska, E.; Kamiński, K.; Paluch, M. The Role of Interfacial Energy and Specific Interactions on the Behavior of Poly(propylene glycol) Derivatives under 2D Confinement. *Macromolecules* **2018**, *51*, 4840–4852.
- (60) Park, J.-Y.; McKenna, G. B. Size and Confinement Effects on the Glass Transition Behavior of Polystyrene/o-Terphenyl Polymer Solutions. *Phys. Rev. B: Condens. Matter Mater. Phys.* **2000**, *61*, 6667.
- (61) Li, L.; Zhou, D.; Huang, D.; Xue, G. Double Glass Transition Temperatures of Poly(methyl methacrylate) Confined in Alumina Nanotube Templates. *Macromolecules* **2013**, *47*, 297–303.
- (62) Tamacka, M.; Madejczyk, O.; Kamiński, K.; Paluch, M. Time and Temperature as Key Parameters Controlling Dynamics and Properties of Spatially Restricted Polymers. *Macromolecules* **2017**, *50*, 5188–5193.
- (63) Brubach, J.-B.; Mermet, A.; Filabozzi, A.; Gerschel, A.; Roy, P. Signatures of the Hydrogen Bonding in the Infrared Bands of Water. *J. Chem. Phys.* **2005**, *122*, 184509.
- (64) Crupi, V.; Longo, F.; Majolino, D.; Venuti, V. Dependence of Vibrational Dynamics of Water in Ion-Exchanged Zeolites A: A Detailed Fourier Transform Infrared Attenuated Total Reflection Study. *J. Chem. Phys.* **2005**, *123*, 154702.
- (65) Le Caër, S.; Pin, S.; Esmouf, S.; Raffy, Q.; Renault, J. P.; Brubach, J.-B.; Creff, G.; Roy, P. A Trapped Water Network in Nanoporous Material: The Role of Interfaces. *Phys. Chem. Chem. Phys.* **2011**, *13*, 17658.
- (66) Baum, M.; Rieutord, F.; Juranyi, F.; Rey, C.; Rébiscoul, D. Dynamical and Structural Properties of Water in Silica Nanoconfinement: Impact of Pore Size, Ion Nature, and Electrolyte Concentration. *Langmuir* **2019**, *35*, 10780.
- (67) Burris, P. C.; Laage, D.; Thompson, W. H. Simulations of the infrared, Raman, and 2D-IR photon echo spectra of water in nanoscale silica pores. *J. Chem. Phys.* **2016**, *144*, 194709.
- (68) Moilanen, D. E.; Fenn, E. E.; Wong, D.; Fayer, M. D. Water dynamics in large and small reverse micelles: From two ensembles to collective behavior. *J. Chem. Phys.* **2009**, *131*, 014704.
- (69) Thompson, W. H. Perspective: Dynamics of confined liquids. *J. Chem. Phys.* **2018**, *149*, 170901.
- (70) Zanotti, J.-M.; Judeinstein, P.; Dalla-Bernardina, S.; Creff, G.; Brubach, J.-B.; Roy, P.; Bonetti, M.; Olivier, J.; Sakellariou, D.; Bellissent-Funel, M.-C. Competing coexisting phases in 2D water. *Sci. Rep.* **2016**, *6*, 25938.
- (71) Knight, A. W.; Kalugin, N. G.; Coker, E.; Ilgen, A. G. Water properties under nano-scale confinement. *Sci. Rep.* **2019**, *9*, 8246.
- (72) Li, L.; Chen, J.; Deng, W.; Zhang, C.; Sha, Y.; Cheng, Z.; Xue, G.; Zhou, D. Glass Transitions of Poly(methyl methacrylate) Confined in Nanopores: Conversion of Three- and Two-Layer Models. *J. Phys. Chem. B* **2015**, *119*, 5047–5054.
- (73) Adrjanowicz, K.; Winkler, R.; Chat, K.; Duarte, D. M.; Tu, W.; Unni, A. B.; Paluch, M.; Ngai, K. L. Study of Increasing Pressure and Nanopore Confinement Effect on the Segmental, Chain, and Secondary Dynamics of Poly(methylphenylsiloxane). *Macromolecules* **2019**, *52*, 3763–3774.
- (74) Tamacka, M.; Kamiński, K.; Mapesa, E. U.; Kamińska, E.; Paluch, M. Studies on the Temperature and Time Induced Variation in the Segmental and Chain Dynamics in Poly(propylene glycol) Confined at the Nanoscale. *Macromolecules* **2016**, *49*, 6678–6686.
- (75) Shi, G.; Guan, Y.; Liu, G.; Müller, A. J.; Wang, D. Segmental Dynamics Govern the Cold Crystallization of Poly(lactic acid) in Nanoporous Alumina. *Macromolecules* **2019**, *52*, 6904–6912.

(76) Adrjanowicz, K.; Paluch, M. Discharge of the Nanopore Confinement Effect on the Glass Transition Dynamics via Viscous Flow. *Phys. Rev. Lett.* **2019**, *122*, 176101.

## OŚWIADCZENIA WSPÓLAUTORÓW

Dr hab. Magdalena Tarnacka, prof. UŚ  
Instytut Fizyki  
Wydział Nauk Ścisłych i Technicznych,  
Uniwersytet Śląski w Katowicach  
Ul. 75 Pułku Piechoty 1A  
41-500 Chorzów

Chorzów, 5.05.2021 r.

### OŚWIADCZENIE

Oświadczam, że w poniższych pracach mój wkład był następujący:

- A1. A. Talik; M. Tarnacka; I. Grudzka-Flak; P. Maksym; M. Geppert-Rybczynska; K. Wolnica; E. Kaminska; K. Kaminski; M. Paluch. **The Role of Interfacial Energy and Specific Interactions on the Behavior of Poly(propylene glycol) Derivatives under 2D Confinement.** *Macromolecules*, 2018, 51,13, 4840-4852

*Mój wkład polegał na opracowaniu koncepcji badań, wykonaniu pomiarów kalorymetrycznych, analizie danych, interpretacji wyników oraz pomocy przy przygotowaniu manuskryptu doktorantce, której jestem promotorem pomocniczym.*

- A2. A. Talik, M. Tarnacka, M. Geppert-Rybczynska, A. Minecka, E. Kaminska, K. Kaminski, M. Paluch. **Impact of the Interfacial Energy and Density Fluctuations on the Shift of the Glass-Transition Temperature of Liquids Confined in Pores.** *Journal of Physical Chemistry C*, 2019, 123, 9, 5549-5556

*Mój wkład polegał na opracowaniu koncepcji badań, wykonaniu pomiarów kalorymetrycznych, analizie danych, interpretacji wyników oraz pomocy przy przygotowaniu manuskryptu doktorantce, której jestem promotorem pomocniczym.*

- A3. A. Talik, M. Tarnacka, M. Wojtyniak, E. Kaminska, K. Kaminski, M. Paluch. **The influence of the nanocurvature on the surface interactions and molecular dynamics of model liquid confined in cylindrical pores.** *Journal of Molecular Liquids*, 2019, 111973.

*Mój wkład polegał na wykonaniu pomiarów przy pomocy skaningowej kalorymetrii różnicowej, analizie otrzymanych wyników kalorymetrycznych i ich dyskusji oraz pomocy przy przygotowaniu manuskryptu doktorantce, której jestem promotorem pomocniczym.*

- A4. A. Talik; M. Tarnacka; M. Geppert-Rybczynska; B. Hachuła; R. Bernat; A. Chrzanowska; K. Kaminski; M. Paluch. **Are hydrogen supramolecular structures being suppressed upon nanoscale confinement? The case of monohydroxy alcohols.** *Journal of Colloid and Interface Science*, 576, 2020, 217-229.

*Mój wkład polegał na dyskusji otrzymanych wyników, pomocy przy przygotowaniu manuskryptu doktorantce, której jestem promotorem pomocniczym.*

A.S.A. Talik; M. Tarnacka; M. Geppert-Rybczynska; B. Hachuła; K. Kaminski; M. Paluch.  
**Impact of Confinement on the Dynamics and H-Bonding Pattern in Low-Molecular Weight Poly(propylene glycols).** *Journal of Physical Chemistry C*, 2020, 124, 17607–17621

*Mój wkład polegał na nadzorowaniu przeprowadzonych pomiarów i analiz oraz pomocy przy przygotowaniu manuskryptu doktorantce, której jestem promotorem pomocniczym.*

Geppert-Rybczynska  
Tarnacka



dr Iwona Grudzka-Flak

Chorzów, 5.05.2021 r.

#### OŚWIADCZENIE

Oświadczam, że w pracy :

A1. A. Talik; M. Tarnacka; I. Grudzka-Flak; P. Maksym; M. Geppert-Rybczynska; K. Wolnica; E. Kaminska; K. Kaminski; M. Paluch. **The Role of Interfacial Energy and Specific Interactions on the Behavior of Poly(propylene glycol) Derivatives under 2D Confinement.** *Macromolecules*, 2018, 51,13, 4840-4852

*Mój wkład polegał na wykonaniu syntezy pochodnych glikolu polipropylenowego*

Iwona Grudzka-Flak

Dr inż. Paulina Maksym  
Wydział Nauk Ścisłych i Technicznych  
Instytut Fizyki  
Uniwersytet Śląski w Katowicach  
Ul. 75 Pułku Piechoty 1A  
41-500 Chorzów

Chorzów, 5.05.2021 r

### OŚWIADCZENIE

Oświadczam, że w pracy :

A1. A. Talik; M. Tarnacka; I. Grudzka-Flak; P. Maksym; M. Geppert-Rybczyńska; K. Wolnica; E. Kaminska; K. Kaminski; M. Paluch. **The Role of Interfacial Energy and Specific Interactions on the Behavior of Poly(propylene glycol) Derivatives under 2D Confinement.** *Macromolecules*, 2018, 51,13, 4840-4852

*Mój wkład polegał na wykonaniu syntezy pochodnych glikolu polipropylenowego oraz charakterystyce uzyskanych produktów metodą NMR*



Dr hab. Monika Geppert-Rybczyńska, prof. UŚ  
Wydział Nauk Ścisłych i Technicznych  
Instytut Chemii  
Uniwersytet Śląski w Katowicach  
ul. Szkolna 9  
40-006 Katowice

Katowice, 5.05.2021 r.

### OŚWIADCZENIE

Oświadczam, że w poniższych pracach :

A1. A. Talik; M. Tarnacka; I. Grudzka-Flak; P. Maksym; M. Geppert-Rybczyńska; K. Wolnica; E. Kaminska; K. Kaminski; M. Paluch. **The Role of Interfacial Energy and Specific Interactions on the Behavior of Poly(propylene glycol) Derivatives under 2D Confinement.** *Macromolecules*, 2018, 51,13, 4840-4852

*Mój wkład polegał na wykonaniu pomiarów kąta zwilżalności, napięcia powierzchniowego oraz obliczenia energii międzyfazowej substancji i ich analizie oraz dyskusji otrzymanych wyników.*

A2. A. Talik, M. Tarnacka, M. Geppert-Rybczyńska, A. Minecka, E. Kaminska, K. Kaminski, M. Paluch. **Impact of the Interfacial Energy and Density Fluctuations on the Shift of the Glass-Transition Temperature of Liquids Confined in Pores.** *Journal of Physical Chemistry C*, 2019, 123, 9, 5549-5556.

*Mój wkład polegał na wykonaniu pomiarów kąta zwilżalności, napięcia powierzchniowego oraz obliczenia energii międzyfazowej substancji i ich analizie oraz dyskusji otrzymanych wyników.*

A4. A. Talik; M. Tarnacka; M. Geppert-Rybczyńska; B. Hachuła; R. Bernat; A. Chrzanowska; K. Kaminski; M. Paluch. **Are hydrogen supramolecular structures being suppressed upon nanoscale confinement? The case of monohydroxy alcohols.** *Journal of Colloid and Interface Science*, 576, 2020, 217–229.

*Mój wkład polegał na wykonaniu pomiarów kąta zwilżalności, napięcia powierzchniowego oraz obliczenia energii międzyfazowej substancji i ich analizie oraz dyskusji otrzymanych wyników.*

A5. A. Talik; M. Tarnacka; M. Geppert-Rybczyńska; B. Hachuła; K. Kaminski; M. Paluch. **Impact of Confinement on the Dynamics and H-Bonding Pattern in Low-Molecular Weight Poly(propylene glycols).** *Journal of Physical Chemistry C* 2020, 124, 17607–17621.

*Mój wkład polegał na wykonaniu pomiarów kąta zwilżalności, napięcia powierzchniowego oraz obliczenia energii międzyfazowej substancji i ich analizie oraz dyskusji otrzymanych wyników.*

*Monika Geppert-Rybczyńska*

Dr Kamila Wolnica

Katowice, 5.05.2021 r.

### OŚWIADCZENIE

Oświadczam, że w pracy :

A. Talik; M. Tarnacka; I. Grudzka-Flak; P. Maksym; M. Geppert-Rybczyńska; K. Wolnica; E. Kamińska; K. Kamiński; M. Paluch. The Role of Interfacial Energy and Specific Interactions on the Behavior of Poly(propylene glycol) Derivatives under 2D Confinement. *Macromolecules*, 2018, 51,13, 4840-4852

Mój wkład polegał na wykonaniu pomiarów substancji litych za pomocą spektroskopii w podczerwieni (IR) ich analizie i opisie.

*Kamila Wolnica*

mgr Aldona Minecka

Sosnowiec, 5.05.2021 r.

Katedra i Zakład Farmakognozji i Fitochemii

ul. Jagiellońska 4

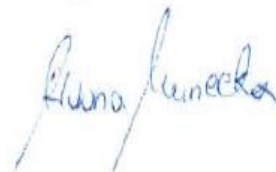
41-200 Sosnowiec

### OŚWIADCZENIE

Oświadczam, że w pracy :

Aż. A. Talik, M. Tarnacka, M. Geppert-Rybczynska, A. Minecka, E. Kaminska, K. Kaminski, M. Paluch. **Impact of the Interfacial Energy and Density Fluctuations on the Shift of the Glass-Transition Temperature of Liquids Confined in Pores.** *Journal of Physical Chemistry C*, 2019, 123, 9, 5549-5556.

*Mój wkład polegał na pomiarach dielektrycznych Hex-IBU oraz analizie wyników.*



mgr inż. Roksana Bernat  
Wydział Nauk Ścisłych i Technicznych  
Instytut Chemii  
Uniwersytet Śląski w Katowicach  
Ul. Szkolna 9  
40-006 Katowice

Katowice, 5.05.2021 r.

#### OŚWIADCZENIE

Oświadczam, że w pracy :

A4. A. Talik; M. Tarnacka; M. Geppert-Rybczyńska; B. Hachuła; R. Bernat; A. Chrzanowska; K. Kaminski; M. Paluch. **Are hydrogen supramolecular structures being suppressed upon nanoscale confinement? The case of monohydroxy alcohols.** *Journal of Colloid and Interface Science*, 576, 2020, 217–229.

*Mój wkład polegał na uczestnictwie w pomiarach za pomocą spektroskopii w podczerwieni (IR) oraz wykonaniu części rysunków.*

Roksana Bernat

Dr Marcin Wojtyniak

Chorzów, 5.05.2021 r.

Wydział Nauk Ścisłych i Technicznych,

Uniwersytet Śląski w Katowicach

ul. 75 Pułku Piechoty 1A

41-500 Chorzów

### OŚWIADCZENIE

Oświadczam, że w pracy :

**A3. A. Talik, M. Tarnacka, M. Wojtyniak, E. Kaminska, K. Kaminski, M. Pałuch. The influence of the nanocurvature on the surface interactions and molecular dynamics of model liquid confined in cylindrical pores. *Journal of Molecular Liquids* 2019, 111973.**

*Mój wkład polegał na wykonaniu pomiarów substancji przy pomocy mikroskopii sił atomowych (AFM), wykonaniu rysunków oraz analizie otrzymanych wyników.*

*Marcin Wojtyniak*

mgr Agnieszka Chrzanowska  
Katedra Chemii Fizycznej  
Uniwersytet Marii Curie-Skłodowskiej  
Pl. Marii Curie-Skłodowskiej 3/222  
20-031 Lublin

Lublin, 5.05.2021 r.

### OŚWIADCZENIE

Oświadczam, że w pracy :

A. Talik; M. Tarnacka; M. Geppert-Rybczynska; B. Hachuła; R. Bernat; A. Chrzanowska; K. Kaminski; M. Paluch. Are hydrogen supramolecular structures being suppressed upon nanoscale confinement? The case of monohydroxy alcohols *Journal of Colloid and Interface Science*, 576, 2020, 217–229.

Mój wkład polegał na wykonaniu analizy i charakterystyki porów krzemowych.

Agnieszka  
Chrzanowska



Dr hab. n. farm. Ewa Kamińska prof. ŚUM  
Katedra i Zakład Farmakognozji i Fitochemii  
ul. Jagiellońska 4  
41-200 Sosnowiec

Sosnowiec, 5.05.2021 r.

### OŚWIADCZENIE

Oświadczam, że w następujących pracach :

A1. A. Talik; M. Tarnacka; I. Grudzka-Flak; P. Maksym; M. Geppert-Rybczynska; K. Wolnica; E. Kaminska; K. Kaminski; M. Paluch. **The Role of Interfacial Energy and Specific Interactions on the Behavior of Poly(propylene glycol) Derivatives under 2D Confinement.** *Macromolecules*, 2018, 51,13, 4840-4852

*Mój wkład polegał na uczestnictwie w tworzeniu i korekcji manuskryptu.*

A2. A. Talik, M. Tarnacka, M. Geppert-Rybczynska, A. Minecka, E. Kaminska, K. Kaminski, M. Paluch. **Impact of the Interfacial Energy and Density Fluctuations on the Shift of the Glass-Transition Temperature of Liquids Confined in Pores.** *Journal of Physical Chemistry C*, 2019, 123, 9, 5549-5556.

*Mój wkład polegał na uczestnictwie w tworzeniu i korekcji manuskryptu.*

A3. A. Talik, M. Tarnacka, M. Wojtyniak, E. Kaminska, K. Kaminski, M. Paluch. **The influence of the nanocurvature on the surface interactions and molecular dynamics of model liquid confined in cylindrical pores.** *Journal of Molecular Liquids* 2019, 111973.

*Mój wkład polegał na uczestnictwie w tworzeniu i korekcji manuskryptu.*

*Ewa Kamińska-Kaminska*

Prof. dr hab. Kamil Kamiński

Chorzów, 5.05.2021

Wydział Nauk Ścisłych i Technicznych,

Instytut Fizyki

Uniwersytet Śląski w Katowicach

Ul. 75 Pułku Piechoty 1A

41-500 Chorzów

### OŚWIADCZENIE

Oświadczam, że w następujących pracach :

A1. A. Talik; M. Tarnacka; I. Grudzka-Flak; P. Maksym; M. Geppert-Rybczynska; K. Wolnica; E. Kaminska; K. Kaminski; M. Paluch. **The Role of Interfacial Energy and Specific Interactions on the Behavior of Poly(propylene glycol) Derivatives under 2D Confinement.** *Macromolecules*, 2018, 51,13, 4840-4852

*Mój wkład polegał na nadzorowaniu przeprowadzonych analiz, dyskusji otrzymanych wyników oraz tworzeniu i korekcji manuskryptu jak i współtworzeniu odpowiedzi do recenzentów.*

A2. A. Talik, M. Tarnacka, M. Geppert-Rybczynska, A. Minecka, E. Kaminska, K. Kaminski, M. Paluch. **Impact of the Interfacial Energy and Density Fluctuations on the Shift of the Glass-Transition Temperature of Liquids Confined in Pores.** *Journal of Physical Chemistry C*, 2019, 123, 9, 5549-5556.

*Mój wkład polegał na nadzorowaniu przeprowadzonych analiz, dyskusji otrzymanych wyników oraz tworzeniu i korekcji manuskryptu jak i współtworzeniu odpowiedzi do recenzentów.*

A3. A. Talik, M. Tarnacka, M. Wojtyniak, E. Kaminska, K. Kaminski, M. Paluch. **The influence of the nanocurvature on the surface interactions and molecular dynamics of model liquid confined in cylindrical pores.** *Journal of Molecular Liquids* 2019. 111973.

*Mój wkład polegał na nadzorowaniu przeprowadzonych analiz, dyskusji otrzymanych wyników oraz tworzeniu i korekcji manuskryptu jak i współtworzeniu odpowiedzi do recenzentów.*

A4. A. Talik; M. Tarnacka; M. Geppert-Rybczynska; B. Hachuła; R. Bernat; A. Chrzanowska; K. Kaminski; M. Paluch. **Are hydrogen supramolecular structures being suppressed upon nanoscale confinement? The case of monohydroxy alcohols.** *Journal of Colloid and Interface Science*, 576, 2020, 217–229.

*Mój wkład polegał na nadzorowaniu przeprowadzonych analiz, dyskusji otrzymanych wyników oraz tworzeniu i korekcji manuskryptu jak i współtworzeniu odpowiedzi do recenzentów.*

A5. A. Talik; M. Tarnacka; M. Geppert-Rybczynska; B. Hachuła; K. Kaminski; M. Paluch. **Impact of Confinement on the Dynamics and H-Bonding Pattern in Low-Molecular Weight Poly(propylene glycols).** *Journal of Physical Chemistry C* 2020, 124, 17607–17621

*Mój wkład polegał na nadzorowaniu przeprowadzonych analiz, dyskusji otrzymanych wyników oraz tworzeniu i korekcji manuskryptu jak i współtworzeniu odpowiedzi do recenzentów.*

*Kamil Kamiński*

Prof. dr hab. Marian Paluch  
Wydział Nauk Ścisłych i Technicznych,  
Instytut Fizyki  
Uniwersytet Śląski w Katowicach  
Ul. 75 Pułku Piechoty 1A  
41-500 Chorzów

Chorzów, 5.05.2021 r.

#### OŚWIADCZENIE

Oświadczam, że w poniższych pracach:

A1. A. Talik; M. Tarnacka; I. Grudzka-Flak; P. Maksym; M. Geppert-Rybczynska; K. Wolnica; E. Kaminska; K. Kaminski; M. Paluch. **The Role of Interfacial Energy and Specific Interactions on the Behavior of Poly(propylene glycol) Derivatives under 2D Confinement.** *Macromolecules*, 2018, 51, 13, 4840-4852

*Mój wkład polegał na udziale w dyskusji otrzymanych wyników oraz korekcji manuskryptu*

A2. A. Talik, M. Tarnacka, M. Geppert-Rybczynska, A. Minecka, E. Kaminska, K. Kaminski, M. Paluch. **Impact of the Interfacial Energy and Density Fluctuations on the Shift of the Glass-Transition Temperature of Liquids Confined in Pores.** *Journal of Physical Chemistry C*, 2019, 123, 9, 5549-5556.

*Mój wkład polegał na udziale w dyskusji otrzymanych wyników oraz korekcji manuskryptu*

A3. A. Talik, M. Tarnacka, M. Wojtyniak, E. Kaminska, K. Kaminski, M. Paluch. **The influence of the nanocurvature on the surface interactions and molecular dynamics of model liquid confined in cylindrical pores.** *Journal of Molecular Liquids* 2019, 111973.

*Mój wkład polegał na udziale w dyskusji otrzymanych wyników oraz korekcji manuskryptu*

A4. A. Talik; M. Tarnacka; M. Geppert-Rybczynska; B. Hachula; R. Bernat; A. Chrzanowska; K. Kaminski; M. Paluch. **Are hydrogen supramolecular structures being suppressed upon nanoscale confinement? The case of monohydroxy alcohols.** *Journal of Colloid and Interface Science*, 576, 2020, 217-229.

*Mój wkład polegał na udziale w dyskusji otrzymanych wyników oraz korekcji manuskryptu*

A5. A. Talik; M. Tarnacka; M. Geppert-Rybczynska; B. Hachula; K. Kaminski; M. Paluch. **Impact of Confinement on the Dynamics and H-Bonding Pattern in Low-Molecular Weight Poly(propylene glycols).** *Journal of Physical Chemistry C* 2020, 124, 17607-17621.

*Mój wkład polegał na udziale w dyskusji otrzymanych wyników oraz korekcji manuskryptu*



#### IV. PODSUMOWANIE

W rozprawie doktorskiej składającej się z serii pięciu artykułów naukowych przedstawiono wyniki badań dynamiki molekularnej różnego rodzaju nisko- i wysokocząsteczkowych substancji formujących stan szklisty, infiltrowanych do mezoporowatych matryc wykonanych z tlenku glinu ( $\text{Al}_2\text{O}_3$ ) oraz tlenku krzemu ( $\text{SiO}_2$ ) o nanometrycznych średnicach porów.

Zestawienie wyników zmian dynamiki śledzonej poprzez zmiany  $T_g$  wraz z zebranymi danymi literaturowymi wskazały, że zachowanie substancji w warunkach geometrycznego ograniczenia przestrzennego może zostać w pewnym stopniu przewidziane biorąc pod uwagę wartości energii międzyfazowej oraz wrażliwości relaksacji strukturalnej/ segmentalnej na zmiany gęstości ( $dT_g/d\rho$ ), a także krzywizny powierzchni.

Zastosowanie pomiarów napięcia powierzchniowego i kąta zwilżania oraz obliczenia energii międzyfazowej ( $\gamma_{SL}$ ) pomiędzy badaną substancją a matrycą ujawniło, że opisywane w literaturze obniżenie  $T_g$  jest związane z temperaturą przejścia szklistego molekuł znajdujących się w rdzeniu porów i jest wynikiem wzrostu  $T_g$  cząsteczek zaadsorbowanych na ścianach. Dzięki tym wynikom możliwe stało się sformułowanie hipotezy, że zachowanie materiałów jedno- i dwuwymiarowych jest rządzone przez te same zależności, a relacje pomiędzy energią międzyfazową a zachowaniem molekuł przyściankowych są istotnym elementem łączącym dotychczas opublikowane dane dla cienkich warstw oraz materiałów infiltrowanych do porów. Ponadto, zestawienie wyników zmian dynamiki molekularnej śledzonej poprzez zmiany w  $T_g$  wskazują, że im większa wrażliwość relaksacji strukturalnej/segmentalnej na zmiany gęstości, wyrażona ilościowo przez współczynnik ciśnieniowy temperatury przejścia szklistego,  $dT_g/d\rho$ , tym niższa temperatura przejścia szklistego substancji w porach w porównaniu z materiałem litym.

Co więcej wykonane eksperymenty dla substancji infiltrowanych do porowatych membran wykazały, że dla pewnych systemów nie obserwuje się efektów ograniczenia przestrzennego. Skorelowanie wyników z modelem Tolmana oraz zastosowanie pionierskich pomiarów siły adhezji za pomocą spektroskopii AFM, dowiodło, że podczas przewidywania zachowania substancji w skali nano oprócz wpływu energii międzyfazowej dla powierzchni planarnych oraz efektu skończonej wielkości należy wziąć pod uwagę stopień zakrzywienia powierzchni.

Prowadzone eksperymenty ujawniły również, że ogromny wpływ na obserwowane zmiany w  $T_g$  oraz w sile oddziaływań mają specyficzne interakcje, m.in. zdolność do tworzenia wiązań wodorowych oraz struktur supramolekularnych. Zastosowanie hydrofilowych oraz hydrofobowych matryc potwierdziło zmianę zachowania badanych substancji oraz siły oddziaływań, wpływając na wartości  $T_g$ . Przedstawione wyniki pomiarów alkoholi pierwszo- i drugorzędowych o różnej lokalizacji grup -OH, wykazały, że wiązania wodorowe stają się słabsze pod wpływem ograniczenia przestrzennego w porównaniu do substancji natywnych, a wpływ układów nano jest większy dla alkoholi pierwszorzędowych. Eksperymenty te ujawniły, że uporządkowana struktura może być zakłócana przez ograniczenie przestrzenne zmieniając tym samym architekturę asocjatyw.

Przedstawione badania różnych nisko- i wysokocząsteczkowych substancji w nanoskali wykazały wpływ wielu parametrów oraz zależności, które należy brać pod uwagę przewidując kierunek oraz wielkość zmian w dynamice molekularnej, temperaturze przejścia szklistego, jak i w dalszym opisie niezbędnym do pozyskiwania nowych nanomateriałów. Poprzez możliwość manipulacji właściwościami fizyko-chemicznymi oraz strukturą wewnętrzną otwierają się nowe perspektywy otrzymywania materiałów wykazujących właściwości wymagane do odpowiednich badań i zastosowań. Uzyskane wyniki bardzo dobrze wpisują się w nadal trwającą debatę nad pozyskiwaniem i modelowaniem nowych inteligentnych materiałów oraz

przyczyniają się w istotny sposób do lepszego zrozumienia zachowania substancji w skali nano, które w dalszej perspektywie mogą znacząco wpływać na aplikacyjność w wielu dziedzinach przemysłu.

## V. Bibliografia

---

- <sup>1</sup> K. Gokulan, S. Khare, C. Cerniglia. Encyclopedia of Food Microbiology, 2nd Edition, Elsevier **2014**, 561–569.
- <sup>2</sup> R. Lyddy. Nanotechnology. Chapter 36: Information Resources in Toxicology (Fourth Edition) **2009**, 321–328.
- <sup>3</sup> R. P. Feynman. Engineering and Science **1960**, 23, 22-36.
- <sup>4</sup> R. P. Feynman. Journal of Microelectromechanical Systems **1992**, 1, 60–66.
- <sup>5</sup> K. S. Soppimath, T. M. Aminabhavi, A. R. Kulkarni, W. E. Rudzinski, J. Control. Release **2001**, 70, 1-20.
- <sup>6</sup> H. Yang, L. Hao, N. Zhao, C. Du, Y. Wang. CrystEngComm. **2013**, 15, 5760–5763.
- <sup>7</sup> J.-H. Jou, S. Kumar, A. Agrawal, T.-H. Li, S. Sahoo. J. Mater. Chem. C **2015**, 3, 2974–3002.
- <sup>8</sup> J. R. Sheats, H. Antoniadis, M. Hueschen, W. Leonard, J. Miller, R. Moon, D. Roitman, A. Stocking. Science **1996**, 273, 884.
- <sup>9</sup> K. S. Novoselov, A. Mishchenko, A. Carvalho, A. H. C. Neto. Science **2016**, 353, 6298.
- <sup>10</sup> D.W. Hobson. Comprehensive Biotechnology, Industrial Biotechnology and Commodity Products (Second Edition), Elsevier **2011**.
- <sup>11</sup> C. B. Carter, M. G. Norton. Ceramic Materials: Science and Engineering. Springer Science & Business Media Berlin, **2007**.
- <sup>12</sup> P. G. Debenedetti, F. H. Stillinger. Nature **2001**, 410, 259–267.
- <sup>13</sup> S. Napolitano, E. Glynos, N. B. Tito. Rep. Prog. Phys. **2017**, 80, 036602.
- <sup>14</sup> M. Alcoutlabi, G.B. McKenna. J. Phys. Condens. Matter **2005**, 17, R461-R524.
- <sup>15</sup> F. Kremer, A. Schönhal, Broadband Dielectric Spectroscopy, Springer, Berlin **2003**.
- <sup>16</sup> H. Sillescu. J. Non-Cryst. Solids **1999**, 243, 81–108.
- <sup>17</sup> A.D. McNaught, A. Wilkinson, A. IUPAC Compendium of Chemical Terminology, 2nd ed. (the "Gold Book") Blackwell Science **1997**.
- <sup>18</sup> M.D. Angell, C.A. Nagel, S.R.J. Phys. Chem. **1996**, 100, 13200.
- <sup>19</sup> P.W. Bridgman. Collected Experimental Papers. Harvard University Press, Cambridge **1964**.
- <sup>20</sup> G. Adam, J.H. Gibbs, J. Chem. Phys. **1965**, 43, 139.
- <sup>21</sup> D. Cangialosi, A. Alegría, J. Colmenero. Physical Review E **2007**, 76, 011514.
- <sup>22</sup> P. Ehrenfest, Proc. Acad. Sci. (Amsterdam) **1993**, 36, 153.
- <sup>23</sup> L. Berthier, G. Biroli, J.-P. Bouchaud, L. Cipelletti, D. El Masri, D. L'Hôte, F. Ladieu, M. Pierno. Science **2005**, 310, 1797-1800.

- 
- <sup>24</sup> K. Koperwas, A. Grzybowski, K. Grzybowska, Ź. Wojnarowska, M. Paluch. *J. Chem. Phys.* **2015**, 143, 024502.
- <sup>25</sup> H. K. Nguyen, D. Wang, T P. Russell, K. Nakajima. *Soft Matter* **2015**, 11, 1425–1433
- <sup>26</sup> F. Kremer. *Dynamics in Geometrical Confinement*, Springer, Berlin **2014**.
- <sup>27</sup> X. Qiu, X, M.D. Ediger. *J. Phys. Chem. B* **2003**, 107, 459–464.
- <sup>28</sup> C. L. Jackson, G. B. McKenna. *J. Non-Cryst. Solids* **1991**, 131, 221–224.
- <sup>29</sup> C. J. Ellison, J. M. Torkelson, *Nat. Mat.* **2003**, 2, 695–700.
- <sup>30</sup> G. Reiter. *Europhys. Lett.* **1993**, 23, 579–584.
- <sup>31</sup> J. L. Keddie, R. A. L. Jones, R. A. Cory. *Europhys. Lett.* **1994**, 27, 59–64.
- <sup>32</sup> T. S. Chow. *J. Phys.: Condens. Matter* **2002**, 14, 1333–1339.
- <sup>33</sup> J. Baschnagel, F. Varnik. *J. Phys.: Condens. Matter* **2005**, 17, 851–953.
- <sup>34</sup> H. Meyer, J. Baschnagel. *Eur. Phys. J. E* **2003**, 12, 147–151.
- <sup>35</sup> J. Baschnagel, K. Binder, M. Mareschal. *Eur. Phys. J. E* **2003**, 12, 167–171.
- <sup>36</sup> D. S. Fryer, R. D. Peters, E. J. Kim, J. E. Tomaszewski, J. J. de Pablo, P. F. Nealey, C. C. White, W. L. Wu. *Macromolecules* **2001**, 34, 5627–5634.
- <sup>37</sup> K. Fukao, Y. Miyamoto. *Phys. Rev. E* **2000**, 61, 1743–1754.
- <sup>38</sup> S. Napolitano, D. Prevosto, M. Lucchesi, P. Pingue, M. D’Acunto, P. Rolla. *Langmuir*, **2007**, 23, 2103–2109.
- <sup>39</sup> K. Adrjanowicz, K. Kolodziejczyk, W. K. Kipnusu, M. Tarnacka, E. U. Mapesa, E. Kaminska, S. Pawlus, K. Kaminski, M. Paluch. *J. Phys. Chem. C* **2015**, 119, 14366–14374.
- <sup>40</sup> M. Arndt, R. Stannarius, W. Gorbatschow, F. Kremer. *Phys. Rev. E* **1996**, 54, 5377–5390.
- <sup>41</sup> S. Napolitano, M. Wubbenhorst. *Nat. Commun.* **2011**, 2, 260.
- <sup>42</sup> A. Schönhals, R. Zorn, B. Frick. *Polymer* **2016**, 105, 393–406.
- <sup>43</sup> J. Xu, L. Ding, J. Chen, S. Gao, L. Li, D. Zhou, X, Li, G. Xue. *Macromolecules* **2014**, 47, 6365–6372.
- <sup>44</sup> J. A. Forrest, K. Dalnoki-Veress, J. R Stevens, J. R. Dutcher. *Phys. Rev. Lett.* **1996**, 77, 2002–2005.
- <sup>45</sup> Z. H. Yang, Y. Fujii, F. K. Lee, C. H. Lam, O. K. C. Tsui. *Science* **2010**, 328, 1676–1679.
- <sup>46</sup> M. D. Ediger, J. A. Forrest, *Macromolecules* **2014**, 47, 471–478.
- <sup>47</sup> J. A. Forrest, K. Dalnoki-Veress. *Adv. Colloid Interface Sci.* **2001**, 94, 167–196.
- <sup>48</sup> Ch. Zhang, L. Li, X. Wang, G. Xue. *Macromolecules* **2017**, 50, 1599–1609.
- <sup>49</sup> R. N. Li, F. Chen, C.-H. Lam, O. K. C. Tsui. *Macromolecules* **2013**, 46, 7889–7893.
- <sup>50</sup> K.-I Akabori, K. Tanaka, A. Takahara, T. Kajiyama, T. Nagamura. *Euro. Phys. J. Special Topics* **2007**, 141, 173–180.



- 
- <sup>51</sup> M. Tress, M. Erber, E. U. Mapesa, H. Huth, J. Muller, A. Serghei, C. Schick, K.-J. Eichhorn, B. Voit, F. Kremer. *Macromolecules* **2010**, 43, 9937–9944.
- <sup>52</sup> S. Napolitano, M. Wubbenhorst. *Nat. Commun.* **2011**, 2, 260.
- <sup>53</sup> J. Wang, G. B. McKenna. *Macromolecules* **2013**, 46, 2485–2495.
- <sup>54</sup> C. J. Ellison, R. L. Ruzskowski, N.J. Fredin, J. M. Torkelson. *Phys. Rev. Lett.* **2004**, 92, 095702.
- <sup>55</sup> J. L. Keddie, R. A. L. Jones, R. A. Cory. *Europhys. Lett.* **1994**, 27, 59.
- <sup>56</sup> Z. Fakhraai, J. S. Sharp, J. A. Forrest, *J. Polym. Sci. B Polym. Phys.* **2004**, 42, 4503–4507.
- <sup>57</sup> C. Yang, R. Onitsuka, I. Takahashi, *Eur. Phys. J. E* **2013**, 36, 1–8.
- <sup>58</sup> J. A. Forrest, K. Dalnoki-Veress, J. R. Dutcher. *Phys. Rev. E* **1997**, 56, 5705–5716.
- <sup>59</sup> D. S. Fryer, P. F. Nealey, J. J. de Pablo. *Macromolecules* **2000**, 33, 6439–6447.
- <sup>60</sup> K.-I. Akabori, K. Tanaka, A. Takahara, T. Kajiyama, T. Nagamura. *Eur. Phys. J. Special Topics* **2007**, 141, 173–180.
- <sup>61</sup> O. Baumchen, J.D. McGraw, J.A. Forrest, K. Dalnoki-Veress. *Phys. Rev. Lett.* **2012**, 109, 055701.
- <sup>62</sup> J. A. Forrest, K. Dalnoki-Veress. *ACS Macro Lett.* **2014**, 3, 310–314.
- <sup>63</sup> C. Rotella, S. Napolitano, L. De Cremer, G. Koeckelberghs, M. Wübbenhorst. *Macromolecules* **2010**, 43, 8686–8691.
- <sup>64</sup> F. Kremer, M. Tress, E. U. Mapesa. *J. Non-Cryst. Solids* **2015**, 407, 277–283.
- <sup>65</sup> S. Alexandris, P. Papadopoulos, G. Sakellariou, M. Steinhart, H.-J. Butt, G. Floudas. *Macromolecules* **2016**, 49, 7400–7414.
- <sup>66</sup> A. Panagopoulou S. Napolitano. *Phys. Rev. Lett.* **2017**, 119, 097801.
- <sup>67</sup> W. K. Kipnusu, M. M. Elmahdy, M. Elsayed, R. Krause-Rehberg, F. Kremer. *Macromolecules* **2019**, 52, 1864–1873.
- <sup>68</sup> S. Napolitano, V. Lupaşcu, M. Wübbenhorst. *Macromolecules* **2008**, 41, 1061–1063.
- <sup>69</sup> W. K. Kipnusu, W. Kossack, C. Iacob, M. Jasiurkowska, J. R. Sangoro, F. Kremer. *Z. Phys. Chem.* **2012**, 226, 797–805.
- <sup>70</sup> L. Linling, Z. Dongshan, H. Dinghai, G. Xue. *Macromolecules* **2014**, 47, 297–303.
- <sup>71</sup> A. Golovoy, K. A. Mazich, M. F. Cheung, V. K. Berry. *Polym. Bull.* **1989**, 22, 175–181.
- <sup>72</sup> J.-Y., Park, G. B. McKenna. *Phys. Rev. B: Condens. Matter Mater. Phys.* **2000**, 61, 6667.
- <sup>73</sup> W. K. Kipnusu, M. Mohamed, R. Krause–Rehberg, F. Kremer. *J. Chem. Phys.* **2017**, 146, 203302.
- <sup>74</sup> K. Shin, S. Obukhov, J.T. Chen, J. Huh, Y. Hwang, S. Mok, P. Dobriyal, P. Thiyagarajan, T.P. Russell. *Nat. Mater.* **2007**, 6(12), 961–965.

- 
- <sup>75</sup> D. Morineau, Y. D. Xia, C. Alba-Simionesco. *J. Chem. Phys.* **2002**, 117, 8966–8972.
- <sup>76</sup> G. B. McKenna. *Comprehensive Polymer Science, Volume 2: Polymer Properties*; ed. by C. Booth, C. Price, Pergamon Press, Oxford, U.K. **1989**, 311–362.
- <sup>77</sup> R. Simha, T. Somcynsky. *Macromolecules* **1971**, 2, 342–350.
- <sup>78</sup> J. H. Gibbs, E. A. DiMarzio. *J. Chem. Phys.* **1958**, 28, 373–83.
- <sup>79</sup> E. A. DiMarzio, J. H. Gibbs. *J. Chem. Phys.* **1958**, 28, 807–813.
- <sup>80</sup> H. W. Spiess. *Macromolecules* **2010**, 43, 5479–5491.
- <sup>81</sup> G. Adam, J. H. Gibbs. *J. Chem. Phys.* **1965**, 43, 139–146.
- <sup>82</sup> C. M. Roland, S. Hensel-Bielowka, M. Paluch, R. Casalini. *Rep. Prog. Phys.* **2005**, 68, 1405-1478.
- <sup>83</sup> A. Patkowski, T. Ruths, E.W. Fischer. *Phys. Rev. E* **2003**, 67, 021501.
- <sup>84</sup> J. Zhang, G. Liu, J. Jonas. *J. Phys. Chem.* **1992**, 96, 3478–3480.
- <sup>85</sup> J.-Y. Park, G. B. McKenna. *Phys. Rev. B* **2000**, 61, 6667.
- <sup>86</sup> C. Gainaru, R. Meier, S. Schildmann, C. Lederle, W. Hiller, E. A. Rössler, R. Böhmer. *Phys. Rev. Lett.* **2010**, 105, 258303.